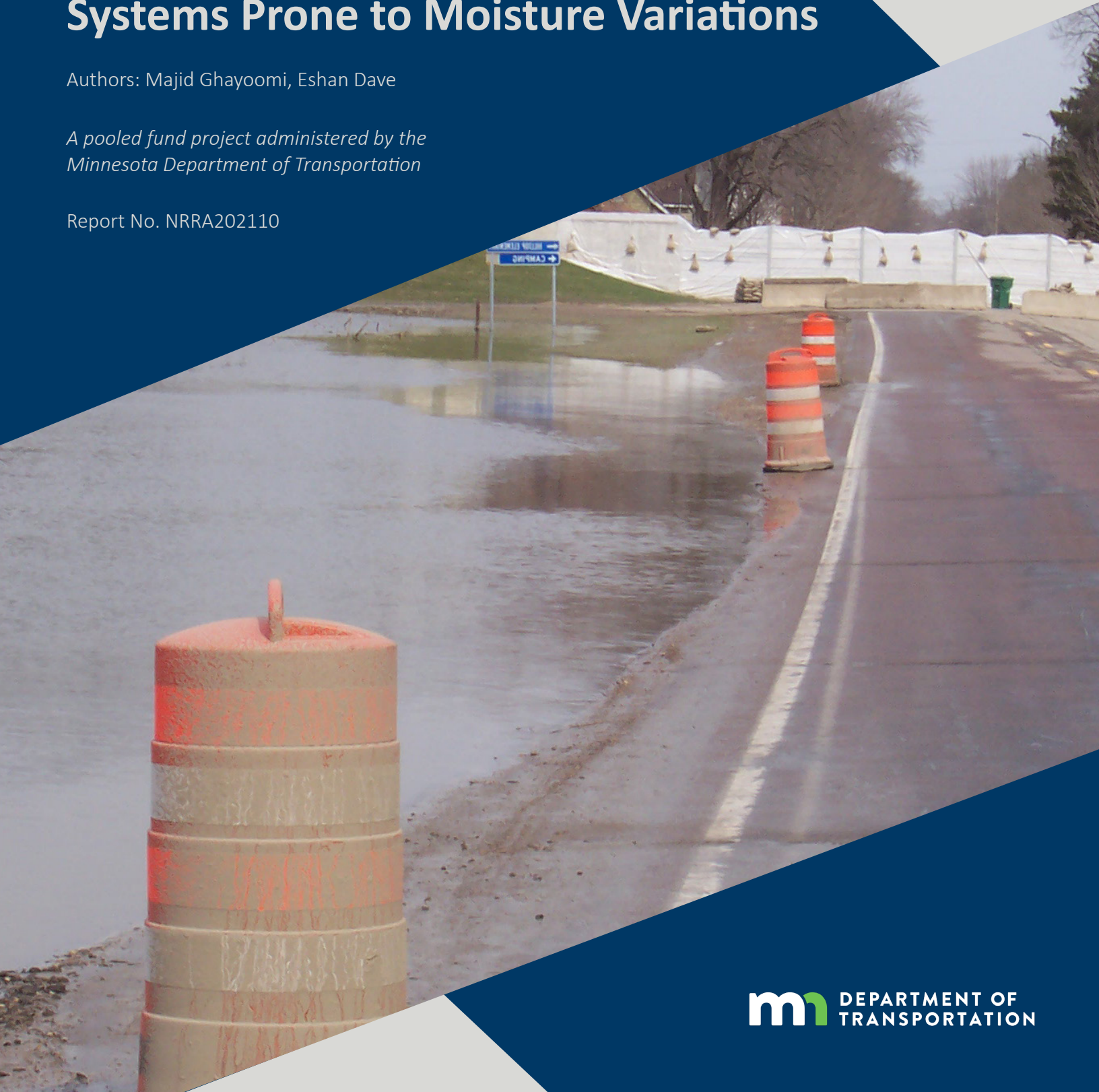


# Mechanistic Load Restriction Decision Platform for Pavement Systems Prone to Moisture Variations

Authors: Majid Ghayoomi, Eshan Dave

*A pooled fund project administered by the  
Minnesota Department of Transportation*

Report No. NRRA202110



To request this document in an alternative format, such as braille or large print, call [651-366-4718](tel:651-366-4718) or [1-800-657-3774](tel:1-800-657-3774) (Greater Minnesota) or email your request to [ADArequest.dot@state.mn.us](mailto:ADArequest.dot@state.mn.us). Please request at least one week in advance.

## Technical Report Documentation Page

1. Report No. <b>NRRA202110</b>	2.	3. Recipients Accession No.	
4. Title and Subtitle <b>Mechanistic Load Restriction Decision Platform for Pavement Systems Prone to Moisture Variations</b>		5. Report Date <b>October 2021</b>	
		6.	
7. Author(s) <b>Majid Ghayoomi, Eshan Dave, Sayedmasoud Mousavi, Francesco Preti</b>		8. Performing Organization Report No.	
9. Performing Organization Name and Address <b>University of New Hampshire, Durham, NH 03824 Department of Civil and Environmental Engineering</b>		10. Project/Task/Work Unit No.	
		11. Contract (C) or Grant (G) No.  <b>(c) 1034192</b>	
12. Sponsoring Organization Name and Address <b>Minnesota Department of Transportation Office of Research &amp; Innovation 395 John Ireland Boulevard, MS 330 St. Paul, Minnesota 55155-1899</b>		13. Type of Report and Period Covered <b>Final Report, 2019-2021</b>	
		14. Sponsoring Agency Code	
15. Supplementary Notes <a href="https://www.mndot.gov/research/reports/2021/NRRA202110.pdf">https://www.mndot.gov/research/reports/2021/NRRA202110.pdf</a>			
16. Abstract (Limit: 250 words) Excessive moisture influences pavement performance by increasing surface deflection and decreasing bearing capacity. Seasonal fluctuation of groundwater, flooding, and spring thaw can all lead to changes in soil moisture and consequently stress states. Load restriction during and after inundation plays a key role in service life and maintenance planning of pavement systems. However, current procedures are either empirical or based on regional historical practices and do not incorporate transient and forecasted moisture profile in pavement response. This signifies the need for a mechanistic, coupled, and risk-based load restriction decision platform to assess pavement performance and determine traffic allowances during and after periods of excessive moisture. The research discussed in this report responds to this need by: (1) identifying key mechanical and environmental stressors and pavement characteristics through system dynamics modeling of hydrological regimes, moisture-dependent material properties, and pavement response models; and (2) developing a mechanistic load restriction decision toolkit validated against independent linear elastic models and field deflection measurement data. System-based univariate and multivariate sensitivity analysis demonstrated how different soil and climatic variables impact the moisture-dependent surface deflection and post-flooding recovery time. Inspired by the outcome of the system dynamics modeling, the first generation of PaveSafe, a flooded pavement assessment app, was prepared and is now available. It is a user-friendly application designed for different agent expertise and application in pavement sections with different model inputs. It is expected that the next generations of PaveSafe will be more computationally efficient, involve more material and modeling options, and be adaptable with other pavement performance packages.			
17. Document Analysis/Descriptors <b>Floods, Flexible pavements, Pavement performance, Dynamic models, Decision Trees, Size and weight regulations</b>		18. Availability Statement	
19. Security Class (this report) <b>Unclassified</b>	20. Security Class (this page) <b>Unclassified</b>	21. No. of Pages <b>218</b>	22. Price

# **Mechanistic Load Restriction Decision Platform for Pavement Systems Prone to Moisture Variations**

## **FINAL REPORT**

Prepared by:

Majid Ghayoomi  
Eshan V. Dave  
Sayedmasoud Mousavi  
Francesco Preti

Department of Civil and Environmental Engineering  
University of New Hampshire

**October 2021**

Published by:

Minnesota Department of Transportation  
Office of Research & Innovation  
395 John Ireland Boulevard, MS 330  
St. Paul, Minnesota 55155-1899

This report represents the results of research conducted by the authors and does not necessarily represent the views or policies of the Minnesota Department of Transportation or the University of New Hampshire. This report does not contain a standard or specified technique.

The authors, the Minnesota Department of Transportation, and the University of New Hampshire do not endorse products or manufacturers. Trade or manufacturers' names appear herein solely because they are considered essential to this report.



## Acknowledgement

This research study would not have been possible without the contribution of a number of individuals and partnership with the National Road Research Alliance (NRRRA) members. We sincerely acknowledge significant efforts made by the technical liaisons for the project, Raul Velasquez and Tim Anderson from the MnDOT Office of Materials and Road Research. The support and feedback of the project Technical Advisory Panel members is also very much appreciated.

# TABLE OF CONTENTS

<b>CHAPTER 1: Introduction.....</b>	<b>1</b>
1.1 Research Project Abstract and Objectives.....	1
1.2 Summary of Research Methodology (SCOPE) .....	1
1.3 Organization of the Report .....	2
<b>CHAPTER 2: Literature Review .....</b>	<b>3</b>
2.1 Effects of Excess Moisture on Pavement Performance.....	3
2.1.1 Introduction.....	3
2.1.2 Moisture Variation Effects on Pavement System Response .....	3
2.1.3 Pertinent Inputs and Models to Assess Pavement Capacity in Context of Excess Moisture States.....	7
2.1.4 Summary .....	12
2.2 Load Restriction Protocols.....	12
2.2.1 Why Are Load Restrictions Needed?.....	12
2.2.2 Minnesota DOT Load Restrictions .....	13
2.2.3 North Dakota DOT Load Restrictions .....	14
2.2.4 Wisconsin DOT Load Restrictions.....	15
2.2.5 Important Factors Considered and Trends Identified .....	17
2.3 Resilient modulus .....	17
2.3.1 Introduction.....	17
2.3.2 Resilient Modulus for A-1 Soil Types.....	18
2.3.3 Resilient Modulus for A-2 and A-3 Soil Types .....	20
2.3.4 Resilient Modulus for A-4 through A-7 Soil Types .....	21
2.3.5 Resilient Modulus Prediction Equation Summary.....	22
2.4 Soil Water Retention Equations and Hydraulic Conductivity Models .....	23
2.4.1 Introduction.....	23

2.4.2 SWRC Modeling Parameters .....	23
2.4.3 Brooks and Corey Model.....	24
2.4.4 Van Genuchten (VG) Model .....	25
2.4.5 Fredlund and Xing (FX) Model .....	26
2.4.6 Hydraulic Conductivity Models .....	26
2.4.7 Summary .....	27
2.5 Pavement Moisture Profile and Hydraulic Modeling .....	27
2.5.1 Introduction.....	27
2.5.2 Unsaturated Soil Flow Models .....	28
2.5.3 Groundwater Recharge Models .....	31
2.5.4 Pavement Moisture Profile and Hydraulic Modeling Summary.....	32
2.6 Literature Review Summary .....	32
2.6.1 Summary .....	32
<b>CHAPTER 3: System Dynamics Framework Development .....</b>	<b>33</b>
3.1 System Dynamics Modeling and VENSIM PRO® Introduction.....	33
3.1.1 Introduction.....	33
3.1.2 System Dynamics Modeling .....	34
3.1.3 Vensim pro® .....	35
3.1.4 A Simple Example of System Dynamics Simulation using Vensim pro® .....	35
3.1.5 Summary .....	38
3.2 Proposed System Dynamics Framework .....	38
3.2.1 Introduction.....	38
3.2.2 System Dynamics Main Structures.....	38
3.2.3 Example of Conventional Flexible Pavement Properties .....	40
3.2.4 Summary .....	41

3.3 Hydrological Structure Model .....	41
3.3.1 Introduction.....	41
3.3.2 Climate Information Variables .....	41
3.3.3 Hydraulics of Unsaturated Subsurface Soil .....	42
3.3.4 Water Movement Simulation within a Conventional Flexible Pavement Example .....	44
3.4 Geotechnical Structure Model .....	48
3.4.1 Introduction.....	48
3.4.2 Geotechnical Structure Variables for Estimation of Resilient Modulus.....	49
3.4.3 Simulation of Geotechnical Structure for the Conventional Flexible Pavement example.....	50
3.5 Pavement Response Structure Model.....	51
3.5.1 Introduction.....	51
3.5.2 Main Components of Pavement Response Structure .....	52
3.5.3 Simulation of Pavement Response Structure for the Conventional Flexible Pavement Example .....	54
3.6 System Dynamics Framework Summary and Conclusions .....	55
3.6.1 Summary and Conclusions .....	55
<b>CHAPTER 4: Sensitivity Analysis and Framework Refinement .....</b>	<b>57</b>
4.1 Overview of the developed System Dynamics Framework.....	57
4.1.1 Introduction.....	57
4.1.2 Developed System Dynamics Framework.....	57
4.1.3 Summary .....	60
4.2 Methodology for Sensitivity Analysis .....	60
4.2.1 Introduction.....	60
4.2.2 Methodology for SDM Sensitivity Analysis .....	61
4.3 Local Sensitivity Analysis .....	68
4.3.1 Introduction.....	68

4.3.2 Local Sensitivity Analysis for Coarse-grained subgrade .....	68
4.3.3 Local Sensitivity Analysis for Fine-grained subgrade .....	82
4.3.4 Sensitivity Analysis Summary and Conclusions .....	93
4.4 Multivariate Global Sensitivity Analysis (GSA).....	94
4.4.1 Introduction.....	94
4.4.2 Global Sensitivity Analysis for Coarse-grained subgrade .....	95
4.4.3 Global Sensitivity Analysis for Fine-grained subgrade .....	100
4.5 Sensitivity Analysis Summary and Conclusions .....	104
4.5.1 Summary and Conclusions .....	104
<b>CHAPTER 5: Load Restriction Decision Platform for Pavement Systems prone to Moisture Variations</b> .....	<b>107</b>
5.1 Technical Background and Assumption.....	107
5.1.1 Introduction.....	107
5.1.2 Hydrological structure.....	107
5.1.3 Geotechnical structure .....	109
5.1.4 Pavement response structure .....	109
5.2 Toolkit User Manual: PaveSafe™ v1.0.4.....	116
5.2.1 Requirements and Installation Procedures.....	116
5.2.2 Introduction.....	120
5.2.3 Password Protection Menu .....	121
5.2.4 Unit System Selection (SI units vs US customary) .....	123
5.2.5 Project Information Panel .....	124
5.2.6 Pavement Structure Panel.....	125
5.2.7 Subgrade Properties Panel .....	126
5.2.8 Hydrology Information Panel .....	128
5.2.9 Results Panel .....	134



5.2.10 Menu Tab .....	137
5.3 Toolkit Summary.....	139
5.3.1 Summary .....	139
<b>CHAPTER 6: Calibration and Preliminary Validation of the Toolkit .....</b>	<b>140</b>
6.1 Verification Procedure and Results .....	140
6.1.1 Introduction.....	140
6.1.2 Adopted Procedure for the Verification of PaveSafe.....	140
6.1.3 Saturation Profile and Resilient Modulus Calculation.....	141
6.1.4 Results for the Verification of PaveSafe .....	143
6.2 Field-Based Validation Procedure and Results .....	148
6.2.1 Introduction.....	148
6.2.2 Field-Based Validation of PaveSafe .....	148
6.2.3 Results for the Field-Based Validation of PaveSafe.....	150
6.3 Calibration and Validation Summary.....	158
6.3.1 Summary .....	158
<b>CHAPTER 7: Summary, Conclusions and Future Work.....</b>	<b>159</b>
7.1 Summary.....	159
7.2 Conclusions.....	159
7.3 Future Work.....	160
<b>REFERENCES.....</b>	<b>162</b>
<b>APPENDIX A. Summary of Resilient Modulus Equations .....</b>	<b>0</b>
<b>APPENDIX B. Sensitivity Analysis Results .....</b>	<b>0</b>

## LIST OF FIGURES

Figure 2-1 Variation of the maximum surface deflection with depth of subsurface water levels (Elshaer et al. 2019) .....	6
Figure 2-2 Variation of bearing capacity with groundwater table levels for the proposed soils (Elshaer et al. 2017) .....	6
Figure 2-3: Soil-Water Characteristic Curves Models Using the Brooks and Corey (1964) Model (Lu and Likos 2004) .....	24
Figure 2-4: Experimental Soil-Water Characteristic Curves Models Using VG (Lu and Likos 2004) .....	25
Figure 2-5: Groundwater Recharge Model (Freeze 1969) .....	31
Figure 3-1: (a) Schematic of the example problem, and (b) the system dynamic model of example problem.....	36
Figure 3-2: Results of system dynamics model simulation using Vensim PRO® .....	37
Figure 3-3: Results of SD model sensitivity simulations using Vensim PRO®. ....	38
Figure 3-4: A conceptual schematic of the SD model structures and their variables.....	40
Figure 3-5: The conventional flexible pavement example.....	40
Figure 3-6: Climate information variables in the system dynamics model. ....	42
Figure 3-7: Hydrological structure of flooded pavement SD model. ....	44
Figure 3-8: Precipitation rate time history.....	45
Figure 3-9: (a) Initial degree of saturation and (b) moisture dependent hydraulic conductivity profile. ...	45
Figure 3-10: Typical results of moisture movement simulation using the SD model formulated in Vensim PRO® in terms of saturation time histories for (a) base aggregate (averaged for whole layer), (b) subbase (averaged for whole layer), (c) subgrade layer 1, and (d) subgrade layer 5.....	47
Figure 3-11: Moisture profile of pavement layers (a) during first period of precipitation, (b) between two periods of precipitation, (c) during the second period of precipitation, and (d) after the second period of precipitation.....	48
Figure 3-12: The geotechnical structure of the proposed SD model.....	49
Figure 3-13: Results of geotechnical structure simulation using the SD model formulated in Vensim PRO®. Results show (a) base aggregate saturation; (b) base aggregate resilient modulus time history; (c) subgrade layer 5 saturation; and (d) subgrade layer 5 resilient modulus time history.....	51

Figure 3-14: Surface deflection simulation using the SD model in Vensim PRO®. ....	53
Figure 3-15: Surface deflection simulation using the example pavement SD model. ....	55
Figure 3-16: A big picture of the SD model structures and variables along with the typical results of the conventional flexible pavement .....	56
Figure 4-1. AC surface deflection time history of the coarse-grained subgrade reference model. ....	66
Figure 4-2. Sensitivity of AC surface deflection (mm) to subgrade $D_{10}$ . Results show surface deflection time histories for 50%, 75%, 95%, and 100% Confidence bounds. ....	67
Figure 4-3. Performance measures used for sensitivity analyses. ....	68
Figure 4-4. AC surface deflection time history of the coarse-grained subgrade reference model. ....	69
Figure 4-5. Sensitivity of peak surface deflection to the variations of subgrade $D_{10}$ . (a) Peak surface deflection versus $D_{10}$ ; (b) change in peak surface deflection versus change in $D_{10}$ . ....	70
Figure 4-6. Sensitivity of peak surface deflection to the variations of subgrade void ratio. ....	71
Figure 4-7. Sensitivity of peak surface deflection to the variations of precipitation (a) rate and (b) duration. ....	71
Figure 4-8. Sensitivity of peak surface deflection to the variations of (a) aggregate base and (b) subbase optimum resilient moduli. ....	72
Figure 4-9. Sensitivity of peak surface deflection to the variations of (a) aggregate base and (b) subbase thicknesses. ....	72
Figure 4-10. Sensitivity of peak surface deflection to the variations of (a) aggregate base and (b) subbase hydraulic conductivities. ....	73
Figure 4-11. Sensitivity of peak surface deflection to the variations of (a) $M_{R,AC}$ and (b) $Th_{AC}$ . ....	73
Figure 4-12. Sensitivity of peak surface deflection to the variations of wheel load. ....	74
Figure 4-13. Comparison of $\delta_p$ and $\delta_p/\delta_0$ as the performance measure index; (a) sensitivity of $\delta_p$ and (b) Sensitivity of $\delta_p/\delta_0$ to $M_{R,AC}$ . ....	75
Figure 4-14. Sensitivity of $\delta_p/\delta_0$ to variation in subgrade (a) $D_{10}$ and (b) $e$ . ....	76
Figure 4-15. Sensitivity of $\delta_p/\delta_0$ to variation in saturated hydraulic conductivity of (a) aggregate base and (b) subbase. ....	76
Figure 4-16. Sensitivity of $\delta_p/\delta_0$ to variation in precipitation rate. ....	77
Figure 4-17. Sensitivity of $t_p$ to variations in subgrade $D_{10}$ . ....	78

Figure 4-18. Sensitivity of $t_R$ to variations in subgrade (a) $D_{10}$ and (b) $e$ .	79
Figure 4-19. Sensitivity of $t_R$ to variations in precipitation (a) rate and (b) duration.	79
Figure 4-20. Sensitivity of $t_R$ to variations in initial GWL.	80
Figure 4-21. Sensitivity of $t_R$ to variations in (a) aggregate base and (b) subbase thicknesses.	81
Figure 4-22. Sensitivity of $t_R$ to variations in AC (a) thickness and (b) resilient modulus.	81
Figure 4-23. Sensitivity of $t_R$ to variations in wheel load.	82
Figure 4-24. Surface deflection time history for (a) the fine-grained subgrade reference and (b) the coarse-grained subgrade reference models.	83
Figure 4-25. Sensitivity of peak surface deflection to the variations of subgrade liquid limit.	84
Figure 4-26. Surface deflection time histories for the fine-grained model with $w_L = 16$ and 17%.	85
Figure 4-27. Sensitivity of peak surface deflection to the variations of precipitation (a) rate and (b) duration.	86
Figure 4-28. Sensitivity of peak surface deflection to the variations of (a) aggregate base and (b) subbase optimum resilient moduli.	86
Figure 4-29. Sensitivity of peak surface deflection to the variations of (a) aggregate base and (b) subbase thicknesses.	87
Figure 4-30. Sensitivity of peak surface deflection to the variations of (a) $M_{R,AC}$ and (b) $Th_{AC}$ .	88
Figure 4-31. Sensitivity of peak surface deflection to the variations of initial GWL.	88
Figure 4-32. Sensitivity of peak surface deflection to the variations of wheel load.	89
Figure 4-33. Sensitivity of $\delta_p/\delta_0$ to variation in subgrade (a) $w_L$ and (b) $e$ .	89
Figure 4-34. Sensitivity of $\delta_p/\delta_0$ to variation in precipitation (a) rate and (b) duration.	90
Figure 4-35. Sensitivity of $\delta_p/\delta_0$ to variation in evaporation rate.	90
Figure 4-36. Sensitivity of $\delta_p/\delta_0$ to variation in (a) AC and (b) aggregate base thicknesses.	91
Figure 4-37. Sensitivity of $t_p$ to variation in subgrade liquid limit.	91
Figure 4-38. Sensitivity of $t_R$ to variations in subgrade (a) $w_L$ and (b) $e$ .	92
Figure 4-39. Sensitivity of $t_R$ to variations in evaporation rate.	93
Figure 5-1. 13-category FHWA vehicle classification (FHWA, 2014).	111

Figure 5-2. Conceptual example of the equivalent footprint method for calculation of induced pressure and radius on AC surface. ....	112
Figure 5-3. Comparisons of AC deflection estimations assuming actual tire configuration and the equivalent footprint method for vehicle class 7 and class 9. (a) Axle spacing 140cm (b) Axle spacing 80cm.....	113
Figure 5-4. Axle weights for different truck sizes from comprehensive truck size and weight study. ....	115
Figure 5-5. Toolkit package folders. ....	116
Figure 5-6. Web installer screenshot. ....	117
Figure 5-7. A screenshot of application installer folder selection tab. ....	117
Figure 5-8. A screenshot of software installer folder selection tab.....	118
Figure 5-9. Matlab runtime license agreement. ....	118
Figure 5-10. Matlab runtime installer tab.....	119
Figure 5-11. A screenshot of Installation completion message.....	119
Figure 5-12. A screenshot of password window. ....	121
Figure 5-13. A screenshot of wrong password message. ....	122
Figure 5-14. A screenshot of correct password message. ....	122
Figure 5-15. A screenshot of dialogue box for unit system selection.....	123
Figure 5-16. A screenshot of project information panel.....	124
Figure 5-17. A screenshot of pavement structure panel. ....	125
Figure 5-18. A screenshot of subgrade properties panel; an example of coarse grained soil.....	126
Figure 5-19. A screenshot of subgrade properties panel; an example of fine grained soil. ....	127
Figure 5-20. A screenshot of subgrade properties panel; an example of fine grained soil with direct hydraulic conductivity input. ....	128
Figure 5-21. A screenshot of hydrological input panel. ....	129
Figure 5-22. A screenshot of hydrological input panel with example precipitation time history. ....	130
Figure 5-23. A screenshot of hydrological input panel with import climate data option. ....	130
Figure 5-24. Generated climate data file name. ....	131



Figure 5-25. Message box for climate data generation. ....	131
Figure 5-26. A screenshot of Excel file format. ....	132
Figure 5-27. A screenshot of Excel file basic inputs. ....	132
Figure 5-28. A screenshot of hydrological input panel with example precipitation time history from input climate data file. ....	133
Figure 5-29. A schematic of pavement layer system with water table elevation. ....	134
Figure 5-30. A screenshot of results panel. ....	134
Figure 5-31. A screenshot of results panel while program is running. ....	135
Figure 5-32. A screenshot of results panel when the analysis is completed. ....	136
Figure 5-33. A screenshot of the menu tab to export the results excel file. ....	137
Figure 5-34. A screenshot of results panel when the results Excel file is successfully generated. ....	138
Figure 5-35. An example of generated results Excel file. ....	138
Figure 5-36. A screenshot of final results Excel file. ....	139
Figure 6-1. Schematic of the pavement cross section. ....	141
Figure 6-2. Saturation profile for the hydrostatic scenario with AASHTO A-3 soil type. ....	142
Figure 6-3: Resilient Modulus profile for the hydrostatic scenario with AASHTO A-3 soil type. ....	142
Figure 6-4. Comparison results from GAMES and PaveSafe for the three scenarios with A-3 subgrade type for vehicle class (V.C.) 5 and 9. ....	144
Figure 6-5. Comparison results from GAMES and PaveSafe for the three scenarios with A-7-6 subgrade type for vehicle class (V.C.) 5 and 9. ....	144
Figure 6-6. Normalized surface deflection for all vehicle classes in hydrostatic scenario with A-3 subgrade type from GAMES and PaveSafe. ....	145
Figure 6-7. Normalized surface deflection for all axle loads in hydrostatic scenario with A-3 subgrade type from GAMES and PaveSafe. ....	146
Figure 6-8. Correlation of results from GAMES and PaveSafe simulations. ....	147
Figure 6-9. Resilient Modulus of subgrade on ND 200. ....	149
Figure 6-10. Results MN 93 (6/24/2010). ....	151

Figure 6-11. Results MN 93 (4/18/2011). .....	152
Figure 6-12. Results MN 93 (4/21/2011). .....	153
Figure 6-13. Results MN 93 (4/25/2011). .....	154
Figure 6-14. Results MN 93 (5/9/2011). .....	155
Figure 6-15. Results ND 200 before flood.....	156
Figure 6-16. Results ND 200 flooded. ....	157
Figure B-1. Sensitivity of peak surface deflection to the variations of subgrade Poisson's ratio for coarse-grained subgrade model. ....	B-1
Figure B-2. Sensitivity of peak surface deflection to the variations of (a) aggregate base and (b) subbase Poisson's ratio for coarse-grained subgrade model. ....	B-1
Figure B-3. Sensitivity of peak surface deflection to the variations of AC Poisson's ratio for coarse-grained subgrade model. ....	B-2
Figure B-4. Sensitivity of $\delta_p/\delta_0$ to variations in (a) precipitation duration and (b) evaporation rate for coarse-grained subgrade model. ....	B-2
Figure B-5. Sensitivity of $\delta_p/\delta_0$ to variations in initial GWL for coarse-grained subgrade model.....	B-3
Figure B-6. Sensitivity of $\delta_p/\delta_0$ to variations in (a) aggregate base and (b) subbase optimum resilient moduli for coarse-grained subgrade model. ....	B-3
Figure B-7. Sensitivity of $\delta_p/\delta_0$ to variations in (a) aggregate base and (b) subbase thicknesses for coarse-grained subgrade model. ....	B-4
Figure B-8. Sensitivity of $\delta_p/\delta_0$ to variations in AC resilient modulus for coarse-grained subgrade model.. .....	B-4
Figure B-9. Sensitivity of $\delta_p/\delta_0$ to variations in wheel load for coarse-grained subgrade model.....	B-5
Figure B-10. Sensitivity of $t_p$ to variations in subgrade void ratio for coarse-grained subgrade model. ...	B-5
Figure B-11. Sensitivity of $t_p$ to variations in precipitation (a) rate and (b) duration for coarse-grained subgrade model. ....	B-6
Figure B-12. Sensitivity of $t_p$ to variations in evaporation rate for coarse-grained subgrade model.....	B-6
Figure B-13. Sensitivity of $t_p$ to variations in initial GWL for coarse-grained subgrade model. ....	B-7
Figure B-14. Sensitivity of $t_p$ to variations in (a) aggregate base and (b) subbase optimum resilient moduli for coarse-grained subgrade model.....	B-7

Figure B-15. Sensitivity of $t_p$ to the variations of (a) aggregate base and (b) subbase hydraulic conductivities for coarse-grained subgrade model. ....	B-8
Figure B-16. Sensitivity of $t_p$ to variations in (a) aggregate base and (b) subbase thicknesses for coarse-grained subgrade model. ....	B-8
Figure B-17. Sensitivity of $t_p$ to variations in AC (a) resilient modulus and (b) thickness for coarse-grained subgrade model. ....	B-9
Figure B-18. Sensitivity of $t_p$ to variations in wheel load for coarse-grained subgrade model for coarse-grained subgrade model. ....	B-9
Figure B-19. Sensitivity of $t_R$ to variations in evaporation rate for coarse-grained subgrade model. ....	B-10
Figure B-20. Sensitivity of $t_R$ to variations in (a) aggregate base and (b) subbase optimum resilient moduli for coarse-grained subgrade model.....	B-10
Figure B-21. Sensitivity of $t_R$ to the variations of (a) aggregate base and (b) subbase hydraulic conductivities for coarse-grained subgrade model. ....	B-11
Figure B-22. Sensitivity of peak surface deflection to the variations of (a) aggregate base and (b) subbase hydraulic conductivities for fine-grained subgrade model.....	B-11
Figure B-23. Sensitivity of $\delta_p/\delta_0$ to variation in initial GWL for fine-grained subgrade model.....	B-12
Figure B-24. Sensitivity of $\delta_p/\delta_0$ to variations in (a) aggregate base and (b) subbase optimum resilient moduli for fine-grained subgrade model.....	B-12
Figure B-25. Sensitivity of $\delta_p/\delta_0$ to the variations of (a) aggregate base and (b) subbase hydraulic conductivities for fine-grained subgrade model.....	B-13
Figure B-26. Sensitivity of $\delta_p/\delta_0$ to variations in (a) aggregate base and (b) subbase thicknesses for fine-grained subgrade model. ....	B-13
Figure B-27. Sensitivity of $\delta_p/\delta_0$ to variations in AC resilient modulus for fine-grained subgrade model.....	B-14
Figure B-28. Sensitivity of $\delta_p/\delta_0$ to variations in wheel load for fine-grained subgrade model. ....	B-14
Figure B-29. Sensitivity of $t_p$ to variations in subgrade void ratio for fine-grained subgrade model.....	B-15
Figure B-30. Sensitivity of $t_p$ to variations in precipitation (a) rate and (b) duration for fine-grained subgrade model. ....	B-15
Figure B-31. Sensitivity of $t_p$ to variations in evaporation rate for fine-grained subgrade model. ....	B-16
Figure B-32. Sensitivity of $t_p$ to variations in initial GWL for fine-grained subgrade model. ....	B-16

Figure B-33. Sensitivity of $t_p$ to variations in (a) aggregate base and (b) subbase optimum resilient moduli for fine-grained subgrade model. ....	B-17
Figure B-34. Sensitivity of $t_p$ to the variations of (a) aggregate base and (b) subbase hydraulic conductivities for fine-grained subgrade model. ....	B-17
Figure B-35. Sensitivity of $t_p$ to variations in (a) aggregate base and (b) subbase thicknesses for fine-grained subgrade model. ....	B-18
Figure B-36. Sensitivity of $t_p$ to variations in AC (a) resilient modulus and (b) thickness for fine-grained subgrade model. ....	B-18
Figure B-37. Sensitivity of $t_p$ to variations in wheel load for coarse-grained subgrade model for fine-grained subgrade model. ....	B-19
Figure B-38. Sensitivity of $t_R$ to variations in precipitation (a) rate and (b) duration for fine-grained subgrade model. ....	B-19
Figure B-39. Sensitivity of $t_R$ to variations in initial GWL for fine-grained subgrade model. ....	B-20
Figure B-40. Sensitivity of $t_R$ to variations in (a) aggregate base and (b) subbase optimum resilient moduli for fine-grained subgrade model. ....	B-20
Figure B-41. Sensitivity of $t_R$ to the variations of (a) base and (b) subbase hydraulic conductivities for fine-grained subgrade model. ....	B-21
Figure B-42. Sensitivity of $t_R$ to variations in (a) base and (b) subbase thicknesses for fine-grained subgrade model. ....	B-21
Figure B-43. Sensitivity of $t_R$ to variations in AC (a) resilient modulus and (b) thickness for fine-grained subgrade model. ....	B-22
Figure B-44. Sensitivity of $t_R$ to variations in wheel load for coarse-grained subgrade model for fine-grained subgrade model. ....	B-22

## LIST OF TABLES

Table 2-1: MnDOT Load Restriction Factors .....	13
Table 2-2: NDDOT Load Restriction Factors.....	15
Table 2-3: WisDOT Load Restriction Factors.....	16
Table 2-4: Regression Constants (Ng et al., 2013) .....	22
Table 3-1: Empirical relations for estimation of hydraulic conductivity of fully saturated soils. ....	43
Table 3-2: Physical and hydraulic properties of hypothetical subgrade.....	46
Table 3-3: Mechanical properties of pavement layers. ....	50
Table 3-4: Mechanical properties of pavement layers. ....	54
Table 3-5: Traffic load information for the pavement example. ....	54
Table 4-1: A summary of the variables associated to climate information. ....	58
Table 4-2: Required input parameters for simulation of moisture infiltration through the SDM.....	59
Table 4-3: Required input parameters in the geotechnical structure of the SDM. ....	59
Table 4-4: Required input parameters in the pavement response structure of the SDM.....	60
Table 4-5: A summary of the climate input parameters and their ranges considered for sensitivity analysis.....	62
Table 4-6: Base and subbase variables and their reference values.....	63
Table 4-7: Empirical relations for estimation of hydraulic conductivity of fully saturated soils. ....	63
Table 4-8: Subgrade variables and their reference values for the first set of the sensitivity analysis. ....	64
Table 4-9: Subgrade variables and their reference values for the second set of the sensitivity analysis. .	65
Table 4-10: Pavement response structure variables ranges and their reference values. ....	65
Table 4-11. Overall qualitative significance of the impact of SDM input parameters on the pavement performance measures from local sensitivity analysis. ....	94
Table 4-12. Select input parameters and their ranges for GSA of coarse-grained subgrade model.....	95
Table 4-13. Summary of the analysis of the sensitivity of peak surface deflection to select input parameters for coarse-grained subgrade model. ....	96



Table 4-14. Summary of the analysis of the sensitivity of $\delta_p/\delta_\theta$ to select input parameters for coarse-grained subgrade model. ....	97
Table 4-15. Summary of the analysis of the sensitivity of $t_p$ to select input parameters for coarse-grained subgrade model. ....	98
Table 4-16. Summary of the analysis of the sensitivity of $t_R$ to select input parameters for coarse-grained subgrade model. ....	99
Table 4-17. Select input parameters and their ranges for GSA of fine-grained subgrade model. ....	100
Table 4-18. Summary of the analysis of the sensitivity of $\delta_p$ to select input parameters for fine-grained subgrade model. ....	101
Table 4-19. Summary of the analysis of the sensitivity of $\delta_p/\delta_\theta$ to select input parameters for fine-grained subgrade model. ....	102
Table 4-20. Summary of the analysis of the sensitivity of $t_p$ to select input parameters for fine-grained subgrade model. ....	103
Table 4-21. Summary of the analysis of the sensitivity of $t_R$ to select input parameters for fine-grained subgrade model. ....	104
Table 4-22. A qualitative summary of the significance of the impact of input parameters on the performance measure indices. ....	106
Table 5-1: Suggested values for fitting parameters in geotechnical structure of the toolkit (Zapata et al. 2007). ....	109
Table 5-2: The axle and tire spacing, and tire pressures considered for each vehicle class.....	114
Table 6-1: Hydrological information for the three scenarios taken into consideration. ....	140
Table 6-2: Cross-section with either A-3 or A-7-6 subgrade type.....	141
Table 6-3: Cross section for MN 93.....	148
Table 6-4: Cross section for ND 200.....	149
Table A-1: Resilient Modulus Equations (1). ....	A-1
Table A-2: Resilient Modulus Equations (2). ....	A-2
Table A-3: Resilient Modulus Equations (3). ....	A-3

## EXECUTIVE SUMMARY:

Adverse effects of excessive moisture within pavement structure are well-known and have been studied in the past. Current pavement design and analysis techniques are often limited to use of optimum moisture conditions to determine pavement vehicular load bearing capacities. Climatic stressors, specifically storm events and snow melt often result in fully saturated conditions for pavement base, subbase and subgrade layers. Flooded pavements can lead to extended periods of water saturation, while their load capacities are tremendously reduced during these periods. At present, minimal capabilities exist to consider climatic history and forecast in planning load restriction strategies that can ensure safe passage of vehicles. While in-situ testing, such as falling weight deflectometer tests, can be used, these are often expensive and not easily available. Further, the use of in-situ testing for load restrictions is only possible in post-storm conditions and does not allow for planning in advance of storms. This study developed a stand-alone application that can enable road agencies to make post-storm, load restriction decisions for different vehicle classes, as well as to plan for future events based on precipitation forecasts.

In this study, a transient system dynamics model was developed that mechanistically integrated hydrological, geotechnical, and structural response attributes of pavements. The system dynamics model was used to conduct comprehensive sensitivity analysis to identify significant variables impacting pavement performance and establish interconnectivities between hydrological, geotechnical and pavement structural response variables. Using system dynamics model as a template and considering outcomes of the sensitivity analysis, a computer application, i.e., PaveSafe, was developed and programmed. PaveSafe is a mechanics-driven decision support system that transportation agencies can adopt to predict pavement response under different vehicular loading and climatic scenarios to ensure safe road operations during and after periods of high moisture. The PaveSafe application was validated using falling weight deflectometer measurements conducted on two roadways in Minnesota and North Dakota in pre-flooded and post-flooded conditions and by using a set of independent linear elastic analysis simulations. Several user experience and efficiency improvements as well as multiscale physical model experiments are identified as next steps in enhancing PaveSafe application and to support its wider adoption.

# CHAPTER 1: INTRODUCTION

## 1.1 RESEARCH PROJECT ABSTRACT AND OBJECTIVES

Excess moisture in aggregate base and subgrade soil layers has detrimental impacts on longevity and serviceability of pavements. Seasonal groundwater level fluctuations, inundations due to storms and post-storm recess, frost penetrations, and freeze-thaw effects lead to continuous moisture hysteresis and change of stress states in pavement foundation. Current analysis and design procedures rely on approximate empirical approaches. This renders their ability to incorporate moisture-dependency and conduct real-time and forecasted pavement capacity and load restriction analyses. A load restriction decision platform is proposed to provide a reliable and mechanistically informed tool for pavement engineers to assess pavement performance and make traffic allowance decisions during and after periods of excessive moisture. This platform encompasses three core attributes: (1) A mechanics-based model that correctly captures soil and base response to saturated and unsaturated soil states, which will be validated using actual field pavement tests such as MnROAD and can be further enhanced through the use of physically modelled scaled pavement sections; (2) a system-based approach to integrate impacts of various stressors (soil moisture state, vehicular loads and volume, climatic conditions, etc.), current pavement conditions, subgrade properties, hydro-geology, and short-term climate forecast. Due to a large number of variables and their inter-dependencies, a system dynamics modelling approach can holistically capture all significant variables and provide a user-friendly system for pavement load restriction decision making and (3) a policy-informed decision-platform that incorporates inputs from transportation agencies and users to facilitate its implementation and realize the cost-effectiveness of such a mechanistic approach.

## 1.2 SUMMARY OF RESEARCH METHODOLOGY (SCOPE)

This project is developing a mechanistic pavement load restriction decision framework using a system dynamics approach. The main outcome of this project will be a toolkit for pavement engineers to make decisions regarding load restrictions due to seasonal soil moisture variations as well as during post-flooding instances. The use of a system-based approach is necessary to integrate impacts of various stressors (soil moisture state, vehicular loads and traffic volume, climatic conditions, etc.), current pavement conditions, subgrade properties, hydro-geology, and short-term climate forecasts. Due to a very large number of variables and their inter-dependencies, a system dynamics modelling approach can holistically capture all significant variables and provide a user-friendly tool for pavement load restriction (both in current time and for future forecasting) decision making. This research is divided into 10 tasks. The study began with the development of an initial memo to quantify research benefits and potential implementation steps (Task 1) and a literature review (Task 2). This was followed with development of the system dynamics framework to mechanistically evaluate pavement load restrictions (Task 3). The next task pertained to conducting sensitivity analysis of the system dynamics model (Task 4). The next step was to develop a user-friendly toolkit that can be readily implemented for a pavement load restriction decision process (Task 5). In Task 6, the results in terms of deflection on the pavement surface from the developed toolkit (called PaveSafe in this report) were compared to a Layered Elastic Analysis (LEA) performed

through the use of the commercial software for pavement evaluation GAMES. In addition, PaveSafe was validated using data from Falling Weight Deflectometer (FWD) testing on pavement sections before and after flooding events. Task 8 finalized the quantification of research benefits and provided guidance on implementation of the research products.

### 1.3 ORGANIZATION OF THE REPORT

This report is organized into 7 chapters, with Chapter 1 being the Introduction.

Chapter 2 represents the literature review portion of the project (Task 2). This chapter includes motivation for pavement load restrictions to emphasize the importance of research study discussed in this report, basic pavement design components to get familiar with how the pavement systems perform, different parameters that affect the performance of the pavement to determine how a change in moisture affects each parameter, and different models that look at how water flows through soil to understand the behavior of water within the pavement system after and during a flooding event.

Chapter 3 discusses the System Dynamics Modeling (SDM) frameworks development (Task 3). This chapter explains how the SDM was developed to simulate real-time behavior of pavement systems due to moisture variations. Three main structures including hydrological, geotechnical, and pavement response were discussed. These were identified to be the ones crucial to development of the SDM.

Chapter 4 focuses on sensitivity analysis and framework refinement (Task 4). This chapter presents a set of sensitivity analyses of the SDM estimations to input variables. In addition, it is shown and described how results of the sensitivity analyses shed light on the sensitivity of pavement performance during periods of excessive moisture with respect to various climatic-, geotechnical-, and pavement-related system parameters.

Chapter 5 presents the load restriction toolkit development (Task 5). In addition, in this chapter, a user manual for PaveSafe v1.0.4 (the latest official version of the toolkit) together with the link for the App website are provided.

Chapter 6 presents the calibration and validation of the toolkit (Task 6). In this chapter the accuracy of PaveSafe application is verified by comparing the results in terms of surface deflection with layered elastic analysis (LEA), using the commercial software for pavement evaluation GAMES. In addition, PaveSafe performance is validated by comparing the results with field data from FWD testing performed on roadway sections in Minnesota (MN 93) and North Dakota (ND 200).

Finally, Chapter 7 summarizes the overall research effort and discusses key study conclusions as well as specific areas of future research to aid in refinement and implementation of research products.

## CHAPTER 2: LITERATURE REVIEW

This chapter is organized in six sections and one appendix (Appendix A). The subsequent six sections provide review of the background on the individual blocks within the load restriction decision system as well as discussion of pertinent literature regarding available equations and models for each of those blocks. The key blocks are determined to be:

- Effects of Excess Moisture on Pavement Performance
- Currently used Seasonal Load Restriction Protocols by Agencies (specifically NRRRA member DOTs)
- Soil Resilient Modulus
- Soil Water Retention and Hydraulic Conductivity Models
- Water flow through Pavement Systems

Lastly, a summary is provided that highlights the key findings from the literature review.

### 2.1 EFFECTS OF EXCESS MOISTURE ON PAVEMENT PERFORMANCE

#### 2.1.1 Introduction

Excess moisture in aggregate base and subgrade soils is one of the parameters that directly related to the structural capacity of pavement systems. The change in groundwater level during freeze-thaw cycles or inundations due to storm and post-storm recess and frost penetrations will cause certain amount of distress on pavement structures. In recent years, researchers showed that the subgrade materials of pavements are generally found in unsaturated condition while most of the equations used in conventional pavement design were developed based on optimum moisture content value. Also, researchers have found that the Resilient Modulus ( $M_R$ ) is also highly affected by the variation of moisture content and soil suction (Yang et al. 2005, Liang et al. 2008, Cary and Zapata, 2010). These effects are important in evaluating the structural performance of pavements especially after hazardous events such as flooding. Pavements are dynamic structures and are affected by several different parameters such as climate, loading conditions, or material properties. To date, the majority of the pavement assessment models are empirical, sometimes incorporating soil index parameters or one representative moisture or suction value. Thus, a mechanistic framework that holistically incorporates all the influential factors is still needed. In the current report, various attributes that have an impact on the capacity of pavement to support vehicular traffic were explored through literature review.

#### 2.1.2 Moisture Variation Effects on Pavement System Response

Vennapusa and White (2015) conducted a comprehensive post-flooding investigation of paved and unpaved roadways in Iowa; their research clearly demonstrated the need for a coupled hydro-mechanical analysis of pavement subgrade to determine the recovery of pavement to traffic bearing conditions. The FHWA Flooded Pavement Evaluation study by Sias et al. (2018) made extensive strides in development of a decision process to determine the time to opening of roadways post-flooding. A decision tree-based



tool has been developed through this study (Qiao et al, 2017) that utilizes in-situ assessment procedures (such as, falling weight deflectometer) for making traffic opening decisions. The current project incorporates real-time analysis as well as future projections on the load restriction decisions along with a mechanistic analysis. These attributes were not explored in the previous flooded pavement evaluation study.

Previous researchers have looked at different parameters that influence the performance of pavement systems, and how moisture variation impacts these parameters and overall performance of the pavement system (e.g. Sultana et al. 2016). About 80% of pavement damage is reported to be directly or indirectly influenced by the presence of excess pore water pressure especially in subgrade soil (Mndawe et al. 2015) while the quality and type of aggregate base, subbase, and subgrade layers controls the overall performance of pavement structure (Santero et al. 2011, Mallick and El-Korchi 2013, Elshaer et al. 2018a).

For example, Hurricane Katrina and Rita, in 2005, resulted in extreme flooding that endangered the integrity of road pavements. Subsequently, many researchers investigated the impact of flooding on pavement deterioration (e.g. Clarke and Cosby 2007, Gaspard et al. 2007, Helali et al. 2008, Zhang et al. 2008, Vennapusa et al. 2013, Chen and Zhang 2014, Daniel et al. 2014, Khan et al. 2015, Mallick et al. 2015, Sultana et al. 2016). However, due to the lack of structural data from prior flooding, it was hard to capture the accurate degradation in pavement capacity; thus, similar systems were targeted. These researchers studied the impact of road elevations, road pavement types, and pavement thickness on the damages on roads during the first week of flooding. The results clearly indicated a loss of stiffness due to post-flooding inundation where more severe for thinner pavements (less or equal than 3 inch of asphalt layer) and pavement sections with lower stiffness (measured using Falling Weight Deflectometer) were more vulnerable to flood water damage (Helali et al. 2008, Zhang et al. 2008).

Clarke and Cosby (2007) looked at the flooded flexible pavements on State Highway 24 in McClain County, Oklahoma after the road was closed to traffic for 14 hours. They observed a 12% reduction in the Falling Weight Deflectometer (FWD) surface deflection after the road closure in comparison with the immediate post-flooding. Vennapusa et al. (2013) visited the flooded sites during Missouri River flooding in 2011, and tested the pavement shortly after water recession and again 6 to 8 months after the flooding on different types of roads at different locations. A 25-28% reduction in subgrade modulus was observed due to the flooding, 20 days after the water receded while similar numbers were reported during the 6 to 8 months post-flooding tests. Sultana et al. (2016) investigated the structural performance of pavements after January 2011 flooding in Queensland, Australia by in-situ testing within 6 weeks and 2 to 4 years post-flooding. A 25-40% reduction in FWD surface deflection and 1.5-50% reduction in Modified Structural Number (SNC) were reported while sections regained their structural strength in 4 years as a result of pavement rehabilitation procedures. Lu et al. (2017) used AASHTOWare Pavement ME to simulate extreme climatic events in Canada (including flooding). Their work demonstrated that current PavementME does not have necessary features to incorporate pavement response post-flooding as well as during events with excessive moisture contents in pavement subgrade.

In general, an increase in moisture content will result is a reduction in soil material moduli (Seed et al. 1962, Hicks and Monismith 1971, Rada and Witczak 1981, Lary and Mahoney 1984, Carmichael and

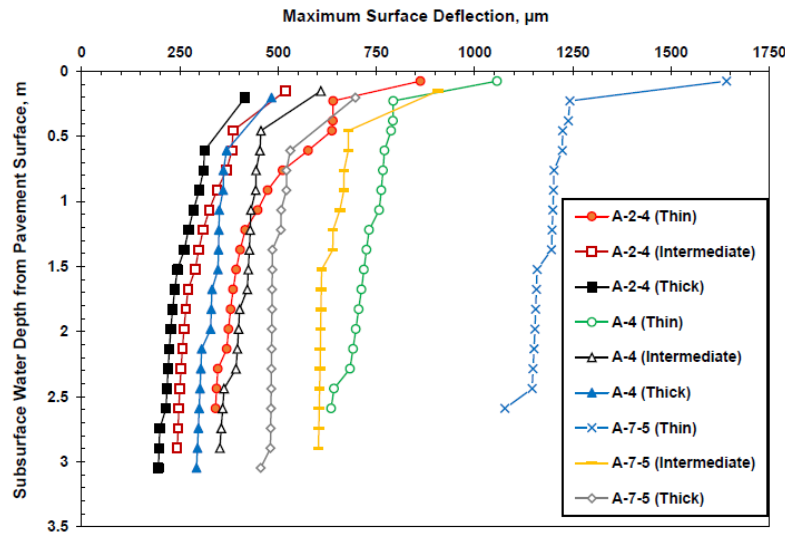
Stewart 1985, Nouredin 1994, Richter 2006, Khoury and Zaman 2004, Cary and Zapata 2010). The deformation that traffic load would introduce on a pavement section is a function of soil type, porosity, of the material, and the rate of loading; thus, the deformation is at its maximum when the subgrade layer is fully saturated; i.e. complete inundation (Ovik et al. 2000). Also, the duration of inundation could result in severe loss of pavement bearing capacity, excessive permanent deformations, material degradation, and loss of bonding among different layers (Salour et al. 2015). Pavement monitoring programs such as the Long Term Pavement Performance (LTPP) that runs a Seasonal Monitoring Program (SMP) on 64 sites would be valuable tool to assess the impacts of environmental factors including temperature, moisture, and freeze-thaw cycles on pavement response (Elkins et al. 2003). Further, Amiri (2004) used a small-scale pavement section to study the “Impact of Moisture Variation of Stiffness Response of Pavements through Small Scale Models” while the moisture was controlled when the soil was compacted. Also, few researchers studied soil moisture variation effects on full scale pavement distress in HMA pavement (Saevarsdottir and Erlingsson 2013, Camacho-Garita et al. 2020).

Laval University has conducted a number of studies to evaluate the damage to flexible pavements in colder climates due to frost and excessive moisture states during spring thaw; for example, Bilodeau et al. (2017) and Badiane et al. (2015). Majority of this work is conducted using a heavy vehicle simulator with a full-scale pavement test section constructed in an indoor test pit. The proposed phase-II of this research project will utilize a physical model to calibrate and refine the system dynamics-based load restriction decision process. Outcomes and data from work conducted at Laval University will be reviewed in that phase.

More recently, Elshaer (2017), as part of FHWA flooded pavement project (Sias et al. 2018) investigated the factors affecting the structural capacity of the pavement in fully saturated condition (flooded pavement), which is important when determining what factors to incorporate in the pavement model. The work also investigated different material types, thicknesses, structural numbers, and loadings. Changing moisture levels were then introduced to the pavement system through exterior environmental effects, changing subsurface water levels, and varying water table depths (Elshaer 2017, Heydinger 2003). To study the pavement response, the horizontal tensile strain at the bottom of the asphalt and the vertical compressive strain at the top of the subgrade layer were evaluated. The effects of soil suction were then considered, which lead to the incorporation of this parameter within the model developed in this research. With all of this information at hand, correlations and estimations could then be made between, the bearing capacity of the pavement in terms of short-term flooding, along with other empirical relationships that were used to estimate physical properties of the materials and stress states within the pavements, such as: resilient modulus, matric suction, poison’s ratio, and structural numbers (Elshaer 2017).

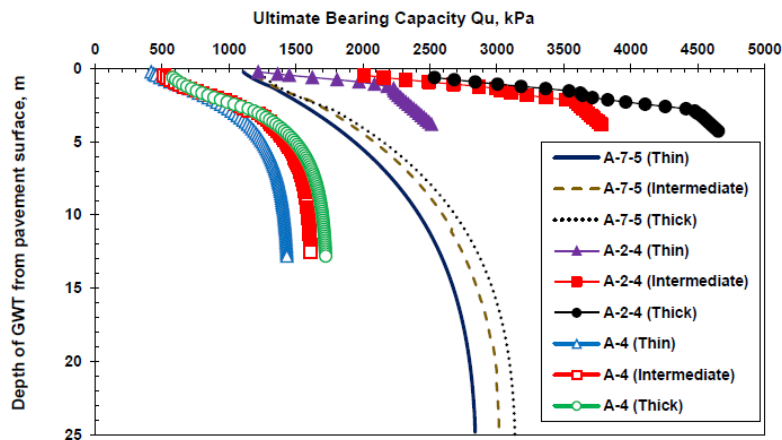
Elshaer et al. (2019) used numerical modeling to study the effect of post-flooding groundwater recession on different pavement performance criteria. For example, in Figure 2-1 the effect of water table on pavement surface deflection is shown considering different pavement sections and soil types. The results emphasized the effects of water inundation on pavement structural capacity. The base aggregate course, subgrade type, and pavement structure resulted in most significant impacts on surface deflection, modified structural number, and vertical strain. However, only pavement structure had noticeable impact

on fatigue performance measured by horizontal strain. Further, gradation and plasticity of unbound material played key roles in pavement structural capacity while they may behave differently in excessive water.



**Figure 2-1 Variation of the maximum surface deflection with depth of subsurface water levels (Elshaer et al. 2019)**

Further, Elshaer et al. (2017) showed how pavement bearing capacity is regained post flooding as the water recedes for different pavement section and subgrade material (Figure 2-2).



**Figure 2-2 Variation of bearing capacity with groundwater table levels for the proposed soils (Elshaer et al. 2017)**

The overall takeaway from these works was that the structural capacity of the pavement decreases significantly when soil is in fully saturated condition. However, the pavement may regain strength once the water dissipates, and the groundwater level lowers. Another takeaway is that temperature and moisture have a significant effect on the pavement, and the influence depth for the subsurface water level is dependent on the pavement structure and material type. Finally, the material type in all layers, along

with thicknesses have a significant effect on the pavements performance, and specifically the base and subgrade are the two most important factors when evaluating changes at the bottom of the asphalt layer, which is a major reference location for determining distresses within the pavement system (Thom & Brown, 1987).

### **2.1.3 Pertinent Inputs and Models to Assess Pavement Capacity in Context of Excess Moisture States**

---

#### **Pavement Structure and Condition**

Pavements are multi-layered structures. Transfer of heavy tire loads to subgrade in flexible pavements rely on concept of load distribution. Whereby the stress levels from top of pavement structure continually decreases until it reaches levels safe for subgrade to carry. Most common configuration of flexible pavement includes asphalt layers, base aggregate layer, subbase layer, prepared subgrade and natural subgrade. The role of each of these layers is different in the pavement structure and their sensitivities to changes on moisture level also vary.

Asphalt layers near the top of pavement structure often comprise of multiple lifts. The thicknesses of these layers depend on the anticipated traffic levels. Usually, the wear course or top-most lift is constructed with more angular aggregates due to very high tire pressures. Wear course is also usually specified with a smaller maximum aggregate size to ensure smoother pavement surface and to increase durability. The non-wear courses experience lower compressive stresses, but often undergo greater tire induced tensile stresses and strain due to flexure of the pavement system under traffic loading. Asphalt layers are sensitive to moisture and often during the design of these materials, testing is conducted to determine moisture damage susceptibility of asphalt mixtures. Typically tests such as modified Lottman test (AASHTO T-283) and Hamburg Wheel Tracking test (AASHTO T 324) are used. In the present research the moisture damage susceptibility of asphalt mixtures is not planned to be considered within the load restriction evaluation. The current asphalt mixture specifications used by NRRRA partner agencies all require testing for moisture susceptibility as part of the mix design process. Hence, the asphalt mixtures from partner agencies are expected to have minimal moisture induced damage potential during the periods of excessive pavement moisture state.

The base aggregate and subbase courses in flexible pavements provide economical layers that not only contribute in stress distribution but also provide lateral drainage to the structure. These layers help in movement of water away from the roadway foundation into drainage ditches. In colder climate regions, these layers also help lower the extent of frost penetration into soil subgrade as well as lower potential for pavement heaving due to prevention of ice lens formation in subbase. Since majority of base aggregate and subbase courses are constructed with natural and processed aggregates, their mechanical properties vary significantly with moisture content. The current MnPAVE system provides a good reference for seasonal adjustment to base aggregate and subbase layer resilient modulus. The AASHTOWare Pavement ME also incorporates the moisture content of base aggregate and subbase layers in determining the modulus of these layers which are then used in the pavement response analysis. Previous research by Elshaer et al. (2019) and Knott (2019) have successfully incorporated impacts of moisture level variations

in base aggregate and subbase layers into adjustments to these layers' resilient moduli. Similar approaches are planned to be adopted in the proposed research. Hydraulic conductivities of these layers will also be incorporated into the proposed system dynamics framework, since the framework is anticipated to include hydraulic analysis for continuous prediction of moisture movement through the pavement structure.

The prepared and natural subgrade properties (stiffness, soil moisture retention as well as hydraulic conductivity) will be critical in the proposed analysis. Later chapters provide substantial insight into the existing literature and relationships that have been developed.

The knowledge of the pavement cross-section (number of layers, their thicknesses and materials types) will be important input to the load restriction decision system. In absence of known cross-section, several typical sections will also be included in the decision toolkit. Use of typical cross-sections will lower reliability of predictions, users will be made aware of this aspect.

The structural condition of the roadway also plays an important role in terms of its load bearing capacity. Due to structural distresses from traffic loads and climatic stressors, the load bearing capacity of roadway often reduces with increasing time (and traffic). Typical pavement design and analysis models (such as, MnPAVE or Pavement ME) adopt miner's hypothesis, whereby the damage functions expressing structural distresses are assumed to be cumulative in nature. Since the proposed research is not focused on life-time simulation of pavement capacity and will be focused only on durations when there is excess moisture within pavement, the pavement condition will be incorporated in the determination of the pavement structural response (such as surface deflection). The pavement condition is anticipated to be estimated from the remaining service life provided by pavement management systems.

### Moisture-Dependent Soil Properties

As discussed in Section 2.1.2 excessive moisture in pavement systems especially in subgrade soils will reduce the pavement foundation capacity and result in surface deflection and cracking. This has been shown through numerical modeling (e.g. Elshaer 2017, Haider and Masud 2018), physical small scale and full scale modeling (e.g. Amiri 2004, Saevardottir and Erlingsson 2013, Camacho-Garita et al. 2020), and field performance assessment (e.g. Clarke and Cosby 2007, Helali et al. 2008, Zhang et al. 2008, Sultana et al. 2016). Soil properties play a key role in pavement response; thus, accurate assessment of these properties under various degree of water saturation is crucial.

Subgrade soil resilient modulus is probably the most influential factor that controls the overall stiffness of the pavement systems. Developing moisture-dependent resilient modulus has been in the forefront of transportation geotechnics research. Especially, with the advance of unsaturated soil mechanics, significant efforts have been made to correlate soil suction and state of stress to resilient modulus in a more mechanistic setting. This is important as vehicular traffic imposes changes in pore pressure or suction in soils. This emphasizes the need for such suction-dependent modulus models that can capture the transient pavement response. 2.3 is devoted to the review of the resilient modulus models and equations. The goal is to develop a set of relatively well-characterized formulations for different soils and

applications that can be used in the proposed system dynamics framework and eventually within the load restriction toolkit.

Suction is proven to be the factor that changes the stress state and impact the soil behavior. However, soil moisture in either gravimetric or volumetric forms are often being measured in the field. Therefore, it is important that these two soil properties be accurately correlated, so they can be interchangeably used in models. Three major soil water retention models are introduced in 2.4 , where their strengths and weaknesses are discussed. In addition, commonly applied unsaturated hydraulic conductivity models are presented and discussed. It is expected that one or two of the models may be implemented within the system dynamics framework for both estimating soil properties and hydraulic analysis.

### Climatic Factors

It is well-known in pavement engineering that the performance and lifespan of pavements are impacted severely by climatic factors. Specifically, temperature and moisture are major stressors for pavements (Huang 2012; Mallick and El-Korchi 2013). Recent research has focused extensively on adapting roadway networks for greater resiliency against changing climatic conditions (Knott, 2019; Pregnolato, Ford, Wilkinson, and Dawson, 2017; EPA, 2017). The link to how this changing climate is affecting the groundwater variation, and therefore affecting the pavements performance, will be an important factor to consider when developing the system dynamics model.

Development of climate projections models is not within scope of this study. Researchers will adopt use of existing climatic forecast data within the system dynamics framework. At this point in time, the short-term meteorological forecast (7 and 14 day) from National Oceanic and Atmospheric Administration (NOAA) will be utilized. The precipitation forecast from this source will be used as user input to the pavement hydraulic analysis to obtain the saturation profiles within pavement structure.

### Groundwater Flow Models

Seasonal fluctuation of groundwater level or water movement through the unsaturated soils during flooding both would impact the soil moisture/suction profile in depth, which in turn, impact the soil properties and overall pavement response. Thus, a well-designed, mechanistic pavement response assessment protocol requires a robust hydraulic analysis of water flow through pavement layers. A review of available approaches and past research is presented in 2.5 . These methods range from complex analytical solutions to simplified approaches and from numerical models to more empirical formulations. The target problem in this research is to track the groundwater level and, as a result, the moisture profile in depth during and after flooding when the water level recedes. In addition, it is planned to incorporate the climatic inputs into these models. Further, the goal is to have a model that is reasonably accurate, yet simple for practical applications

## Pavement Structural Response Model and Capacity Indicator(s)

Historically, different methods have been proposed to analyze the structural performance of pavement systems. The early models made simple assumptions about the loading and the layered system, while more recent models incorporate more complex soil response and can simulate multi-layer systems. Some of the common approaches are single-layer elastic theory, multi-layer elastic theory, finite element methods, viscoelastic theory, dynamic analysis, thermal models, and nonlinear plastic behavior models.

Single-layer and multi-layer elastic theory are based on fundamental formulations of mechanics of materials, such as Hooke's theory of elasticity. Over time, different assumptions and changes, for either loading or the layered system, were made in these models which made them more accurate. The evolution of these models follows this timeline: half-space space under a point load (Boussinesq, 1885), semi-infinite space due to a circular load (Newark, 1942; Foster & Ahlvin, 1954; Ahlvin & Ulery, 1962), two layers due to a circular load (Burmister, 1943), three-layer systems (Jones, 1962), and finally multilayer systems and finite element models.

The use of multilayer analysis, specifically layered elastic analysis, is current state of practice in the majority of flexible pavement analysis and design systems (such as, MnPAVE, Pavement ME, CalME etc.). In the proposed framework, the pavement surface deflection will be considered as an indicator of the pavement capacity. Furthermore, use of system dynamics for sensitivity analysis and real-time evaluation requires usage of a closed-form solution. Another challenge in evaluating a multi-layer system is the incorporation of moisture variation in depth. Elshaer et al. (2018 a,b) discussed the impact of the modulus equation option and also the selected approach to incorporate variable moisture on pavement response. This included the choice of suction- versus degree of saturation-dependent equation, inclusion of multi-layer subgrade with variable moisture versus incorporating a representative effective moisture content value, and the choice of empirical versus more mechanistic resilient modulus functions. These effects were tested for different soil types and pavement structure. The results indicated the simple models especially for non-plastic soils might be sufficient as long as the depth of stress influence and the effective moisture content is considered. The results were verified against FWD data recorded from the Long-Term Pavement Performance (LTPP) records.

For the load restriction decision system, use of two and three-layer solutions will be adopted in the system dynamics framework. Comparative evaluations will be undertaken to ensure that the results of these solutions are in agreement with multilayer analysis program (such as, WESLEA or JULEA).

## Traffic Loads

When determining what traffic load to use as an input parameter in the load restriction decision system, a few different parameters should be considered. The key parameters in all load cases are the vehicle types (tire and axle configurations, pressure etc.), loading repetitions for each type, and future projections of both loading and repetitions. This is done by observation and quantification of the traffic traveling over a given roadway. Then, past data can be looked at, and with other future estimates, the future traffic on the roadway can be estimated.

There are two approaches to determine the expected loads on the given pavement over its entire design life. One approach is to convert all magnitudes of loading and repetitions of loading to an equivalent unit using approaches such as equivalent damage, a commonly used example for this is equivalent single axial load (ESAL). The other approach is to use a load spectrum, which characterizes loads directly by number of axles, configuration, and weight. This method is typically more complex since the structural analysis requires use of each vehicular combination to be evaluated to obtain relevant responses. Both methods follow typical equations and/or procedures that have been well laid out (such as, AASHTO, 1993 and FHWA, 2019).

For the proposed load restriction decision framework, the use of ESAL approach is not appropriate, since the damage potential from each vehicle type needs to be evaluated. Furthermore, a unique feature of this research is to provide users with a vehicle-class specific load restriction decision. Thus, in this study vehicle class-based traffic inputs will be utilized. At present, the 13-category FHWA vehicle classification will be adopted (FHWA, 2014). The pavement response analysis will be conducted at median, 75<sup>th</sup> percentile and 90<sup>th</sup> percentile load levels for each vehicle class. The nationally applicable load level distributions for each vehicle class are provided in the AASHTOWare Pavement ME system. The higher percentile loads will be adopted on the basis of the criticality of the roadway in question.

### Other Variables

In addition to the parameters that were previously mentioned, there are a few other parameters that can potentially impact the performance of the pavement system. Physical properties of the materials used within the pavement system can affect the overall performance of the system, which was previously mentioned (Huang, 2012). However, some additional soil parameters that have the potential to affect the overall performance of the pavement system could be friction angle and cohesion values of certain soils. Also, other parameters of cohesive soil could have an effect on the performance of the pavement system, such as both liquid limit and over-consolidation ratio. Compaction and consolidation characteristics themselves should be considered for all materials and soils used within the pavement system, since they both have a direct relationship in terms of both strength and drainage within the pavement system (Holtz, 2011).

Another consideration that should be made that would have an effect on the pavement performance is the surrounding environment. For example, if the pavement system is located next to an ocean, a changing climate or flooding events may lead to the pavement system being exposed to more moisture than other systems (FHWA2019). If the surrounding terrain tends to drain additional water into the pavement, this would also expose this pavement to more moisture than other systems. In conjunction with this consideration, the direction of the flow of water should also be considered as an important factor that may affect the overall performance of the pavement system.

Construction considerations should be made as an important factor that may affect the overall performance of the pavement system (Huang, 2012). For example, if the compaction requirements that were called for and accounted for in the model, were not what was implemented in the actual pavement system, then this would affect the overall performance of the pavement in a negative way.



#### 2.1.4 Summary

---

A well-designed and user-friendly load restriction decision platform would heavily rely on 1) an accurate assessment of pavement response under excessive and fluctuating water in base aggregate, subbase, and subgrade layers; 2) a mechanistic evaluation of pavement performance that can holistically incorporate several key influential factors; 3) the capacity of the platform to prioritize the impactful factors in the response analysis and rank the load restriction recommendation; 4) the ease of access by users with different expertise and input data.

The project will leverage system dynamics sensitivity analysis and statistical approach to develop a load restriction decision protocol that can meet the above qualifications. The analysis will be based on the list of expected key players in pavement response analysis during and after inundation. The following chapters discuss the history and state-of-the-art in some of these influential factors that are considerably sensitive to amount of moisture.

## 2.2 LOAD RESTRICTION PROTOCOLS

### 2.2.1 Why Are Load Restrictions Needed?

---

Seasonal road restrictions are weight limits that are enforced by various state's Department of Transportation (DOT) as well as local highway agencies. These limitations are put in place in order to reduce the amount of damage that a certain roadway will experience. These restrictions are put in place when the pavement system is most vulnerable to experience damage; this usually occurs when the frost from the winter season thaws into the spring season or after inundation due to flooding. This results in excessive water within the pavement system itself, causing a weaker system. The load limitations are then removed when the roadway is able to carry legal traffic weight without accelerated damage to the structure. Each road load limitation varies from state to state and depends on a number of various parameters such as loading scenarios, local temperature, and roadway types and conditions.

Eight National Road Research Alliance (NRRRA) states DOTs (California, Illinois, Iowa, Michigan, Minnesota, Missouri, North Dakota, and Wisconsin) were investigated to understand how agencies are already evaluating load restrictions on given roadways and how road closures and opening decisions are made. Some of these parameters include, but not limited to frost depth, temperature forecasts, and pavement strength. Looking at current policies of different agencies allows to establish a baseline to determine what important information are needed when setting a load restriction. If a certain factor, such as temperature, was repeated throughout multiple NRRRA states, it was then noted that the factor should be used when investigating whether a road should have a load restriction. Creating this baseline for important factors in setting a load restriction will be useful when incorporating different factors into the proposed model. Load restriction state specific data was successfully found and collected for the following NRRRA states: Minnesota, North Dakota, and Wisconsin. The following states did not have information publicly available: California, Iowa, Missouri, Michigan, and Illinois. Although the specific limits and restrictions were not listed for these states, similar factors were discussed when determining load restrictions for roadways.

### 2.2.2 Minnesota DOT Load Restrictions

Minnesota is also a NRRA state that uses four different factors to determine whether a roadway should have a load restriction. These four factors include: daily temperature forecasts, future temperature forecasts, a parameter called the cumulative thawing index, and the depth at which the frost is located below the ground. The table below shows each factor in the guideline along with some specific notes and limitations used by the Minnesota Department of Transportation (MnDOT) when setting or lifting a load restriction. (Minnesota Department of Transportation Engineering Services Division, 2014).

**Table 2-1: MnDOT Load Restriction Factors**

MnDOT	
Factor in Posting of Load Restriction	Notes
Temperature	Load restrictions will be scheduled when the 3-Day weather forecast indicates (CTI) will exceed 25F degree-days and longer-range forecasts predict continued warmth
Cumulative Thawing Index (CTI)	Used in conjunction with temperature forecasts to set load restrictions within each different frost zone
Frost Depths	With other key parameters located at each frost zone, this help place an end date to the load restriction
Forecast Daily Air Temperature	

A major parameter that MnDOT uses is called the cumulative thawing index (CTI). This index represents a running total of each day's thawing index that starts from a value of zero degrees Fahrenheit during the winter freeze. The daily thawing index is the amount the daily average temperature is above the reference temperature for that day, and the reference temperature is based on the monthly average temperature. The department has a specific set of rules, limitations, examples, and equations when dealing with CTI (Chiglo 2014).

As Table 2-1 describes, MnDOT uses both daily and future forecasted temperatures to help determine if a road requires a load restriction enforced on it. This observed temperature forecast is then used along with the CTI to determine load restrictions. The department specifically looks for the time when the three-day weather forecast indicates that the CTI for a specific frost zone will exceed 25 degree-days and long-range temperature forecast predicts for warm days to come. If this condition holds true, then restrictions will be scheduled and the advance notice for the public will be released.

The next factor used in determining load restrictions is the depth of the frost table under the ground surface. This is important because it indicates at what level the frozen water table is located near the ground surface, and if too close to the surface that would be a cause for concern. The speed at which this frost table lowers, and thaws depends on several factors such as; depth, soil moisture content, and spring weather patterns (Guthrie et al., 2016). All these parameters can vary from year to year, therefore the load restrictions in each year will also vary and will depend heavily on the past experience of the department.

### **2.2.3 North Dakota DOT Load Restrictions**

---

North Dakota's DOT (NDDOT) uses four different factors to determine whether or not a certain road should have a load restriction posted or not. These factors include; current temperature in the roadway, temperature forecasts, current strength of the roadway, and previous experience. The following table describes each factor in more detail along with any notes and or limitations that apply to each (North Dakota Department of Transportation, 2019).

The first factor used by NDDOT when determining if a certain roadway needs a load restriction is the temperature within the base aggregate layer. Temperature probes are placed within the base aggregate of different roadway systems throughout the state. The temperature is then observed and recorded for each section of roadway. NDDOT begins planning the posting of load restrictions when the temperature in the base aggregate layer begins to approach 32 degrees Fahrenheit. The next factor used by NDDOT is the long-range temperature forecast within each region. When the department observes consistent forecasted daily temperatures that have daily highs in the range of upper 30's or 40's (degrees Fahrenheit), load restrictions are then planned. The next factor that the NDDOT uses when determining whether a roadway needs a load restriction is the actual strength of the particular roadway. The way this strength is measured is by using Falling Weight Deflectometer (FWD). This allows for measuring both the strength of the roadway base along with the strength of the asphalt surface. The data collected from FWD along with long range weather forecasts and moisture conditions over the whole area, provide the basic information needed for NDDOT to both initiate and lift a load restriction on a given roadway.

**Table 2-2: NDDOT Load Restriction Factors**

NDDOT	
Factor in Posting of Load Restriction	Notes
Temperature in Base Layer	Probes put into base layer of pavement section. When approach 32F, planning of posting begins
Long Range Temperature Forecast	When indicate low temp. approaches freezing point and the daily highs are in the upper 30's or 40's, restrictions are planned
Falling Weight Deflectometer (FWD)	Measures strength of roadway bases. Used for both initiating and lifting load restrictions in combination with long range forecasts and area wide moisture conditions
Past Experience	Most significant damage occurs during first 4 weeks after spring thaw. Lead to close monitoring of weather forecasts and sub-base temps.

The last factor, and most significant factor used by NDDOT when determining load restrictions is past data and experience (North Dakota Department of Transportation, 2019). Using past information, the department has been able to limit the time frame to when the most significant damage is seen on a given roadway. NDDOT recognized that the most significant pavement damage occurs during the first four weeks after the onset of spring thaw. This allows for closer monitoring of weather forecasts and sub-base temperatures during this time to either enforce load restrictions or lift them in a shorter time frame.

#### **2.2.4 Wisconsin DOT Load Restrictions**

---

Wisconsin's department of transportation (WisDOT) is the third NRRA state that describes how load restrictions are set for specific roadways within the state. WisDOT uses five different parameters when determining if a road should have a load restriction enforced or if a restriction should be lifted, which can be seen below in. The five factors are the following: temperature forecasts, the depth at which the frost level is below the ground, visual inspection, axle configuration along with vehicle weight, and the trip type that the vehicle driving over the specific roadway is taking (Wisconsin Department of Transportation, 2018).

**Table 2-3: WisDOT Load Restriction Factors**

<b>WisDOT</b>	
<b>Factor in Posting of Load Restriction</b>	<b>Notes</b>
Rising Temperatures	Use weather forecasts and Cornell Pavement Frost Model (CPFM) (Miller et al. 2015) to estimate when restrictions are needed
Frost Tube Readings	Frost tube should be checked on Mondays and Thursday and reported to BHM until seasonal posted roads restrictions are declared in each zone
Frost Depth	Reaches 6 inches below pavement surface
Road Level	Seasonal Posted Roads cannot be declared until Class II road restrictions are declared, and Seasonal Posted Roads must end before Class II road restrictions are ended
Maintenance	Weekly monitoring for weeping and pumping, advising Bureau of Highway Maintenance Freight Engineer when Seasonal Postings shall end for each zone
Axle Configuration and Vehicle Weight	Posted limits are normally 6 tons per single-axle and 10 tons for any 2 axles less than 8' apart  Gross vehicle weight or combo of group axles is 24 tons
Trip Type	All single trip and most annual overweight travel is not permitted during this time on seasonal posted road sections

WisDOT uses future and daily weather forecasts in conjunction with MnDOT's frost model in order to set and lift certain roadway load restrictions. The next parameter that the department considers when enforcing load restrictions is the depth at which the frost table is located beneath the ground surface. This is done by using frost tubes that are placed into a hole with undisturbed and uncompacted soil. The readings are reported two times a week until the frost level is no longer six inches from the pavement surface, which is the limiting distance for setting the load restriction (Wisconsin Department of Transportation, 2018). Another factor used by WisDOT is visual inspection during maintenance of a

specific roadway. Weekly monitoring is mandatory with the intention of looking for signs of weeping and pumping within the roadway. If signs of these conditions are shown, it must be brought to the attention of the Bureau of Highway Maintenance (Bureau of Highway Maintenance WisDOT, 2019) where then a restriction will be enforced, or if these conditions are no longer occurring for a steady amount of time then a restriction can be lifted.

The department also limits the axle configuration and vehicle type when enforcing a load restriction. This is to ensure that the ultimate strength of the roadway will not be impaired if overloaded during its weaker timeframe. WisDOT has certain expectations and procedures for this limitation that are outlined on the DOT's website (Wisconsin Department of Transportation, 2018).

### **2.2.5 Important Factors Considered and Trends Identified**

---

Looking at the three NRRRA states that had available information for how load restrictions are set and lifted, certain factors and parameters showed up multiple times across the three states. The major factor used in all three states was looking at temperature forecasts for both the future along with current conditions. The next factor that is being consistently used is the depth of the frost layer. Along with this factor, there was a stress to focus on how the water drained with the current soil conditions once the frost layer thawed. The last factor that constantly was used in all three NRRRA states was setting a certain axial configuration, trip type, and vehicle weight which is the basis for the load restriction. Further, past experience is also commonly considered in load restriction decisions.

In this research, these factors will be implemented in a decision model, where the model will encompass the following breakthroughs:

- A mechanistic load restriction protocol will be developed that include an analytical or empirical hydro-mechanical analysis.
- The effect of moisture variability is investigated through a holistic sensitivity analysis.
- The load restriction protocols will be extended to flooded zones where water in inundated zones recedes and the load restriction can be lifted.

## **2.3 RESILIENT MODULUS**

### **2.3.1 Introduction**

---

The effects of moisture on soil's resilient modulus have been investigated by many researchers in the past (e.g. Sauer and Monismith 1968, Edris and Lytton 1976, Fredlund and Morgenstern 1977, Nouredin 1994, Drumm et al. 1997, Ceratti et al. 2004, Yang et al. 2008, Khoury and Khoury 2009, Sawangsuriya et al. 2009, Khoury et al. 2010, Cary and Zapata 2010, Han and Vanapalli 2015). As a result of these investigations several analytical and empirical models have been proposed to estimate the resilient modulus of subgrade soil under various moisture and stress states; some being simple and applied and some being complex and mechanistic (e.g. Seed et al. 1967, Moossazadeh and Witczak 1981, Witczak and Uzan 1988, Witczak et al. 2000, Khoury and Zaman 2004, Yang et al. 2005, Liang et al. 2008, Cary and

Zapata 2010 and 2011, Sivakumar et al. 2013, Khosravifar et al. 2015). A master list of several resilient modulus prediction equations has been developed and a subset of this list is provided in the Appendix A.

To date, the most commonly used equation is the extended version of MEPDG equation for resilient modulus at optimum water content from the results of extensive experimental material evaluation (Zapata et al. 2007). In this method, Equation 2-1 is used to adjust the estimated resilient modulus at optimum water content calculated using Equation 2-2, based on the degree of water saturation.

$$\log \left( \frac{M_R}{M_{R-OPT}} \right) = a + \frac{b - a}{1 + \exp \left[ \ln \left( -\frac{b}{a} \right) + k_m (S - S_{OPT}) \right]}$$

Equation 2-1

$$M_{R-OPT} = k_1 p_a \left( \frac{\theta_b}{p_a} \right)^{k_2} \left( \frac{\tau_{oct}}{p_a} + 1 \right)^{k_3}$$

Equation 2-2

where  $S$  = degree of saturation (in decimals);  $S_{OPT}$  = degree of saturation at optimal water content (in decimals);  $a$  = minimum of  $\log (M_R/M_{R-OPT})$ ;  $b$  = maximum of  $\log \log (M_R/M_{R-OPT})$ ; and  $k_m$  = regression parameter. Parameter values  $a = -0.5934$ ,  $b = 0.4$ , and  $k_m = 6.1324$  are suggested for fine-grained soils, and parameter values  $a = -0.3123$ ,  $b = 0.3$ , and  $k_m = 6.8157$  are suggested for coarse-grained soils. Also, where  $p_a$  = atmosphere pressure (i.e., 101.3 kPa),  $\theta_b$  = bulk stress,  $\tau_{oct}$  = octahedral shear stress; and  $k_1$ ,  $k_2$ , and  $k_3$  = model parameters.

Due to the advance of the mechanics of unsaturated soils, more mechanistic equations were proposed incorporating the state of stress and soil suction. Han and Vanapalli (2016) reported a summary of a suite of these equations to estimate or predict suction or moisture-dependent resilient modulus for pavement base-course and subgrade soils. These equations were broken up into three categories: empirical relationships, constitutive models incorporating the soil suction into applied shearing or confining stresses, and constitutive models extending the independent stress state variable approach.

After reviewing these predictive equations, representative formulas are selected based on the target soil type recommended and the model's performance in predicting the resilient modulus values. Soil types were broken into three different categories according to AASHTO classification: A-1 soils, A-2 and A-3 soils, and A-4 through A-7 soils (AASHTO, 1993). The corresponding soil types by the Unified Soil Classification (UCS) system definitions are; (GP, GW, SP-SM, SM, and SP) for A-1 soils, (GM or GC, SM, SC, and SM-SC) for A-2 and A-3 soils, and (CH, CL, CL-ML, MH, ML, SC, SM, SM-SC, A-6) for A-4 through A-7 soils (Natural Resources Conservation Service, 2019).

### 2.3.2 Resilient Modulus for A-1 Soil Types

The research that was performed on the Canadian Long-Term Performance Project (C-LTPP) resulted in a generalized model that quantifies the modulus-water sensitivity of typical base material (Doucet & Dore'

2004). The proposed model is an empirical relationship developed through resilient modulus tests on several partially crushed and crushed granular materials, based on the following equations:

$$\Delta M_R = -8700(u_a - u_w) - 17,000$$

Equation 2-3

$$M_R = 1060\theta_b - 8700\psi + 57000$$

Equation 2-4

The model uses the matric suction ( $\psi$ ) (kPa) to describe the modulus water sensitivity, and the balance between air pressure ( $u_a$ ) and pore water pressure ( $u_w$ ). Bulk stress is defined as ( $\theta_b$ ), ( $\Delta M_R$ ) is the variation in resilient modulus in kPa, and ( $M_R$ ) is the resilient modulus also expressed in kPa.

Further, research was conducted to develop correction factors (CF) under the National Cooperative Highway Research Program (NCHRP). MEPDG testing methods were performed in order to obtain an in-situ  $M_R$  for underlying materials (MEPDG, 2004). This value was then compared to a laboratory  $M_R$  value, and a correction factor was then developed. Other researchers also participated in the effort to establish the CF of base material, while taking into account stress state and in-situ moisture content for Florida granular materials (Oh et al. 2012). Laboratory test data on resilient modulus and soil suction, the relationship between resilient modulus, stress state, and moisture content was investigated. After reviewing the resilient modulus from the MEPDG (MEPDG, 2004), the following equation was developed, presented in Equation 2-5; where bulk stress is modeled by  $\theta$ , the octahedral shear stress is  $\tau_{oct}$ ,  $\psi$  is suction, and  $P_a$  is atmospheric pressure (100kPa).

$$M_R = k_1 P_a \left( \frac{\theta_b + 3k_4 \psi \theta}{P_a} \right)^{k_2} \left( \frac{\tau_{oct}}{P_a} + 1 \right)^{k_3}$$

Equation 2-5

The equation also includes four regression constants,  $k_1$  through  $k_4$ . One constant specifically,  $k_4$ , accounts for the effect of moisture content variation on the bulk stress term.

Through a micromechanical approach to model partially saturated soils, a relationship between the mean principal stress acting on the system and the Helmholtz free energy per unit initial volume was developed (Lamborn 1986). From this equation, a relationship between the mean principal stress and the change in soil suction was developed (Chandra et al. 1989). Based on this relationship, Equation 2-6 was proposed, which is similar to Equation 2-5; in which  $S$  is suction and  $V_w$  is the volumetric water content.

$$M_R = k_1 P_a \left( \frac{\theta_b + 3k_4 S V_w}{P_a} \right)^{k_2} \left( \frac{\tau_{oct}}{P_a} + 1 \right)^{k_3}$$

Equation 2-6

The mean principal stress is known to be one third of the bulk stress; this means the change in bulk stress due to soils suction can then be calculated. The change in soil suction equates to an additional



confinement being imparted, which is then added to the bulk stress associated with surface loads and gravimetric stresses.

### 2.3.3 Resilient Modulus for A-2 and A-3 Soil Types

Cary and Zapata (2011) studied the effect of moisture variation on the resilient modulus of unbound materials in a pavement structure. Earlier, there were models developed that attempted to capture how moisture variation affected a pavement structure. However, these models were based on a total stress analysis and were mostly empirical. The goal in Cary and Zapata's research was to understand the relationship between pore water pressure and the resilient modulus response. They introduced matric suction, which is a fundamental stress variable, as a predictive variable in the Universal Model adopted by the MEPDG (MEPDG, 2004).

Testing was done on a Triaxial system that allowed full control and measurement of pore water and pore air pressures. The system was also capable of simulating both drained and undrained conditions, in this study both conditions were tested, and resilient modulus was measured. The materials tested in this study were a typical granular base material found in Arizona and a subgrade material that was commonly found in the Phoenix Valley and was classified to be a clayey sand.

After testing, successful modeling of the effects of suction on modulus resulted in a smooth transition from unsaturated soil conditions to saturated conditions. This led to modifications being made to the Universal Model, and gave the proposed equation shown below

$$M_R = k'_1 * P_a * \left( \frac{\theta_{net} - 3 * \Delta u_{w-sat}}{P_a} \right)^{k'_2} * \left( \frac{\tau_{oct}}{P_a} + 1 \right)^{k'_3} * \left( \frac{(\psi_{m_0} - \psi_m)}{P_a} + 1 \right)^{k'_4}$$

Equation 2-7

Where,  $P_a$  = atmospheric pressure,  $k'_1$  through  $k'_4$  are regression constants that depend on material type,  $\theta_{net} = \theta - 3u_a$ , net bulk stress and  $u_a$  is pore air pressure,  $\Delta u_{w-sat}$  = build-up of pore water pressure under saturated conditions, in such cases  $\Delta \psi_m = 0$ ,  $\tau_{oct}$  = octahedral shear stress,  $\psi_{m_0}$  = initial matrix soil suction, and  $\Delta \psi_m$  = relative change of matric soil suction with respect to  $\psi_{m_0}$  due to build-up of pore water pressure under saturated conditions, in this case  $\Delta u_{w-sat} = 0$ .

Net bulk stress is used over bulk stress to accommodate for modeling the transition between unsaturated and saturated soil states. This is because as the condition happens, pore air pressure will approach zero, and the net bulk stress will approach the bulk stress again. The third factor is the new term that makes this model different from the Universal Model. This is the term that attempts to capture the contribution of matric suction in the overall resilient response of the material under saturated, undrained conditions. These conditions are in effect when the relative change of matric suction approaches zero. The actual matric suction at the time of the resilient modulus measurement can be obtained by subtracting the relative change in matric suction from the initial matric suction.

The plus one term after the octahedral shear stress is to avoid the same problem of constants approaching zero. This term is also normalized by the atmospheric pressure, and therefore keeps the regression constants non-dimensional. Once this term approaches one, the model allows for saturated conditions, and therefore matrix suction doesn't contribute to resilient modulus anymore. When the excess pore water pressure becomes equal to the external applied loads, the effective stress in the material approaches zero. The regression constants were obtained for each of the base aggregate and subgrade material by plotting the predicted resilient modulus against the measured resilient modulus.

In another study by Sahin et al. (2013) Equation 2-8 was developed for granular bases. This model is based on micromechanics theory and thermodynamics laws.

$$M_R = k_1 P_a \left[ \frac{\theta_b - 3f\theta \left( \psi_0 + \beta \frac{\theta_b}{3} + \alpha \tau_{oct} \right)}{P_a} \right]^{k_2} \left( \frac{\tau_{oct}}{P_a} + 1 \right)^{k_3}$$

**Equation 2-8**

Where;  $k_1$  through  $k_4$  are model parameters,  $\tau_{oct}$  = octahedral shear stress,  $\psi_0$  = initial matrix soil suction,  $P_a$  is atmospheric pressure,  $\theta_b$  is bulk stress,  $\theta$  = volumetric water content,  $f$  = saturation factor ( $1 < f < \frac{1}{\theta}$ ), and  $\alpha$  and  $\beta$  are Henkel pore-water pressure parameters.

### 2.3.4 Resilient Modulus for A-4 through A-7 Soil Types

Yang et al. (2005) and Ng et al. (2013) proposed equations that deal with A-4 through A-7 soil types. For example, when dealing with A-4 through A-7 soil types, Equation 2-9 was developed by Yang et al. (2005). The soils examined in this research project consisted of two fine-grained subgrade soils (one A-7-5 soil and one A-7-6 soil) from Taiwan, China, over the soil suction range of 0–10,000 kPa.

$$M_R = k_1 (\sigma_d + X^\psi)^{k_2}$$

**Equation 2-9**

where,  $\sigma_d$  = deviator stress,  $X$  = Bishop's effective stress parameter,  $\psi$  = soil suction, and  $k_1$  and  $k_2$  are model regression parameters. The regression parameter values depend on the material being used. For the A-7-5 soil type  $k_1 = 274.2$  and  $k_2 = 1.24$ , and for the A-7-6 soil type  $k_1 = 111.5$  and  $k_2 = 1.27$ .

This equation uses a single model parameter ( $k_2$ ), derived from regression studies, to predict the behavior of the resilient modulus with respect to both matric suction and deviator stress. Positive  $k_2$  values indicate that resilient modulus increases with both matric suction and deviator stress, while negative values do the opposite and show a negative trend in resilient modulus. It is documented through this study that this model reasonably captures the behavior in resilient modulus with respect to matric suction.

The effect of moisture on resilient modulus of a material, through a suction-controlled triaxial apparatus was studied by Ng et al. 2013. The material tested was a decomposed tuff material that was collected in Hong Kong. It can be classified as a silt (ML) by USCS or as A-7-6 soil type by AASHTO (AASHTO, 1993). In

this research, the effect of two stress-state variables (matric suction and net stress) along with the wetting and drying history and how it affected the resilient modulus of the material were investigated. Also, they studied the effect of load repetitions on the material. The results yielded Equation 2-10 for the resilient modulus of a material under both saturated and unsaturated conditions.

$$M_R = M_0 \left( \frac{\theta_{net}}{\theta_{ref}} \right)^{k_1} \left( \frac{q_{cyc}}{\theta_{ref}} \right)^{k_2} \left( 1 + \frac{\psi}{\theta_{net}} \right)^{k_3}$$

**Equation 2-10**

Where;  $M_R$  and  $M_0$  are the resilient modulus and initial modulus respectively,  $\theta_{net}$  = the net mean stress,  $\theta_{ref}$  = the reference stress state,  $q_{cyc}$  = cyclic stress,  $\psi$  = matrix suction, and  $k_1$  through  $k_3$  are regression constants that depend on the material at hand. Table 2-4 shows the recommended regression constants for different material.

**Table 2-4: Regression Constants (Ng et al., 2013)**

Material	AASHTO (2000) classification	Specific gravity	Plastic limit	Liquid limit	Plasticity index	$M_0$	$k_1$	$k_2$	$k_3$	$R^2$	Se/Sy
CDT	A-7-6	2.73	29	43	14	8.32	1.00	-0.65	1.01	0.98	0.14
Keuper Marl	A-7-6	2.69	18	37	19	6.32	1.00	-0.65	1.01	0.66	0.60
Gault clay	A-7-5	2.69	25	61	36	0.61	1.00	-0.36	1.31	0.98	0.14
London clay	A-7-5	2.73	23	71	48	0.53	1.00	-0.36	1.31	0.96	0.21

The first term on the right side of the equation denoted the resilient modulus at the reference stress state where the matric suction is equal to zero. The second term quantifies the influence of net mean stress on resilient modulus, showing the increase in stiffness with an increase in confinement. The third term reflects the variation of resilient modulus with cyclic stress, and the fourth term accounts for the effect of matric suction on the resilient modulus. When the matric suction is equal to zero this fourth term reduces to one, and therefore can be applied to saturated soils to find resilient modulus from effective confining pressure and cyclic stress.

### 2.3.5 Resilient Modulus Prediction Equation Summary

Because the resilient modulus has a significant effect directly on the performance of a pavement system, a detailed literature review of the parameter was performed. The goal was to review state-of-the-art equations that were developed to predict resilient modulus of unsaturated soils. The models were either degree of saturation-based or suction-based while the latter varied from completely empirical to more mechanistic constitutive relations. This review identified some of the models with broader application and better prediction capacity and presented for different soil types. It is expected that these models would be implemented in the forthcoming system dynamics model, which would provide the opportunity to better predict the response of pavements with different subgrade material.

## 2.4 SOIL WATER RETENTION EQUATIONS AND HYDRAULIC CONDUCTIVITY MODELS

### 2.4.1 Introduction

Three commonly used predictive Soil Water Retention Curve (SWRC) models are introduced in this section including: Brooks and Corey (BC) Model (Brooks & Corey, 1964), van Genuchten (VG) Model (van Genuchten, 1980), and the Fredlund and Xing (FX) Model (Fredlund & Xing, 1994). A good relationship between the moisture content within a soil and soil suction can be made with direct measurements of the SWRC using different experimental techniques (Lu and Likos 2004). However, these direct measurements are expensive and time consuming. Also, acquiring enough samples from the field to create SWRCs would be expensive given the transportation, lab preparation, and monitoring. Thus, alternative methods were needed to create SWRCs. Numerical approaches, graphical plots, and parameter identification methods were all developed as the alternatives. The three models previously mentioned are examples of these models, which will be discussed.

### 2.4.2 SWRC Modeling Parameters

In numerical modeling of SWRC, there are several different parameters whether they pertain to a certain condition or are an empirical fitting constant. The parameters that pertain to a certain condition such as the soil suction at a specific condition or certain water content include full saturation, residual saturation, and air entry pressure (Lu and Likos 2004). The fitting constants are either empirical or semi-empirical that are selected to capture the general shape of the curve between fixed points; there are two or more within each model.

Some common parameters used within all numerical models are discussed in this section (Lu and Likos 2004). The volumetric water content is expressed as  $\theta$  and, the saturated water content is represented by  $\theta_s$  and describes the point where all available pore space within the soil is taken by water. This is usually shown on the curve by the corresponding desorption. The air entry pressure describes the suction on the desorption branch when air first begins entering the largest pores and desaturation begins and is represented by  $\psi_m$ . The condition where very little pore water resides in the soil and very large amounts of energy are required to remove it from the matrix is described by the residual water content,  $\theta_r$ . The degree of saturation is expressed as  $S$ , and the effective and residual degrees of saturation are expressed as,  $S_e$  and,  $S_r$  respectively. An effective degree of saturation can be normalized by the condition ( $S = 1$ ), and if the residual degree of saturation

is equal to zero then the effective degree of saturation is equal to the degree of saturation. The commonly used parameter is a dimensionless water content variable,  $\Theta$ , which is used for modeling purposes. It can be defined by normalizing the volumetric water using Equation 2-11.

$$\Theta = \frac{\theta - \theta_r}{\theta_s - \theta_r}$$

Equation 2-11

### 2.4.3 Brooks and Corey Model

In 1964, Brooks and Corey developed one of the first numerical approaches for modeling the SWRC based on observations from a large array of experiments where water content and suction were directly measured (Brooks and Corey 1964). The equation proposed was a two-part power law relationship that incorporated a “pore size distribution index”, ( $\lambda$ ), allowing for different gradations of soil to be modeled. The equation can be both expressed in terms of air entry as in Equation 2-12 or in terms of suction head ( $h$ ) and air-entry head ( $h_b$ ) as shown in Equation 2-13.

$$\Theta = S_e = \begin{cases} 1 & \psi < \psi_b \\ \left(\frac{\psi_b}{\psi}\right)^\lambda & \psi \geq \psi_b \end{cases}$$

Equation 2-12

$$\Theta = S_e = \begin{cases} 1 & h < h_b \\ \left(\frac{h_b}{h}\right)^\lambda & h \geq h_b \end{cases}$$

Equation 2-13

Figure 2-3 shows the results of data collected for three different soils from a silty sand to a poorly graded sand and was collected using a Tempe cell apparatus. The parameters, gradation index, and porosity for all three different soil types can be seen on the figure (Lu and Likos 2004). Overall, the BC model works best for relatively coarse grained soils where the drainage occurs of a low and narrow range of suction. Once  $\theta_r$  is being approached and higher values of suction are present, the model becomes less accurate and less applicable.

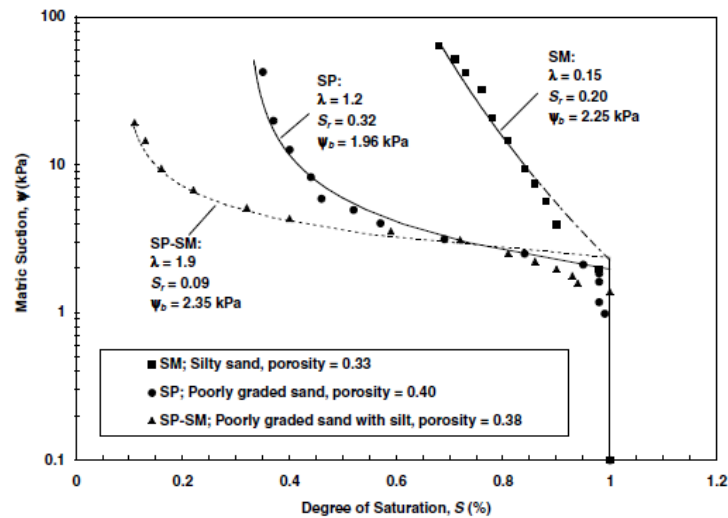


Figure 2-3: Soil-Water Characteristic Curves Models Using the Brooks and Corey (1964) Model (Lu and Likos 2004)

#### 2.4.4 Van Genuchten (VG) Model

In 1980, van Genuchten proposed a three-parameter model for the SWRC in a smooth and closed form (van Genuchten, 1980). Smooth transitions at the air-entry pressure and for suction approaching residual condition are more effectively captured, and a wider soil suction range is able to be obtained. The three fitting parameters for the model are represented by  $\alpha$ ,  $n$ , and  $m$ . The model is shown in Equation 2-14.

$$\Theta = S_e = \left[ \frac{1}{1 + (\alpha\psi)^n} \right]^m$$

Equation 2-14

The  $n$  and  $m$  fitting parameters correspond to both pore size distribution and the overall symmetry of the characteristic curve. The  $m$  parameter is frequently constrained by direct relation to the  $n$  parameter, i.e. Equation 2-15 and Equation 2-16, where Equation 2-15 can be used when the residual saturation condition is equal to zero. The  $\alpha$  parameter has a unit of inverse pressure.

$$m = 1 - \frac{1}{n}$$

Equation 2-15

$$m = 1 - \frac{1}{2n}$$

Equation 2-16

Figure 2-4 also shows data for three sandy soils where the model parameters can be seen for each corresponding soil on the figures. The model shows an excellent fit to the experimental data over the entire range if the parameters are all fitted independently.

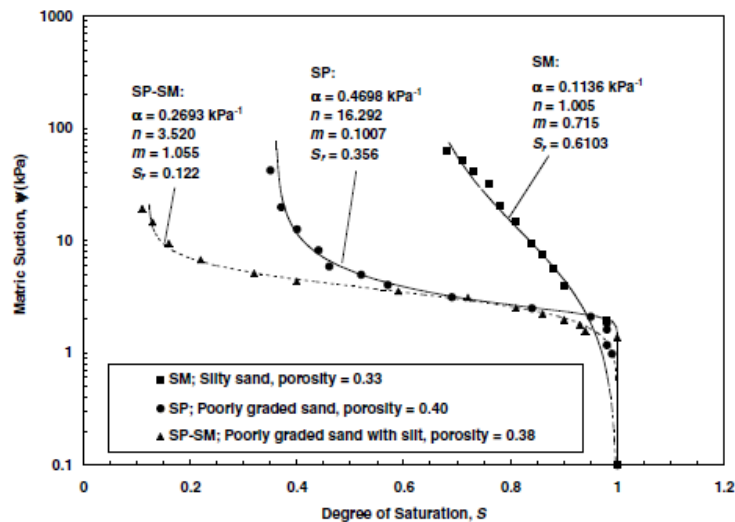


Figure 2-4: Experimental Soil-Water Characteristic Curves Models Using VG (Lu and Likos 2004)

#### 2.4.5 Fredlund and Xing (FX) Model

---

In 1994, Fredlund and Xing developed a similar model to VG model in by considering the pore size distribution (Fredlund and Xing, 1994). The model can be seen in Equation 2-17. If the residual water content is assumed to be equal to zero, the model can be written in terms of normalized water content or degree of saturation by dividing both sides of the equation by the volumetric water content.

$$\theta = C(\psi)\theta_s \left[ \frac{1}{\ln \left[ e + \left( \frac{\psi}{a} \right)^n \right]} \right]^m$$

Equation 2-17

The fitting parameters in the equation are  $a$ ,  $n$ , and  $m$ . These can be estimated from inflection points located on the measured characteristic curve. Similar to the VG model, the  $n$  parameter is related to the pore size distribution and the  $m$  parameter is related to the overall symmetry of the characteristic curve. For small values of  $m$ , the air-entry value can be used as  $a$ . For larger  $n$  values, sharper corners near the air-entry value are produced, also more uniform pore distribution are simulated. The  $m$  parameter controls the slope of the curve in the higher end of the suction range, where smaller  $m$  values result in a steeper slope at higher suction values.

The  $e$  parameter is the natural logarithmic constant, and the  $C(\psi)$  is a correction factor. This correction forces the model to a suction value of  $10^6$  kPa at zero water content and can be calculated from Equation 2-18.

$$C(\psi) = \left[ 1 - \frac{\ln(1 + \frac{\psi}{\psi_r})}{\ln(1 + \frac{10^6}{\psi_r})} \right]$$

Equation 2-18

#### 2.4.6 Hydraulic Conductivity Models

---

As the degree of saturation decreases from the fully saturated condition, the hydraulic conductivity (or permeability) also decreases. This will become important in the hydraulic water flow analysis. Similar to SWRC, there are several approaches to incorporate the degree of saturation, water content, suction, or head in hydraulic conductivity functions. Among the several available methods Equation 2-19 by Gardner (1958) and Equation 2-20 by Brooks and Corey (1964) are simple and commonly used empirical models.

$$k(\psi) = k_s \exp(-\alpha\psi)$$

Equation 2-19

where  $k_s$  is the saturated hydraulic conductivity and  $\alpha$  is indicative of pore size distribution.

$$k(\psi) = \begin{cases} k_s & \psi < \psi_b \\ k_s \left(\frac{\psi_b}{\psi}\right)^\eta & \psi \geq \psi_b \end{cases}$$

Equation 2-20

where  $\eta$  is a fitting parameter.

Also, van Genuchten (1980) and Fredlund et al. (1994) proposed two closed-form solutions developed based on the statistical pore size distribution concept, which are very popular. For example, Equation 2-21 shows the equation by van Genuchten (1980).

$$k(\psi) = \frac{[1 - (\alpha\psi)^{n-1}[1 + (\alpha\psi)^n]^{-m}]^2}{[1 + (\alpha\psi)^n]^{m/2}}$$

Equation 2-21

#### 2.4.7 Summary

The soil water characteristic curve describes the relationship between the water content and the suction of a specific soil. Three very commonly used SWRC models were presented and discussed. Although Brooks and Corey model has a smaller number of input parameters but it is less favorable due to its two section equation and less accurate prediction near air entry value. However, the other two models are both effective and would be implemented in the proposed system dynamics model. Further, among different hydraulic conductivity models available in the literature some of the most commonly applied ones were discussed. One model from the simplified approach and one from statistics-based approach will be implemented in the proposed system dynamics simulation.

### 2.5 PAVEMENT MOISTURE PROFILE AND HYDRAULIC MODELING

#### 2.5.1 Introduction

Literature was reviewed to investigate how water flows through pavement layers, and how that behavior changes in depth in a given soil. This is a very complex boundary value problem because the way water flows through a given soil depends on several different factors. These factors include pavement structure, the type of soil that the water is flowing through, the hydraulic conductivity of the soil, the current moisture state of the soil, the amount of water that is being introduced to the soil, and the subsurface water level or groundwater level. The other complex piece to this modeling is that depending on these parameters they can all be changing, and the rates at which they change over a given time may be different from one another.

Due to these complexities in this type of system, unsaturated soil models were reviewed based on their simplicity. The boundary conditions of these models will then be attempted to be modified to create more accurate models that may be more applicable to real world scenarios a pavement may experience. Even



though an actual pavement system may have saturated soil or partially saturated soil, modeling these systems in a dynamic process becomes more complicated. Also, a review into groundwater recharge and discharge equations was done, to see how the groundwater level changes and how the water moves through a soil system.

### 2.5.2 Unsaturated Soil Flow Models

---

There are several different approaches and hydraulic models that are built into pavement design, among them is the Drainage Requirement in Pavement (DRIP) (FHWA, 2002) and Enhanced Integrated Climatic Model (EICM) (Larson and Dempsey, 1997). The DRIP manual from FHWA provides well laid out requirements on pavement subsurface drainage design, several considerations are recommended to be made when creating a hydraulic model for a pavement system. These considerations include: geometric, physical properties of the soil, and the water that enters the pavement system (FHWA, 2002). The geometric considerations primarily focused on the slope of the pavement system. Particularly the resultant, longitudinal, and cross slope of the pavement. Within this information and given the equations, the resultant flow length can be calculated (FHWA, 2002). In terms of the physical properties of the soil, the coefficient of permeability is required and can be calculated based on  $D_{10}$  of the soil along with experimental constants. The other physical property of the soil that is required is porosity, which could be difficult to measure without taking a sample of the soil within the pavement system. To include the total water that can enter the pavement, infiltration through cracks, joints, shoulders, and side ditches were incorporated, along with meltwater. Groundwater variation was mentioned as an important factor, but no equations were presented to estimate the effect of this variation. To estimate infiltration, two different methods are recommended, the crack infiltration method and the infiltration ratio method. These equations are based on infiltration rates, both pavement and soil, geometric properties of the cracks, rainfall rates, and experimental constants (FHWA, 2002).

A challenge with the DRIP model is that it is focused on the flow of water into the pavement, through cracks and different forms. This is valuable when one desires to recognize the factors that should be built into the proposed model. However, it is also important to know how the groundwater moves within the soil. That is why additional models were reviewed, particularly models that deal with unsaturated soil flow. EICM, which is also used in the Pavement ME system, relies on a 1D finite difference modelling of moisture flow through pavement. A limitation though for EICM is that it does use a constant groundwater table boundary condition. Also, EICM relies on 1-D modeling which does not accurately replicate the 3-D flow problem.

In terms of soil moisture movement models, some of these are empirical in nature such as: Kostiaikov's Equation, Horton's Equation and the SCS equation (Ravi and Williams, 1998). These models are a good basis, but they are empirical. The other two models that were reviewed are the Green-Ampt Model and the Richards' Equation. The Richards' Equation is one of the most commonly used method and the most accurate one. The problem with this equation is that it involves many differential equations and boundary conditions, which make it very complex. Therefore, the Green-Ampt model was reviewed, which is also an accurate model, but makes some assumptions that results in a simpler equation to be modeled. More details on this model are provided next.

The Green-Ampt Model was developed in 1911, by Green and Ampt. The model was one of the first models commonly used to describe how water moves through soil based on the simplicity of the model and the accurate results that it yielded (Ravi and Williams, 1998). The basic parameters that the model includes is the water pressure from infiltrating water from above the soil, the hydraulic conductivity of the soil, the volumetric water content of the soil, and time. Knowing the physical properties of the soil and properties of the infiltration rate on the soil, the wetting front level, which can be related to the groundwater level, can be estimated for any given time. To find the critical time, which is defined as the duration of flooding needed to cause a completely saturated base course condition, can be estimated with an explicit form of the Green-Ampt equation shown below in Equation 2-22 (FHWA, 2019).

$$t = \frac{\theta_s - \theta_i}{k} [L_f - (h_L - \phi_f) \ln \left( \frac{h_L + L_f - \phi_f}{h_L - \phi_f} \right)]$$

Equation 2-22

Where:

$\theta_s$  = volumetric moisture content at saturation

$\theta_i$  = initial volumetric moisture content

$L_f$  = thickness of (HMA + base course), m

$\phi_f$  = suction, m

$h_L$  = depth of ponded water, m

$t$  = time to infiltrate, seconds

$k$  = permeability, m/s

In order to account for the flow of water through the HMA layer above the base aggregate course material, an effective permeability is estimated (FHWA, 2019). This estimation can be made with Equation 2-23.

$$k_{effective} = \frac{h_{HMA} + h_{Base}}{\frac{h_{HMA}}{k_{HMA}} + \frac{h_{Base}}{k_{Base}}}$$

Equation 2-23

Where:

$k_{effective}$  = effective permeability in m/s

$h_{HMA}$  = thickness of HMA, m

$h_{Base}$  = thickness of base aggregate course, m

$k_{HMA}$  = permeability of HMA, m/s

$k_{Base}$  = permeability of base course, m/s

Through iterations of analyzing the pavement system with the Green-Ampt model, several conclusions could be made (FHWA, 2019). The first is that the critical time is significantly affected by the HMA layer permeability, and in almost all cases this critical time was within six hours and frequently within two hours. Another conclusion is that cracks within the pavement system, especially for thin HMA surfaces, can

greatly increase the amount of water that enters into the pavement system. The most vulnerable time for HMA pavements was observed to be right after construction due to the voids in the system being relatively high. Finally, climatic considerations and locations are important factors, as temperature and distance to nearby water sources have the possibility to significantly affect the HMA system (FHWA, 2019).

However, this model has a few issues based on the assumptions made. One of these issues is that the model assumes completely unsaturated soil and a water table depth at some level below the soil. This is an unfavorable assumption, because in a case where a pavement system becomes flooded, the soil would be completely saturated. Another issue this model has is that an estimate is made with an effective permeability to explain how water flows through the pavement material; however, this isn't necessarily the most accurate estimation. The final problem with the model is that it assumes one dimensional flow straight down from the surface into the pavement, while in reality, water may be flowing in multiple directions (Ravi and Williams, 1998).

There are different hydraulic analysis software that have been used in the literature such as MnDrain (FHWA, 2019) or VADOSE/W (GeoSlope, 2019). MnDrain is a software developed by the Minnesota Department of Transportation for dealing with unsaturated flow within a pavement system. Within this software the Brooks and Corey model is used to relate hydraulic conductivity and pressure, or moisture content (FHWA, 2019). The equations used in this software can be seen below in Equation 2-24 and Equation 2-25. VADOSE/W is also part of Geo-Studio package that deals with flow in unsaturated soil zones above the water table.

$$K = K_{sat} \left[ \frac{\theta - \theta_{res}}{\theta_{sat} - \theta_{res}} \right]^{\lambda_2}$$

Equation 2-24

$$\theta = \begin{cases} 0.0001 (\psi - \psi_b) + \theta_{sat} & \psi < \psi_b \\ (\theta_{sat} - \theta_{res}) \left( \frac{\psi}{\psi_b} \right)^{-\lambda_1} + \theta_{sat} & \psi \geq \psi_b \end{cases}$$

Equation 2-25

Where:

K = Hydraulic conductivity

$K_{sat}$  = Saturated hydraulic conductivity

$\lambda_1$  and  $\lambda_2$  = material constants

Among other developed models for flow through pavement systems is the FLODEF package (Long et al. 2006). In this model the moisture flow is simulated using a 2D Finite Element numerical model based on Lytton's approach for moisture flow-soil deformation response. The method used a simplified Mitchell and Avalle's (1984) procedure for solving a moisture diffusion problem. In this method, the suction-permeability relation for unsaturated soil is based on the relationship proposed by Laliberte et al. (1966), which is similar in form to the one proposed by Brooks and Corey (1964). In a similar study, Espinoza and

Bourdeau (1992) developed a computer program PURDRAIN to model the water infiltration with the pavement systems, which was based on theories of water flow in unsaturated soils.

### 2.5.3 Groundwater Recharge Models

The next type of models are groundwater recharge and discharge models. There are several different types of these models, but similarly to the unsaturated flow models, many of them are empirical or too complex (Freeze 1969, Pathak 2014). Among these a model by Freeze (1965) is reviewed here. The model assumes one dimensional vertical flow in an unsaturated system. This model can be seen in Figure 2-5 (Freeze, 1969). As seen, the model incorporates the pressure heads, volumetric water content of the soil, depth, and other physical properties. Also, the model incorporates both infiltration and evaporation into the system. The issue with the model is that it most likely will not be able to be directly incorporated into the proposed model. This is for the same reason as the Green-Ampt Model, because both are solved for a wetting front moving down in an unsaturated zone, which is different than the recession of groundwater level. However, the proposed differential equation forms can be adapted for the given boundary value problem in the proposed project, in order to understand how the water recedes after flooding and to estimate the moisture profile in depth.

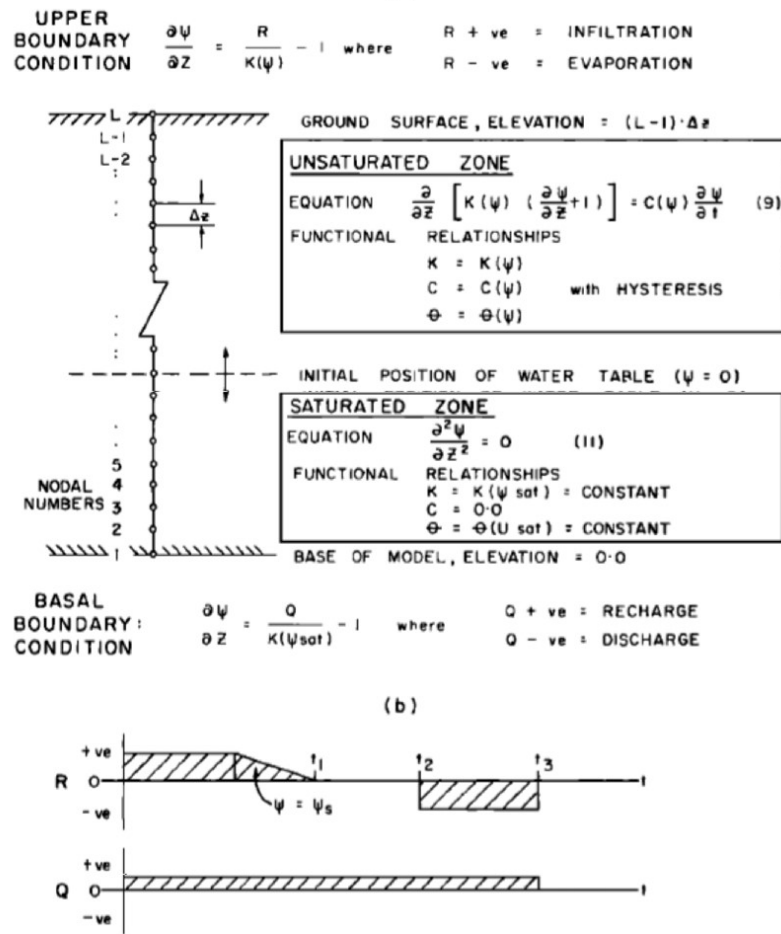


Figure 2-5: Groundwater Recharge Model (Freeze 1969)

#### **2.5.4 Pavement Moisture Profile and Hydraulic Modeling Summary**

---

A key factor in accurate assessment of pavement performance during and after inundation is the understanding of how water flows within the pavement system. In an event of flooding the soil is first saturated, but as water dissipates through the soil, the soil then becomes unsaturated and then unsaturated. Thus, a correct model should incorporate a dynamic flow system with a suction (or degree of saturation) – dependent permeability. Among the different classes of models presented in the review, the Green-Ampt model or the groundwater recharge models can be adjusted for the given hydrologic scenarios of interest. Starting with the core differential equations in these methods and solving for the boundary value problem, a simple semi-analytical procedure will be included in the proposed system dynamics model.

### **2.6 LITERATURE REVIEW SUMMARY**

#### **2.6.1 Summary**

---

Literature was reviewed in order to prepare for the next steps within this research project. This included: why load restrictions were needed to understand the importance of this research, basic pavement design components to get familiar with how the systems perform, different parameters that affect the performance of the pavement to see how a change in moisture affects each parameter, and different models that look at how water flows through soil to understand the behavior of water within the pavement system after and during a flooding event. As already mentioned, multi-directional flow was not fully investigated. Another area of literature that was not reviewed was climatic predictions. These were not within the scope of the project, and only public domain climatic forecast data will be used in the current work. However, the model can be adapted and cross-linked in future for climatic forecasting.

Key findings from the literature review resulted in understanding what parameters have a significant impact on the performance of the pavement system. Predictive equations for each of these parameters were then identified, which can ultimately be used in the system dynamics model to help predict the overall performance of the pavement system due to a storm event (or other events that result in excessive moisture within pavement system). For resilient modulus, the equations were based on how they were used in previous implementations, these were presented in section 2.3 . For the soil water retention curves, the two most commonly used models were chosen to incorporate into the system dynamics model, along with the two of the hydraulic conductivity models. These models were presented in section 2.4 . Incorporating these reviewed models in a system dynamics approach, will help to have a better understanding of how pavement performance is affected by a change in moisture within the system. Section 2.5 presented alternative approaches on simulating the water flow in pavement layers and subgrade soils, which is key to estimation of the moisture profile in depth.

## CHAPTER 3: SYSTEM DYNAMICS FRAMEWORK DEVELOPMENT

This chapter is organized in six sections. The subsequent six sections introduce system dynamics modeling, the embedded system dynamics structures, and the analysis of the developed model for evaluation of pavement deformation under variable soil moisture condition. In order to better introduce the proposed system dynamics framework, the key structures and their performance are discussed through practical examples of a conventional flexible pavement system. Lastly, a summary is provided that highlights the key findings from the proposed system dynamics framework.

The key components of this chapter consist of:

- System dynamics modeling and Vensim Pro® introduction
- Proposed system dynamics framework
- Hydrological structure and variables
- Geotechnical structure and variables
- Pavement response structure and variables
- System dynamics framework summary and conclusions

### 3.1 SYSTEM DYNAMICS MODELING AND VENSIM PRO® INTRODUCTION

#### 3.1.1 Introduction

There is a growing recognition of complexities and uncertainties in the management of pavement foundations subjected to moisture variations and, with it, the need for robust policy and decision-making that embraces these complexities and uncertainties. Pavements are dynamic structures and are affected by several complex interdependent parameters such as climatic and mechanical stressors and hydro-geological material properties. To consider this interdependent response, public and private agencies must transition from reductionist empirical approaches to mechanistically informed decision-making processes, as pavements are influenced by a multitude of interacting factors that may not initially appeared to be related.

To date, the majority of the pavement assessment efforts with respect to excess subgrade moisture conditions are based on direct field observation or empirical models, sometimes incorporating soil index parameters or one representative moisture or suction value. Empirical or observation-based methods for complex problems such as flooded pavement systems can be insufficient, limited, and ambiguous, and are often affected by biased evidence-based decision of an expert. Therefore, these methods are often limited in their ability to explain causation and the effect of non-linear interactions and feedback on the behavior of complex systems. This can result in unintended faulty decisions with consequences that create new problems or exacerbate the original problem. Decision-makers are required to integrate scientific and mechanistic-based evidence into decision making.

System dynamics modelling (SDM) is a problem-oriented modelling approach to help agencies better understand complex dynamic problems. The use of system-based approach for pavements

subjected to moisture variation is a necessary step to integrate and understand complex interaction of key factors affecting their overall performance. Due to a very large number of variables and their interdependencies, a system dynamics approach can holistically capture all significant variables and provide a user-friendly tool to study and visualize governing factors and their effects on pavement response under variable initial and boundary conditions. The system dynamics modeling can provide engineers with an instructive basis to understand significant factors impacting pavement response to moisture variation and also develop a mechanistic approach for load restriction (both in current time and for future forecasting) decision making. This chapter describes SDM concept and Vensim PRO®, a software utilized to simulate and visualize problems in the context of SDM.

### 3.1.2 System Dynamics Modeling

---

System dynamics (SD) is a problem-oriented modelling approach originated by Jay Forrester and his colleagues in the late 1950's, which initiated by applying concepts from feedback control theory to industrial problems (Forrester 1987). It is an approach to study and manage complex systems that change over time. System dynamics modeling has been used to model and understand complex dynamic systems in various fields; some examples include environmental science, management, economics, natural and social sciences, and healthcare systems (Bixler et al. 2019; Currie et al 2018; Forrester 1987). SD involves causal mapping and visualization of behavior of a system as well as interaction between system structures and components with the aid of computer simulation. This provides a strong tool specifically for decision makers to experiment the consequences of their decision before implementation in real world. In addition, while conventional approaches tend to tackle problems by studying individual components of a system (e.g., effect of moisture on subgrade resilient modulus or effect of subgrade resilient modulus on pavement response), a SD approach centers around the idea of integrating dynamic system structures and components considering their interactions over time (e.g., simultaneous evaluation of moisture movement in pavement considering the impact of moisture on hydro-mechanical soil properties as well as pavement response over time).

A SD model consists of three basic elements including (1) level variables, (2) flow variables, (3) information variables. Levels are the key components of each system showing the state of system over time. An example of levels in a flooded pavement system can be the level of ponded water on top of pavement or moisture content in a given layer of soil. Levels can only change through flow variables. Flow variables are defined as the amounts of material added (inflow) or expelled (outflow) from the level. An example of inflow in a pavement system can be the rate of water flowing into the ponded water due to precipitation and an example of outflow can be the rate of water infiltrating into pavement layers from the ponded water. Thus, the level variable in a system is mainly controlled by flow variables and most often are calculated by numerical integration of net flow over time. The quantity and sequence of material flow in a dynamic system is controlled by information variable. An example of information variable in a pavements system can be hydraulic conductivity of soil or precipitation rate and duration which control the rate of inflow and outflow in the system. One key component of SD is causal loop or feedback loop. Causal loop is a closed sequence of material and information flow that establishes the causal effects of different variables in a closed loop (Kirkwood 1998). In recent years several computer programs such as

Vensim® and Stella® are developed and employed to simulate and visualize complex system dynamics. The following section describes Vensim PRO®, a system dynamics simulation software utilized in this research to study and simulate the behavior of pavement system under moisture variations.

### 3.1.3 Vensim pro®

---

Vensim PRO® (Ventana Systems, Harvard, Massachusetts) is a computer software that allows to conceptualize, document, simulate, visualize, and analyze complex dynamic systems. The software has extensive features including causal loop diagrams, stock and flow diagrams, in built-functions (e.g., if then else, random number generation, etc.), simulation and visual analysis, data use, sensitivity testing, reality check, and more. It is widely used to simulate and visualize complex SD in various fields (e.g., Khan et al. 2009; Rashedi and Hegazy 2016; Whang and Yuan 2017).

Different types of variables such as level variable, rate variable, auxiliary variable, data variable, constant variables are used in Vensim PRO®. Level variables show the current state of dynamics components of the system. The quantity of level at each time step is controlled by the magnitude of cumulative net flow into the level and is computed by numerical integration of difference between inflow and outflow as follows:

$$Level(t) = \int_0^t (inflow - outflow) dt + Level(t = 0)$$

Equation 3-1

Specifically, rate variables control the inflow and outflow into a level. Auxiliary variables are computed through defining analytical equations and functions by using other variables at a given time. Constant variables define constant values for given variables over time. Data variables enable users to define variables that change over time but are independent of changes in the system. Variables in Vensim are connected through arrows indicating that there is either material or information flow between the two given variables. Several numerical integration techniques including Euler and second order and fourth order Runge-Kutta integration are available in the software. The following sections are intended to describe the capabilities of SD modeling in simulating and understanding the system behavior while being presented in a context of a hypothetical one-dimensional (1-D) moisture flow example.

### 3.1.4 A Simple Example of System Dynamics Simulation using Vensim pro®

---

The flow example consists of a fully saturated column of soil subjected to inflow and outflow of water as shown in Figure 3-1 (a). A SD model was developed to simulate the ponded water height and outflow of water to the outflow container using Vensim PRO®. The notations used in Vensim for depicting the defined variables are shown in Figure 3-1 (b). In the software, the material flow is shown by double arrows, information flow is shown by single arrows, level variables are shown in boxes, and auxiliary, constant, and data variables are shown by words. In Figure 3-1 (b), ponded water height ( $h_p$ ) and accumulated outflow ( $h_a$ ) are the level variables in the system. Inflow rate ( $q_{in}$ ), Infiltration rate ( $q_{out}$ ), and evaporation rate ( $q_e$ ) are rate variables controlling the rate of water flux to and from the ponded water. The ponded



water height can be calculated as an integral of water flux in and out of the soil surface using Equation 3-2.

$$h_{p,t} = \int_0^t (q_{in,t} - q_{E,t} - q_{out,t}) dt + h_{p,t=0}$$

Equation 3-2

Vensim PRO® uses numerical integration techniques to compute accumulated level of ponded water at a given time. Inflow can be defined as a constant variable or data variable by defining time dependent data (e.g., providing precipitation time history as an input). Effective soil size for which 10% of soil grains are smaller than that size ( $D_{10}$ ), soil void ratio ( $e$ ), and soil thickness ( $Th$ ) are constant variables. Saturated hydraulic conductivity of soil ( $k_s$ ) and infiltration rate are examples of auxiliary variables.  $k_s$  in this example was calculated based on a semi-empirical equation which uses soil  $D_{10}$  and void ratio,  $e$ , to estimate hydraulic conductivity of sandy soils (Chapuis 2004).

$$k_s = 2.46[D_{10}^2 \frac{e^3}{(1+e)}]^{0.78}$$

Equation 3-3

Although  $k_s$  is an auxiliary variable in this example, its magnitude does not change over time since it is function of two constant variables. However, infiltration rate, the other auxiliary variable changes over time as it is a function of ponded water height, which is a level and time dependent variable. The infiltration rate in this example can be calculated using Darcy's law:

$$q_{out,t} = k_s \frac{\delta h_t}{\delta z}$$

Equation 3-4

where  $\delta h_t$  is the change in total pressure head over a given distance,  $\delta z$ .

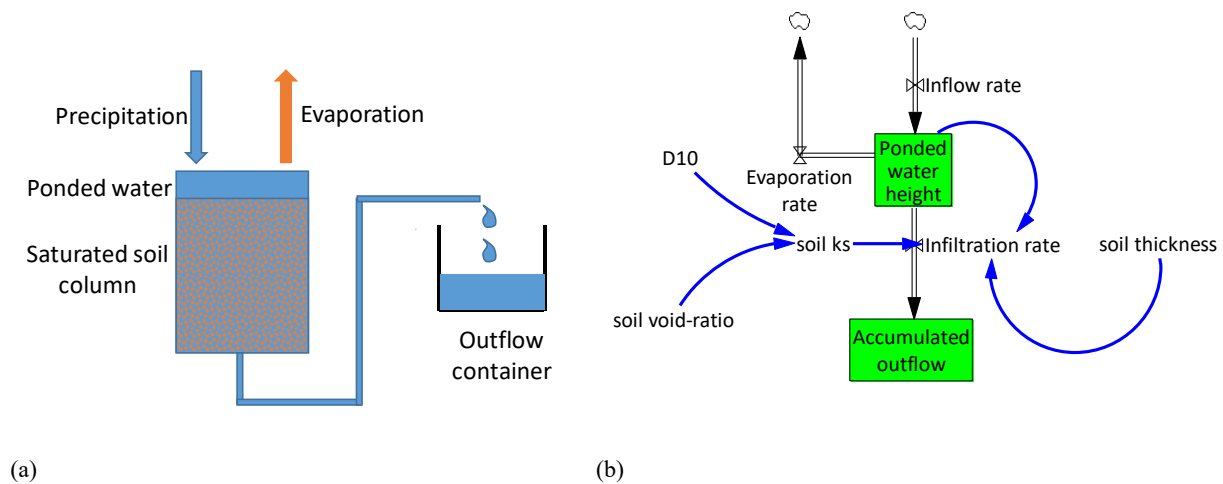
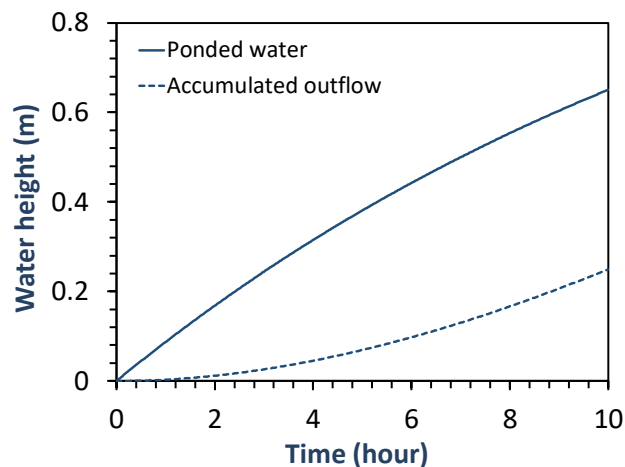


Figure 3-1: (a) Schematic of the example problem, and (b) the system dynamic model of example problem.

Vensim uses the initial and time dependent data to compute auxiliary and time dependent variables at each time step. Results of SD model simulation are produced in terms of time histories. Examples of these results for ponded water height and accumulated outflow are presented in Figure 3-2 in terms of ponded water height and accumulated outflow time series. SD model simulation indicated no ponded water and accumulated outflow at the initial time. This is in agreement with the system's initial condition where total head of water at the soil surface and the end of the outflow tube are the same and the system is at equilibrium. Time history for elevation of ponded water (water height) showed an increasing trend with time, however, with decreasing rate in time. This is because the increase in ponded water height resulted in an increase in hydraulic gradient and subsequently infiltration rate. This is evident in the accumulated outflow curve where the rate of water accumulation was increased with time. Overall, the results of simulation indicated a very good agreement between the SD model predictions and the expected trends. This shows that SD can be a useful tool to model moisture flow through soil systems.

One of the most important advantages of SD modeling using Vensim PRO® is the capability of running sensitivity analysis. This is specifically of great importance for complex systems such as flexible pavements under moisture hysteresis where the existence of complex interdependent components increases the complications of understanding the influential factors governing the system behavior.



**Figure 3-2: Results of system dynamics model simulation using Vensim PRO®.**

For the flow example presented herein, the sensitivity of the ponded water height to variations of effective soil particle size (i.e.,  $D_{10}$ ) and soil thickness was examined. The input variables were changed over a range of  $\pm 50\%$  and the resulting influence of these changes on the ponded water height over 10 hours were investigated. Figure 3-3 presents the sensitivity of ponded water height to  $D_{10}$  and soil thickness variations. Regardless of the type of input variable, a significant change in model response in terms of ponded water height was observed by a change in input variables. The simulation results showed higher sensitivity of ponded water to  $D_{10}$  than soil thickness for positive changes in input variables. Overall, results showed that sensitivity analysis of SD model provides a useful tool to understand the significant influence of input variables on model behavior.

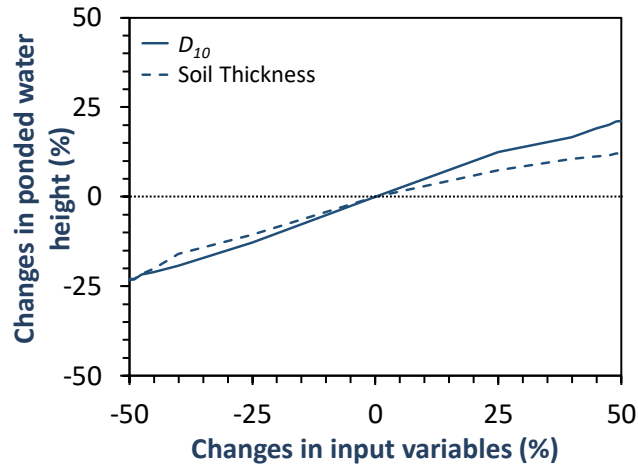


Figure 3-3: Results of SD model sensitivity simulations using Vensim PRO®.

### 3.1.5 Summary

Pavements are dynamic structures that are affected by several complex interdependent stressors and material properties. The use of a system-based approach for pavements subjected to moisture variations that integrates these interactions is needed. SDM, an approach to study and manage complex systems which change over time, is an approach that can address this challenge. This approach holistically captures all significant variables and provide a user-friendly tool to study and visualize the pavement response. In this chapter, Vensim PRO®, was successfully used to model 1-D flow through a saturated soil system while demonstrating some of the SD capabilities.

## 3.2 PROPOSED SYSTEM DYNAMICS FRAMEWORK

### 3.2.1 Introduction

The first step in modeling any dynamic system in the context of SD is the identification of influential factors and establishing the relationship between them. In the case of pavements with moisture variations, several parameters such as climate conditions, hydro-geological properties, loading patterns, and pavement structural properties contribute to overall pavement system response. A complete SD model should incorporate all influential variables as well as their interdependency to capture overall pavement system response to moisture movement in real time. This chapter focuses on identification of different system dynamics structures and variables contributing to overall pavement system response to moisture variation.

### 3.2.2 System Dynamics Main Structures

Previous studies have shown that about 80% of pavement damage is directly or indirectly influenced by the presence pore water especially in subgrade soil (e.g. Sultana et al. 2016; Mndawe et al. 2015) while the quality and type of base aggregate, subbase, and subgrade layers control the overall performance of

pavement system (Santero et al. 2011, Mallick and El-Korchi 2013, Elshaer et al. 2018a). Moisture movement in pavement structure and subsurface layers can significantly affect the soil and unbound aggregate layers' mechanical properties and thus pavement response to traffic loading (Sauer and Monismith 1968, Edris and Lytton 1976, Fredlund and Morgenstern 1977, Noureldin 1994, Drumm et al. 1997, Ceratti et al. 2004, Yang et al. 2005, Khoury and Khoury 2009, Sawangsuriya et al. 2009, Khoury et al. 2010, Cary and Zapata 2010, Han and Vanapalli 2015). Thus, modeling moisture movement and factors affecting its mechanism is the first step in mechanistic pavement response assessment in the context of SDM.

Heavy storm precipitation and low permeability of subgrade soil result in ponding water on top of natural subgrade. In the case of highly permeable base and subbase material, the floodwater easily permeates through these layers which results in inundation of layers within ponded water depth. The level of ponded water depends on climatic conditions (i.e., precipitation and evaporation rates), the topography of pavement, and rate of water infiltration to subsurface soil. The infiltration of water into the subsurface is highly affected by subsurface hydro-geological conditions including soil moisture/suction profile in depth, hydraulic conductivity, and elevation of groundwater table. Thus, a well-designed, mechanistic pavement response assessment protocol requires a robust hydrological analysis of water flow through pavement layers in real time. Moisture movement in the proposed system dynamics framework is conducted under a hydrological structure.

The next step in the mechanistic assessment of pavement response to moisture variation is the analysis of the impact of moisture variation on the mechanical properties of various pavement layers and subgrade layers. This analysis should incorporate the soil moisture/suction profile time series obtained from hydrological analysis as inputs and estimates the mechanical properties of pavement layers in real time as an output. This is performed using a geotechnical structure as the second main structure in the SD model.

The final step in the proposed SD framework is the estimation of pavement structural response to traffic loading. It is well established that weakening of pavement layers due to moisture variation and excessive deformations is the main cause of damage to pavement systems (Gaspard et al., 2007; Helali et al., 2008; Zhang et al., 2008; Vennapusa et al., 2013). The analysis of pavement response should consider the variable, moisture-dependent mechanical properties of pavement layers, pavement current conditions due to existing distresses, and vehicular axle loads and configuration. The pavement response can be analyzed in terms of vertical deflection and peak stresses. This is performed using a pavement response structure, which incorporates the results of analysis of hydrological and geotechnical structures, and pavement and traffic inputs to estimate pavement response in real time.

These three major structures of the SD model will be integrated while each structure contains multiple interrelated variables. Figure 3-4 provides a snapshot of how these three structures work within the SD model.

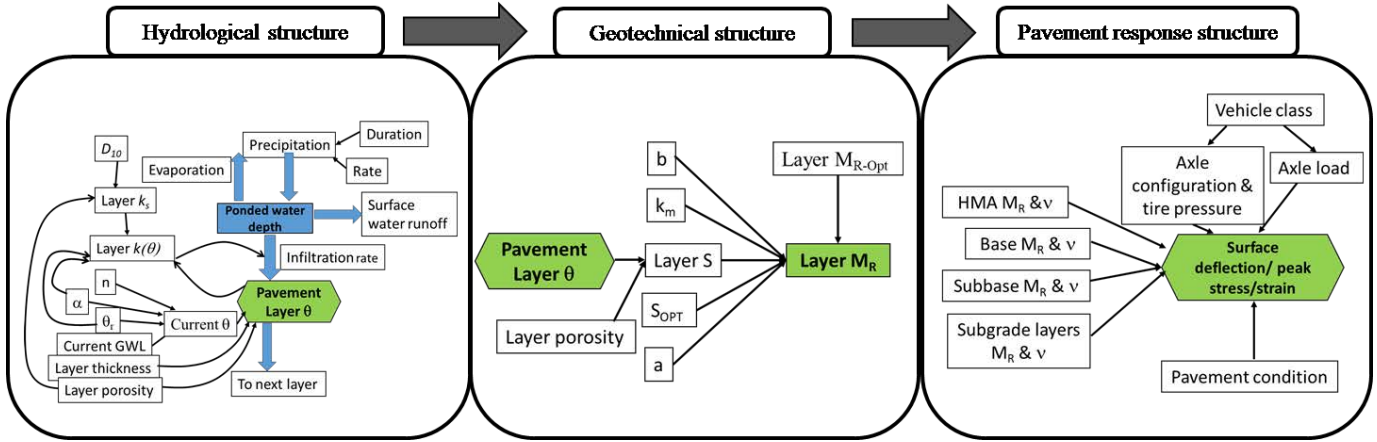


Figure 3-4: A conceptual schematic of the SD model structures and their variables.

### 3.2.3 Example of Conventional Flexible Pavement Properties

In order to better explain the application of the SD, the framework development process is discussed by evaluating the response of a conventional flexible pavement system with hypothetical material properties and given hydrological and climate conditions. Figure 3-5 presents the schematic of this conventional flexible pavement example which consists of a 0.1 m (~4 inch) thick Hot Mix Asphalt (HMA) layer, 0.3 m (~12 inch) thick base aggregate, and 0.1 m (~4 inch) thick subbase placed on top of natural subgrade. Groundwater table (GWT) is assumed to be located 2 m (~6.56 ft.) deep from natural ground surface and bedrock is at a depth of 10 m (~32.8 ft.) from natural ground surface. Since different physical and mechanical characteristics of subgrade soil is depth-dependent, the subgrade above GWT is divided to 10 layers. The normal seasonal groundwater level is assumed to be 2 m deep.

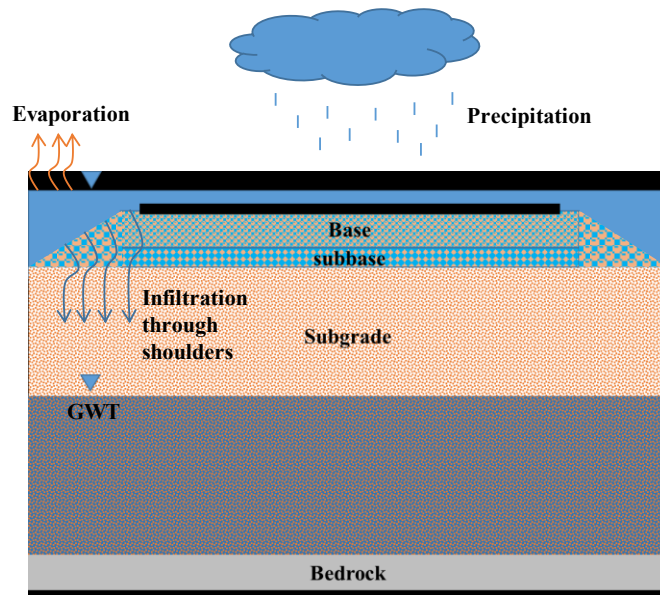


Figure 3-5: The conventional flexible pavement example.

### 3.2.4 Summary

---

Any SD framework for pavement response analysis during moisture hysteresis should include three general structures, (1) a hydrological structure, (2) a geotechnical structure, and (3) a pavement response structure. Such framework should be able to model the interaction between these three structures. The overall pavement response during moisture variation depends on the concurrent interactions between the three structures and their components over time. Each of these structures are described in following chapters.

## 3.3 HYDROLOGICAL STRUCTURE MODEL

### 3.3.1 Introduction

---

The hydrological structure of the proposed SD model simulates the moisture flux in and out of pavement layers due to precipitation, evaporation, or groundwater level (GWL) fluctuation. This is governed by complex interaction of two main components including climate information (e.g., precipitation duration and rate, evaporation rate, surface water runoff) and unsaturated soil hydraulics (e.g., moisture-dependent hydraulic properties of soil layers, current moisture state of the soil, and subsurface GWL). The hydrological structure models the complex interaction between these components to capture variation of moisture content and soil suction profiles during a period of time for consequent geotechnical and pavement response assessment. The following sections are intended to describe each component and related variables of hydrological structure. To better understand the function of each variable, their performance is discussed using the conventional flexible pavement example introduced in Chapter 3.

### 3.3.2 Climate Information Variables

---

The climate information provides material and information data that controls water flux into and out of the soil surface (i.e., flows associated with water infiltration and discharge). Climate information variables include evaporation rate, initial post flooding ponded water height, rate of surface run-off, and precipitation rate. The initial post flooding ponded water height can be treated as a constant variable based on forecasted data. It can also be estimated from subtraction of evaporation, surface runoff, and infiltration rates from precipitation rate. The surface water runoff depends on the location of pavement, and it can be assumed to be zero for “flat areas” and equals precipitation minus infiltration and evaporation for pavements with significant grades. The evaporation/precipitation can be treated as constant input based on average regional evaporation/precipitation rate. Also, the short-term climate forecast can be directly utilized as an input. The SD model has the capability to utilize past precipitation time series for calibration and validation purposes. Figure 3-6 presents the defined climate information variables in the SD model.

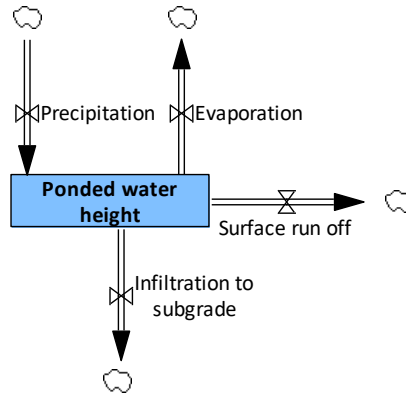


Figure 3-6: Climate information variables in the system dynamics model.

### 3.3.3 Hydraulics of Unsaturated Subsurface Soil

The water flux out and into unsaturated subgrade layers can be estimated by Richards' equation (Richards 1931). Richards' equation for the one-dimensional transient unsaturated flow through subgrade layers to the groundwater table in an isotropic soil deposit can be expressed as follows:

$$\frac{\delta \theta}{\delta t} = \frac{\delta}{\delta z} [K_{(\theta)} \left( \frac{\delta h}{\delta z} + 1 \right)]$$

Equation 3-5

where,  $\theta$  is the volumetric water content,  $z$  is the depth from the subgrade surface,  $h$  is the soil pressure head,  $t$  is time, and  $K_{(\theta)}$  is the moisture dependent hydraulic conductivity of soil. The initial volumetric water content profile of subgrade can be estimated using Soil Water Retention Curve (SWRC) predictive models. Several SWRC predictive models including Brooks and Corey Model (Brooks and Corey 1964), van Genuchten (VG) Model (van Genuchten 1980), and Fredlund and Xing Model (Fredlund and Xing 1994) were introduced previous chapters. The van Genuchten's formula was implemented in the current SD model due to its accuracy in predicting SWRC and its common use. The model has the following form:

$$\frac{\theta - \theta_r}{\theta_s - \theta_r} = \left[ \frac{1}{1 + (\alpha h)^{n_{VG}}} \right]^{m_{VG}}$$

Equation 3-6

where  $\theta_r$  is residual volumetric water content,  $\theta_s$  is saturated volumetric water content, and  $m_{VG}$  and  $n_{VG}$  are VG model fitting parameters ( $m_{VG} = 1 - 1/n_{VG}$ ). The moisture-dependent hydraulic conductivity at each soil layer soil can, then, be calculated according to Mualem (1976):

$$K(\theta) = K_{sat} \left( \frac{\theta - \theta_r}{\theta_s - \theta_r} \right)^{0.5} \left[ 1 - \left( 1 - \left( \frac{\theta - \theta_r}{\theta_s - \theta_r} \right)^{\frac{1}{m_{VG}}} \right)^2 \right]^2$$

Equation 3-7

where  $K_{sat}$  is the hydraulic conductivity of soil at fully saturated state. The hydraulic conductivity of fully saturated soil layer can be obtained from field tests or be estimated by semi-empirical equations. Table 3-1 summarizes some empirical equations for estimating the hydraulic conductivity of soils in fully saturated state.

**Table 3-1: Empirical relations for estimation of hydraulic conductivity of fully saturated soils.**

Reference	Equation number	Hydraulic conductivity (cm/s)	Notation	Remarks
Hazen (1911)	<b>Equation 3-8</b>	$k_s = cD_{10}^2$	$c$ = constant.	$c \approx 1$ , applicable for fairly uniform sand
Chapuis (2004)	<b>Equation 3-9</b>	$k_s = 2.46[D_{10}^2 \frac{e^3}{(1+e)}]^{0.78}$	$e$ = void ratio of soil	Applicable for uniform gravel and sand and non-plastic silty sands
Mbonimpa et al. (2002)	<b>Equation 3-10</b>	$k_s = C_p \frac{\gamma_w}{\mu_w} \frac{e^{3+x}}{(1+e)} \frac{1}{\rho_s^2 w_L^{2x}}$	$\gamma_w$ =unit weight of water (kN/m <sup>3</sup> ) $\mu_w$ = Water dynamic viscosity (Pa·s) $\rho_s$ = Density (kg/m <sup>3</sup> ) of solids $W_L$ = Liquid limit (%) $x = 7.7W_L^{-0.15} - 3$	Applicable for plastic soils, $\gamma_w \approx 9.8$ , $\mu_w \approx 10^{-3}$ , $\chi = 1.5$

While Richards' equation is one of the most accurate methods to model the moisture infiltration into unsaturated soils, it requires a numerical solution due to the challenges in setting the initial and boundary conditions. Yang et al. (2009) suggested a simple numerical solution of Equation 3-5 for water movement in unsaturated soils and demonstrated that the solution works satisfactorily. The solution uses the integration of Equation 3-5, vertically, over the soil layer to simulate moisture movement in unsaturated soil layers (Yang et al. 2009):

$$\Delta\theta = \left( \frac{v_{wi} - v_{wi+1}}{\Delta z} \right) \Delta t$$

**Equation 3-11**

where  $i$  is the number of layer,  $\Delta t$  is time step,  $\Delta z$  is the soil layer thickness,  $v_{wi}$  and  $v_{wi+1}$  are the water flow rate from layer  $i$  to  $i+1$ . The flow rate at each layer is calculated based on the volumetric water content, moisture dependent hydraulic conductivity, and soil pressure head at a given time step:

$$v_{wi} = K_{(\theta_i)} \left( \frac{\Delta h_{i,t-1}}{\Delta z} + 1 \right)$$

**Equation 3-12**

$$v_{wi+1} = K_{(\theta_{i+1})} \left( \frac{\Delta h_{i,i+1}}{\Delta z} + 1 \right)$$

**Equation 3-13**



where  $\Delta h_{i,i-1}$  and  $\Delta h_{i,i+1}$  represent the differences in soil total head between the given layer and its adjacent top and bottom layers. In order to simulate water movement in subgrade layers, the simplified numerical solution of Equation 3-5 was formulated into the SD model. The SD model incorporates the climate variables and variables related to the flow in unsaturated soil layers to simulate the moisture movement in real time. Figure 3-7 presents the interrelation of these variables in the hydrological structure of SD model.

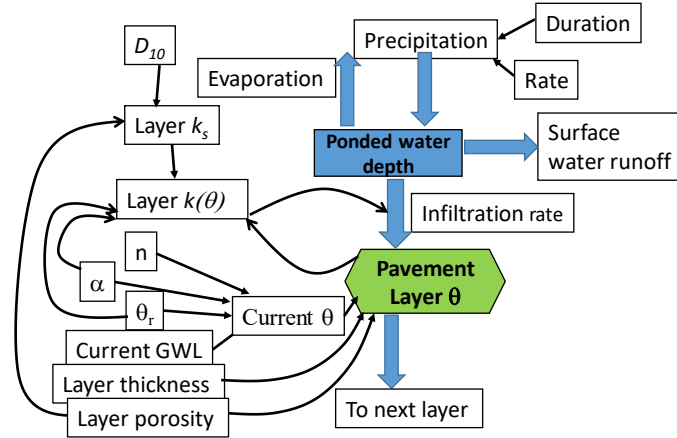


Figure 3-7: Hydrological structure of flooded pavement SD model.

### 3.3.4 Water Movement Simulation within a Conventional Flexible Pavement Example

In order to highlight the capability of the SD model to simulate moisture movement in pavement layers, the conventional flexible pavement example (described in Chapter 9) was simulated in Vensim PRO®. In this regard, a hypothetical climate scenario was defined in the software. It was assumed that the pavement section with the given initial and boundary condition would be subjected to two discrete periods of heavy precipitation; first with a rate of 0.2 m per hour for 10 hours and second with a rate of 0.1 m per hour for 5 hours while they occur 20 hours apart. The evaporation rate and run off were assumed to be negligible during the period of simulation. This hypothetical precipitation time history is shown in Figure 3-8, it was used as an input to the SD model demonstrated in this chapter.

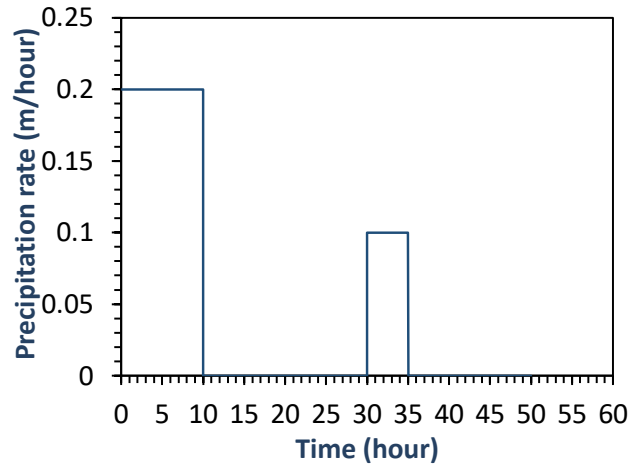


Figure 3-8: Precipitation rate time history.

In order to simulate the moisture flow in subsurface, physical properties were assumed for the pavement layers (as shown in Table 3-2). The SD model used the input information and Equation 3-6 and Equation 3-7 to estimate initial soil degree of saturation,  $S = \theta/n$  ( $n$ = soil porosity), and hydraulic conductivity profile. These are shown in Figure 3-9.

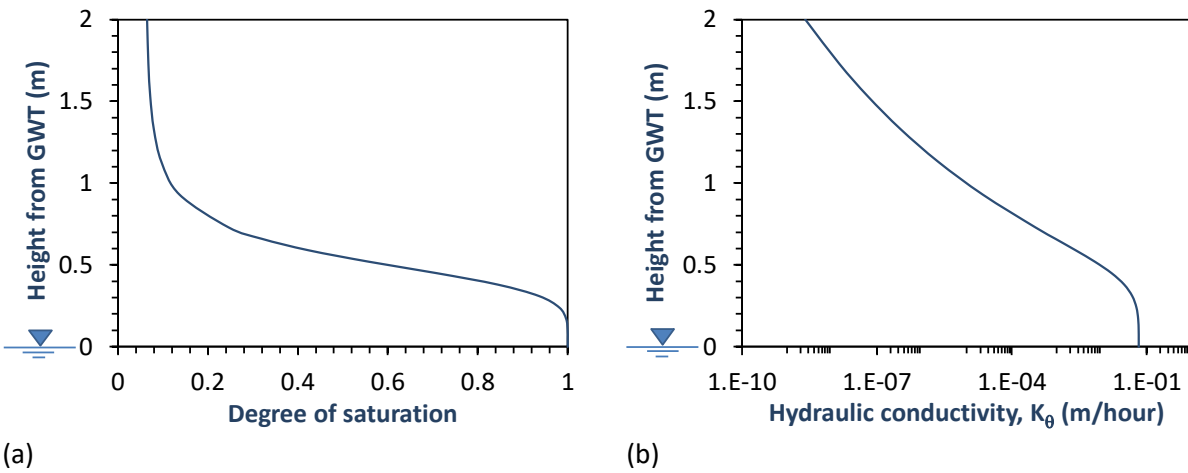
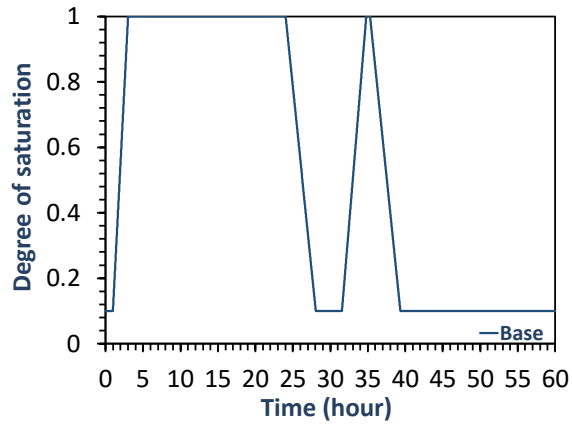


Figure 3-9: (a) Initial degree of saturation and (b) moisture dependent hydraulic conductivity profile.

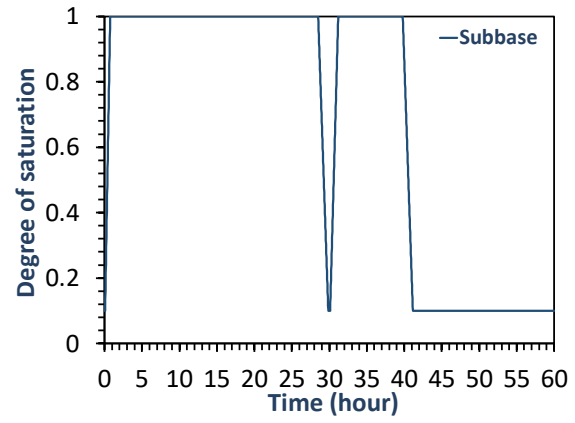
**Table 3-2: Physical and hydraulic properties of hypothetical subgrade.**

Properties	Attributes/Value
Soil type	Silty sand
Void ratio ( $e$ )	0.5
Effective grain size ( $D_{10}$ )	0.035 (mm)
$n_{vG}$	5
$a_{vG}$	2
Residual volumetric water content ( $\theta_r$ )	0.02
Saturated water content ( $\theta_s$ )	0.3

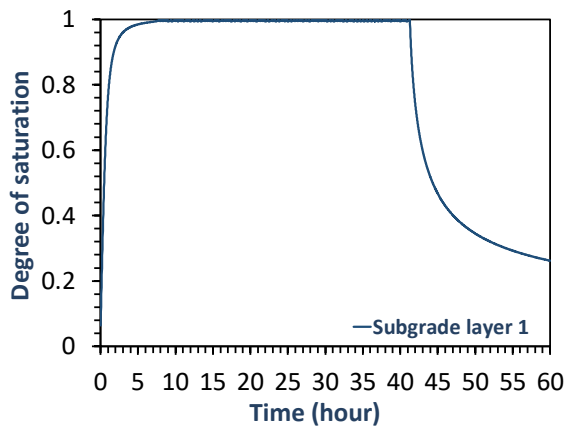
The SD model incorporated the input climate data, unsaturated soil hydraulic variables, and formulations to simulate moisture movement through pavement layers and to estimate the degree of saturation of each layer in time steps. It is noteworthy that pavement base aggregate and subbase layers typically consist of granular material with relatively high permeability and very low water retainability. Therefore, for the case of flooded pavement with granular base and subbase layers, it is reasonable to assume free water movement in these layers. Accordingly, the degree of saturation in these layers is assumed to be a function of the ponded water height and the total layer thickness, i.e., degree of saturation is calculated by dividing the portion of the layer under the ponded water to the total thickness of the layer. Figure 3-10 presents the SD simulation results (in form of degree of saturation for various layers) associated with the conventional flexible pavement example using the proposed hydrological structure. Figure 3-11 illustrates the moisture profiles within the pavement layers at different periods of time. Subgrade layer 1 presented in Figure 3-10 was located at the natural soil surface (0 to 0.2m) and subgrade layer 5 was 1 meter deep from the surface (1 to 1.2m) (i.e., 1 meter to GWL). The SD simulation indicated that after approximately 2.5 hours from the first period of precipitation the subbase and base aggregate layers become fully saturated. The 20 hours stop in precipitation resulted in full desaturation recovery of both layers. However, 5 hours of rain, even in a lower rate was enough to re-saturate both layers. The infiltration of rainwater into subgrade layers resulted in gradual saturation of the subgrade layers. The full saturation of layer 1 and layer 5 occurred in about 5 and 8 hours, respectively, after the first period of precipitation. Both layers remained fully saturated for more than 40 hours. Then, the recession of ponded water resulted in desaturation of both base aggregate and subbase layers and also redistribution of water in subgrade layers. This resulted in a gradual reduction in subgrade layers' degree of saturation toward their initial value (i.e., SWRC equilibrium level). In general, results show expected trends in pavement layers' degree of saturation due to the precipitation. This provides confidence in the suitability of hydrological structure of the SD model to capture moisture movement in pavement systems.



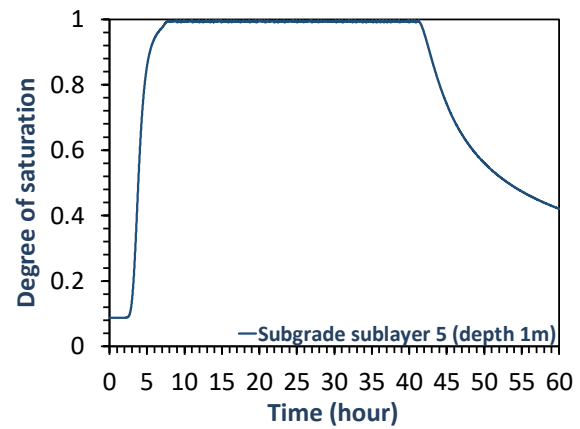
(a)



(b)



(c)



(d)

Figure 3-10: Typical results of moisture movement simulation using the SD model formulated in Vensim PRO® in terms of saturation time histories for (a) base aggregate (averaged for whole layer), (b) subbase (averaged for whole layer), (c) subgrade layer 1, and (d) subgrade layer 5.

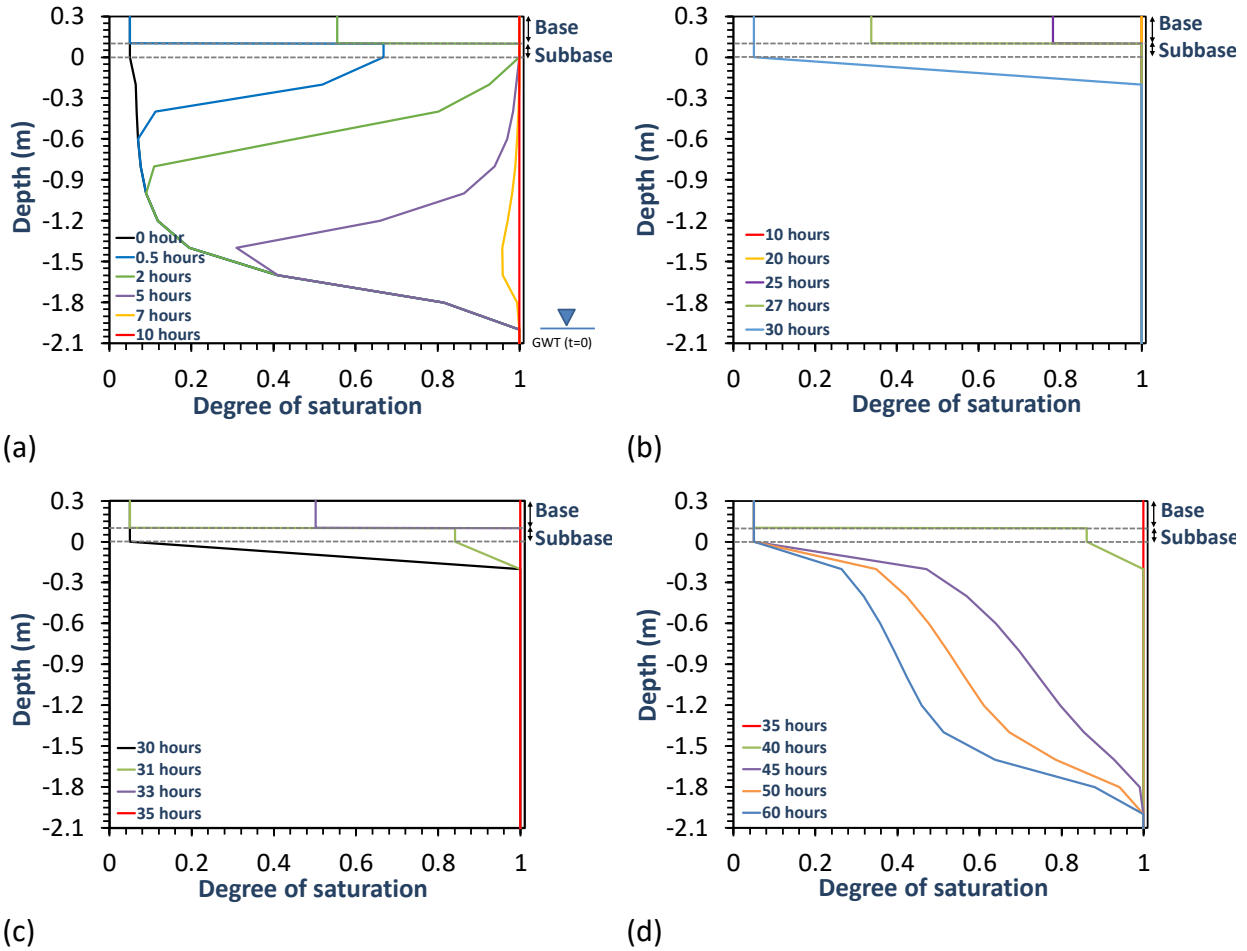


Figure 3-11: Moisture profile of pavement layers (a) during first period of precipitation, (b) between two periods of precipitation, (c) during the second period of precipitation, and (d) after the second period of precipitation.

### 3.4 GEOTECHNICAL STRUCTURE MODEL

#### 3.4.1 Introduction

Excessive moisture in pavement systems especially in subgrade soils reduces the pavement foundation stiffness and results in surface deflection and cracking. This has been shown through numerical modeling (e.g., Elshaer et al. 2017, Haider and Masud 2018), physical small-scale and full-scale modeling (e.g., Amiri 2004, Saevarsdottir and Erlingsson 2013), and field performance assessment (e.g., Zhang et al. 2008, Sultana et al. 2016). Geotechnical properties of soils play a key role in pavement response; thus, accurate assessment of these properties under various degrees of water saturation is crucial. Resilient modulus of subgrade soil is one of the most influential factors that controls the overall stiffness of the pavement system. Developing moisture-dependent resilient modulus has been in the forefront of transportation geotechnics research. Especially, with the advancement of unsaturated soil mechanics, significant efforts have been made to correlate soil suction and state of stress to resilient modulus in a more mechanistic

setting. The geotechnical structure of the proposed SD model incorporates the moisture/suction variation of soil layers obtained from the hydrological structure at each time step to estimate resilient modulus of the pavement layer subjected to moisture variations. The following sections discuss the variables used in the geotechnical structure of the SD model.

### 3.4.2 Geotechnical Structure Variables for Estimation of Resilient Modulus

Several analytical and empirical models have been proposed to estimate the resilient modulus,  $M_R$ , of soil under various moisture and stress states; some being simple and empirical whereas other being complex and mechanistic (e.g., Yang et al. 2005, Liang et al. 2008, Cary and Zapata 2010, Seed et al. 1967, Khoury and Zaman 2004, Khosravifar et al. 2015). To date, the most commonly used equation is the extended version of Mechanistic-Empirical Pavement Design Guide (MEPDG) equation for resilient modulus at optimum water content from the results of extensive experimental material evaluation (Zapata et al. 2007). In this method, Equation 3-14 is used to determine resilient modulus at any degree of saturation by adjusting the resilient modulus at optimum water content.

$$\log \left( \frac{M_R}{M_{R-OPT}} \right) = a + \frac{b - a}{1 + \exp \left[ \ln \left( -\frac{b}{a} \right) + k_m (S - S_{OPT}) \right]}$$

Equation 3-14

where  $S_{OPT}$  = degree of saturation at optimal water content (in decimals);  $a$  = minimum of  $\log (M_R/M_{R-OPT})$ ;  $b$  = maximum of  $\log$ - $\log (M_R/M_{R-OPT})$ ; and  $k_m$  = regression parameter. Parameter values  $a = -0.5934$ ,  $b = 0.4$ , and  $k_m = 6.1324$  are suggested for fine-grained soils, and parameter values  $a = -0.3123$ ,  $b = 0.3$ , and  $k_m = 6.8157$  are suggested for coarse-grained soils.  $M_{R-OPT}$  can be estimated based on soil type and properties, laboratory tests, or back calculated from field tests (e.g., Falling Weight Deflectometer, FWD) (Christopher et al. 2006).

Equation 3-14 was implemented in the SD model to capture the moisture variation impacts on the resilient modulus of base aggregate, subbase and subgrade layers. The proposed geotechnical structure for a given layer of pavement is presented in Figure 3-12. The proposed SD model uses the estimated values of degree of saturation from hydrological analysis and  $M_{R-OPT}$  and fitting parameters in Equation 3-14 to estimate moisture-dependent  $M_R$  for each pavement layer and at each time step.

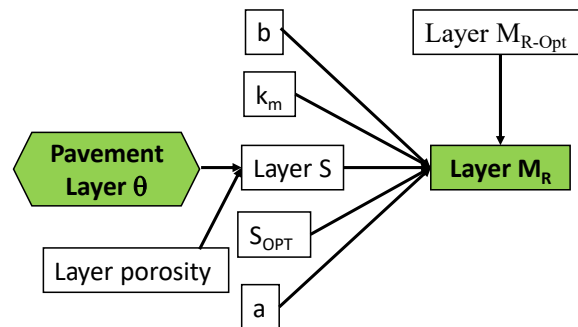


Figure 3-12: The geotechnical structure of the proposed SD model.

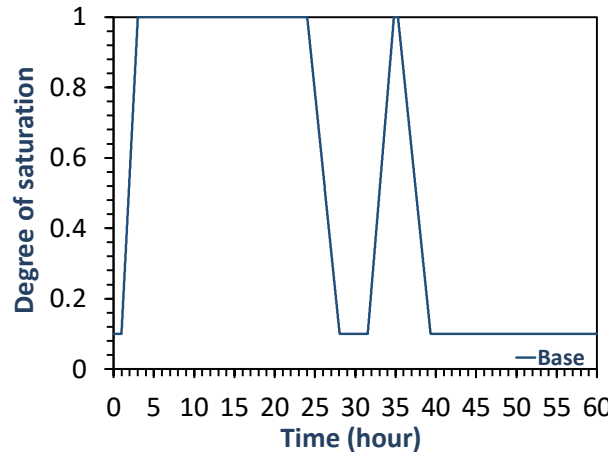
### 3.4.3 Simulation of Geotechnical Structure for the Conventional Flexible Pavement example

The conventional flexible pavement example introduced in Chapter 9 in conjunction with the hydrological solution presented in Chapter 10 under the given precipitation scenario was simulated in Vensim PRO®. This will highlight the capability of the proposed SD model to estimate  $M_R$  variation with moisture movement in pavement layers. In this regard, a set of typical mechanical properties were assigned to the pavement layers (as presented in Table 3-3). The initial moisture-dependent properties were estimated according to the initial moisture distribution in Chapter 10 and were concurrently updated throughout the simulation as moisture moved through the soil layer.

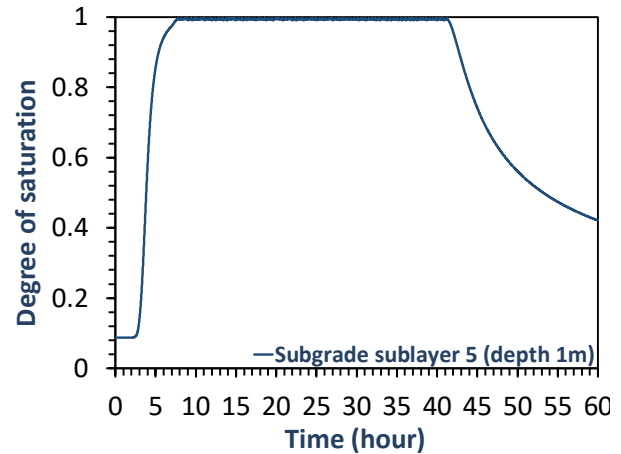
**Table 3-3: Mechanical properties of pavement layers.**

Property/parameter (at optimum moisture content)	value
Base resilient modulus ( $M_{R,B-OPT}$ )	200 MPa (~30 ksi)
Subbase resilient modulus ( $M_{R,SB-OPT}$ )	137 MPa (~20 ksi)
Subgrade resilient modulus ( $M_{R,Sg-OPT}$ )	70 MPa (~10 ksi)
$a$	-0.3123
$b$	0.3
$K_m$	6.8157

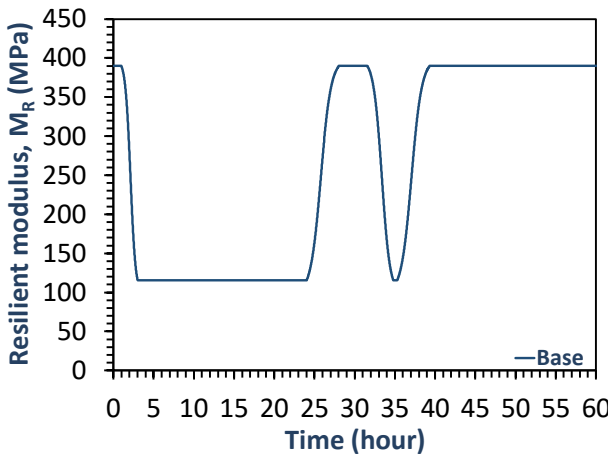
Figure 3-13 illustrates the results of SD simulation for analysis of moisture-dependent resilient modulus variation with moisture movement in the conventional flexible pavement example. The resilient modulus time histories are presented along with the degree of saturation time histories for the base aggregate layer and the 5<sup>th</sup> subgrade layer (located 1 m above the seasonally normal GWT). A comparison of the resilient modulus time histories with moisture showed good agreement between the trends observed in both figures. This suggests that the SD model could successfully capture the interaction between geotechnical and hydrological structures. The resilient modulus of the base aggregate layer decreased to almost a quarter of its initial value when the first period of raining resulted in full saturation of the base aggregate from its initial degree of saturation. The SD model predicted full recovery of the base layer's resilient modulus after approximately 16 hours from the end of the first period of precipitation followed by a sudden drop during the second period of raining. This was in a very good agreement with the degree of saturation variation with time. Similar results were also observed for the selected subgrade layer. In general, results showed the capability of geotechnical structure to capture the effect of moisture movement on the subgrade resilient modulus. Specifically, simultaneous simulation of hydrological and geotechnical structures enabled real time prediction of moisture movement as well as resilient modulus variations based on climate forecast.



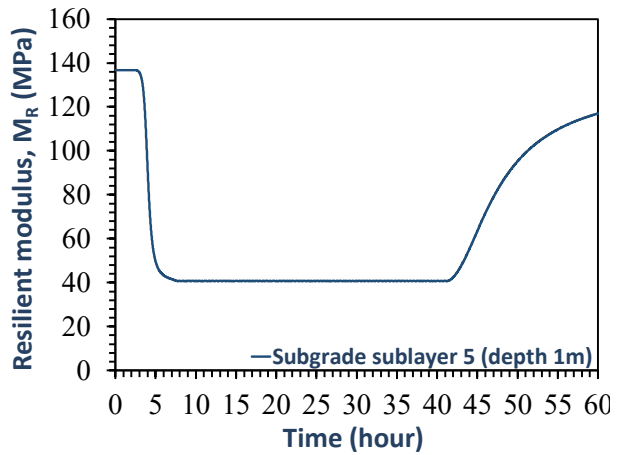
(a)



(c)



(b)



(d)

**Figure 3-13: Results of geotechnical structure simulation using the SD model formulated in Vensim PRO®. Results show (a) base aggregate saturation; (b) base aggregate resilient modulus time history; (c) subgrade layer 5 saturation; and (d) subgrade layer 5 resilient modulus time history.**

### 3.5 PAVEMENT RESPONSE STRUCTURE MODEL

#### 3.5.1 Introduction

In the proposed framework, the pavement surface deflection will be considered as an indicator of the overall pavement load carrying capacity. This choice was based on the literature review, pavement surface deflection under loading is often able to quickly discern safe passage of a vehicle versus of that where unsafe conditions in terms of pavement failure may prevail. Furthermore, pavement surface deflection has been shown in other previous researches on post-flooding assessment as a reliable indicator of damage potential to roadways due to allowance of traffic before full recovery. Deflection of pavement surface layer during moisture variation requires real time information on moisture-dependent mechanical properties of pavement layers, current pavement condition (i.e., age and distresses), and traffic



information. The pavement response structure considers the interaction between all these components to estimate real-time surface deformation of pavement considering moisture movement in pavement layers. Therefore, a pavement structure should incorporate the real time moisture movement and pavement layers' mechanical variables from hydrological and geotechnical structures to estimate surface deflection based on traffic and current pavement condition information. This chapter describes the main components of pavement structure and the methodology to estimate the pavement surface deflection during moisture variation.

### 3.5.2 Main Components of Pavement Response Structure

---

#### Traffic information

There are two approaches to determine the expected loads on the given pavement over its entire design life. One approach is to convert all magnitudes of loading and repetitions of loading to an equivalent unit using approaches such as equivalent damage; a commonly used example for this is equivalent single axial load (ESAL). The other approach is to use a load spectrum, which characterizes loads directly by number of axles, configuration, and weight. The latter method is typically more complex since the structural analysis requires the use of each vehicular combination to be evaluated to obtain relevant responses. Both methods follow standard equations and/or procedures that have been well laid out in the literature (such as, AASHTO, 1993 and FHWA, 2019). For the proposed SD framework, the use of ESAL approach is not appropriate, since the damage potential from each vehicle type needs to be evaluated. Thus, vehicle class-based traffic inputs can be more appropriate for the current system. In this regard, the 13-category FHWA vehicle classification was adopted (FHWA, 2014). The traffic variables include axle loads, axle configurations, and tire pressures.

#### Pavement structural performance

Historically, different methods have been proposed to analyze the structural performance of pavement systems. The use of multilayer analysis, specifically layered elastic analysis, is the current state-of-the-practice in the majority of flexible pavement analysis and design systems (such as, MnPAVE, PavementME, CalME etc.). However, the use of these methods requires an iterative numerical scheme, which is not easily implementable in Vensim Pro®. Thus, the use of a closed form solution such as Boussinesq (1885)'s theory for an elastic half-space was considered in this research. In this regard, Odemark's Equivalent Thickness Method (ETM) was employed to reduce the multilayer elastic pavement system to an equivalent single half-space layer (Ullidtz 1987). ETM is also used in MnPAVE to reduce multiple asphalt concrete layers into single layer. ETM uses each layer's elastic modulus ( $E$ ) and Poisson ratio ( $\nu$ ) to convert the layered pavement system to a single homogenous half-space layer according to Equation 3-15:

$$H_{Eq} = H_n + \sum_i^n C_i H_i \left[ \frac{E_i(1 - \nu_n^2)}{E_n(1 - \nu_i^2)} \right]^{1/3}$$

Equation 3-15

Where  $H_{Eq}$ , is the equivalent thickness of pavement layers,  $H_n$  is the thickness of layer  $n$  with young's modulus=  $E_n$  and Poisson ratio=  $\nu_n$ , and  $H_i$  is the thickness of layer  $i$  with young's modulus=  $E_i$  and Poisson ratio=  $\nu_i$ , and  $C_i$  is a fitting parameter and depends on the ratio of modulus of the equivalent pavement ( $E_n$ ) and the pavement layer thickness ( $E_i$ ). Preliminary analyses using Equation 3-15 and layered elastic analysis software (e.g., WinJULEA) indicated less than 20% error in stress distribution estimations when  $E_n = E_{Subgrade}$ ,  $\nu_n = \nu_{Subgrade}$ , and  $C_{HMA} = 0.5$ ,  $C_{Base} = 0.7$ ,  $C_{Subbase} = 0.85$ , and  $C_{subgrade} = 1$ . Equation 3-15 converts each pavement layer to a new layer with equivalent thickness and mechanical properties to ones in layer  $n$ . The total equivalent pavement thickness is obtained by summation of equivalent thicknesses of all the layers. The stress distribution and vertical strain in each layer can then be calculated using Boussinesq (1885) theory for a homogenous and isotropic linear elastic half-space system in axisymmetric condition (Equation 3-16, Equation 3-17, and Equation 3-18):

$$\sigma_z = q \left( 1 - \frac{z^3}{(a^2 + z^2)^{1.5}} \right)$$

Equation 3-16

$$\sigma_r = \frac{q}{2} \left[ 1 + 2\nu_i - \frac{2(1 + \nu_i)z}{(a^2 + z^2)^{0.5}} - \frac{z^3}{(a^2 + z^2)^{1.5}} \right]$$

Equation 3-17

$$\epsilon_z = \frac{1}{E_z} [\sigma_z - \nu_z(2\sigma_r)]$$

Equation 3-18

where  $a$  is the equivalent tire radius and is calculated based on wheel load and tire pressure ( $q$ ),  $\epsilon_z$  is the vertical strain at depth  $z$ ,  $\sigma_r$  is the horizontal stress, and  $E_z$  and  $\nu_z$  are the young modulus and Poisson ratio of layer  $i$  located at depth  $z$ . Vertical strain in each layer is multiplied to layer thickness to obtain layer deflection, cumulation of these deflections provide surface deflection. The SD model calculates the deflections imposed by each wheel to estimate maximum deflection using the superposition principle. The conceptual structure for simulation of pavement response is shown in Figure 3-14.

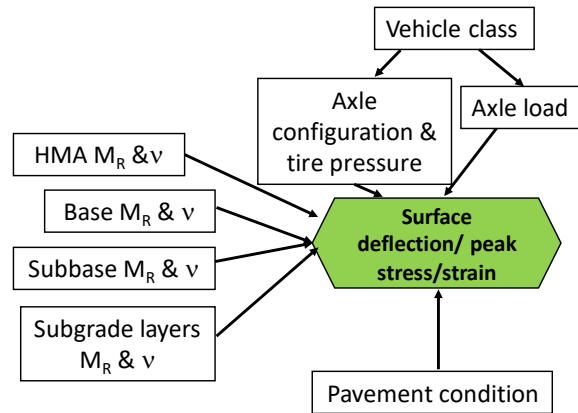


Figure 3-14: Surface deflection simulation using the SD model in Vensim PRO®.

### 3.5.3 Simulation of Pavement Response Structure for the Conventional Flexible Pavement Example

The previously described pavement system example is used to evaluate the ability of the pavement response structure to simulate the impact of moisture movement on pavement deflection under traffic load. In this regard, the pavement response structure was incorporated in the SD model to connect all three structures (i.e., hydrological, geotechnical, and pavement response) and simultaneously evaluate the impact of moisture variations on different variables in the system. The mechanical properties of the pavement layers for the deflection analysis were assumed to be as shown in Table 3-4. The effect of pavement age and existing distresses will be accounted for by adjusting these mechanical properties. In the current example, no adjustments were made.

**Table 3-4: Mechanical properties of pavement layers.**

properties	value
AC resilient modulus ( $M_{R,AC}$ )	2500 MPa (~360 ksi)
AC Poisson's ratio ( $\nu_{AC}$ )	0.35
Base Aggregate Poisson's ratio ( $\nu_B$ )	0.3
Subbase Poisson's ratio ( $\nu_{Sb}$ )	0.3
Subgrade Poisson's ratio ( $\nu_{Sg}$ )	0.4

**Table 3-5: Traffic load information for the pavement example.**

Traffic information	Value
Tire pressure	550 kPa (80 psi)
Wheel load	45 kN (10 kips)

The flexible pavement system's surface deflection was analyzed in Vensim PRO® under the given precipitation scenarios in Chapter 10. The analysis was performed for a single tire with loading characteristics presented in Table 3-5. The SD model used the moisture-dependent properties of pavement layers obtained from hydrological and geotechnical structures to simulate deflection of pavement surface at each time step using the assumed traffic and mechanical material properties. Figure 3-15 presents results of surface deflection simulation of the flexible pavement example. Results showed a very good agreement between trends in surface deflection and moisture and resilient modulus variations in the pavement layers. The full saturation of the pavement layers resulted in almost a 150% increase in surface deflection during both periods of raining. The results showed that although the surface deflection partially recovers after 20 hours from the first period of precipitation, the second period of precipitation, even with a lower rate and duration, could result in full saturation of pavement layers and significant increase in deflection and thus vehicular traffic during this duration can potentially damage the

pavement foundation. This highlighted the significant importance of simulating pavement systems in context of SD to capture real time, post-inundation pavement response using forecasted climate data.

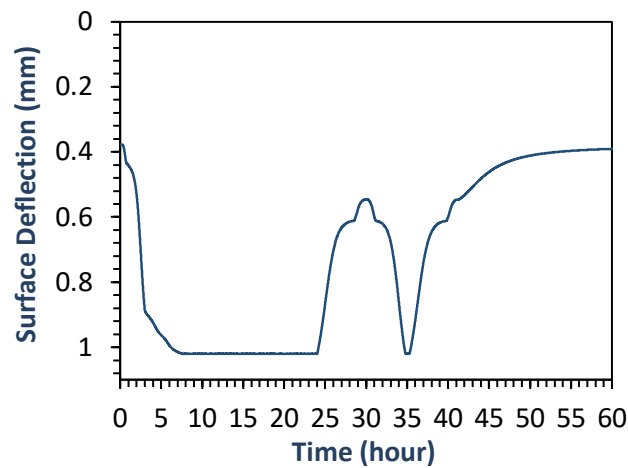


Figure 3-15: Surface deflection simulation using the example pavement SD model.

## 3.6 SYSTEM DYNAMICS FRAMEWORK SUMMARY AND CONCLUSIONS

### 3.6.1 Summary and Conclusions

A SD model was developed to simulate the real time behavior of pavement systems due to moisture variations. Three main structures including hydrological, geotechnical, and pavement response structures were identified to be crucial to develop the SD model. A detailed discussion on components and variables required to model each structure and the interaction between them was provided in this chapter. A practical example of a conventional flexible system, simulated using the developed SD model, was also provided to highlight the suitability of the SD model to address this problem. Figure 3-16 illustrates a big picture of the SD model structures and variables along with the typical results of the conventional flexible pavement example. The new SD model could holistically incorporate pavement structure, climatic forecast, traffic loads, and moisture movement processes within a pavement system. The comparison between input variables and output charts using the developed SD model indicated the capability of the model to simultaneously model interactions between hydrological, geotechnical, and pavement response structures.

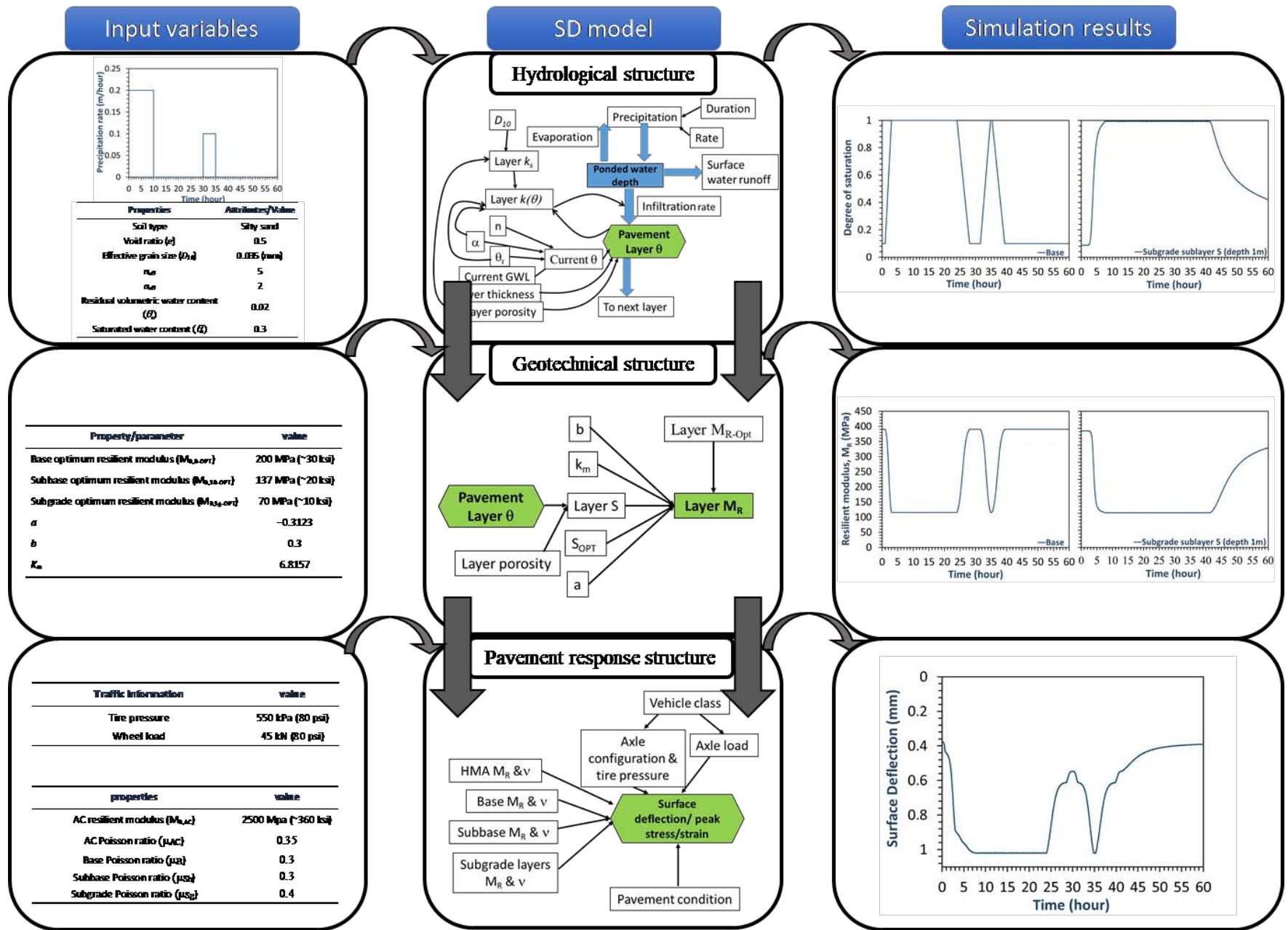


Figure 3-16: A big picture of the SD model structures and variables along with the typical results of the conventional flexible pavement

## CHAPTER 4: SENSITIVITY ANALYSIS AND FRAMEWORK REFINEMENT

This chapter is organized in six sections and one appendix (Appendix B). The subsequent six chapters review the developed system dynamics model along with a set of sensitivity analysis. This includes a brief overview of the developed system dynamics model for evaluating pavement response to traffic loading during moisture variations that was previously discussed in chapter 3 in detail, the methodology for sensitivity analysis, local sensitivity analysis to identify the important parameters, and global sensitivity analysis to identify main contributors in overall system response. Lastly, a summary is provided that highlights the key findings from the proposed system dynamics framework.

### 4.1 OVERVIEW OF THE DEVELOPED SYSTEM DYNAMICS FRAMEWORK

#### 4.1.1 Introduction

---

A System dynamics-based approach was adopted in this study to integrate and understand complex interaction of key factors affecting the overall performance of flexible pavements prone to moisture variations. The model was developed to simulate the real time behavior of pavement systems due to moisture variations. Three main structures including hydrological, geotechnical, and pavement response structures were identified to be crucial in order to develop the System dynamics model (SDM). A detailed discussion on components and variables required to model each structure and the interaction between them was provided in previous chapter. This chapter briefly review the developed SDM and its key components in simulating moisture movement and pavement system performance during moisture variations. In addition, the improvements in the framework are discussed in this chapter.

#### 4.1.2 Developed System Dynamics Framework

---

Figure 3-4 presented the three major structures of the SDM and the interaction between them and their variables. The first step in the mechanistic analysis of pavement response to moisture variations is the simulation of moisture movement in pavement layers. This is performed through the hydrological structure. The hydrological structure consists of two main components: (1) climate information and (2) unsaturated soil hydraulics. The climate information provides material and information data that controls water flux into and out of the soil surface (i.e., flows associated with water infiltration and discharge). A summary of the input variables associated with the climate information is provided in Table 4-1: A summary of the variables associated to climate information.

**Table 4-1: A summary of the variables associated to climate information.**

Climate information	Variables	Note
Precipitation	Rate ( $P_r$ ) and duration ( $P_d$ )	Can be input based on real or forecast precipitation time history
Evaporation	Rate ( $E_r$ )	Can be input based on real or forecast evaporation time history
Ponded water	Height of accumulated water above natural subgrade ( $H_p$ )	Can be input based on real or forecast climate condition
Surface water runoff	Rate ( $SR_r$ )	Zero for pavements located on “flat natural ground” with poor drainage system, otherwise equals precipitation minus infiltration and evaporation

The second component in hydrological structure of the SDM is the unsaturated soil hydraulics. This component includes the variables and governing equations related to estimation of initial pavement layers' moisture content, moisture movement in unsaturated pavement layers, and their time dependent moisture content. The initial moisture content of the layers is estimated based on layers' soil water retention curve (SWRC) data and initial groundwater level (GWL) where GWL is defined as the depth of groundwater from subgrade soil surface. It is noteworthy that the infiltration process in this study was assumed to occur through pavement shoulders. Since the permeability of aggregate base and subbase layers are typically much higher than natural subgrade soil, the infiltration of water through these layers may result in ponding of water above subgrade layer. Therefore, the degree of saturation in these layers is governed by both water infiltration in these layers and ponded water height above the subgrade. Accordingly, the aggregate base and subbase layers' degree of saturation are calculated based on the weighted average of the inundated portion and the unsaturated portion of each layer. The moisture movement in subgrade soil is governed by its hydraulic properties including saturated and unsaturated hydraulic conductivity and moisture content. The methodology and governing equations for simulating moisture movement in unsaturated subgrade layers and estimating their time dependent moisture content were elaborated in previous chapters. A summary of input parameters for unsaturated soil hydraulic component of the hydrological structure is provided in Table 4-2.

The second structure in the SDM is the geotechnical structure. The geotechnical structure incorporates the time dependent moisture content of pavement layers estimated from the hydrological structure to estimate their resilient modulus. This is performed by using Equation 3-14 which estimates unbound pavement layers' resilient modulus ( $M_R$ ) based on their resilient modulus at the optimum degree of saturation ( $M_{R-OPT}$ ) (Zapata et al. 2007).

$$\log \left( \frac{M_R}{M_{R-OPT}} \right) = a + \frac{b - a}{1 + \exp \left[ \ln \left( -\frac{b}{a} \right) + k_m (S - S_{OPT}) \right]}$$

Equation 4-1

where  $S_{OPT}$ = degree of saturation at optimal water content (in decimals);  $a$ = minimum of log ( $M_R/M_{R-OPT}$ );  $b$ = maximum of log-log ( $M_R/M_{R-OPT}$ ); and  $k_m$ = regression parameter. Table 4-3 summarizes the required input values for geotechnical structures and their values.

Table 4-2: Required input parameters for simulation of moisture infiltration through the SDM.

Parameters	Description	Note
$K_s$	Pavement layer saturated hydraulic conductivity	Required for aggregate base, subbase, and subgrade. Can be estimated based on empirical equations.
$\alpha_{vG}$ and $n_{vG}$	van Genuchten 1980 SWRC fitting parameters	Required for subgrade.
$\theta_r$	Pavement layer residual volumetric water content	Required for aggregate base, subbase, and subgrade.
$\theta_s$	Pavement layer saturated water content	Required for aggregate base, subbase, and subgrade.
Initial GWL	Initial groundwater level	-
Th <sub>Base</sub>	Base thickness	-
Th <sub>Subbase</sub>	Subbase thickness	-

Table 4-3: Required input parameters in the geotechnical structure of the SDM.

Parameters	Value/note
$a$	=-0.3123 for coarse grained soils =-0.5934 for fine grained soils
$b$	=0.3 for coarse grained soils =0.4 for fine grained soils
$S_{OPT}$	Depends on soil type/initial conditions. Can be estimated based on empirical equations.
$k_m$	6.8157
$M_{R-OPT}$	Can be estimated based on pavement layer type and properties, or obtained from field/lab tests



Lastly, the pavement response structure incorporates the results of hydrological and geotechnical structures along with traffic load information to predict pavement response in terms of surface deflection time history. The input variables required to estimate pavement response include those related to mechanical pavement layers properties and traffic loading. A summary of these parameters is presented in Table 4-4.

**Table 4-4: Required input parameters in the pavement response structure of the SDM.**

parameter	Note
Asphalt concrete resilient modulus ( $M_{R,AC}$ )	Depends on pavement current condition
Asphalt concrete thickness ( $Th_{AC}$ )	-
Layer Poisson's ratio ( $\nu$ )	Required for each pavement layer
Tire pressure	Depends on vehicle type
Wheel load	Depends on vehicle type

#### 4.1.3 Summary

This section reviewed the structures and components of the developed system dynamics model for evaluation of surface deflection of flexible pavement systems during moisture variations. In general, 32 input variables are required to estimate surface deflection of a flexible pavement system during moisture variations. These variables are subject to uncertainty, so sensitivity analysis is an important task for understanding the significance of each parameter on the SDM output and the reliability of simulation results. Following sections describe comprehensive sensitivity analyses and statistical modeling to address this challenge.

## 4.2 METHODOLOGY FOR SENSITIVITY ANALYSIS

### 4.2.1 Introduction

Accurate estimation of pavement performance during moisture variations relies on a sound understanding of the key contributing parameters and their interaction in the system. However, the collection of accurate information about all contributing parameters, such as subgrade hydraulic conductivity, may not be feasible. Large number of variables and their interaction within the system, and high uncertainties in their values warrant a detailed understanding of the significance of various uncertainties on the performance of flexible pavements. This can be addressed by sensitivity analysis which shed light on how variations in output (i.e., surface deflection) can be apportioned to different source of variations (e.g., subgrade hydraulic conductivity). Furthermore, sensitivity analysis not only determines the significance of each parameter on the model output, but it also helps to develop intuition

about model structure and guides the data collection efforts based on significance of the parameter of interest. In other words, the sensitivity analysis could identify the need for additional data collection for the parameters that significantly impact the output behavior (Saltelli et al. 2008).

Uncertainties in physical phenomena are often analyzed using two major sensitivity analyses approaches; (1) local sensitivity analysis method (LSA), and (2) global sensitivity analysis (GSA) (Tang et al. 2007; Wei 2013). The LSA techniques are also referred as to univariate sensitivity analysis and commonly investigate the individual effects of each input parameter while other parameters are maintained at a reference value. Although these methods require relatively low computational demand, the sensitivity results are dependent on and may only be valid for the select reference values. For the systems with high number of variables, such as flexible pavement systems, nonlinear interactions among variables may become more significant. The local sensitivity analysis methods, however, are not able to capture this. On the other hand, global sensitivity analysis methods use a multivariate analysis approach and consider a wide range of variables and the high-ranking interaction between them. Considering that a large number of input parameters are involved in the SDM, GSA methods require a significantly large number of simulations to reliably identify the significance of each parameter. However, this is not computationally feasible. In order to address this challenge, an LSA was first performed to understand the significance of each input parameter in overall system behavior (i.e., surface deflection time history). Then, the most significant parameters were identified and refined to conduct a GSA. Following sections describe the methodologies for performing LSA and GSA in this study.

#### **4.2.2 Methodology for SDM Sensitivity Analysis**

---

Sensitivity analysis of a system response requires identification of independent input variables contributing to the overall system behavior. Therefore, the first step in sensitivity analysis was to identify independent input parameters in the SDM. Then, possible range of each input parameter was determined by using published information or assigning logical values. The next step was to use a sampling strategy to conduct simulations for the select range of the variables. Depending on the sensitivity analysis method (i.e., LSA versus GSA) several numbers of simulation were performed using the programed SDM in Vensim Pro® and the response was obtained in terms of surface deflection time histories. Since the behavior of the surface deflection is dependent on time, the evaluation of the sensitivity of response to select parameters was evaluated in terms of time dependent behavior and selected “performance measure indices”. The performance measure indices determine the key performance attributes during a moisture variation event (e.g., peak surface deflection during and after moisture variation event). Lastly, the results were statistically analyzed using regression method and each parameter was ranked based on its significant importance. The following sections provide relevant information about above mentioned steps.

##### **Selection of Input Parameters and Their Ranges**

The primary goal of this section is to identify the least number of interdependent variables and their ranges to run sensitivity analysis and to assign reference values for local sensitivity analysis. In general, 32 input variables were identified in the SDM. These include variables associated with the (1) climate data,

(2) unsaturated soil hydrology, (3) geotechnical structure, and (4) pavement response structure. For climate data, precipitation rate, duration, and evaporation rate were considered as independent variables for the sensitivity analysis. Surface water runoff which results in removal of excess moisture from the pavement foundation (i.e., AC, aggregate base, and subbase layers) was considered to be zero in this study. Table 4-5 summarizes the range of climate data input variables.

**Table 4-5: A summary of the climate input parameters and their ranges considered for sensitivity analysis.**

Variables	Ranges	Reference value
Precipitation rate ( $P_r$ )	0 to 0.1 m/hour (~0 to 4 inch/hour)	0.05 m/hour (~ 2 inch/hour)
Precipitation duration ( $P_d$ )	5 to 20 hours	10 hours
Evaporation rate ( $E_r$ )	0.0001 to 0.001 m/hour (~ 0.004 to 0.04 inch)	0.005 m/hour (0.2 inch/m)

The parameters required for unsaturated soil hydrological component and geotechnical structure of the SDM are to be selected for aggregate base and subbase, and subgrade soil. In this study, it was assumed that the aggregate base and subbase layers consist of granular material. Table 4-6 presents the reference values and the ranges of parameters for aggregate base and subbase layers.

Among the required input parameters for simulation of moisture movement in unsaturated subgrade layers, saturated hydraulic conductivity and van Genuchten (1980) SWRC model's fitting parameters are interdependent. In order to define independent parameters and their ranges for subgrade, these variables were estimated based on fundamental soil properties. Due to difference in material properties of fine-grained and coarse-grained soils, two types of subgrade soils were considered, and two sets of sensitivity analysis were performed, accordingly. The subgrade soil for the first set was assumed to be a coarse-grained soil (such as, fine sand) and the second set assumed a fine-grained soil with variable plasticity (representative of clayey or silty soil).

For the first set of sensitivity analysis, the hydraulic conductivity of sand was estimated based on its void ratio ( $e$ ) and effective grain diameter ( $D_{10}$ ); according to Equation 4-2 presented in Table 4-7. Parameters  $a_{vG}$  and  $n_{vG}$  were assumed to be linearly related to  $D_{10}$  where  $a_{vG}= 5 \text{ m}^{-1}$  at  $D_{10}= 0.07$ ,  $a_{vG}= 25 \text{ m}^{-1}$  at  $D_{10}= 0.42$ ,  $n_{vG}= 1.7$  at  $D_{10}= 0.07$ , and  $n_{vG}= 3.7$  at  $D_{10}= 0.42$ . Further, subgrade optimum resilient modulus ( $M_{R-OPT,Subgrade}$ ) was assumed to be linearly correlated to its void ratio where  $M_{R-OPT,Subgrade}= 50 \text{ kPa}$  at  $e= 0.8$  and  $M_{R-OPT,Subgrade}= 150 \text{ kPa}$  at  $e= 0.4$ . It should be noted that these assumptions are not intended to and may not provide an accurate estimation of the SWRC parameters and  $M_{R-OPT,Subgrade}$ . However, they can establish a logical interdependency between these parameters and soil properties for the purpose of sensitivity analysis. Table 4-8 presents the reference values and the ranges of parameters for the coarse-grained subgrade soil.

**Table 4-6: Base and subbase variables and their reference values.**

Parameters	Description	Range	Reference value
$K_{s,Base}$	Aggregate base hydraulic conductivity	12 to 160 m/hour (472 to 6300 inch/hour)	50 m/hour (~1968 inch/hour)
$K_{s,Subbase}$	Subbase hydraulic conductivity	4 to 40 m/hour (157 to 1574 inch/hour)	12 m/hour (~472 inch/hour)
$Th_{Base}$	Aggregate base thickness	0 to 0.5 m (0-20 inch)	0.3 m (~12 inch)
$Th_{Subbase}$	Subbase thickness	0 to 0.3 m (~0 to 12 inch)	0.1 m (~4 inch)
$a_{base}=a_{subbase}$	Equation 3-14 fitting parameters	-	-0.3123
$b_{base}=b_{subbase}$	Equation 3-14 fitting parameters	-	0.3
$S_{OPT-Base}$	Aggregate base optimum degree of saturation	-	0.45
$S_{OPT-Subbase}$	Subbase optimum degree of saturation	-	0.5
$M_{R-OPT,Base}$	Aggregate base optimum resilient modulus	200 to 300 MPa (~ 29 to 43 ksi)	250 MPa (~36 ksi)
$M_{R-OPT,Subbase}$	Subbase optimum resilient modulus	100 to 200 MPa (~14 to 29 ksi)	150 MPa (~22ksi)

**Table 4-7: Empirical relations for estimation of hydraulic conductivity of fully saturated soils.**

Reference	Equation number	Hydraulic conductivity (cm/s)	Notation	Remarks
(Chapuis 2004)	<b>Equation 4-2</b>	$k_s = 2.46[D_{10}^2 \frac{e^3}{(1+e)}]^{0.78}$	$e$ = void ratio of soil $D_{10}$ = effective grain diameter	Applicable for uniform gravel and sand and non-plastic silty sands
(Mbonimpa et al. 2002)	<b>Equation 4-3</b>	$k_s = C_p \frac{\gamma_w}{\mu_w} \frac{e^{3+x}}{(1+e)} \frac{1}{\rho_s^2 W_L^{2x}}$	$\gamma_w$ =unit weight of water (kN/m <sup>3</sup> ) $\mu_w$ = Water dynamic viscosity (Pa·s) $\rho_s$ = Density (kg/m <sup>3</sup> ) of solids $W_L$ = Liquid limit (%) $x = 7.7 W_L^{-0.15} - 3$	Applicable for plastic soils, $\gamma_w \approx 9.8$ , $\mu_w \approx 10^{-3}$ , $C_p=5.6$ , $\chi=1.5$

Table 4-8: Subgrade variables and their reference values for the first set of the sensitivity analysis.

Subgrade soil type/Parameters	Description	Range	Reference soil/value
Sand	SW/SP/A-1b/A-3	Fine to medium sand	Fine sand
$D_{10-subgrade}$	Subgrade effective grain diameter	0.07 to 0.42 mm (~0.003 to 0.017 inch)	0.24 mm (~0.01 inch)
$e_{Subgrade}$	Subgrade void ratio	0.45 to 0.75	0.6
$K_{s,Subgrade}$	Subgrade saturated hydraulic conductivity	correlated to $e$ and $D_{10}$ (See Equation 4-2)	2 m/hour (~78 inch/hour)
$\alpha_{vG}$	-	Linearly correlated to $D_{10}$	15
$n_{vG}$	-	Linearly correlated to $D_{10}$	2.7
$a_{Subgrade}$	Equation 3-14 fitting parameters	-	-0.3123
$b_{Subgrade}$	Equation 3-14 fitting parameters	-	0.3
$S_{OPT-Subgrade}$	Subgrade optimum degree of saturation	-	0.6
$M_{R-OPT,Subgrade}$	Subgrade optimum resilient modulus	linearly correlated to $e_{subgrade}$	100 MPa (~14.5 ksi)

For the second set of sensitivity analysis, the hydraulic conductivity of silt/clay was estimated based on its void ratio ( $e$ ) and liquid limit ( $w_L$ ); according to Equation 4-3 presented in Table 3-1. Parameters  $a_{vG}$  and  $n_{vG}$  were assumed to be linearly related to soil  $w_L$  where  $a_{vG}= 0.5 \text{ m}^{-1}$  at  $w_L = 40$ ,  $a_{vG}= 2 \text{ m}^{-1}$  at  $w_L = 5$ ,  $n_{vG}= 1.1$  at  $w_L = 40$ , and  $n_{vG}= 1.5$  at  $w_L = 5$ . Further, subgrade optimum resilient modulus ( $M_{R-OPT,Subgrade}$ ) was assumed to be linearly correlated to its void ratio where  $M_{R-OPT,Subgrade}= 10 \text{ kPa}$  at  $e= 1.5$  and  $M_{R-OPT,Subgrade}= 100 \text{ kPa}$  at  $e= 0.5$  present the reference values and the ranges of parameters for the fine subgrade soil.

The groundwater depth from subgrade soil surface was assumed to range between 1 to 5 m for the sensitivity analysis and was assumed to be located at 3 m for the reference model. The reference values and the ranges of the parameters considered for the pavement structure analysis is shown in Table 4-10.

**Table 4-9: Subgrade variables and their reference values for the second set of the sensitivity analysis.**

Subgrade soil type/Parameters	Description	Range	Reference soil/value
Clay/Silt	ML-CL/A-4 to A-6	Low plasticity silt/clay	ML
$w_{L,subgrade}$	Subgrade liquid limit	5 to 40	20
$e_{Subgrade}$	Subgrade void ratio	0.6 to 1.4	1
$K_{s,Subgrade}$	Subgrade saturated hydraulic conductivity	correlated to $w_L$ and $e$ (See Equation 4-3)	$1.8 \times 10^{-5}$ m/hour (~0.0007 inch/hour)
$\alpha_{vG}$	-	Linearly correlated to $w_L$	1
$n_{vG}$	-	Linearly correlated to $w_L$	1.3
$a_{Subgrade}$	Equation 3-14 fitting parameters	-	-0.59
$b_{Subgrade}$	Equation 3-14 fitting parameters	-	0.4
$S_{OPT-Subgrade}$	Subgrade optimum degree of saturation	-	0.85
$M_{R-OPT,Subgrade}$	Subgrade optimum resilient modulus- linearly correlated to $e_{subgrade}$	-	55 MPa (~8 ksi)

**Table 4-10: Pavement response structure variables ranges and their reference values.**

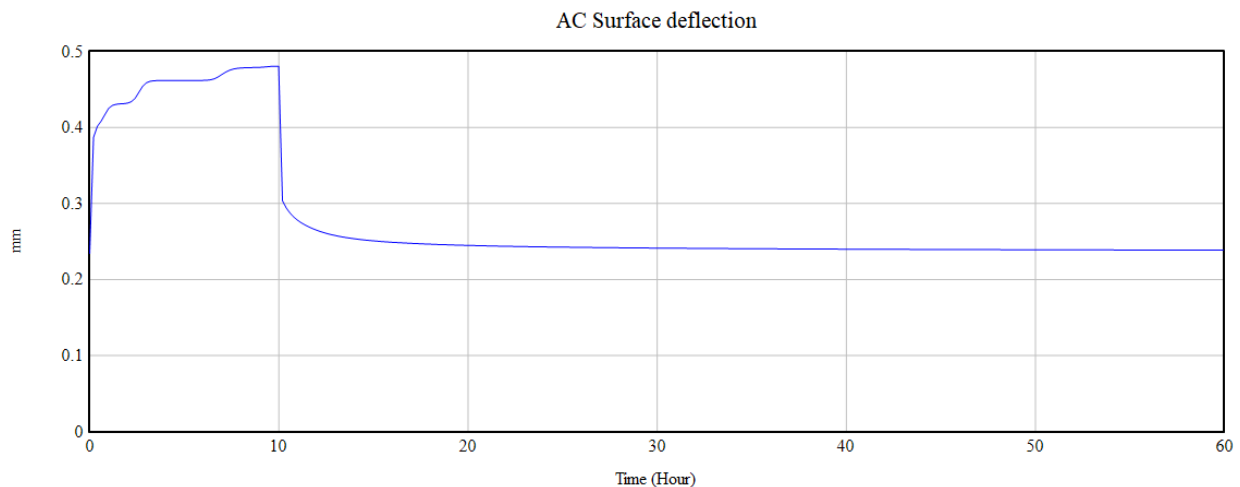
parameter	Range	Reference value
$M_{R,AC}$	700 to 7000 MPa	3000 MPa
$Th_{AC}$	0.05 to 0.5 m	0.15 m
AC Poisson's ratio ( $\nu_{AC}$ )	0.3 to 0.4	0.35
Aggregate base Poisson's ratio ( $\nu_{Base}$ )	0.25 to 0.4	0.3
Subbase Poisson's ratio ( $\nu_{Subbase}$ )	0.25 to 0.4	0.3
Subgrade Poisson's ratio ( $\nu_{Subgrade}$ )	0.3 to 0.5	0.4
Tire pressure	-	550 kPa
Wheel load	20 to 90 kN	45 kN

## Univariate and Multivariate Sensitivity Simulations

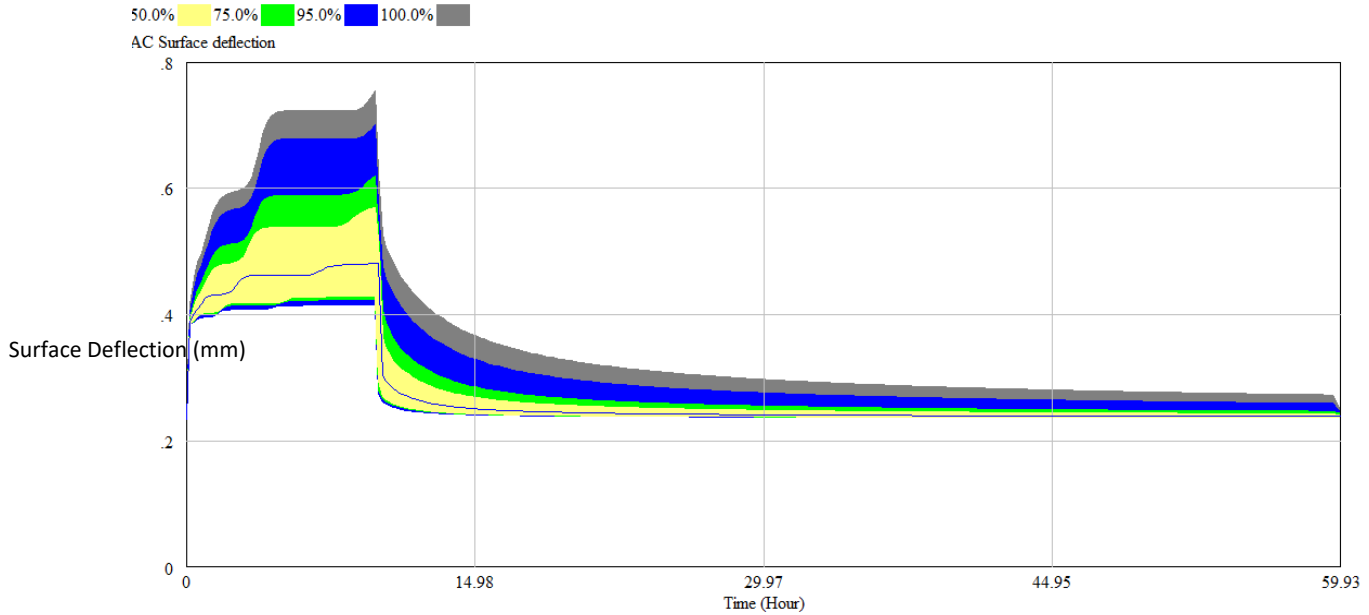
Selection of an appropriate sampling methodology is the next step in sensitivity analysis after determination of independent parameters and their ranges. There are several sampling strategies such as random sampling using Monte Carlo (MC) simulation and Latin Hypercube Sampling (LHS). Monte Carlo simulation randomly assign N points for the selected ranges of the variables. However, this method relies on pure randomness of the input and may be inefficient in capturing the response ranges (i.e., requires a large number of simulations to minimize sampling error). On the other hand, LHS method spread the sample points more evenly across all possible values. The LHS method was used in this study for the sensitivity simulations. The simulation assumed a random uniform distribution for the ranges of input variables. For the univariate sensitivity simulations, each parameter was changed while the other parameters were kept at the reference values. A minimum of 20 simulations were performed for each parameter using Vensim Pro® Sensitivity Simulation tool and the results were obtained in terms of surface deflection time history for each simulation. The multivariate sensitivity analysis was performed by simultaneously changing select variables using LHS method. This included 2000 simulations for each set of sensitivity analysis (i.e., coarse-grained subgrade and fine-grained subgrade).

## Selection of Performance Measure Indices

After performing each set of simulations, the sensitivity simulation data including values of the model parameters and surface deflection time histories were obtained for each simulation run. Further, Vensim Pro® shows the confidence bounds for select variable and simulation run. For example, Figure 4-1 presents the estimated asphalt concrete (AC) surface deflection time history assuming reference values for the coarse-grained subgrade and Figure 4-2 illustrate 50%, 75%, 95%, and 100% confidence bounds for the analysis of sensitivity of AC surface deflection to subgrade  $D_{10}$ .



**Figure 4-1. AC surface deflection time history of the coarse-grained subgrade reference model.**



**Figure 4-2. Sensitivity of AC surface deflection (mm) to subgrade  $D_{10}$ . Results show surface deflection time histories for 50%, 75%, 95%, and 100% Confidence bounds.**

While the results in terms of time history provide useful information about the time dependent performance of the flexible pavement under moisture variation, further analysis is required to statistically quantify the significance of each parameter on pavement performance. In this regard, the time dependent performance of pavement was evaluated using four key performance index measures including (1) peak surface deflection ( $\delta_p$ ), (2) Peak to initial surface deflection ratio ( $\delta_p/\delta_i$ ), (3) time to peak surface deflection ( $t_p$ ), and (4) Recovery time ( $t_{rec.}$ ). The peak surface deflection shows the maximum surface deflection that the pavement would experience during a moisture variation event. The peak to initial surface deflection ratio is the ratio of the peak surface deflection to the surface deflection right before precipitation (i.e., Hydrostatic condition). Time to peak surface deflection shows the time required to reach the peak surface deflection and lastly, the recovery time measures the time that it takes to reach 80% recovery from the peak surface deflection. The recovery is defined as the ratio of current surface deflection to the peak minus the initial surface deflection.



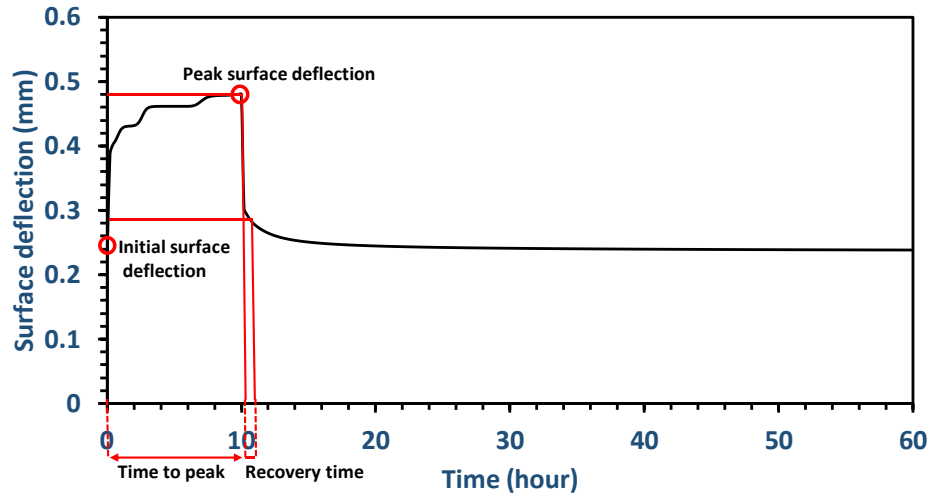


Figure 4-3. Performance measures used for sensitivity analyses.

## Statistical Analysis

The extracted data for sensitivity simulations including values of input parameters and key performance measures were used for statistical analysis. In this study, linear regression method was utilized to comparatively evaluate the importance of each input parameter for each performance measure. In this regard, the data were analyzed using JMP software and standard regression coefficients including PValue, LogWorth, and t-ratio were used for statistical comparison of the significance of the effect of each parameter on the given performance measure.

## 4.3 LOCAL SENSITIVITY ANALYSIS

### 4.3.1 Introduction

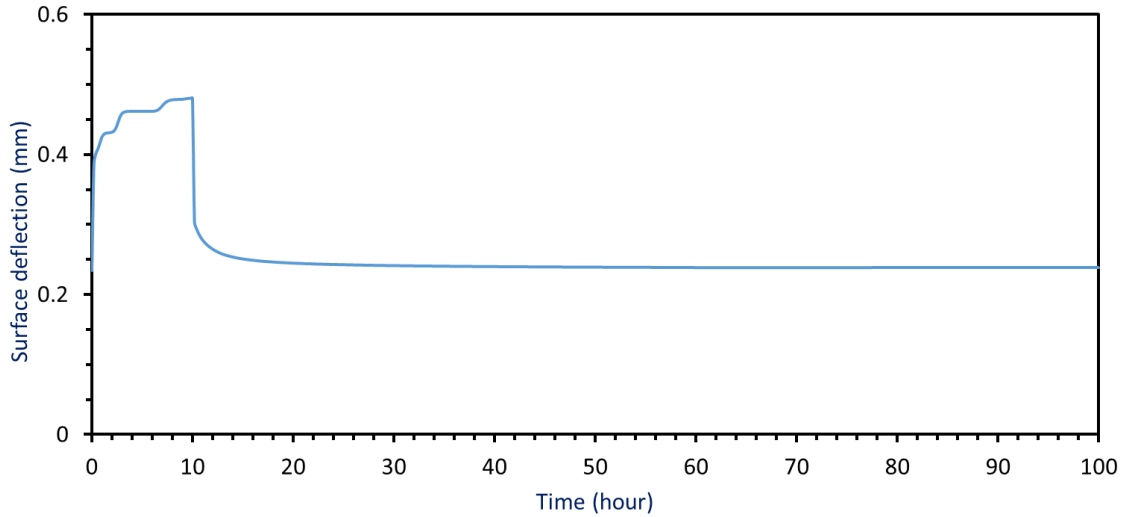
The local sensitivity analysis is intended to investigate the impact of uncertainty in individual variables on the system performance. This included two sets of sensitivity simulations for coarse-grained and fine-grained soils. The results were interpreted in terms of surface deflection time histories and performance measure indices introduced in Chapter 3. Following sections describe the local sensitivity analysis results for each set of simulations.

### 4.3.2 Local Sensitivity Analysis for Coarse-grained subgrade

#### Reference model response

Simulation of moisture variation impact on pavement surface deflection was performed using the developed SDM and the reference model values presented in Chapter 3. The results are shown in Figure 4-4. According to this figure, 10 hours of precipitation initially resulted in a dramatic increase in the AC

surface deflection followed by a gradual increase in surface deflection. This is followed by a relatively quick recovery of surface deflection after the end of precipitation. The main reason for such behavior is the high hydraulic conductivity of the pavement layers which resulted in movement of the excess moisture out of the pavement layers.



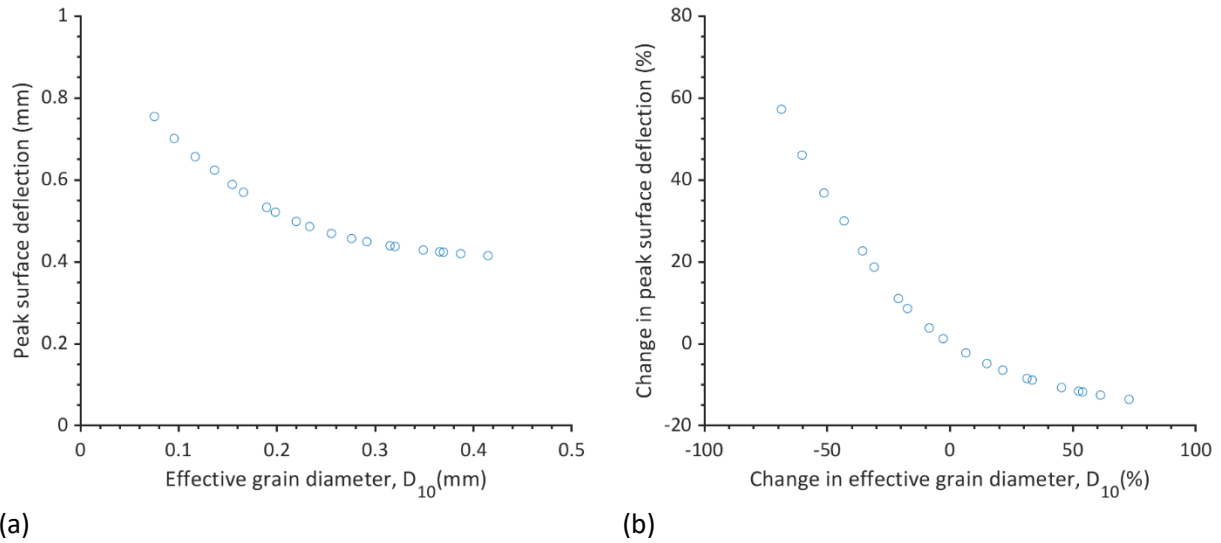
**Figure 4-4. AC surface deflection time history of the coarse-grained subgrade reference model.**

#### Univariate sensitivity simulation results

Univariate simulations were performed by changing an independent parameter while maintaining the other parameters at the reference model value. The reference model values and the ranges of each parameter for sensitivity simulations were reported in Chapter 3. The simulation results are interpreted and discussed in terms of key performance measures.

##### Sensitivity of peak surface deflection ( $\delta_p$ ):

Figure 4-5 presents the variations of peak surface deflection with subgrade  $D_{10}$ . Sensitivity simulations indicated that a reduction in  $D_{10}$  from the reference model value can considerably increase the peak surface deflection experienced during the moisture variation event (Figure 4-5a). According to Figure 4-5b, a 60% reduction in  $D_{10}$  resulted in almost 46% increase in  $\delta_p$ , compared to the value for reference model. However, the impact of  $D_{10}$  on  $\delta_p$  became less pronounced for  $D_{10}$  values higher than the reference value. For example, a 60% increase in  $D_{10}$  from the reference model resulted in only 12% reduction in  $\delta_p$  (Figure 4-5b). These results suggest that for relatively medium to coarse sand particles, an increase in particle size has less significant impact on the pavement performance during moisture variation events. However, a decrease in particle size can potentially elevate the chance of damage to pavement structure.



**Figure 4-5. Sensitivity of peak surface deflection to the variations of subgrade  $D_{10}$ . (a) Peak surface deflection versus  $D_{10}$ ; (b) change in peak surface deflection versus change in  $D_{10}$ .**

The sensitivity of  $\delta_p$  to subgrade void ratio was analyzed by changing void ratio values from 0.45 to 0.75. These values correspond to relative density,  $D_r = 12.5\%$  and  $87.5\%$ , respectively, for the given soil. Figure 4-6 presents the sensitivity simulation results in terms of percent change in  $\delta_p$  versus percent change in void ratio relative to the reference model values. The results indicate that a reduction in void ratio increases  $\delta_p$ . The main reason for this observation is that in the SDM, the subgrade soil void ratio would impact both subgrade resilient modulus and its hydraulic conductivity. Although a soil with lower void ratio would have higher resilient modulus at a given moisture content, it would have lower hydraulic conductivity. This would result in poor drainage of water and potentially, elevation of excess moisture in pavement structural layers. Thus, higher surface deflection observed for the soil can be attributed to its lower hydraulic conductivity which result in poor drainage of water and inundation of pavement structural layers.

Figure 4-7 illustrates the change in  $\delta_p$  with precipitation rate and duration. Results indicate that while a change in precipitation rate is likely to have a substantial impact on pavement surface deflection, a change in its duration between the ranges tested in this study (i.e., 5 to 15 hours) is less likely to impact the magnitude of  $\delta_p$ . The main reason for such observation is high hydraulic conductivity of the subgrade soil. In general, if the hydraulic conductivity of soil is higher than the precipitation rate, it is expected that the subgrade soil reaches the steady state infiltration at a given degree of saturation. In this case, an increase in precipitation duration would not impact the steady state degree of saturation of soil. However, a change in precipitation rate can alter the steady state infiltration rate and consequently the soil's degree of saturation.

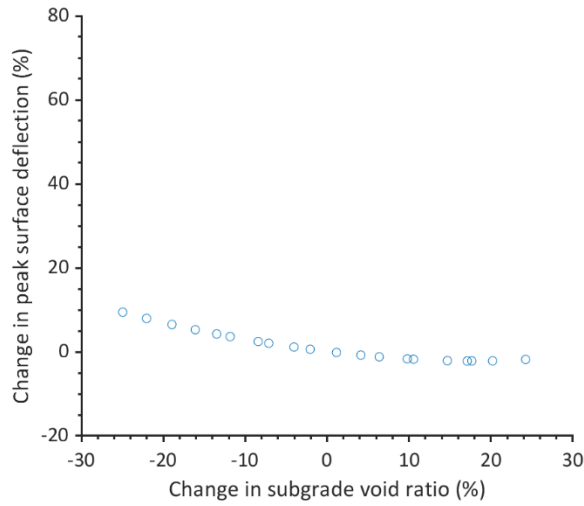


Figure 4-6. Sensitivity of peak surface deflection to the variations of subgrade void ratio.

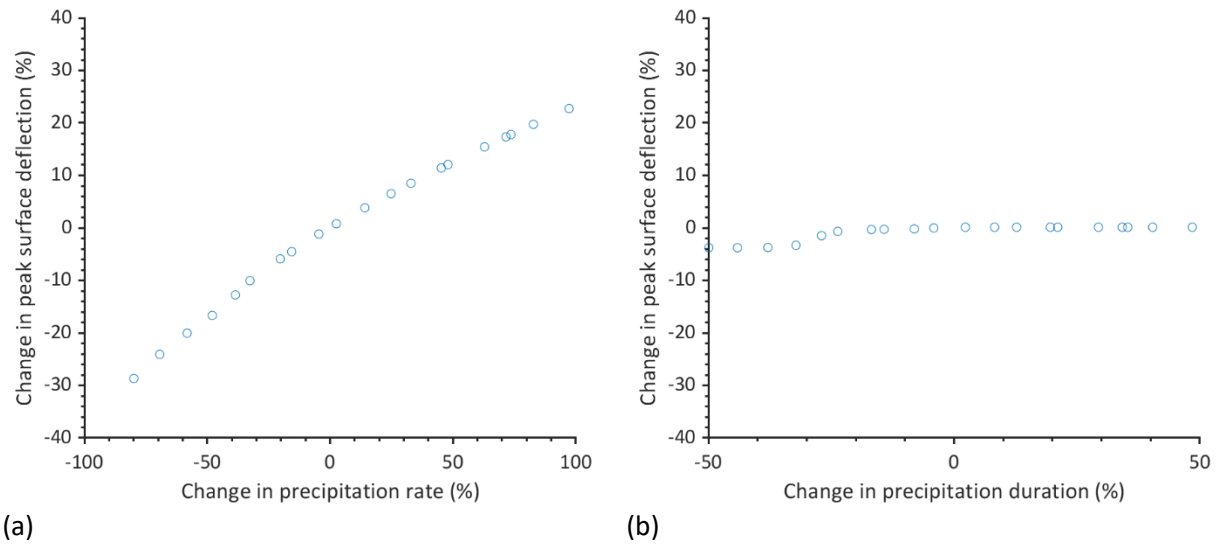
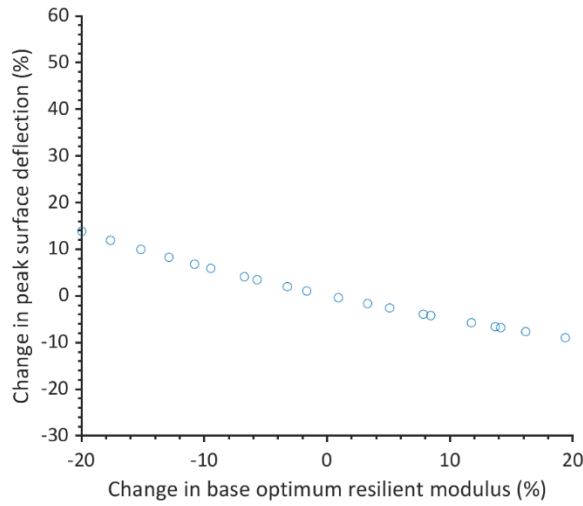
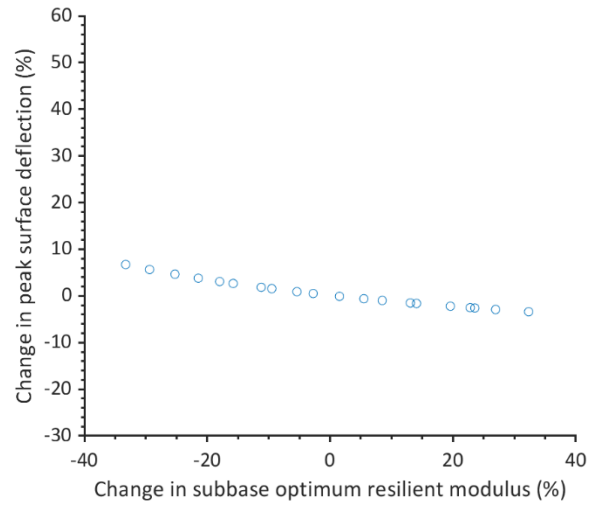


Figure 4-7. Sensitivity of peak surface deflection to the variations of precipitation (a) rate and (b) duration.

Figure 4-8 shows the results of sensitivity simulations for aggregate base and subbase optimum resilient modulus ( $M_{R-OPT,Base}$  and  $M_{R-OPT,Subbase}$ , respectively). Results indicate that  $M_{R-OPT,Base}$  and  $M_{R-OPT,Subbase}$  are inversely proportional to  $\delta_p$ . The comparison of  $M_{R-OPT,Base}$  versus peak surface deflection curves and those of subbase indicate that a change in  $M_{R-OPT,Base}$  would have higher impact on peak surface deflection than  $M_{R-OPT,Subbase}$ . Similar observations were also made for the comparisons of the impact of aggregate base and subbase thicknesses on peak surface deflection (Figure 4-9).

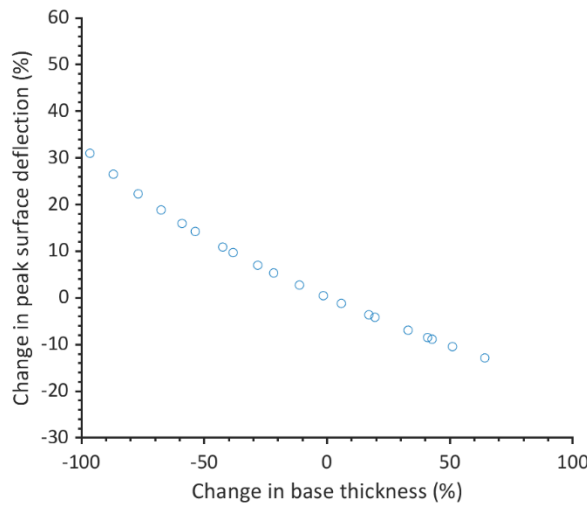


(a)

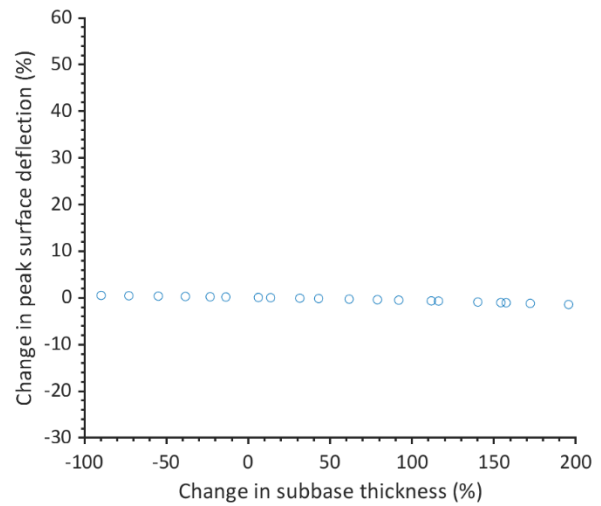


(b)

**Figure 4-8. Sensitivity of peak surface deflection to the variations of (a) aggregate base and (b) subbase optimum resilient moduli.**



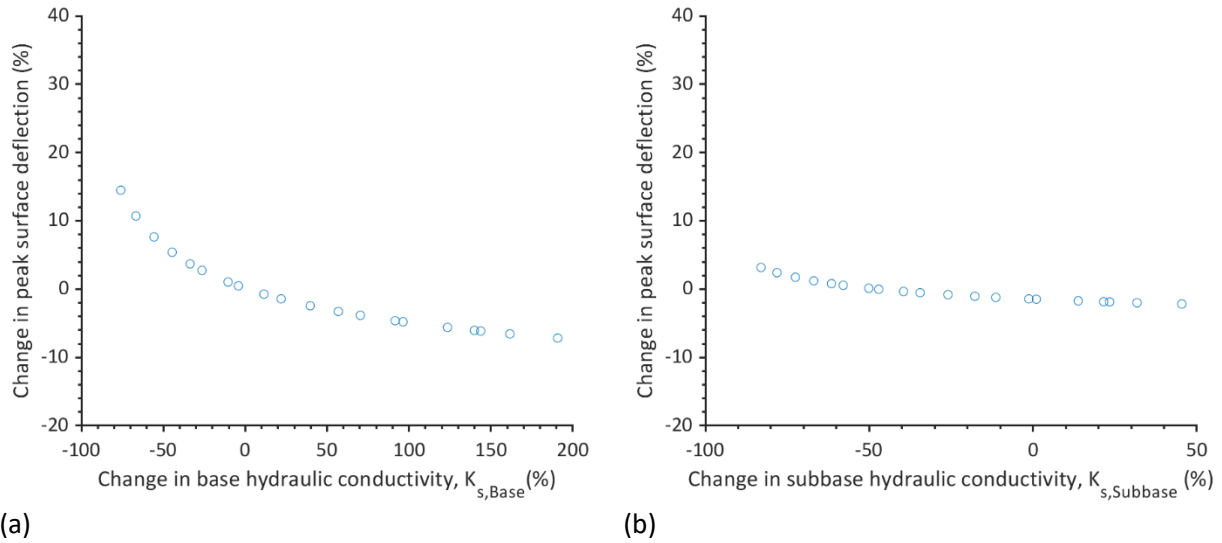
(a)



(b)

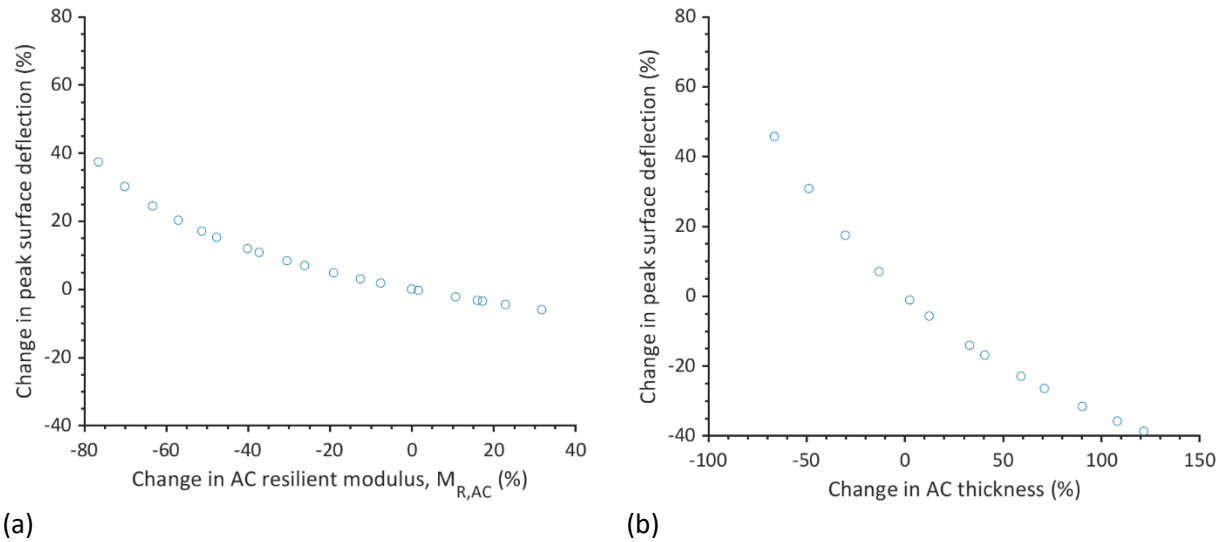
**Figure 4-9. Sensitivity of peak surface deflection to the variations of (a) aggregate base and (b) subbase thicknesses.**

Figure 4-10 presents variations in  $\delta_p$  with changes in aggregate base and subbase hydraulic conductivities ( $K_{s,Base}$  and  $K_{s,Subbase}$ , respectively). Results indicate a nonlinear relationship between peak surface deflection and  $K_{s,Base}$  and  $K_{s,Subbase}$ , where reduction in the hydraulic conductivity increases the peak surface deflection. The results also indicate that peak surface deflection is more sensitive to change in aggregate base hydraulic conductivity than subbase.



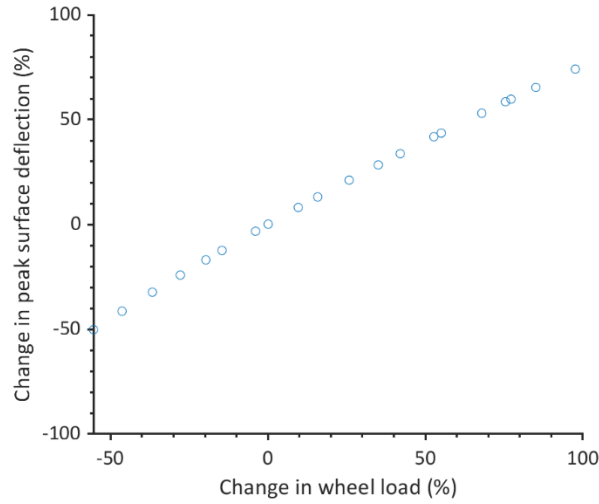
**Figure 4-10. Sensitivity of peak surface deflection to the variations of (a) aggregate base and (b) subbase hydraulic conductivities.**

Figure 4-11 presents the results of  $\delta_p$  sensitivity simulations to changes in asphalt concrete resilient modulus ( $M_{R,AC}$ ) and thickness ( $Th_{AC}$ ). Results show that a decrease in  $M_{R,AC}$  or  $Th_{AC}$  leads to a substantial increase in  $\delta_p$  during a moisture variation event. However, peak surface deflection is more sensitive to a change in  $Th_{AC}$  than  $M_{R,AC}$ .



**Figure 4-11. Sensitivity of peak surface deflection to the variations of (a)  $M_{R,AC}$  and (b)  $Th_{AC}$ .**

Figure 4-12 presents the variations of peak surface deflection with change in wheel load. Results indicate a substantial impact of wheel load on the peak surface deflection.

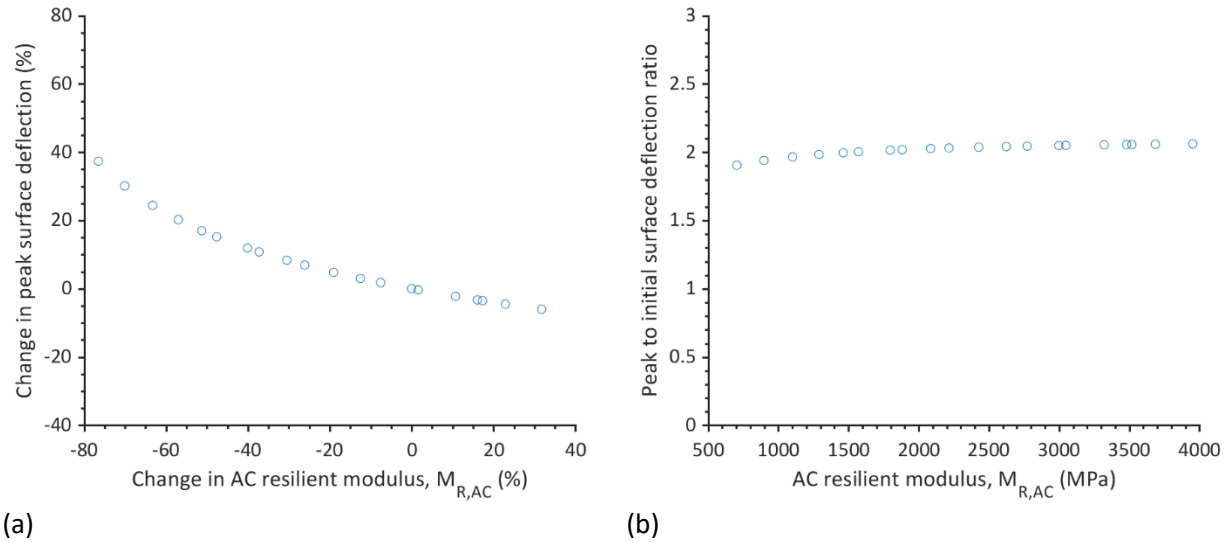


**Figure 4-12. Sensitivity of peak surface deflection to the variations of wheel load.**

For the ranges of GWL and layers'  $\nu$ , and the reference model considered in this study, the sensitivity analyses indicated minimal impact of these variables on the  $\delta_p$ . Results of sensitivity simulations for these parameters are shown in the Appendix B.

Sensitivity of peak to initial surface deflection ratio ( $\delta_p/\delta_0$ ):

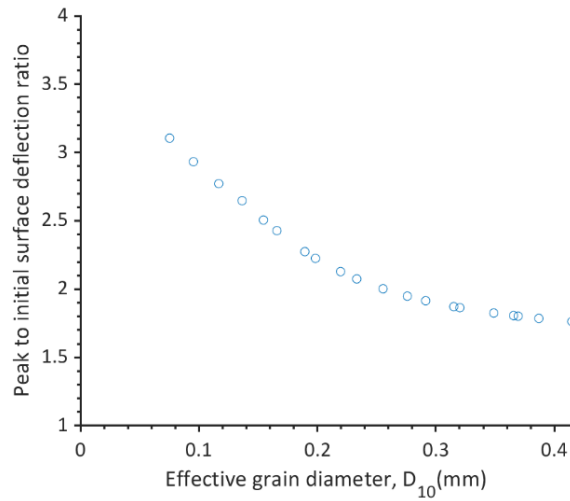
Although peak surface deflection provides a good information about the impact of a certain variable on general performance of pavement, it provides little information on the extent of its impact during moisture variation compared to initial condition. For example, increase in  $M_{R,AC}$  reduces both initial (i.e., before precipitation) and the peak surface deflection during moisture variation event. Therefore, peak surface deflection provides no information about the extent to which a change in  $M_{R,AC}$  would impact pavement performance relative to the initial condition. For this purpose, the normalized peak to initial surface deflection defined in this study provides a better measure of the impact of a certain variable on the change in surface deflection during moisture variation events. This can be confirmed by comparing the results for sensitivity of  $\delta_p$  and  $\delta_p/\delta_0$  to  $M_{R,AC}$  shown in Figure 4-13. According to this figure, while an approximately 80% reduction in  $M_{R,AC}$  from the reference value (i.e., 3000 MPa) resulted in almost 40% increase in  $\delta_p$  (Figure 4-13a), 80% reduction in  $M_{R,AC}$  resulted in only a slight reduction in  $\delta_p/\delta_0$ .



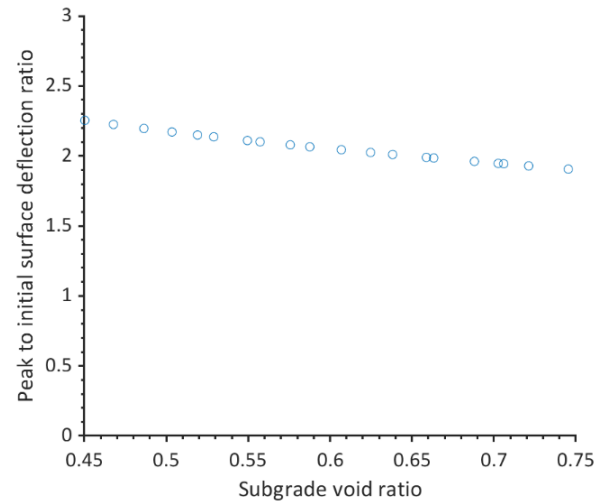
**Figure 4-13. Comparison of  $\delta_p$  and  $\delta_p/\delta_0$  as the performance measure index; (a) sensitivity of  $\delta_p$  and (b) Sensitivity of  $\delta_p/\delta_0$  to  $M_{R,AC}$ .**

Figure 4-14 illustrates the variation of  $\delta_p/\delta_0$  with subgrade  $D_{10}$  and  $e$ . This figure shows similar trends between  $\delta_p/\delta_0-D_{10}$  and  $\delta_p/\delta_0-e$  curves to what were observed in  $\delta_p-D_{10}$  and  $\delta_p-e$  curves in Figure 4-5 and Figure 4-6, respectively. According to the results presented in Figure 4-14a, if two pavement systems with different subgrade  $D_{10}$  of 0.4 and 0.1 mm are subjected to a precipitation event, the one having the smaller  $D_{10}$  would experience a surface deflection approximately 200% higher than that of hydrostatic condition (before precipitation). On the other hand, for the pavement system with subgrade  $D_{10}$  of 0.4 mm, the same precipitation event would lead to only 60% increase in initial surface deflection. Since  $D_{10}$  and  $e$  are directly proportional to soil hydraulic conductivity, the results presented in Figure 4-14 indicate that a change in hydraulic conductivity of subgrade can considerably impact the extent to which an extreme climatic event can damage the pavement structure.





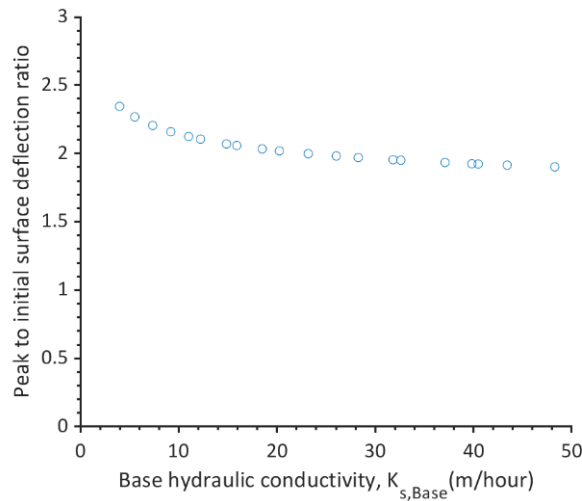
(a)



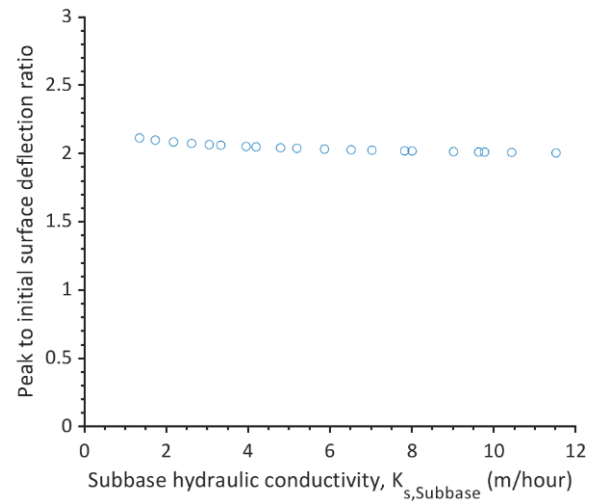
(b)

**Figure 4-14. Sensitivity of  $\delta_p/\delta_0$  to variation in subgrade (a)  $D_{10}$  and (b)  $e$ .**

Results of analysis of sensitivity of  $\delta_p/\delta_0$  to aggregate base and subbase saturated hydraulic conductivity yields similar conclusions to the subgrade saturated hydraulic conductivity. As it is shown in Figure 4-15, reduction in  $K_{s,Base}$  or  $K_{s,Subbase}$ , can adversely impact the potential effects of a precipitation event on the integrity of a pavement system.



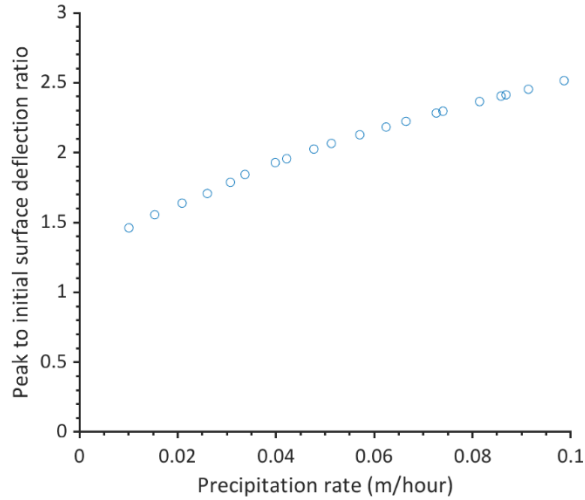
(a)



(b)

**Figure 4-15. Sensitivity of  $\delta_p/\delta_0$  to variation in saturated hydraulic conductivity of (a) aggregate base and (b) subbase.**

Figure 4-16 presents the variation of  $\delta_p/\delta_0$  with the precipitation rate. Results of sensitivity analysis show a substantial impact of precipitation rate on  $\delta_p/\delta_0$ . While a precipitation event with  $P_r = 0.02$  m/hour results in approximately 50% increase in initial surface deflection, the surface deflection would increase up to 150% of its initial value for  $P_r = 0.1$  m/hour.



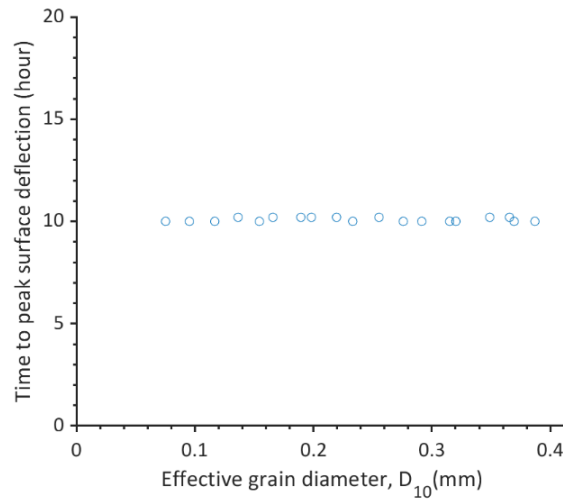
**Figure 4-16. Sensitivity of  $\delta_p/\delta_0$  to variation in precipitation rate.**

The SDM simulations indicated that resilient moduli and thicknesses of pavement layers have minimal impact on  $\delta_p/\delta_0$ . This indicates that  $\delta_p/\delta_0$  is mostly controlled through variables related to hydrology of the pavement system (e.g., hydraulic conductivity of layers and precipitation rate), rather than the variables that control the stiffness of the pavement system. It should be emphasized that this conclusion may hold valid only for the pavement systems with similar condition to the reference model evaluated in this study. A GSA is required to understand the significance of each variable in general condition.

#### Sensitivity of time to peak surface deflection ( $t_p$ ):

The time to peak surface deflection indicates how quickly a pavement section reaches its highest surface deflection under a certain traffic load and during a certain precipitation event. SDM simulations for the range of variables considered in this study indicated no considerable impact of the input parameters on the  $t_p$ . For example, Figure 4-17 shows the sensitivity of  $t_p$  to subgrade  $D_{10}$ . According to this figure, the peak surface deflection occurs after approximately 10 hours from the initiation of the precipitation, which is the same as the end of precipitation period. This explains why  $t_p$  is insensitive to change in input

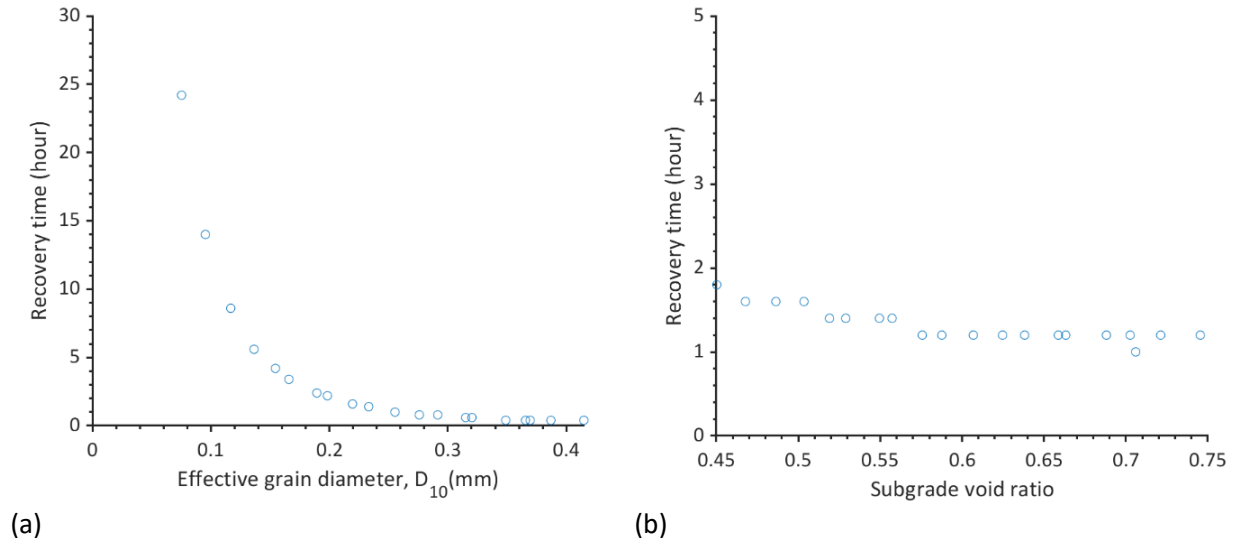
parameters, as for the given reference model and the defined range of variables, the highest surface deflection always occurs at the end of precipitation period.



**Figure 4-17. Sensitivity of  $t_p$  to variations in subgrade  $D_{10}$ .**

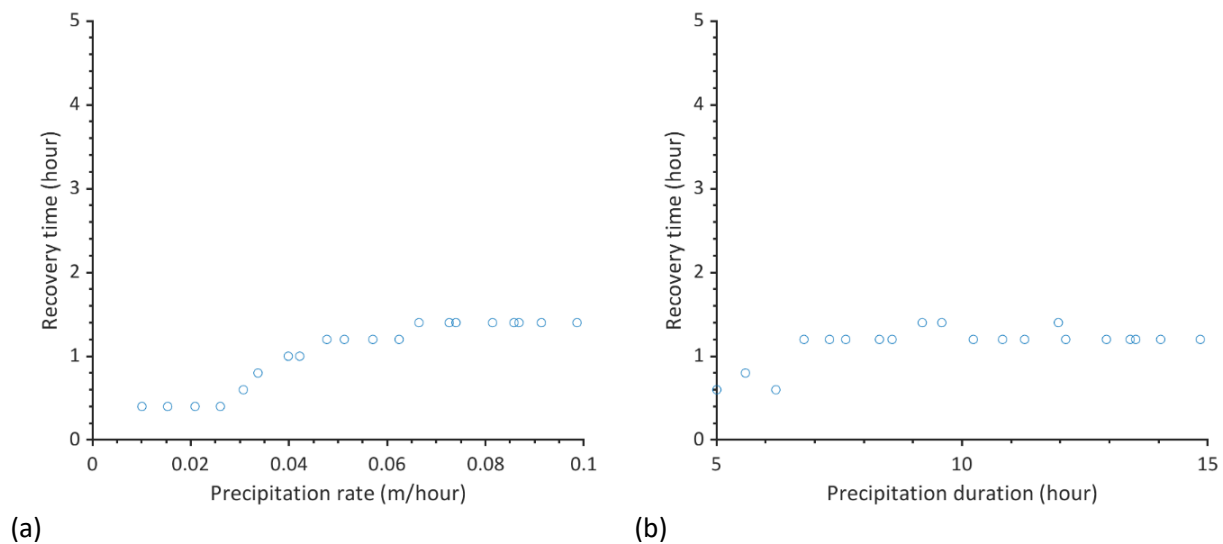
#### Sensitivity of recovery time ( $t_R$ ):

The recovery time reflects the time it takes for the excess moisture to redistribute within the pavement layers so that 80% of the excess surface deflection is recovered. Figure 4-18 exhibits the variations of  $t_R$  with subgrade  $D_{10}$  and  $e$ . According to Figure 4-18a, subgrade  $D_{10}$  can considerably impact the recovery time. The impact of  $D_{10}$  is more significant for  $D_{10}$  values approximately less than 0.2 mm. For  $D_{10} > 0.25$  mm, the recovery time is less than an hour. This can mainly be due to the impact of  $D_{10}$  on hydraulic conductivity of soil. The redistribution of moisture is expected to be slower in soils with lower hydraulic conductivity. On the other hand, if the hydraulic conductivity is large enough, moisture moves almost freely within the soil and redistribution of moisture can happen relatively quickly. Similar to  $D_{10}$ , although in lower extents, an increase in subgrade void ratio resulted in reduction in recovery time (Figure 4-18b). This is because hydraulic conductivity of coarse-grained soils is more impacted by its  $D_{10}$  than void ratio.



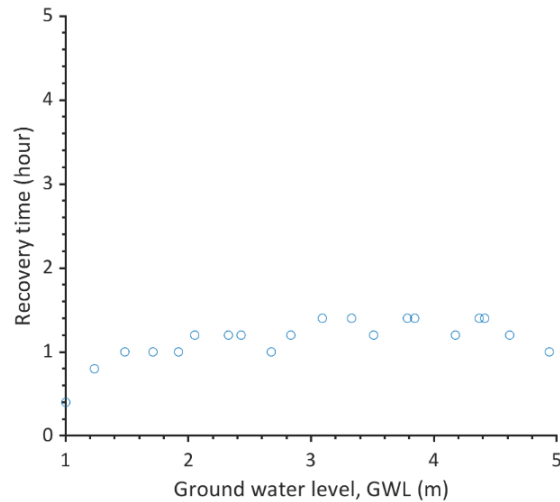
**Figure 4-18. Sensitivity of  $t_R$  to variations in subgrade (a)  $D_{10}$  and (b)  $e$ .**

The impact of precipitation rate and duration on  $t_R$  is presented in Figure 4-19. An increase in precipitation rate increased  $t_R$  (Figure 4-19a). This means that a longer time is required for redistribution of moisture in pavement layers for higher precipitation rates which is due to higher amount of water being accumulated in pavement layers. An increase in precipitation duration from 5 to 7 hours resulted in an increase in  $t_R$  (Figure 4-19b). However, further increase in precipitation rate did not impact  $t_R$ . This is due to a change in moisture movement from transient to steady state after 7 hours of precipitation. For steady state infiltration, the pavement layers' degree of saturation is controlled by the rate of precipitation rather than its duration. Therefore, once the steady state condition is achieved, an increase in precipitation duration has no impact on its degree of saturation and consequently the time required for redistribution of the excess moisture.



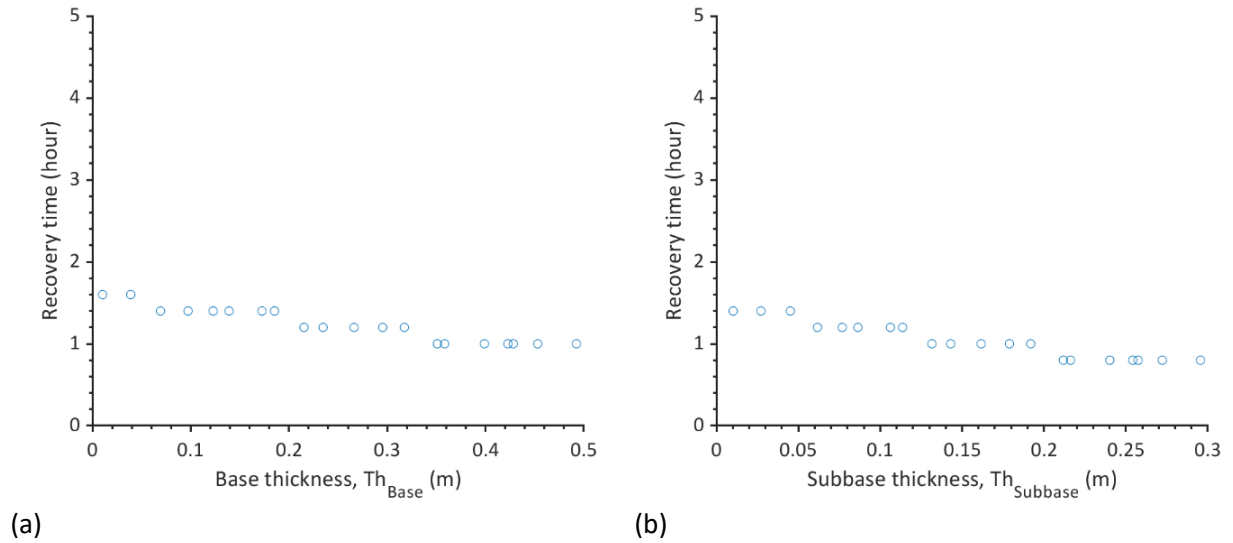
**Figure 4-19. Sensitivity of  $t_R$  to variations in precipitation (a) rate and (b) duration.**

Figure 4-20 presents the variation of  $t_R$  with GWL. According to this figure,  $t_R$  gradually increases as the GWL increases. For a hydrostatic condition (i.e., before precipitation) and a given depth above GWL, soil degree of saturation decreases with an increase in the depth of the groundwater. Therefore, in a moisture variation event and for deeper groundwater levels, redistribution of moisture may take longer for a deeper GWL than a shallower one since soil moisture content would need to go back to a lower value.

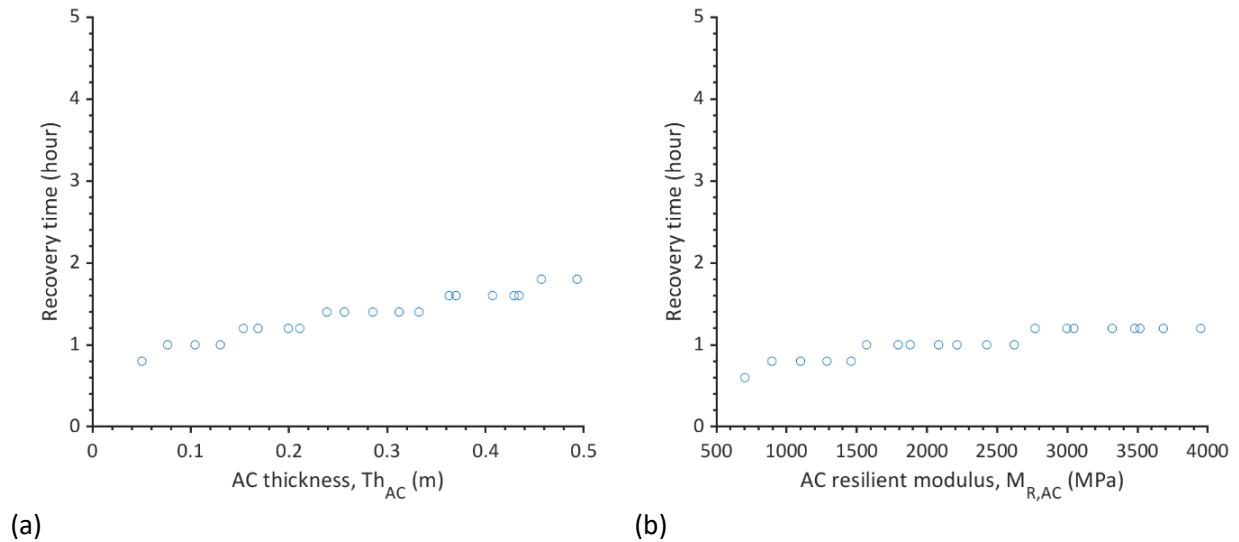


**Figure 4-20. Sensitivity of  $t_R$  to variations in initial GWL.**

Figure 4-21 presents results of sensitivity simulation in terms of aggregate base and subbase thickness versus  $t_R$ . An increase in either thickness of aggregate base or subbase resulted in reduction in recovery time. This is due to higher permeability of these layers that accelerated the redistribution of moisture in pavement layers. On the other hand, an increase in AC thickness or resilient modulus increase the recovery time in Figure 4-22.

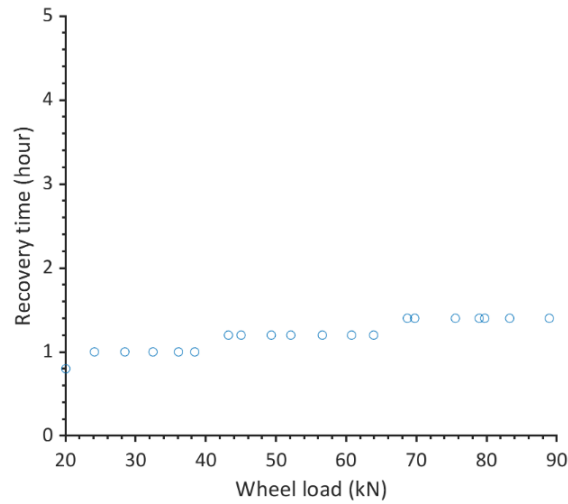


**Figure 4-21. Sensitivity of  $t_R$  to variations in (a) aggregate base and (b) subbase thicknesses.**



**Figure 4-22. Sensitivity of  $t_R$  to variations in AC (a) thickness and (b) resilient modulus.**

Figure 4-23 shows the variation of recovery time with wheel load. Results presented in this figure suggest that a longer time is required for the recovery of pavements under higher wheel loads.

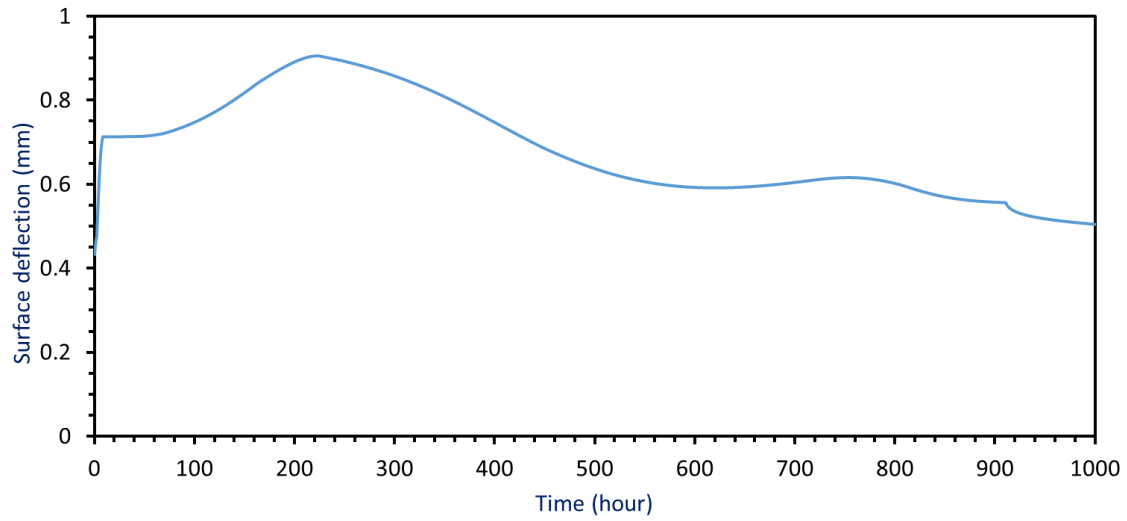


**Figure 4-23. Sensitivity of  $t_R$  to variations in wheel load.**

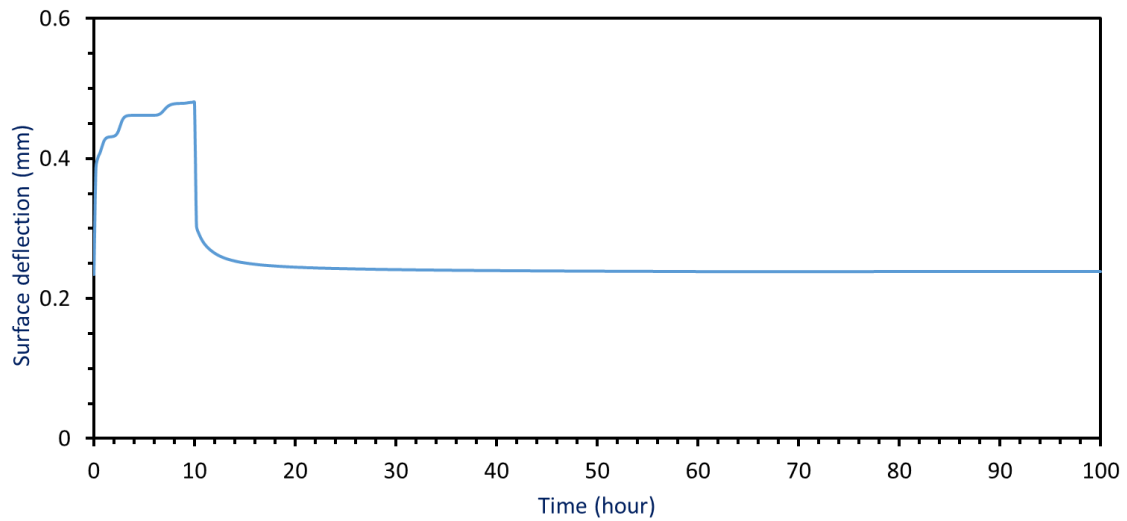
#### 4.3.3 Local Sensitivity Analysis for Fine-grained subgrade

##### Reference Model Response

For this set of analysis, the subgrade reference model input parameters and their ranges were assigned based on values presented for a fine-grained subgrade in Table 4-9. Figure 4-24 presents the surface deflection time history for the fine-grained subgrade reference model (Figure 4-24a) along with the one for the coarse-grained subgrade (Figure 4-24b). Similar to the coarse-grained subgrade model, results presented in Figure 4-24a indicate a sharp increase in AC surface deflection with start of rain. This is due to inundation of subbase and aggregate base coarse material under the ponded water which resulted in a drastic reduction in their stiffness and resistance against loading. Unlike the coarse-grained subgrade reference model, the surface deflection continues to increase after when the precipitation stops. This is due to gradual saturation of subgrade layers with a very low hydraulic conductivity. Because of this, the surface deflection reaches the peak value approximately 170 hours (~one week) after the end of precipitation. The evaporation of ponded water and the infiltration and redistribution of water within the subgrade layers resulted in a gradual recovery of surface deflection. However, due to significantly lower hydraulic conductivity of fine-grained subgrade, its recovery time is considerably slower than that of the coarse-grained reference model. While the surface deflection almost completely recovers after 30 hours in coarse-grained subgrade model, the full recovery was not achieved even after 1000 hours for fine-grained subgrade reference model.



(a)



(b)

**Figure 4-24. Surface deflection time history for (a) the fine-grained subgrade reference and (b) the coarse-grained subgrade reference models.**

### Univariate sensitivity simulation results

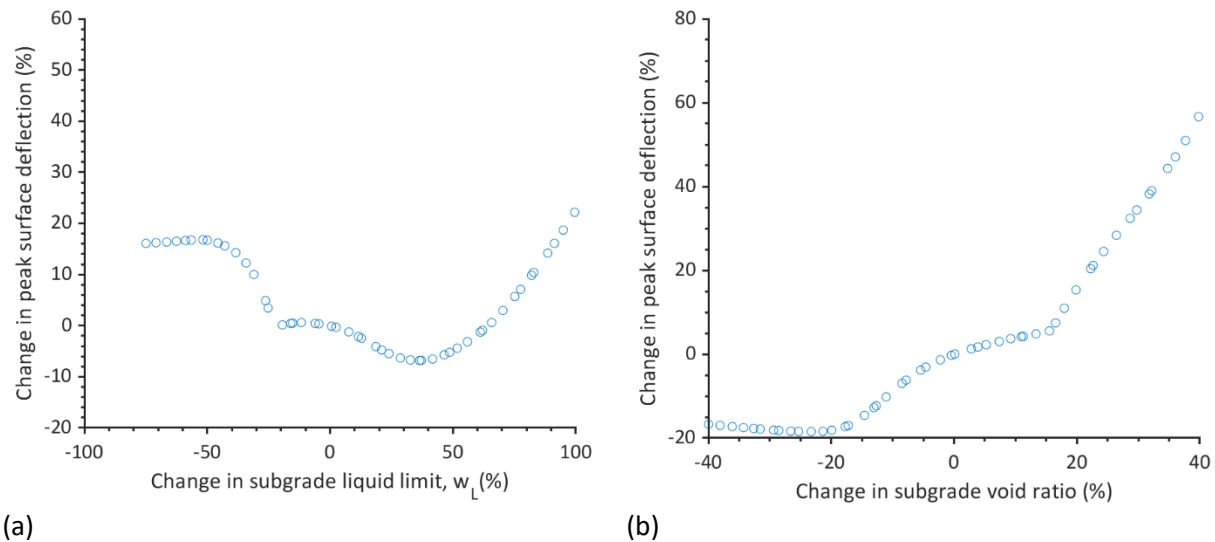
Univariate SDM simulations were performed by changing an independent parameter while maintaining the other parameters at the reference model value. The reference model values and the ranges of each parameter for sensitivity simulations were reported in Chapter 3. The simulation results are interpreted and discussed in terms of key performance measures.



#### Sensitivity of peak surface deflection ( $\delta_p$ ):

Figure 4-25 presents the variations of peak surface deflection with subgrade liquid limit and void ratio. Results indicated a highly non-linear relationship between  $\delta_p$  and  $w_L$  (Figure 4-25a). This is due to the complex impact of  $w_L$  on pavement response to traffic loading. The subgrade liquid limit impacts both water retainability (i.e., SWRC fitting parameters) and hydraulic conductivity. In general, soils with higher liquid limit would have higher water retainability. Therefore, at a given depth above the GWL, it is likely that soils with higher liquid limit would have higher degree of saturation, and consequently, lower stiffness. On the other hand, lower hydraulic conductivity is expected for soils with higher  $w_L$ . The interaction of these two factors explains the nonlinearity and multiple points of inflection observed in  $\delta_p$  versus  $w_L$  curve.

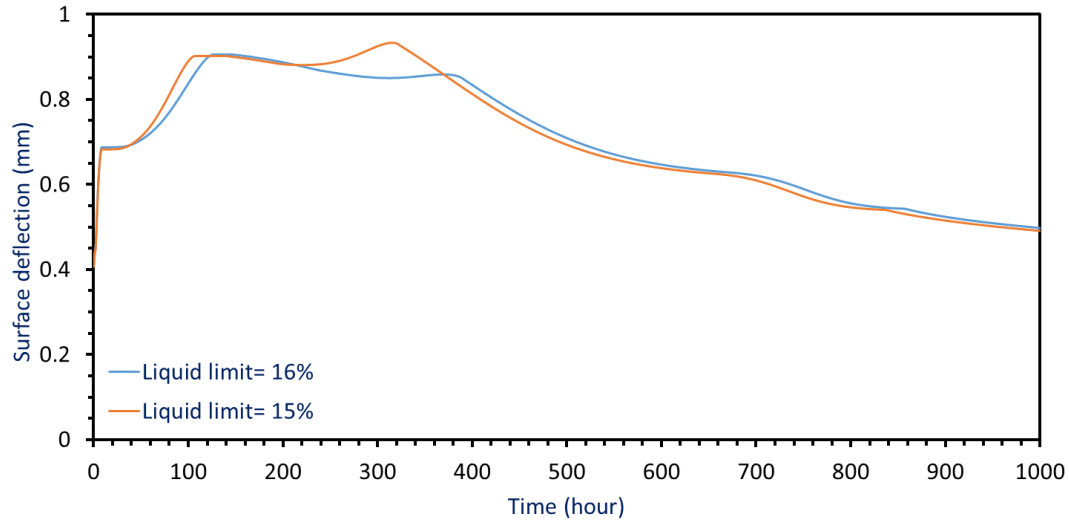
The peak surface deflection during precipitation was substantially affected by change in void ratio (Figure 4-25b). In general, an increase in void ratio increased the  $\delta_p$ . This is in contrast with what was observed for the coarse-grained case. This is a result of the interaction of soil stiffness and hydraulic conductivity in fine-grained soils. While the effect of subgrade  $e$  on its hydraulic conductivity was likely to be the dominant factor affecting  $\delta_p$  in a coarse-grained soil, the change in subgrade stiffness most likely plays more important role in  $\delta_p$  in a fine-grained subgrade.



**Figure 4-25. Sensitivity of peak surface deflection to the variations of subgrade liquid limit.**

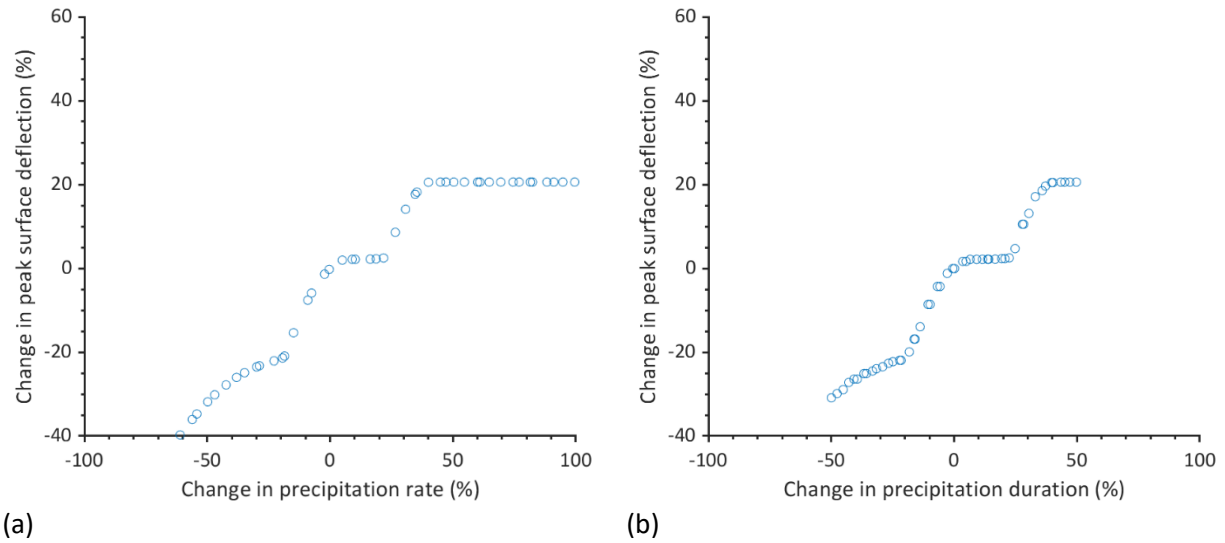
The results presented in Figure 4-25a and b showed several points of inflection in peak surface deflection versus  $w_L$  or  $e$  curves. The reason for this observation is a transition in mode of saturation in the layers. Moisture movement from a layer to another layer results in sequences of saturation and desaturation of layers. The complex interaction of hydro-mechanical properties of soil and climatic factors may change these sequences and time dependent pavement behavior. In order to better illustrate this, time histories of surface deflection for the inflection point between -20 to -30% change in  $w_L$  (i.e,  $w_L=16$

to 17%) are reviewed in Figure 4-26. According to the results presented in this figure, due to saturation and desaturation of pavement layers, a double peak behavior is observed in the surface deflection versus time curves. The first peak is due to saturation of shallow pavement layers while the second peak is attributed to the movement of moisture to deeper soil and desaturation of aggregate base layer. While for  $w_L=16\%$  the first peak controls the highest surface deflection, the highest surface deflection is controlled by the second peak when  $w_L=15\%$ . This change in time dependent surface deflection behavior is expected to dramatically change the time to peak surface deflection and recovery time as will be observed in following figures.



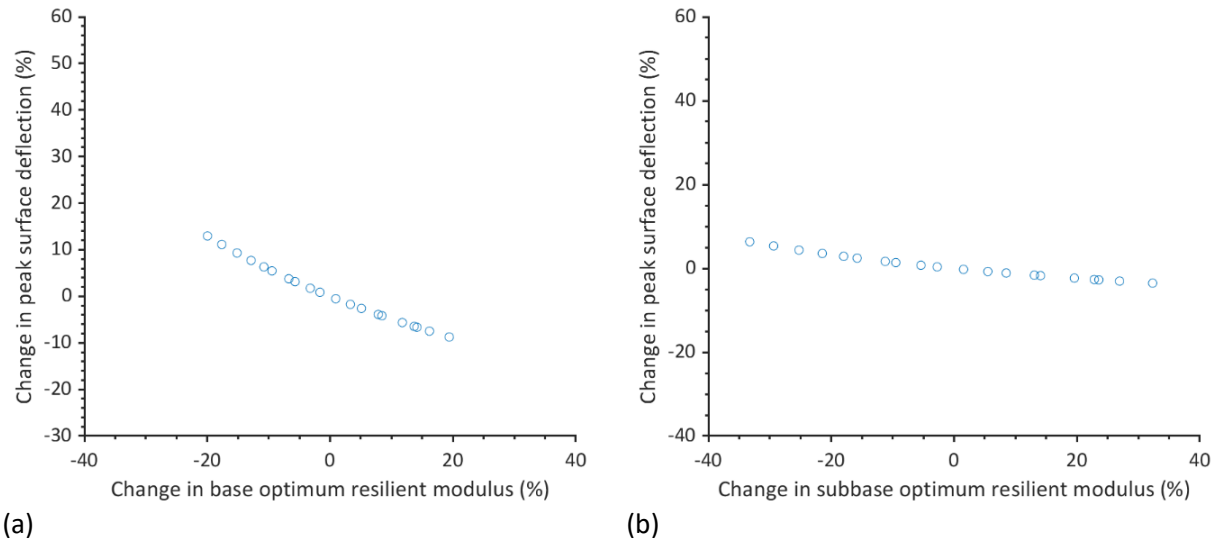
**Figure 4-26. Surface deflection time histories for the fine-grained model with  $w_L= 16$  and  $17\%$ .**

Figure 4-27 illustrates variations of  $\delta_p$  with precipitation rate and duration. Results indicate substantial impact of both  $P_r$  and  $P_d$  on  $\delta_p$ . The trend observed in  $\delta_p - P_r$  curve is almost consistent with what was observed for coarse-grained subgrade case. While in coarse-grained case,  $\delta_p$  was almost insensitive to change in  $P_d$ , it was considerably increased with an increase in  $P_d$ . Higher precipitation duration allows infiltration of moisture through fine-grained subgrade layers while maintaining moisture content of the structural pavement layers at a high level.



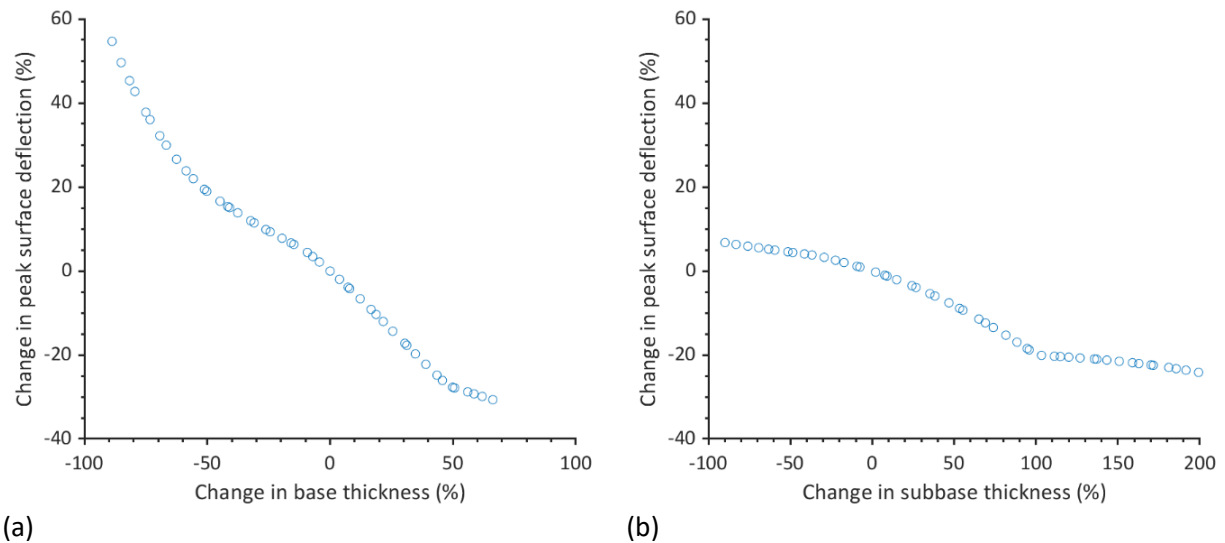
**Figure 4-27. Sensitivity of peak surface deflection to the variations of precipitation (a) rate and (b) duration.**

Figure 4-28 shows the results of sensitivity simulations for aggregate base and subbase optimum resilient modulus. Results indicate that  $M_{R-OPT,Base}$  and  $M_{R-OPT,Subbase}$  are inversely proportional to  $\delta_p$ . Results showed that  $\delta_p$  is more sensitive to change in  $M_{R-OPT,Base}$  than  $M_{R-OPT,Subbase}$ . Similar observations were also made for the comparisons of the impact of aggregate base and subbase thicknesses on peak surface deflection (Figure 4-9).



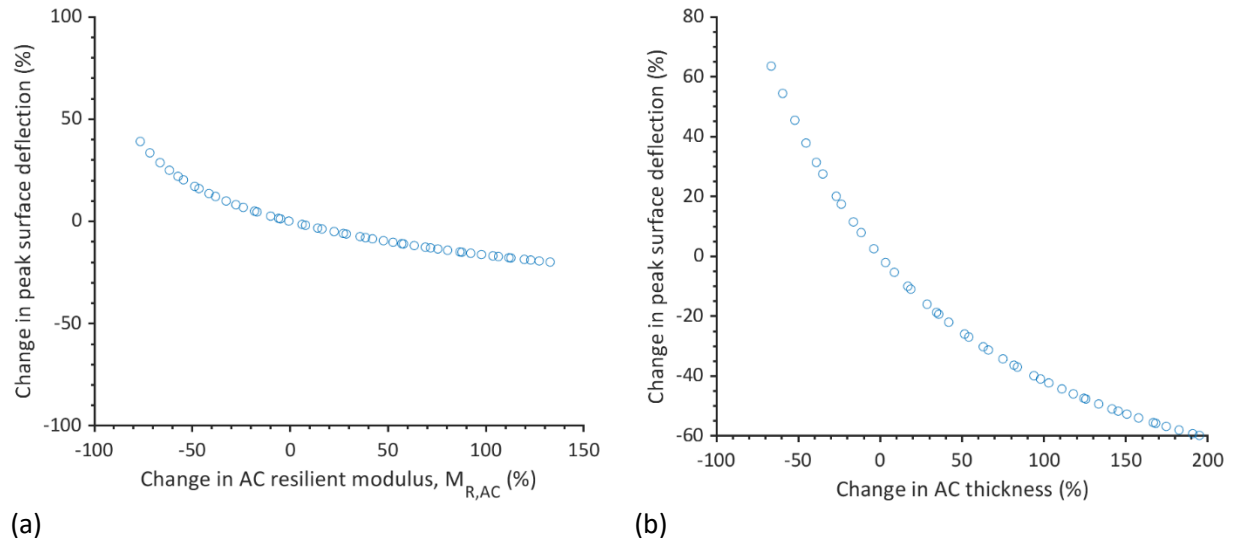
**Figure 4-28. Sensitivity of peak surface deflection to the variations of (a) aggregate base and (b) subbase optimum resilient moduli.**

The SDM simulations indicate a substantial impact of aggregate base and subbase thickness on  $\delta_p$  (Figure 4-29). Results indicate that 50% increase in aggregate base thickness reduces the peak surface deflection by almost 30% (Figure 4-29a). Similar trend, although in lower rates were observed for aggregate subbase thickness (Figure 4-29b). A comparison between Figure 4-29 and Figure 4-10 indicates that  $d_p$  in fine-grained subgrade model is more sensitive to aggregate base and subbase thickness than in the coarse-grained subgrade model. For a pavement system with low permeable fine-grained subgrade, it is more likely that aggregate base and subbase layers become fully saturated. The high thickness of these layers above natural subgrade surface helps them to stay above the ponded water height.



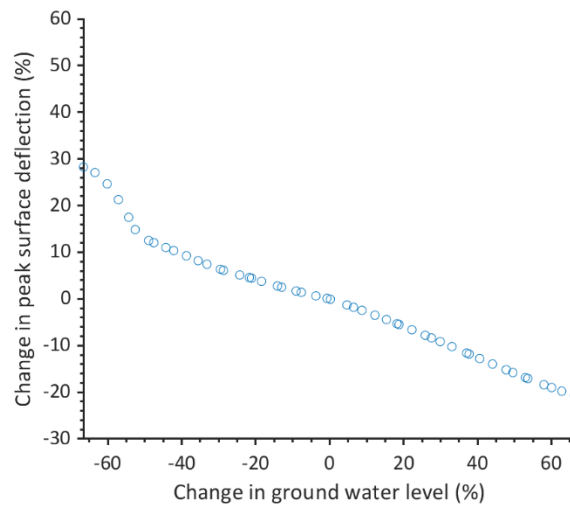
**Figure 4-29. Sensitivity of peak surface deflection to the variations of (a) aggregate base and (b) subbase thicknesses.**

Figure 4-30 presents the results of  $\delta_p$  sensitivity simulations to  $M_{R,AC}$  and  $Th_{AC}$ . Results show that a decrease in  $M_{R,AC}$  or  $Th_{AC}$  leads to a substantial increase in  $\delta_p$  during a moisture variation event. However, peak surface deflection is more sensitive to a change in  $Th_{AC}$  than  $M_{R,AC}$ .



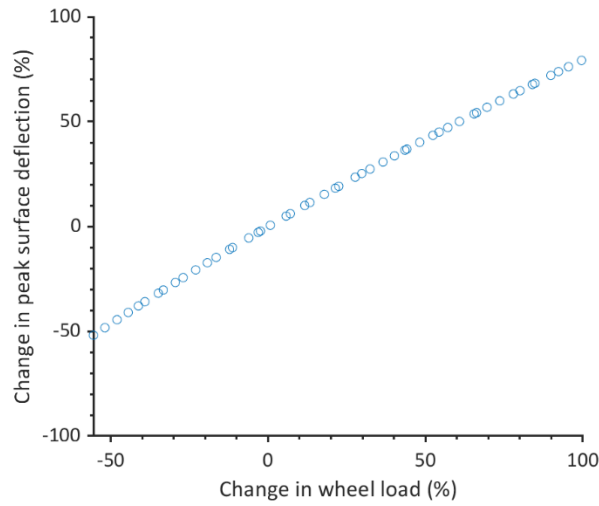
**Figure 4-30. Sensitivity of peak surface deflection to the variations of (a)  $M_{R,AC}$  and (b)  $Th_{AC}$ .**

Figure 4-31 presents the sensitivity of peak surface deflection to initial GWL. Results show lower surface deflection as the initial GWL becomes deeper.



**Figure 4-31. Sensitivity of peak surface deflection to the variations of initial GWL.**

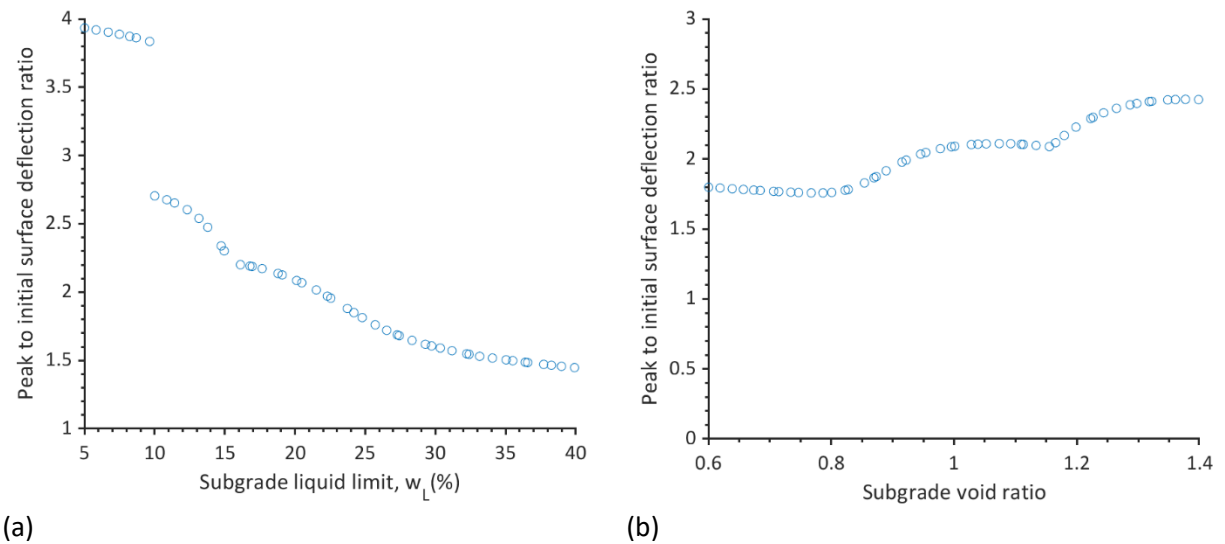
Figure 4-32 presents the variations of peak surface deflection with changes in wheel load. Results indicate a substantial impact of wheel load on the peak surface deflection.



**Figure 4-32. Sensitivity of peak surface deflection to the variations of wheel load.**

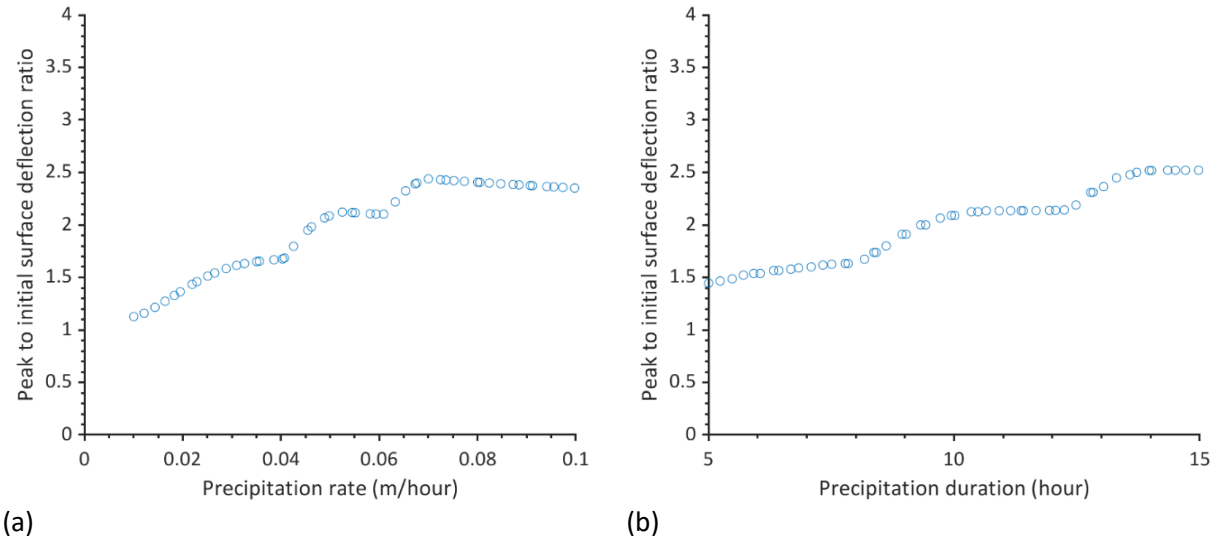
Sensitivity of peak to initial surface deflection ratio ( $\delta_p/\delta_0$ ):

Figure 4-33 illustrates the variation of  $\delta_p/\delta_0$  with subgrade  $w_L$  and  $e$ . Results indicate considerable impacts of  $w_L$  and  $e$  on  $\delta_p/\delta_0$ . The ratio of  $\delta_p/\delta_0$  decreased from approximately 4 to 1.5 as  $w_L$  increased from 5 to 40.

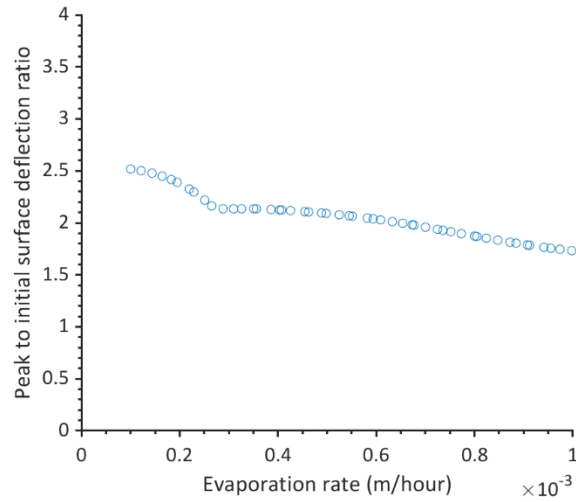


**Figure 4-33. Sensitivity of  $\delta_p/\delta_0$  to variation in subgrade (a)  $w_L$  and (b)  $e$ .**

Figure 4-34 presents the variation of  $\delta_p/\delta_0$  with precipitation rate and duration. Results show similar trends as what was observed for the peak surface deflection under variable  $P_r$  and  $P_d$ . Similar observation were also made for  $\delta_p/\delta_0$  versus evaporation rate (Figure 4-35).

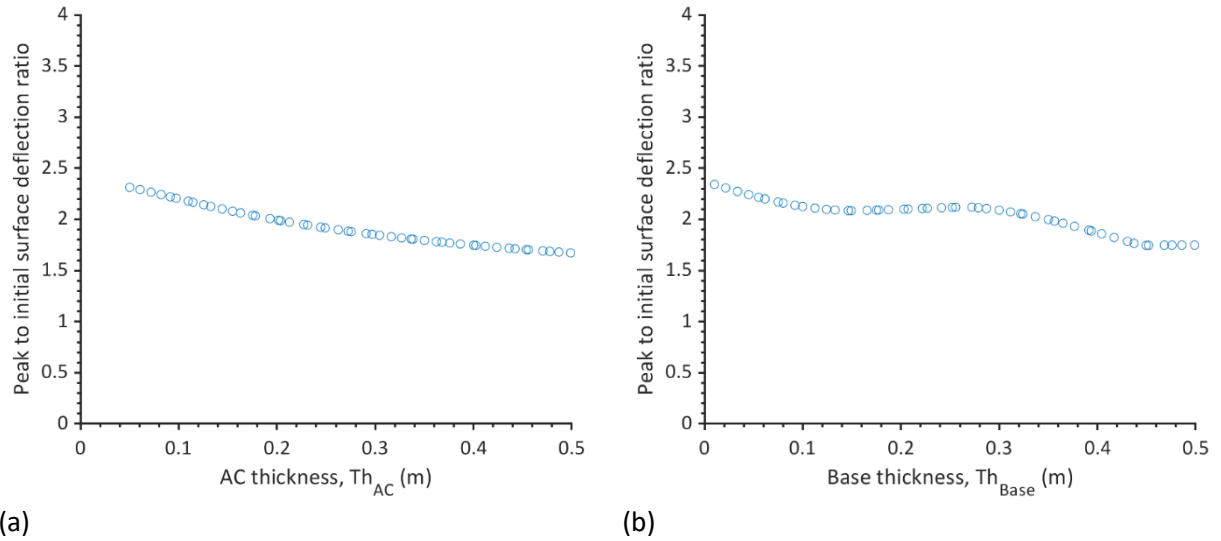


**Figure 4-34. Sensitivity of  $\delta_p/\delta_0$  to variation in precipitation (a) rate and (b) duration.**



**Figure 4-35. Sensitivity of  $\delta_p/\delta_0$  to variation in evaporation rate.**

Unlike the coarse-grained subgrade reference model, results show substantial impact of pavement layers' thicknesses on  $\delta_p/\delta_0$  for fine-grained case (Figure 4-36).

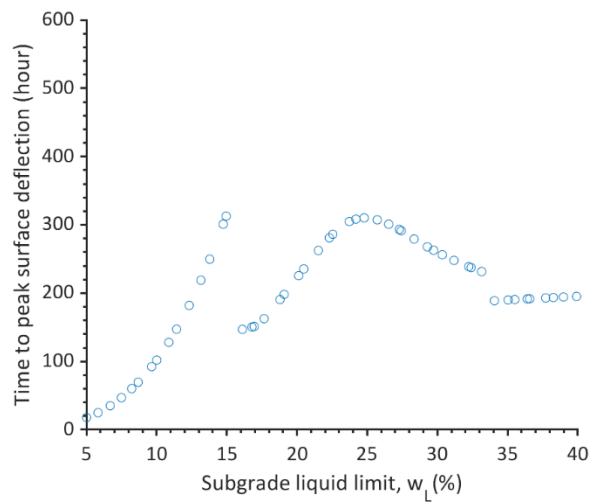


**Figure 4-36. Sensitivity of  $\delta_p/\delta_0$  to variation in (a) AC and (b) aggregate base thicknesses.**

Like the SDM simulation for coarse-grained subgrade model, resilient moduli of pavement layers had minimal impact on  $\delta_p/\delta_0$ . The SDM simulations for other parameters are provided in the Appendix B.

**Sensitivity of time to peak surface deflection ( $t_p$ ):**

The SDM simulations indicated a nonlinear relationship between  $t_p$  and evaporation rate, precipitation rate and duration, subgrade void ratio and liquid limit, and aggregate base and subbase thicknesses. Figure 4-37 presents, as an example, results of the analysis of sensitivity of  $t_p$  to subgrade liquid limit. The SDM simulations for other parameters are provided in the Appendix B.

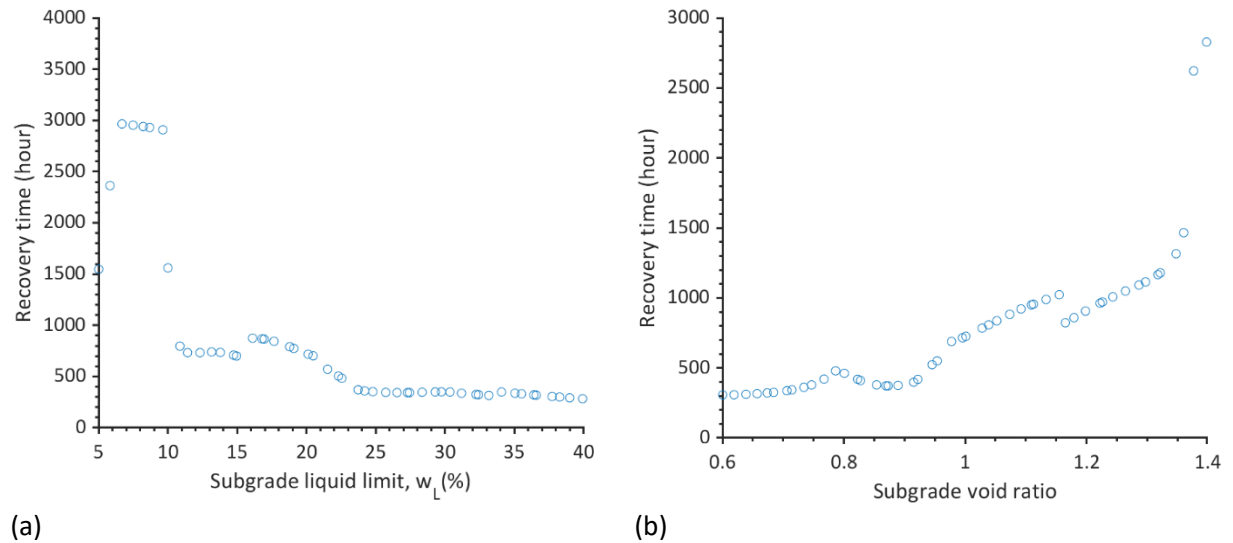


**Figure 4-37. Sensitivity of  $t_p$  to variation in subgrade liquid limit.**

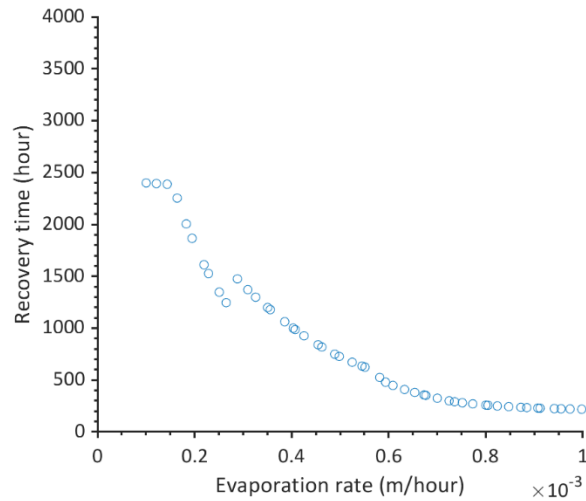


### Sensitivity of recovery time ( $t_R$ ):

Figure 4-38 illustrates the variations of  $t_R$  with subgrade  $w_L$  and  $e$ . Results show high sensitivity of  $t_R$  to these parameters. According to the results presented in Figure 4-38a,  $t_R$  increase as  $w_L$  increases from 5% up to approximately 7%. However, for the liquid limit values greater than 7%,  $w_L$  is inversely proportional to  $t_R$ . This implies that the recovery time decreases as the hydraulic conductivity increases which is in contrast with what was observed for the coarse-grained case. Void ratio versus recovery time results also support this conclusion (Figure 4-38b). The change in the mechanism of excess moisture removal from the system can be responsible for this. As the hydraulic conductivity of subgrade becomes relatively very low, less water infiltrates through the subgrade and most of the moisture is removed through evaporation. As the redistribution of moisture in a fine-grained subgrade is typically very slow, this accelerates the recovery process. This can be confirmed by evaluating the sensitivity of  $t_R$  to evaporation rate (Figure 4-39). While evaporation had minimal impact on  $t_R$  for coarse-grained subgrade case, it plays a significant role in  $t_R$  of fine-grained subgrade reference model.



**Figure 4-38. Sensitivity of  $t_R$  to variations in subgrade (a)  $w_L$  and (b)  $e$ .**



**Figure 4-39. Sensitivity of  $t_R$  to variations in evaporation rate.**

Results of SDM simulation for pavement structural layers thicknesses, and precipitation rate and duration indicated a considerable impact of these variables on  $t_R$ . However, similar to sensitivity analysis for coarse-grained subgrade, pavement structural layers moduli and hydraulic conductivity, traffic load, and GWL had minimal impact on the recovery time for fine-grained pavement model. The sensitivity results for these variables are provided in the Appendix B.

#### 4.3.4 Sensitivity Analysis Summary and Conclusions

Two sets of univariate sensitivity simulations, one considering a coarse-grained subgrade and one considering a fine-grained subgrade were performed to understand the significance of the SDM input variables on pavement system performance during moisture variation and under traffic loading. The pavement performance was evaluated using four performance measures, namely, peak surface deflection, peak to initial surface deflection ratio, time to peak surface deflection, and recovery time. Results of the analysis indicated that the significance of the impact of input parameters is dependent on the type of the subgrade soil. Table 4-11 qualitatively summarizes the overall significance of the impact of each input parameter on performance measures for coarse-grained and fine-grained subgrade models. It should be emphasized that the results and conclusions presented herein may only hold valid for the reference model, ranges of variables, and select relationships used for the analysis.

**Table 4-11. Overall qualitative significance of the impact of SDM input parameters on the pavement performance measures from local sensitivity analysis.**

Variable		Performance measure index							
		$(\delta_p)_{\text{coarse}}^a$	$(\delta_p)_{\text{fine}}^b$	$(\delta_p/\delta_0)_{\text{coarse}}$	$(\delta_p/\delta_0)_{\text{fine}}$	$(t_p)_{\text{coarse}}$	$(t_p)_{\text{fine}}$	$(t_R)_{\text{coarse}}$	$(t_R)_{\text{fine}}$
$D_{10, \text{Subgrade}}$	↑	***↓	NA	***↓	NA	-	NA	***↓	NA
$w_{L, \text{Subgrade}}$	↑	NA	**↓↑	NA	***↓	NA	***↓↑	NA	***↓
$e_{\text{Subgrade}}$	↑	*↓	***↓	*↓	*↑	-	***↓↑	*↓	***↑
$P_r$	↑	***↑	**↑	***↑	**↑	-	***↓↑	*↑	***↑
$P_d$	↑	*↑	***↑	-	**↑	***↑	***↓↑	*↑	***↑
$E_r$	↑	-	**↓	-	**↓	-	***↓↑	-	***↓
GWL	↑	*↓	***↓	-	*↓↑	**↑	***↓↑	*↑	*↓↑
$K_{s, \text{base}}$	↑	**↓	-	**↓	*↑	-	-	-	*↑
$K_{s, \text{subbase}}$	↑	*↓	-	*↓	-	-	-	-	-
$Th_{\text{base}}$	↑	**↓	***↓	-	**↓	-	***↓	*↓	***↓
$Th_{\text{subbase}}$	↑	*↓	**↓	-	*↓	-	**↓	*↓	**↓
$M_{R, \text{opt}, \text{base}}$	↑	**↓	**↓	-	-	-	-	*↑	-
$M_{R, \text{opt}, \text{subbase}}$	↑	*↓	*↓	-	-	-	-	-	-
$M_{R, \text{AC}}$	↑	**↓	***↓	-	-	-	-	*↑	-
$Th_{\text{AC}}$	↑	***↓	***↓	**↓	**↓	-	-	*↑	*↑
Wheel load	↑	***↑	***↑	-	-	-	-	*↑	-

<sup>a</sup> Coarse-grained subgrade reference model.

<sup>b</sup> Fine-grained subgrade reference model.

“\*\*\*” indicates relatively substantial impact, “\*\*” indicates relatively moderate impact, \* indicates relatively low impact, “-” indicates minimal impact, and “↑” shows the direction of the impact on the given performance measure as a result of an increase “↑” in input variables. “↑” implies increase, “↓” implies decrease, and “↓↑” implies nonlinear behavior.

## 4.4 MULTIVARIATE GLOBAL SENSITIVITY ANALYSIS (GSA)

### 4.4.1 Introduction

Univariate sensitivity simulations presented in the previous section provided instructive information about the importance of each parameter and its overall contribution to pavement system behavior. However, due to complex interaction of input variables and extreme nonlinearity in response in most cases, the results may only be applicable to the reference model values. For example, while the recovery time is likely to be insensitive to evaporation for highly permeable subgrades, it is likely to be substantially

impacted by evaporation for subgrades with relatively low permeability. Therefore, the interaction of evaporation and permeability of subgrade is expected to become critically important for design or evaluation of a pavement system prone to moisture variations. While a local sensitivity analysis may not be able to explain the interaction between different parameters, a global sensitivity analysis can holistically assess the significance of input variables and their interaction on critical pavement performance indicators during and after a moisture variation event. This section presents the results of global sensitivity analysis for coarse-grained and fine-grained subgrade cases.

#### 4.4.2 Global Sensitivity Analysis for Coarse-grained subgrade

Based on univariate sensitivity analysis results, input parameters that had low to substantial impact on the pavement performance measures during and after moisture variation event were selected for global sensitivity analysis. In addition, due to substantial impact of evaporation rate on the response of fine-grained subgrade reference model, it was considered in the multivariate simulations. The multivariate simulations included 2000 SDM simulations using LHS method for the select parameters and their ranges, as shown in Table 4-12. Results of the simulations were interpreted in terms of the four performance measure indices. Statistical analysis, using JMP software was performed to understand the significant importance of each parameter and to rank them based on their significant impact.

**Table 4-12. Select input parameters and their ranges for GSA of coarse-grained subgrade model.**

Parameters	Range
$D_{10, Subgrade}$	0.07 to 0.2
$e_{Subgrade}$	0.45 to 0.75
$P_r$	0.01 to 0.1 m/hour
$P_d$	5 to 15 hours
$E_r$	0.0001 to 0.001
GWL	1 to 5m
$K_{s,base}$	12 to 160 m/hour
$K_{s,subbase}$	4 to 40 m/hour
$Th_{base}$	0 to 0.5 m
$Th_{subbase}$	0 to 0.3 m
$M_{R-opt,base}$	200 to 300 MPa
$M_{R-opt,subbase}$	100 to 200 MPa
$M_{R,AC}$	700 to 7000 MPa
$Th_{AC}$	0.05 to 0.5 m

### Sensitivity of $\delta_p$ to Select Parameters

Results of sensitivity analysis of peak surface deflection to variations in select input parameters for coarse-grained subgrade case are provided in Table 4-13. p-values reported in the table provides evidence to support or reject null hypothesis that the response and input parameters are not correlated. A p-value greater than 0.05 indicates strong evidence for the null hypothesis. Logarithm of worth ( $\log(\text{worth})$ ) present the significance of each model effect, defined as  $\log_{10}(\text{p value})$ . Parameter t Ratio is the ratio of parameter coefficient in linear regression model to its standard error and it indicates the significance and direction of the impact.

According to the results presented in Table 4-13,  $Th_{AC}$  may have the most significant impact on peak surface deflection. The negative “t Ratio” value obtained for  $Th_{AC}$  indicates its inverse relationship with the peak surface deflection (i.e., an increase in  $Th_{AC}$  results in decrease in the peak surface deflection).  $P_r$ ,  $M_{R,AC}$ ,  $D_{10,Subgrade}$ ,  $M_{R-OPT,Base}$ , and  $Th_{Base}$  are other parameters that would play a substantial role in estimation of the peak surface deflection. Further, similar to univariate sensitivity simulations, the results indicate that the peak surface deflection is insensitive to variations of evaporation rate between the ranges examined in this study.

**Table 4-13. Summary of the analysis of the sensitivity of peak surface deflection to select input parameters for coarse-grained subgrade model.**

Ranking	Variable	Log (worth)	t Ratio	p value
1	$Th_{AC}$	644.97	-95.4	<.0001
2	$P_r$	380.842	57.14	<.0001
3	$M_{R,AC}$	340.603	-52.13	<.0001
4	$D_{10,Subgrade}$	236.403	-39.67	<.0001
5	$M_{R-OPT,Base}$	217.196	-37.41	<.0001
6	$Th_{Base}$	198.948	-35.25	<.0001
7	$K_{s,Base}$	23.952	-10.44	<.0001
8	$M_{R-OPT,Subbase}$	21.986	-9.97	<.0001
9	$TH_{Subbase}$	20.536	-9.61	<.0001
10	$K_{s,Subbase}$	17.119	-8.71	<.0001
11	$P_d$	14.014	7.82	<.0001
12	Initial GWL	8.997	6.15	<.0001
13	$e_{Subgrade}$	3.44	-3.57	0.0004
14	$E_r$	0.832	1.45	0.1472

### Sensitivity of $\delta_p/\delta_0$ to Select Parameters

Results of the analyses for sensitivity of  $\delta_p/\delta_0$  to variations of the select parameters indicate that precipitation rate ( $P_r$ ) and subgrade effective grain diameter ( $D_{10,Subgrade}$ ) may have the most influential effect on  $\delta_p/\delta_0$  (Table 4-14). The results indicate that, as long as  $\delta_p/\delta_0$  is concerned, evaporation rate may become an important contributor to the pavement system response. Further,  $\delta_p/\delta_0$  is insensitive to the subbase resilient modulus variations between the ranges tested in this study.

**Table 4-14. Summary of the analysis of the sensitivity of  $\delta_p/\delta_0$  to select input parameters for coarse-grained subgrade model.**

Ranking	Variable	Log (worth)	t Ratio	p value
1	$P_r$	684.758	87.8	<.0001
2	$D_{10,Subgrade}$	386.467	-53.52	<.0001
3	$Th_{AC}$	175.536	-31.43	<.0001
4	$M_{R,AC}$	133.721	26.7	<.0001
5	$Th_{Base}$	97.578	-22.28	<.0001
6	$e_{Subgrade}$	66.691	-18.03	<.0001
7	$K_{s,Base}$	59.425	-16.93	<.0001
8	Initial GWL	37.26	13.16	<.0001
9	$K_{s,Subbase}$	29.203	-11.55	<.0001
10	$P_d$	26.998	11.08	<.0001
11	$M_{R-OPT,Base}$	11.626	7.06	<.0001
12	$Th_{Subbase}$	3.218	-3.43	0.0006
13	$E_r$	1.501	-2.15	0.0316
14	$M_{R-OPT,Subbase}$	0.089	0.24	0.8142

### Sensitivity of $t_p$ to Select Parameters

Results of analyses for sensitivity of  $t_p$  to variations of the select parameters indicate that precipitation duration and initial GWL may have the most substantial impact on  $t_p$  (Table 4-15). While LSA results indicated that variations of  $P_r$ ,  $D_{10,Subgrade}$ , and  $e_{Subgrade}$  may have minimal impact on  $t_p$ , the GSA results indicate that these parameters may significantly impact  $t_p$ . According to GSA results presented in Table 4-15, the rest of select parameters do not have significant impact on  $t_p$ .

**Table 4-15. Summary of the analysis of the sensitivity of  $t_p$  to select input parameters for coarse-grained subgrade model.**

Ranking	Variable	Log (worth)	t Ratio	p value
1	$P_d$	594.402	76.64	<.0001
2	Initial GWL	142.733	27.75	<.0001
3	$P_r$	89.123	-21.17	<.0001
4	$D_{10,Subgrade}$	3.56	-3.64	0.0003
5	$e_{Subgrade}$	2.814	3.17	0.0015
6	$Th_{Base}$	0.73	-1.32	0.1860
7	$M_{R,AC}$	0.558	1.09	0.2764
8	$M_{R-OPT,Subbase}$	0.354	-0.77	0.4426
9	$Th_{Subbase}$	0.332	0.73	0.4656
10	$E_r$	0.219	0.52	0.6043
11	$M_{R-OPT,Base}$	0.182	0.44	0.6579
12	$K_{s,Base}$	0.167	-0.41	0.6809
13	$K_{s,subbase}$	0.011	0.03	0.9761
14	$Th_{AC}$	0	0	0.9999

### Sensitivity of $t_R$ to Select Parameters

Table 4-16 presents the summary of the sensitivity of  $t_R$  to variations of the select parameters evaluated in this study. Results indicate that subgrade effective grain diameter may have the most significant impact on  $t_R$ . This might have been expected, as it was also observed in LSA results, for a pavement with coarse-grained subgrade, the redistribution of excess moisture after an extreme moisture variation event is primarily governed by its hydraulic properties. The results presented in Table 4-16 indicate that the hydraulic conductivity of aggregate base and subbase layers do not significantly impact  $t_R$ . This is mainly

because these layers are assumed to be consisted of granular material with relatively high permeability, if permeability of these layers are reduced, their impact on recovery time will become significant.

**Table 4-16. Summary of the analysis of the sensitivity of  $t_R$  to select input parameters for coarse-grained subgrade model.**

Ranking	Variable	Log (worth)	t Ratio	p value
1	$D_{10,Subgrade}$	303.309	-44.87	<.0001
2	<i>Initial GWL</i>	66.572	18.01	<.0001
3	$P_r$	45.755	14.7	<.0001
4	$Th_{Base}$	35.639	-12.85	<.0001
5	$M_{R,AC}$	35.042	12.74	<.0001
6	$P_d$	21.283	9.76	<.0001
7	$M_{R-OPT,Base}$	12.228	7.25	<.0001
8	$Th_{Subbase}$	11.036	-6.86	<.0001
9	$e_{Subgrade}$	9.682	-6.39	<.0001
10	$E_r$	2.354	2.85	0.0044
11	$Th_{AC}$	1.484	2.14	0.0328
12	$M_{R-OPT,Subbase}$	1.309	1.97	0.0491
13	$K_{Ssubbase}$	0.048	0.13	0.8955
14	$K_{S,Base}$	0.001	0	0.9986



#### 4.4.3 Global Sensitivity Analysis for Fine-grained subgrade

Similar to coarse-grained subgrade case, the GSA was investigated by performing 2000 multivariate simulations using the SDM. The select parameters and their ranges, as shown in Table 4-12. Results of the simulations were interpreted in terms of the four performance measure indices. Statistical analysis, using JMP software was performed to understand the significant importance of each parameter and to rank them based on their significant impact.

**Table 4-17. Select input parameters and their ranges for GSA of fine-grained subgrade model.**

Parameters	Range
$w_L$	5 to 40
$e_{Subgrade}$	0.6 to 1.4
$P_r$	0.01 to 0.1 m/hour
$P_d$	5 to 15 hours
$E_r$	0.0001 to 0.001
GWL	1 to 5m
$K_{s,base}$	12 to 160 m/hour
$K_{s,subbase}$	4 to 40 m/hour
$Th_{base}$	0 to 0.5 m
$Th_{subbase}$	0 to 0.3 m
$M_{R-opt,base}$	200 to 300 MPa
$M_{R-opt,subbase}$	100 to 200 MPa
$M_{R,AC}$	700 to 7000 MPa
$Th_{AC}$	0.05 to 0.5 m

### Sensitivity of $\delta_p$ to Select Parameters

Table 4-18 presents results of analyses for sensitivity of  $\delta_p$  to variations of the select parameters. Similar to the coarse-grained subgrade model results,  $Th_{AC}$  may have the most significant impact on the peak surface deflection during a moisture variation event and under a given traffic load. Unlike the coarse-grained subgrade model, the results indicate that evaporation rate may have a significant impact on  $\delta_p$  while  $\delta_p$  is not significantly affected by the variations of aggregate base and subbase hydraulic conductivity. This is due to initial assumption that aggregate base and subbase layers consist of relatively highly permeable material. However, the results indicate that the use of these permeable layers and a change in their thicknesses can significantly impact  $\delta_p$ .

**Table 4-18. Summary of the analysis of the sensitivity of  $\delta_p$  to select input parameters for fine-grained subgrade model.**

Ranking	Source	Log (worth)	t Ratio	p value
1	$Th_{AC}$	160.15	-95.4	<.0001
2	$P_r$	46.66	57.14	<.0001
3	$M_{R,AC}$	41.64	-52.13	<.0001
4	$Th_{Base}$	40.98	-39.67	<.0001
5	$e_{Subgrade}$	32.84	-37.41	<.0001
6	Initial GWL	20.88	-35.25	<.0001
7	$P_d$	18.42	-10.44	<.0001
8	$Th_{Subbase}$	10.56	-6.8	<.0001
9	$M_{R-OPT,Subbase}$	4.40	-4.14	<.0001
10	$E_r$	4.20	-4.07	<.0001
11	$w_L$	2.94	-3.27	0.0010
12	$M_{R-OPT,Base}$	2.29	2.81	0.0051
13	$K_{Subbase}$	0.53	1.06	0.291
14	$K_{S,Base}$	0.52	1.03	0.3055

### Sensitivity of $\delta_p/\delta_0$ to Select Parameters

Table 4-19 presents results of analyses for sensitivity of  $\delta_p/\delta_0$  to variations of the select parameters for the fine-grained subgrade model. Similar to the coarse-grained model, results indicate high sensitivity of  $\delta_p/\delta_0$  to input parameter governing the precipitation and hydrology of the subgrade. In addition, results indicate that  $\delta_p/\delta_0$  in fine-grained subgrade model can significantly be affected by the evaporation rate.  $\delta_p/\delta_0$  is less sensitive to stiffness of pavement layers compared to other parameters listed in Table 4-19.

**Table 4-19. Summary of the analysis of the sensitivity of  $\delta_p/\delta_0$  to select input parameters for fine-grained subgrade model.**

Ranking	Variable	Log (worth)	t Ratio	p value
1	$w_L$	348.65	-53.09	<.0001
2	$P_r$	181.712	33.19	<.0001
3	$P_d$	82.621	20.59	<.0001
4	$Th_{AC}$	55.069	-16.4	<.0001
5	$E_r$	19.933	-11.19	<.0001
6	$e_{Subgrade}$	19.345	-9.44	<.0001
7	$Th_{Base}$	9.764	9.3	<.0001
8	$Th_{Subbase}$	6.547	5.19	<.0001
9	Initial GWL	3.71	3.91	<.0001
10	$K_{s,Base}$	3.63	3.73	0.0002
11	$K_{s,Subbase}$	2.456	-2.95	0.0033
12	$M_{R-OPT,Subbase}$	2.424	2.91	0.0037
13	$M_{R,AC}$	1.811	2.43	0.0153
14	$M_{R-OPT,Base}$	0.619	1.18	0.2367

### Sensitivity of $t_p$ to Select Parameters

Results of analyses for sensitivity of  $t_p$  to variations of the select parameters indicate that climatic related data may have the most substantial impact on  $t_p$  (Table 4-20). Further,  $t_p$  is expected to be significantly affected by the thicknesses of aggregate base and subbase layers.

**Table 4-20. Summary of the analysis of the sensitivity of  $t_p$  to select input parameters for fine-grained subgrade model.**

Ranking	Variable	Log (worth)	t Ratio	p value
1	$P_r$	245.115	39.12	<.0001
2	$E_r$	141.436	-27.71	<.0001
3	$P_d$	114.124	24.43	<.0001
4	$Th_{Base}$	68.488	-18.33	<.0001
5	$Th_{Subbase}$	33.105	-12.37	<.0001
6	$w_{L, Subgrade}$	28.394	11.39	<.0001
7	$e_{Subgrade}$	9.044	-6.16	<.0001
8	$M_{R,AC}$	2.075	2.64	0.0084
9	$Th_{AC}$	1.653	-2.29	0.0222
10	<i>Initial GWL</i>	1.231	1.89	0.0587
11	$M_{R-OPT,Base}$	1.103	-1.76	0.0788
12	$M_{R-OPT,Subbase}$	0.992	1.64	0.1019
13	$K_{s, subbase}$	0.954	-1.59	0.1112
14	$K_{s,Base}$	0.914	1.55	0.122

## Sensitivity of $t_R$ to Select Parameters

Table 4-21 presents the summary of the sensitivity of  $t_R$  to variations of the select parameters evaluated in this study. Results indicate that subgrade liquid limit and precipitation rate may have the most significant impact on  $t_R$ . Also, unlike the coarse-grained model, evaporation rate may play a significant role in accelerating the recovery of surface deflection in pavements with fine-grained subgrade.

**Table 4-21. Summary of the analysis of the sensitivity of  $t_R$  to select input parameters for fine-grained subgrade model.**

Ranking	Variable	Log (worth)	t Ratio	p value
1	$W_{L,Subgrade}$	145.202	-28.78	<.0001
2	$P_r$	109.695	24.28	<.0001
3	$E_r$	48.835	-15.35	<.0001
4	$P_d$	32.818	12.37	<.0001
5	$e_{Subgrade}$	32.557	12.31	<.0001
6	$Th_{Subbase}$	8.641	-6.01	<.0001
7	$Th_{Base}$	6.708	-5.23	<.0001
8	Initial GWL	4.911	4.39	<.0001
9	$M_{R,AC}$	3.103	3.36	0.0008
10	$K_{S,Subbase}$	3.026	3.31	0.0009
11	$Th_{AC}$	1.891	-2.49	0.0129
12	$K_{S,Base}$	0.702	1.29	0.1985
13	$M_{R-OPT,Base}$	0.217	0.51	0.6066
14	$M_{R-OPT,Subbase}$	0.02	0.06	0.9547

## 4.5 SENSITIVITY ANALYSIS SUMMARY AND CONCLUSIONS

### 4.5.1 Summary and Conclusions

This section presented sets of sensitivity analysis of the SDM estimations to input variables. Results of the sensitivity analyses shed light on sensitivity of pavement performance during periods of excessive moisture with respect to various climatic, geotechnical and pavement related system parameters. The

pavement performance was interpreted in terms of four key performance measures: (1) peak surface deflection during moisture variation and under a certain traffic load, (2) the ratio of peak surface deflection and the surface deflection before precipitation event, (3) time to reach peak surface deflection, and, (4) required time for recovery of pavement system. A summary of key findings is provided herein:

- The performance of the pavement during a moisture variation event and the significance of input parameters are highly dependent on the permeability of subgrade soil.
- Regardless of the type of subgrade soil, climate data including precipitation rate and duration play a significant role in estimation of pavement performance. Accurate estimation of these parameters is of critical importance for a reasonable prediction of pavement performance during moisture variation.
- For pavements with subgrade of relatively low permeability and poor drainage system, evaporation rate may have a significant impact on pavement system performance during and after a moisture variation event.
- Thickness and mechanical properties of AC layer may significantly impact the peak surface deflection during excessive moisture conditions; however, they may have a minimal impact on the extent of the impact of moisture variation relative to the initial condition and the required time for recovery of the pavement.
- Thickness of compacted granular base and subbase layers with relatively high permeability can significantly impact the performance of pavement systems during and after excessive moisture variation. This impact is expected to be more substantial in pavements with subgrade of relatively lower permeability.
- For pavements with relatively permeable granular base and subbase layers, variation of the layers' hydraulic conductivity may not substantially impact the performance of pavement systems with fine-grained subgrade; however, it may substantially impact the performance of pavement systems with coarse-grained subgrade.
- Hydraulic properties of subgrade soil including hydraulic conductivity and water retainability can substantially impact its behavior during moisture variations. For soils with relatively high permeability (such as, clean sand), a decrease in permeability can adversely impact pavement performance while for subgrades with relatively very low permeability (i.e., clay), reduction in permeability may improve the pavement capacity during moisture variation.
- GWL may have a complex impact on the performance of pavements systems during moisture variations. While an increase in the depth of groundwater may lower peak surface deflection experienced during moisture variation, it may increase the recovery time.

The significant importance of each parameter relies on the performance measure for design or evaluation of the pavement section prone or subjected to moisture variation. Table 4-22 qualitatively presents the relative importance of input parameters for evaluation of flexible pavement performance measures based on LSA and GSA.

**Table 4-22. A qualitative summary of the significance of the impact of input parameters on the performance measure indices.**

Variable	Performance measure index							
	$(\delta_p)_{\text{coarse}}$	$(\delta_p)_{\text{fine}}$	$(\delta_p/\delta_\theta)_{\text{coarse}}$	$(\delta_p/\delta_\theta)_{\text{fine}}$	$(t_p)_{\text{coarse}}$	$(t_p)_{\text{fine}}$	$(t_R)_{\text{coarse}}$	$(t_R)_{\text{fine}}$
$D_{10, \text{Subgrade}}$		NA		NA		NA		NA
$w_{L, \text{Subgrade}}$	NA		NA		NA		NA	
$e_{\text{Subgrade}}$								
$P_r$								
$P_d$								
$E_r$								
Initial GWL								
$K_{s, \text{base}}$								
$K_{s, \text{subbase}}$								
$Th_{\text{base}}$								
$Th_{\text{subbase}}$								
$M_{R\text{-opt}, \text{base}}$								
$M_{R\text{-opt}, \text{subbase}}$								
$M_{R, AC}$								
$Th_{AC}$								
Wheel load								

	Very significant impact
	Significant impact
	Moderate impact
	Minimal impact

## CHAPTER 5: LOAD RESTRICTION DECISION PLATFORM FOR PAVEMENT SYSTEMS PRONE TO MOISTURE VARIATIONS

This chapter is organized in three sections. The first section describes the technical background and assumptions for development of the load restriction toolkit. The second section presents the toolkit components and provides a manual for users. The last section briefly presents a summary of the toolkit and the next step in improving the application.

### 5.1 Technical Background and Assumption

#### 5.1.1 Introduction

---

A coupled hydro-mechanical model was programmed in MATLAB to evaluate the performance of flexible pavements prone to moisture variations. The model was developed to simulate the real time behavior of pavement systems due to moisture variations. Similar to the system dynamics model presented in chapter 3, the model included three coupled structures: (1) a hydrological structure to capture moisture movement in saturated and unsaturated pavement layers; (2) a geotechnical structure to capture moisture-dependent mechanical properties of geomaterial; and (3) a pavement response structure to estimate pavement performance in terms of surface deflection. This section describes formulations and assumptions made for development of each structure.

#### 5.1.2 Hydrological structure

---

##### Technical background and formulations

The first step in the mechanistic analysis of pavement response to moisture variations is the simulation of moisture movement in pavement layers. This is performed through the hydrological structure. The hydrological structure consists of two main components; (1) climate information and (2) unsaturated soil hydraulics. The climate information provides material and information data that controls water flux into and out of the soil surface (i.e., flows associated with water infiltration and discharge). This includes precipitation rate and duration, evaporation rate, surface water runoff, and the height of water ponded on top of the subgrade surface. The current toolkit version obtains the precipitation data for up to 5 precipitation events with given duration and rates. The evaporation rate can be obtained based on the local weather information. Surface water runoff pertains to the portion of precipitated water (in percent) that is excluded from the pavement structure (i.e., aggregate base and subbase layers) and it depends on the topography of the natural ground and performance of pavement drainage systems. A surface water runoff of 100% is expected for pavements with significant grades or proper drainage system and a surface water runoff of 0% is expected for pavements located in flat areas with no drainage systems.

The second component in hydrological structure of the toolkit is the unsaturated soil hydraulics. This component includes the variables and governing equations related to estimation of initial pavement layers' moisture content, moisture movement in unsaturated pavement layers, and their time dependent moisture



content. The initial moisture content of the subgrade is estimated based on the soil water retention curve (SWRC) data and initial groundwater level (GWL) (i.e., depth of groundwater to the subgrade natural surface). In this regard, van Genuchten's formula (van Genuchten 1980) was implemented in the toolkit due to its accuracy in predicting SWRC and its common use. The model has the form expressed in Equation 3-6.

The initial moisture content (i.e., before precipitation initiation) of aggregate base and subbase layers were assumed to be equal to their residual water content. It is noteworthy that the infiltration process in this study was assumed to occur through pavement shoulders. Since the permeability of aggregate base and subbase layers are typically much higher than natural subgrade soil, the infiltration of water through these layers may result in ponding of water above subgrade layer. Therefore, the degree of saturation in these layers is governed by both water infiltration in these layers and ponded water height above the subgrade. Accordingly, the aggregate base and subbase layers' degree of saturation are calculated based on the weighted average of the inundated portion and the unsaturated portion of each layer. The moisture movement in subgrade soil is governed by its hydraulic properties including saturated and unsaturated hydraulic conductivity and moisture content. Richards' equation for the one-dimensional transient unsaturated flow through subgrade layers to the groundwater table in an isotropic soil deposit can be expressed as in Equation 3-5. The moisture-dependent hydraulic conductivity at each soil layer soil can, then, be calculated according to Mualem (1976), as in Equation 3-7. The hydraulic conductivity of fully saturated soil layer can be obtained from field tests or be estimated by semi-empirical equations. Table 4-7 summarized empirical equations for estimating the hydraulic conductivity of soils in fully saturated state used in the toolkit. While Richards' equation is one of the most accurate methods to model the moisture infiltration into unsaturated soils, it requires a numerical solution due to the challenges in setting the initial and boundary conditions. Yang et al. (2009) suggested a simple numerical solution of Equation 3-5 for water movement in unsaturated soils and demonstrated that the solution works satisfactorily. The solution uses the integration of Equation 3-5, vertically, over the soil layer to simulate moisture movement in unsaturated soil layers (Yang et al. 2009), as in Equation 3-11. The flow rate at each layer is calculated based on the volumetric water content, moisture dependent hydraulic conductivity, and soil pressure head at a given time step using Equations 3-12 and 3-13. To simulate water movement in subgrade layers, the simplified numerical solution of Equation 3-5 was formulated into MATLAB. The toolkit incorporates the climate variables and variables related to the flow in unsaturated soil layers to simulate the moisture movement in real time.

### Assumptions and limitations

The assumptions and limitations of the hydrological structure formulated in the toolkit are as follows:

1. The hydrological structure considers one dimensional vertical flow into the pavement layers. Although the impact of ground topography can be incorporated by adjusting surface water runoff, it is not directly modeled in the toolkit. A two- or three-dimensional model is to be developed to consider the impact of topography and complex hydrology of the area.
2. The toolkit assumes constant groundwater level throughout the analysis. In other words, it is assumed that the water entering the groundwater flows out from the system with the same rate. A complex model considering the hydrology of the specific location is to be developed to consider groundwater level fluctuations during and after extreme weather.

3. The hydrological structure assumes a homogenous subgrade layer. The results of analyses may not be applicable to subgrade soils with highly variable soil layers.
4. The aggregate base and subbase layers are assumed to be clean granular (i.e., fines content less than 10%) material with relatively high permeability and low water retainability.

### 5.1.3 Geotechnical structure

#### Technical background and formulations

The second structure in the toolkit is the geotechnical structure. The geotechnical structure incorporates the time dependent moisture content of pavement layers estimated from the hydrological structure to estimate their resilient modulus. This is performed by using Equation 3-14 which estimates unbound pavement layers' resilient modulus ( $M_R$ ) based on their resilient modulus at the optimum degree of saturation ( $M_{R-OPT}$ ) (Zapata et al. 2007) using Equation 3-14. Based on soil type, Zapata et al. (2007) suggested some typical values for fitting parameters  $a$ ,  $b$ , and  $k_m$ , as summarized in Table 5-1.

**Table 5-1: Suggested values for fitting parameters in geotechnical structure of the toolkit (Zapata et al. 2007).**

Parameters	Value/note
$a$	=-0.3123 for coarse grained soils =-0.5934 for fine grained soils
$b$	=0.3 for coarse grained soils =0.4 for fine grained soils
$k_m$	=6.8157 for coarse grained soils = 6.1324 for fine grained soils

#### Assumptions and limitations

The assumptions and limitations of the geotechnical structure formulated in the toolkit are as follows:

1. The geotechnical structure does not consider the stress dependency of resilient modulus. In other words, the optimum resilient modulus of each layer is to be input based on estimated stress level in that layer and does not update with a change in stress levels during the analysis.
2. The model assumes homogenous aggregate base, subbase, and subgrade layers. An equivalent resilient modulus may be used for nonhomogeneous layers.

### 5.1.4 Pavement response structure

#### Technical background and formulations

The pavement surface deflection is considered as an indicator of the pavement performance indicator in the current pavement response structure. Therefore, the pavement structure incorporates the real time moisture

movement and pavement layers' mechanical variables from hydrological and geotechnical structures to estimate surface deflection based on traffic and current pavement condition information. In this regard, Odemark's Equivalent Thickness Method (ETM) is employed to reduce the multilayer elastic pavement system to an equivalent single half-space layer (Ullidtz 1987). ETM is also used in MnPAVE (Minnesota Department of Transportation 2012) to reduce multiple asphalt concrete (AC) layers into single layer. ETM uses each layer's elastic modulus ( $E$ ) and Poisson ratio ( $\nu$ ) to convert the layered pavement system to a single homogenous half-space layer according to Equation 3-15. Analyses using Equation 3-15 and layered elastic analysis software, General Analysis of Multi-layered Elastic Systems (GAMES) (Maina and Matsui 2004) indicated less than 20% error in stress distribution estimations when  $E_n = E_{\text{Subgrade}}$ ,  $\nu_n = \nu_{\text{Subgrade}}$ , and  $C_{AC} = 0.5$ ,  $C_{\text{Base}} = 0.7$ ,  $C_{\text{Subbase}} = 0.85$ , and  $C_{\text{subgrade}} = 1$ . Equation 3-15 converts each pavement layer to a new layer with equivalent thickness and mechanical properties to ones in layer  $n$ . The stress distribution and deflection in each layer can then be calculated using (Boussinesq 1885) theory for a homogenous and isotropic linear elastic half-space system in axisymmetric condition as in the following equations (re-written based on Equation 3-16, Equation 3-17, and Equation 3-18):

$$\sigma_z = q \left( 1 - \frac{z^3}{(R^2 + z^2)^{1.5}} \right)$$

Equation 5-1

$$\sigma_r = \frac{q}{2} \left[ 1 + 2\nu_z - \frac{2(1 + \nu_z)z}{(R^2 + z^2)^{0.5}} - \frac{z^3}{(R^2 + z^2)^{1.5}} \right]$$

Equation 5-2

$$\epsilon_z = \frac{1}{E_z} [\sigma_z - \nu_z (2\sigma_r)]$$

Equation 5-3

where  $R$  is the equivalent tire radius and is calculated based on wheel load ( $L$ ) and tire pressure ( $q$ ):

$$R = \sqrt{\frac{L}{q \times \pi}}$$

Equation 5-4

$\epsilon_z$  is the vertical strain at depth  $z$ ,  $\sigma_r$  is the horizontal stress, and  $E_z$  and  $\nu_z$  are the young modulus and Poisson ratio of layer  $i$  located at depth  $z$ . The wheel load and tire pressure are assigned based on vehicle tire and axle configuration and loading. In this regard, the 13-category FHWA vehicle classification shown in Figure 5-1 is adopted (FHWA, 2014).

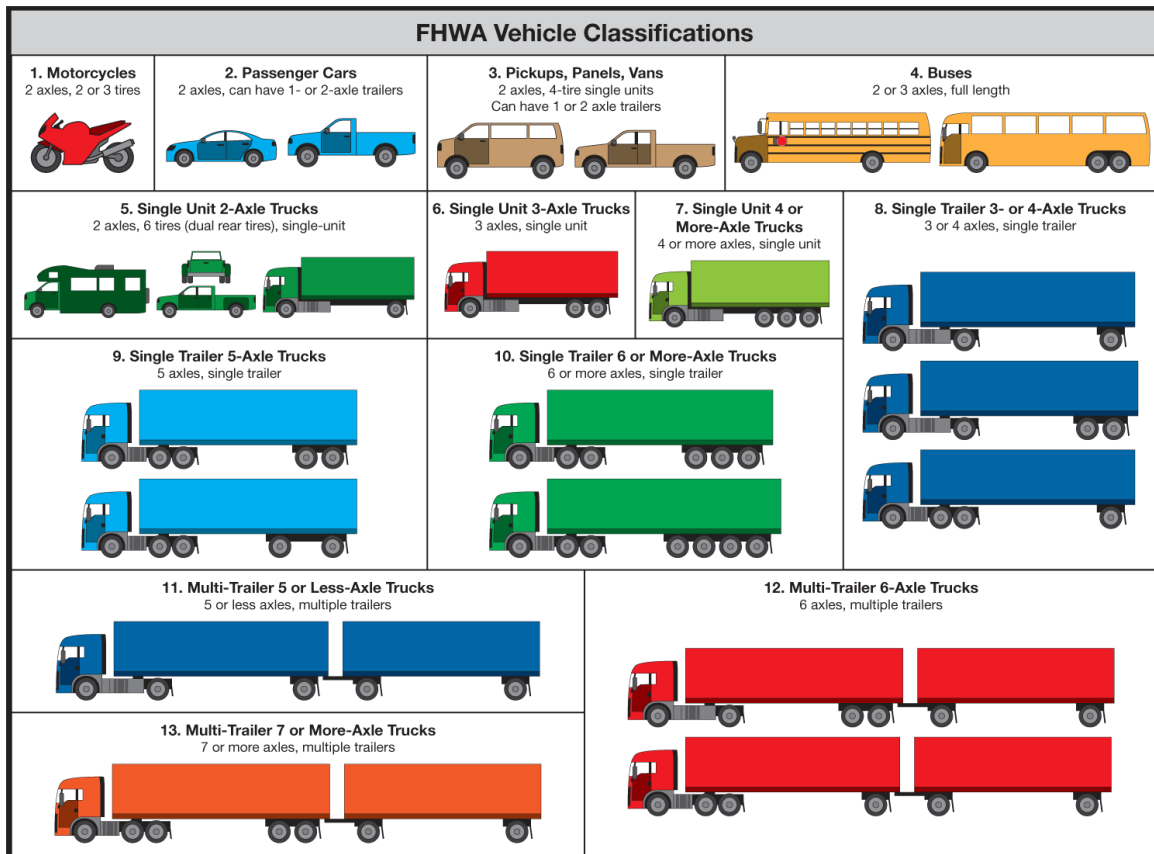
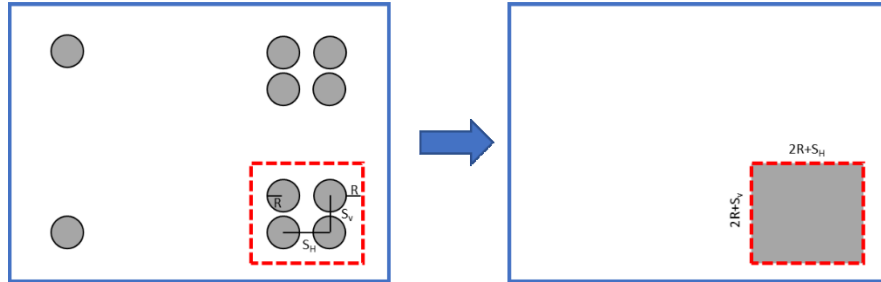


Figure 5-1. 13-category FHWA vehicle classification (FHWA, 2014).

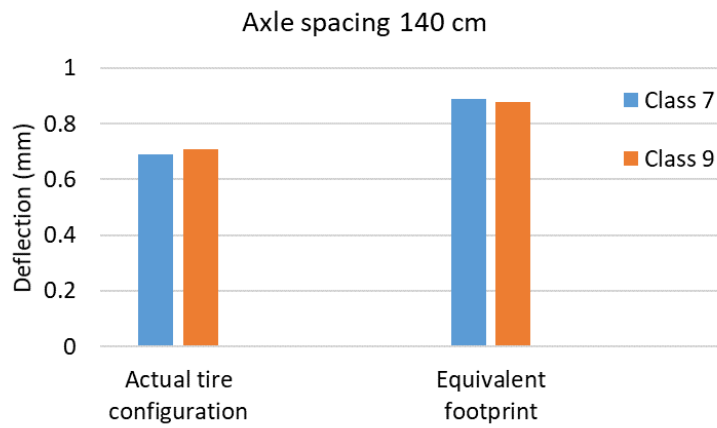
The induced stress on AC surface by each vehicle class is calculated by an equivalent footprint method. In this method, the axle loads are assumed to be distributed uniformly in a rectangular footprint enclosing the tandem/tridem and dual tires on one side of the axle. For example, Figure 5-2 presents a conceptual schematic of the equivalent footprint method to calculate induced pressure and its radius for vehicle class 6. According to this figure, it is assumed that the loads applied on the tandem dual tires of the rear axle is distributed uniformly over a rectangular area with  $2R+S_H \times 2R+S_V$  dimensions; where  $R$  is the equivalent radius of the tire footprint calculated based on tire load and pressure (See Equation 5-4),  $S_H$  is the spacing between tandem tires, and  $S_V$  is the spacing between dual tires. The equivalent footprint radius and the equivalent pressure is calculated by having the rectangular area and the load on the four tires.

**6. Single Unit 3-Axle Trucks**  
3 axles, single unit

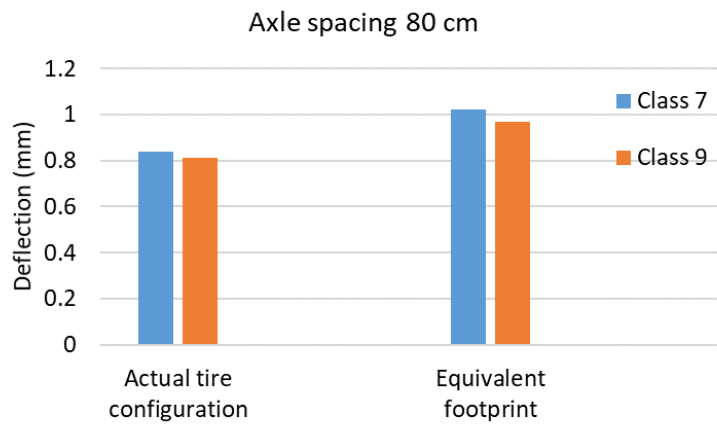


**Figure 5-2. Conceptual example of the equivalent footprint method for calculation of induced pressure and radius on AC surface.**

The layered elastic analysis software, GAMES, was used to evaluate the accuracy of the equivalent footprint method in estimating the induced deflection on AC surface. In this regard, the deflections on AC surface of a given flexible pavement system were analyzed by (1) considering the actual tire configuration (this does not refer to the actual tire footprint. It just means the actual arrangement of the wheels as opposed to an equivalent block footprint) and (2) equivalent footprint method. Results of analyses indicate that the equivalent footprint method leads to a conservative estimation of AC surface deflection as shown in Figure 5-3. In general, the surface deflections estimated considering the equivalent footprint method were approximately 20-25% higher than the ones estimated considering the actual tire configuration.



(a)


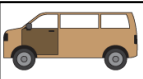









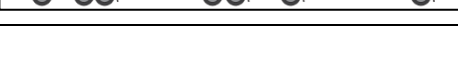


(b)

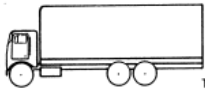
**Figure 5-3. Comparisons of AC deflection estimations assuming actual tire configuration and the equivalent footprint method for vehicle class 7 and class 9. (a) Axle spacing 140cm (b) Axle spacing 80cm.**

The maximum allowable axle loads from comprehensive truck size and weight study (based on a Report prepared for FHWA, 1995), shown in Figure 5-4, were considered to estimate the load on equivalent footprint for each vehicle class. The axle and tire spacing, and tire pressures considered for each vehicle class are summarized in Table 5-2.

**Table 5-2: The axle and tire spacing, and tire pressures considered for each vehicle class.**

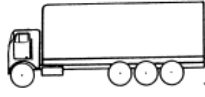
Vehicle class	Representative configuration	Tire Spacing meter (inch)	Axle spacing meter (inch)	Tire pressure kPa (psi)
2		-	-	275.8 (40)
3		-	-	551.6 (80)
4		0.35 (13.5)	1.37 (54)	689.476 (100)
5		0.35 (13.5)	1.37 (54)	689.476 (100)
6		0.35 (13.5)	1.37 (54)	689.476 (100)
7		0.35 (13.5)	1.37 (54)	689.476 (100)
8		0.35 (13.5)	1.37 (54)	689.476 (100)
9		0.35 (13.5)	1.37 (54)	689.476 (100)
10		0.35 (13.5)	1.37 (54)	689.476 (100)
11		0.35 (13.5)	1.37 (54)	689.476 (100)
12		0.35 (13.5)	1.37 (54)	689.476 (100)
13		0.35 (13.5)	1.37 (54)	689.476 (100)

(a) Three-Axle Single-Unit Truck



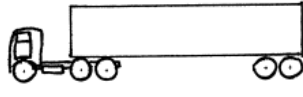
Weight (lb 000s)	16	32	48	Total
ESALs				
Flexible	0.62	0.86	1.48	
Rigid	0.60	1.50	2.10	

(b) Four-Axle Single-Unit Truck



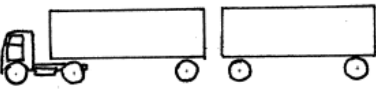
Weight (lb 000s)	16	40	56	Total
ESALs				
Flexible	0.62	0.49	1.11	
Rigid	0.60	1.18	1.78	

(c) Five-Axle Tractor-Semitrailer (3-S2)



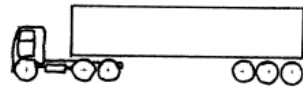
Weight (lb 000s)	12	34	34	Total
ESALs				
Flexible	0.19	1.09	1.09	2.37
Rigid	0.17	1.95	1.95	4.07

(d) Five-Axle Double (2-S1-2)



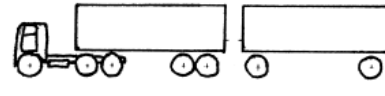
Weight (lb 000s)	9	20	19	16	18	Total
ESALs						
Flexible	0.06	1.51	1.24	0.62	0.62	4.05
Rigid	0.05	1.58	1.26	0.60	0.60	4.09

(e) Six-Axle Tractor-Semitrailer (3-S3)



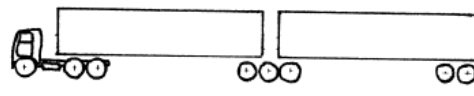
Weight (lb 000s)	12	34	42	Total
ESALs				
Flexible	0.19	1.09	0.60	1.88
Rigid	0.17	1.95	1.45	3.57

(f) Seven-Axle Double (3-S2-2)



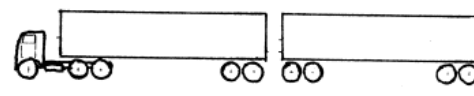
Weight (lb 000s)	9	31	30	16	15	101	Total
ESALs							
Flexible	0.06	0.75	0.66	0.62	0.48	2.57	
Rigid	0.05	1.31	1.14	0.60	0.46	3.56	

(g) Eight-Axle B-Train Double (3-S3-2)



Weight (lb 000s)	12	34	42	34	Total
ESALs					
Flexible	0.19	1.09	0.60	1.09	2.97
Rigid	0.17	1.95	1.45	1.95	5.52

(h) Nine-Axle Double (3-S2-4)



Weight (lb 000s)	12	33	28	28	28	Total
ESALs						
Flexible	0.19	0.97	0.50	0.50	0.50	2.66
Rigid	0.17	1.71	0.85	0.85	0.85	4.43

Figure 5-4. Axle weights for different truck sizes from comprehensive truck size and weight study.

## Assumptions and limitations

The assumptions and limitations in the pavement structure formulated in the toolkit are as follows:

1. The model assumes homogenous aggregate base, subbase, and subgrade layers. The variations in layers strength with depth is not considered in this study.
2. Although the ETM method with equivalent footprint used in the toolkit provides an approximate estimation of stress distribution in pavement layers, layered elastic formulations can provide more accurate estimations.
3. For the axle loads, and axle and tire configurations and vehicle classes considered in this study, the equivalent footprint method may provide a conservative estimation of stresses and deformations induced in pavement layers. Consideration of other configurations and loads are beyond the scope of this study.
4. The model assumes homogenous aggregate base, subbase, and subgrade layers. An equivalent resilient modulus may be used for nonhomogeneous layers.
5. The toolkit is developed for estimation of surface deflection in flexible pavement systems prone to moisture variations. The estimation of surface deflection in other pavement systems such as rigid pavement is beyond the scope of this study.



6. The pavement response structure does not consider the mechanical behavior of problematic soils such as expansive clay and collapsible soils.
7. The impact of freeze and thaw on geo-hydro-mechanical behavior is not considered in this study.

## 5.2 TOOLKIT USER MANUAL: PAVESAFE™ V1.0.4

### 5.2.1 Requirements and Installation Procedures

The toolkit “PaveSafe™” is currently at version v1.0.4. The toolkit requires MATLAB Compiler Runtime (MCR) to be installed on the host system.

MCR inherits identical system requirements as of the MATLAB version used to build the toolkit. MATLAB 2019b Update 3 has been used for toolkit development.

General MCR requirements are listed below:

1. For Macintosh systems: <https://www.mathworks.com/content/dam/mathworks/mathworks-dot-com/support/sysreq/files/system-requirements-release-2019b-macintosh.pdf>
2. For Windows systems: <https://www.mathworks.com/content/dam/mathworks/mathworks-dot-com/support/sysreq/files/system-requirements-release-2019b-windows.pdf>
3. For Linux systems: <https://www.mathworks.com/content/dam/mathworks/mathworks-dot-com/support/sysreq/files/system-requirements-release-2019b-linux.pdf>

#### Installation Procedure:

**Step 1:** The toolkit package is provided in two folders:

- PaveSafe Application
- MyAppInstaller

Users can choose to use the PaveSafe Application folder which contains the toolkit to run the application, given, MCR already configured in the host system.

If MCR is not configured on the host system, users may need to use the MyAppInstaller folder and launch the contained installer file “MyAppInstaller\_web”. Detailed installation procedure using the installer is mentioned in the following steps

 MyAppInstaller	5/21/2021 8:14 AM	File folder
 PaveSafe Application	5/21/2021 9:07 AM	File folder

Figure 5-5. Toolkit package folders.

**Step 2:** Open the MyAppInstaller\_web installer.

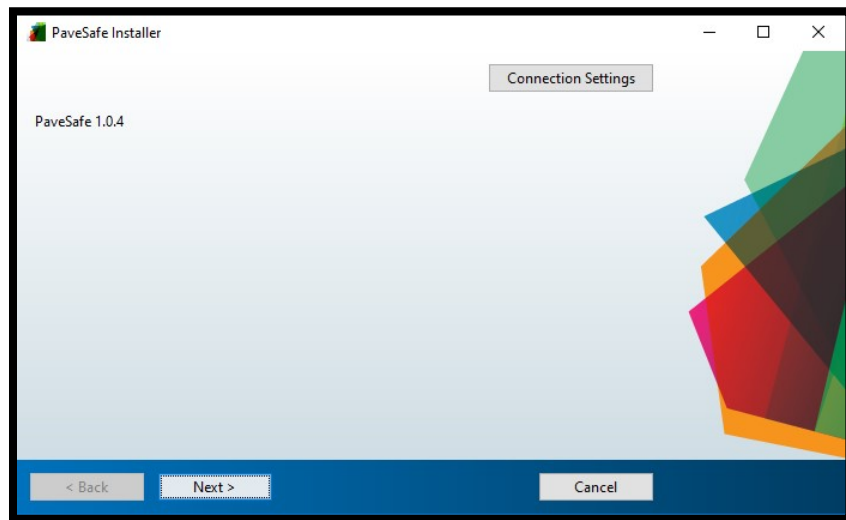


Figure 5-6. Web installer screenshot.

**Step 3:** Select the application installation folder.

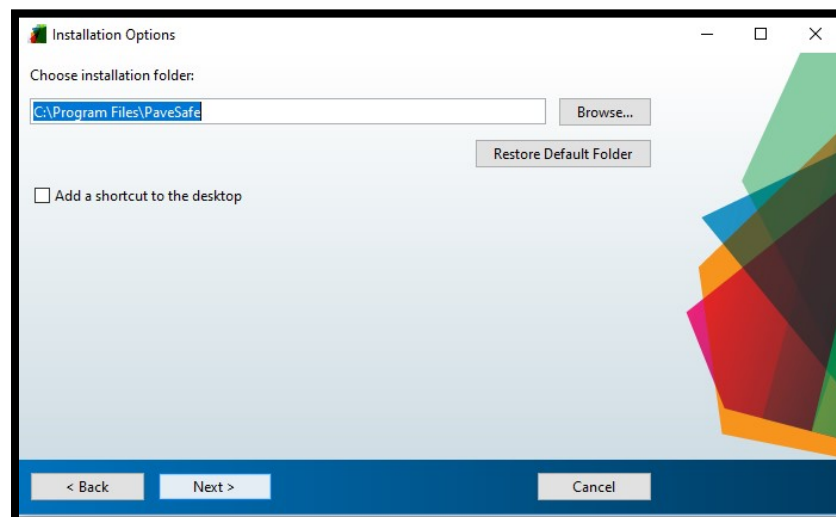


Figure 5-7. A screenshot of application installer folder selection tab.

**Step 4:** Installer will detect if the MRC is installed on the host computer. If it is not already configured, a prompt for choosing the installation folder appears.

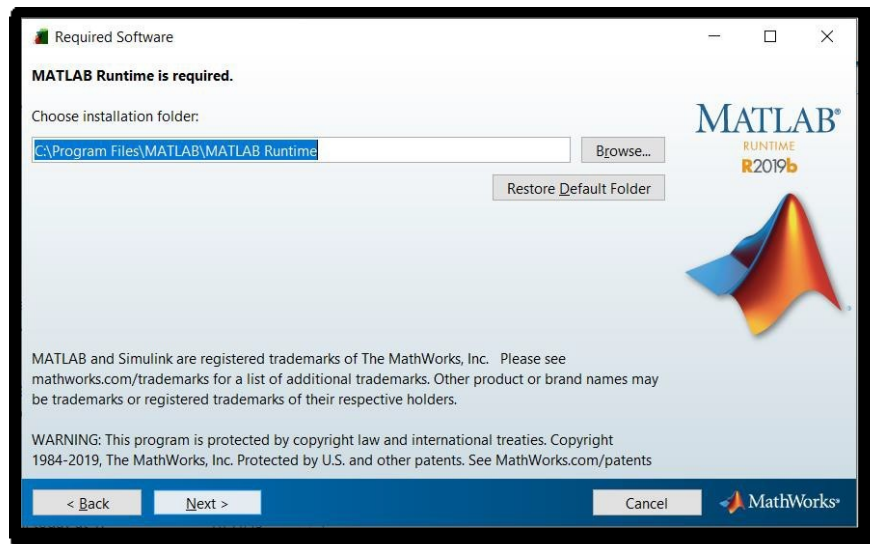


Figure 5-8. A screenshot of software installer folder selection tab.

**Step 5:** Accept the license agreement, confirm, and wait until installation is completed.

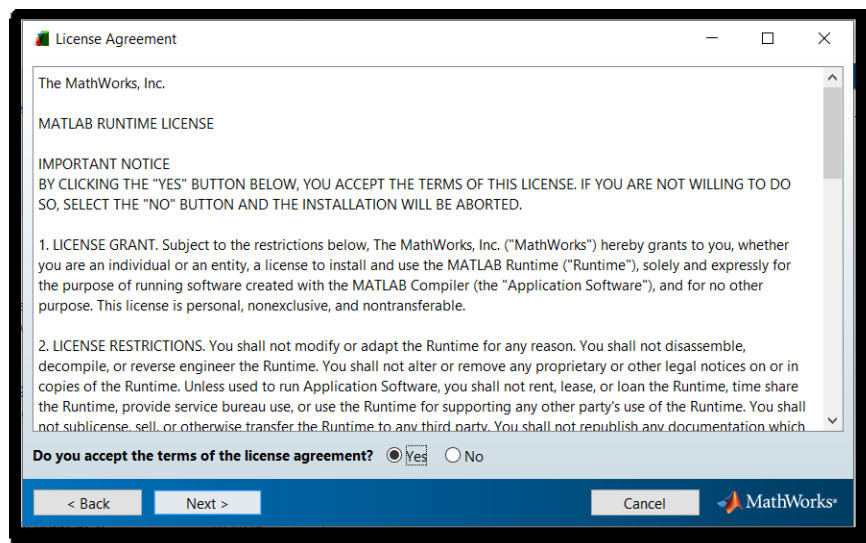


Figure 5-9. Matlab runtime license agreement.

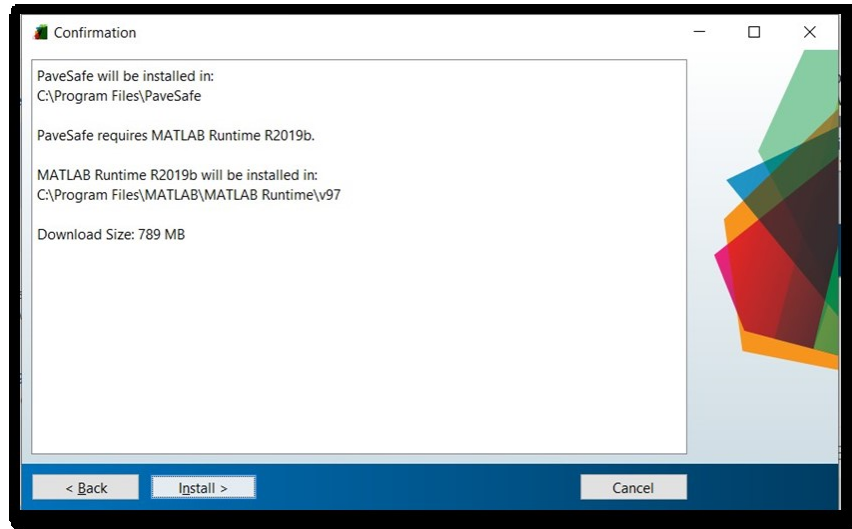


Figure 5-10. Matlab runtime installer tab.

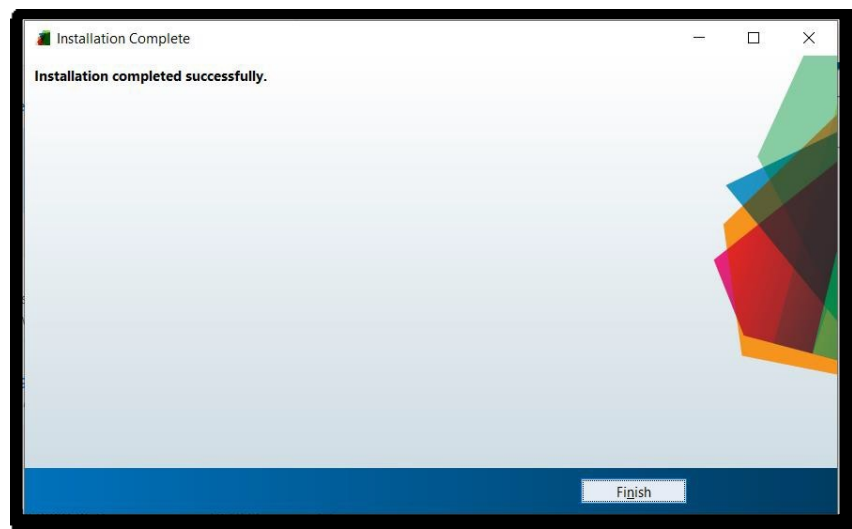


Figure 5-11. A screenshot of Installation completion message.

### 5.2.2 Introduction

---

The toolkit PaveSafe™ v1.0.4 is password protected via password protected window and requires the user to provide inputs across 5 panels after correct password has been provided. In addition to these sections, the toolkit offers the Menu Tab on top of the PaveSafe application window. In the version PaveSafe™ v1.0.4 we have added the flexibility for user to select SI Units or use US Customary instead.

The application collectively contains the following sections:

- Password Protection Window
- SI Units vs US Customary Selection Stage
- Project Information Panel
- Pavement Structure Panel
- Subgrade Properties Panel
- Hydrological Information Panel
- Results Panel
- Menu Tab

These panels and windows are described in more detail in the upcoming sections.

### 5.2.3 Password Protection Menu

---

Inherently, MATLAB does not provide a password protection for the generated applications. A password protection window that secures the app from unauthorized access is prepared.

**Disclaimer:** Please note that there is no underlying encryption mechanism which protects the application from people who have intentions to misuse the application. Simple methods such as brute force (example – John the Ripper password cracking software) can still break the password. It is advised to share the application with the intended users only. In workspaces, users should be trained to be aware of attacks such as Shoulder Surfing, Tailgating, Phishing and other forms of Social Engineering attacks. The host systems can be secured by using anti-virus and setting up appropriate firewall settings. These preventive measures along with provided password protection can reduce the risk of misuse. We do not guarantee complete protection against hackers or take accountability for any misuse of the application. It is the responsibility of the intended users to keep the application secure.

On launch, a password protection screen pops out and requires the users to enter the password. After providing the password it is required to press the “Check Password” button in order to proceed.

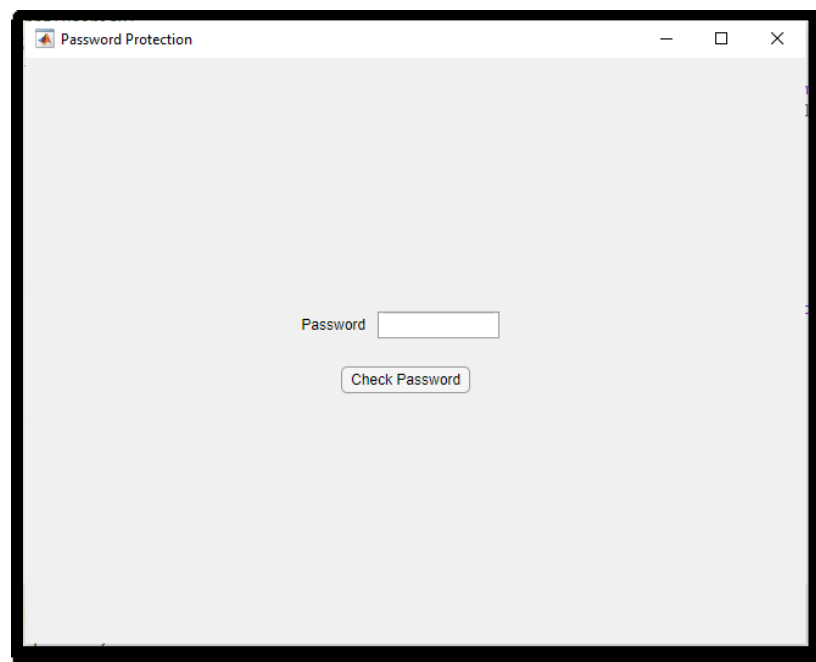
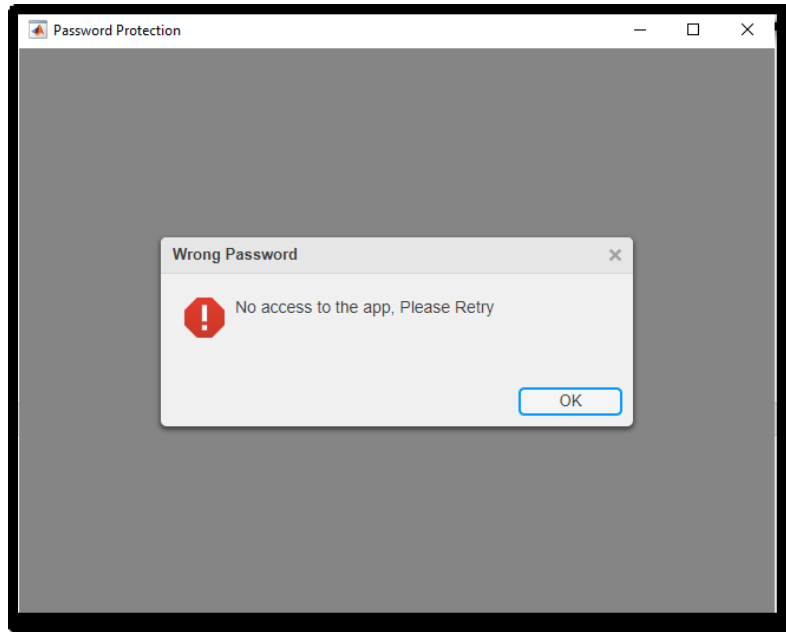


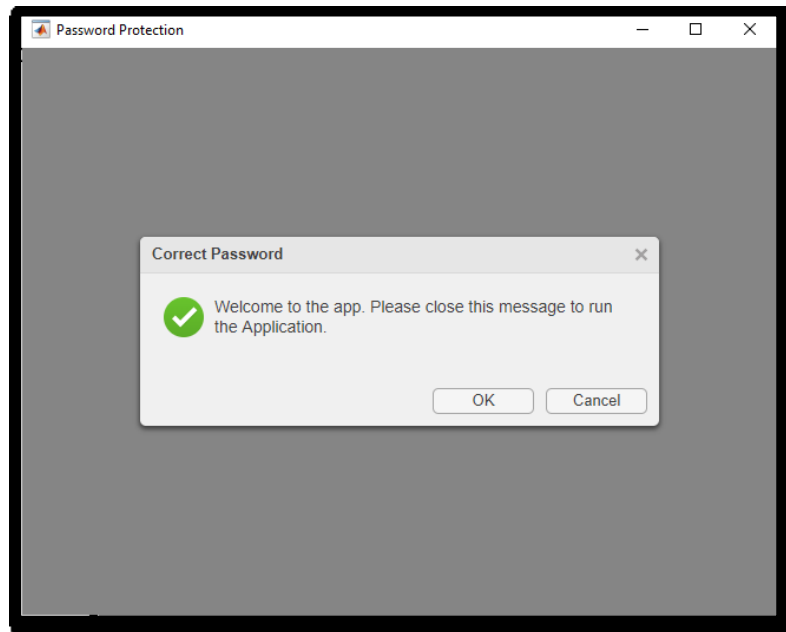
Figure 5-12. A screenshot of password window.

In the event of providing an incorrect password, a wrong password alert box appears on the screen. You may choose to close the alert box or press “OK” to proceed.



**Figure 5-13. A screenshot of wrong password message.**

In the event of providing a correct password, a correct password alert box appears on the screen. You must choose to close the alert box by pressing “OK”, “Cancel” or closing the alert box by clicking the “X” on top right side of the alert box to proceed working with the PaveSafe application.



**Figure 5-14. A screenshot of correct password message.**

#### 5.2.4 Unit System Selection (SI units vs US customary)

---

In this stage, user is required to select the units of measurement.

We have the following units of measurements in place:

- SI Units
- US Customary

A dialogue box will appear requiring the user to select the desired units of measurement. If user chooses to close the dialogue box without selection, SI Units will be default.

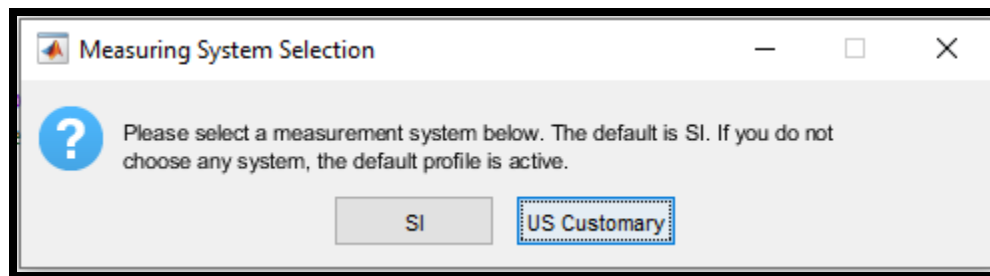


Figure 5-15. A screenshot of dialogue box for unit system selection



### 5.2.5 Project Information Panel

On launch of the application post selecting the desired units of measurement, Project Information panel appears in the application which has the following optional inputs to be provided by the user:

- Project Name:
- Engineer Name:
- Route:
- City:
- Date:
- Notes: Any additional notes to be saved for future reference.

The screenshot shows the 'PavSafe v1.0.4' application window. On the left is a sidebar with four buttons: 'Asphalt Concrete' (selected), 'Subgrade Properties', 'Hydrological Information', and 'Results'. The main area is titled 'Project Information' and contains input fields for 'Project Name', 'Engineer Name', 'Route', 'City', 'Date', and 'Notes'. At the bottom of the main area are logos for 'NRRRA National Road Research Alliance' and 'University of New Hampshire'.

Figure 5-16. A screenshot of project information panel.

The Pavement Structure, Subgrade Properties, Hydrological Information and Results Panels can be accessed by pressing the individual buttons on the left-hand side of the application screen. If these buttons are pressed again then the button is de-selected, and it brings the users back to the Project Information Panel

## 5.2.6 Pavement Structure Panel

The Pavement Structure panel requires the user to input thickness (in units of cm or inch), resilient modulus (in units of MPa or ksi) and saturated hydraulic conductivity (in units of m/hour or ft/s) for Asphalt Concrete, Aggregate Base and Subbase layers. Please note that it is not required to provide saturated hydraulic conductivity for the Asphalt Concrete layer. The users may choose to use the default values provided. The field “Type” was added in PaveSafe v1.0.4 and it provides the user 2 dropdowns to choose default values for AASHTO or MnDOT Class with respect to Aggregate Base and Subbase selection (if other agencies provide us with their default materials and corresponding properties, those will be added to the selection drop-box). Note that, the units will change when US Customary is selected.

**Pavement Structure**

Type	Selection	Layers	Thickness (cm)	Modulus (MPa)	Ks,sat (m/hour)
		Asphalt Concrete	10	3000	
Base Selection	<input checked="" type="checkbox"/>	Base	15	275.8	10
Subbase Selection	<input checked="" type="checkbox"/>	Subbase	25	275.8	5

Base Selection: AASHTO A-1-a ▼  
Subbase Selection: AASHTO A-1-b ▼

Logos: NRRRA, University of New Hampshire

Figure 5-17. A screenshot of pavement structure panel.

In order to remove Aggregate Base and Subbase layers from calculations in case those layers do not exist, users may opt to uncheck the respective selection check boxes. By default, these layers are selected for calculations.

### 5.2.7 Subgrade Properties Panel

The default screen for the Subgrade Properties Panel has the following appearance:

**Pavement Structure**

- Asphalt Concrete
- Base
- subbase

**Subgrade Properties**

Soil Type: Coarse Grained  
Soil Category: A-2-4

Resilient Modulus at OMC (MPa): 65

*van Genuchten's SWRC parameters*

$\alpha vG$  (1/m): 90  
 $nvG$  (-): 3

**Saturated Hydraulic Conductivity**

☐ Input Value ☒ Estimate

Void Ratio,  $e$ : 0.6  
Effective Grain Size,  $D_{10}$  (mm): 0.02  
 $K_s$  saturated (m/hour): 0.002

Estimate  $K_s$

**Hydrological Information**

**Results**

**NRRRA** National Road Research Alliance  
**University of New Hampshire**

Figure 5-18. A screenshot of subgrade properties panel; an example of coarse grained soil.

**Subgrade Properties**

Soil Type: Fine Grained  
 Soil Category: A-4

Resilient Modulus at OMC (MPa): 40

van Genuchten's SWRC parameters  
 $avG$  (1/m): 1.6  
 $nvG$  (-): 1.4

Saturated Hydraulic Conductivity  
☐ Input Value ☒ Estimate

Void Ratio,  $e$ : 0.8  
 Liquid Limit (%): 10  
 $K_s$  saturated (m/hour): 0.0002

Estimate  $K_s$

NRRRA National Road Research Alliance  
 University of New Hampshire

Figure 5-19. A screenshot of subgrade properties panel; an example of fine grained soil.

The Soil Type dropdown menu controls the Soil Category dropdown and default values of other inputs appearing on the screen. The default value of Soil Type dropdown menu is “Coarse Grained” and can be changed to “Fine Grained”.

After the selection of the Soil Type, Soil Category based on AASHTO soil classification system must be selected. Based on the Soil Category default values of other inputs on the screen are populated. Users always have an option to change these values including resilient modulus at optimum moisture content (in units of MPa or ksi), van Genuchten’s SWRC fitting parameters, void ratio, effective grain size ( $D_{10}$ ) (in units of mm or inch).

The saturated hydraulic conductivity will be estimated based on either the default soil parameters or the input values, by pressing “Estimate  $K_s$ ” button. If this button is not pressed, then a default value will be assigned, which may not exactly reflect the Soil Category.

Also, there is an option provided for the user to directly input saturated hydraulic conductivity via selecting the “Input value” radio button under the Saturated Hydraulic Conductivity box, if such value is available (in units of m/hour or ft/s).

**Subgrade Properties**

Soil Type: Fine Grained  
 Soil Category: A-4

Resilient Modulus at OMC (MPa): 40

Saturated Hydraulic Conductivity:  
☒ Input Value ☐ Estimate  
 Ks saturated (m/hour): 0.0002

*van Genuchten's SWRC parameters*

$\alpha vG$  (1/m): 1.6  
 $nvG$  (-): 1.4

NRRA National Road Research Alliance | University of New Hampshire

Figure 5-20. A screenshot of subgrade properties panel; an example of fine grained soil with direct hydraulic conductivity input.

### 5.2.8 Hydrology Information Panel

Hydrological Information Panel has the following required inputs:

- Period of Analysis (in hour): By default, this value is set to be for 10 days of analysis i.e. 240 hours.
- Input Climatic Data: The precipitation events can be provided as input to the application by first selecting the “Precipitation Event” checkbox and then providing the starting and ending hour values with the rate of precipitation (in units of cm/hour or inch/hour). However, if the box assigned for each precipitation event is not checked, that event would not be considered in the analysis.
- Initial Pondered Water Height (in units of m or ft): By default, we assume there is no pondered water above the ground hence default value is 0.
- Evaporation Rate (in units of m/hour or ft/hour): The default value set inside the application is 0.005 m/hour; however, if there is no pondered water above the ground, there will be no evaporation in the calculations.
- Water Runoff (as % of precipitation): This input is the percentage of precipitation water that runs off from the ground.
- Initial Groundwater Depth (in units of m or ft): This is the depth at which groundwater table exists.

By default, 3 meters is taken as input value.

- Initial Saturation Condition: The users can select the initial saturation condition of the ground above the water table to be hydrostatic or fully saturated. The default value set is hydrostatic condition above the water table, meaning linear suction profile with depth.

The default screen appears as below:

**Hydrological Input**

Period of Analysis (hour)

Precipitation Data Method Selection  
☒ Input Climatic Data ☐ Import Climatic Data

Precipitation Event	Start (hour)	End (hour)	Rate (cm/hour)
<input type="checkbox"/>	<input type="text" value="0"/>	<input type="text" value="0"/>	<input type="text" value="0"/>
<input type="checkbox"/>	<input type="text" value="0"/>	<input type="text" value="0"/>	<input type="text" value="0"/>
<input type="checkbox"/>	<input type="text" value="0"/>	<input type="text" value="0"/>	<input type="text" value="0"/>
<input type="checkbox"/>	<input type="text" value="0"/>	<input type="text" value="0"/>	<input type="text" value="0"/>
<input type="checkbox"/>	<input type="text" value="0"/>	<input type="text" value="0"/>	<input type="text" value="0"/>

Initial Poned Water Height (m)

Evaporation Rate (m/hour)

Water Runoff (% of Precipitation)

Initial Ground Water Depth (m)

Initial Saturation Condition  
Hydrostatic Condition ▼

Schematic Help View Plot Clear Plot

NRRRA National Road Research Alliance University of New Hampshire

Figure 5-21. A screenshot of hydrological input panel.

After providing the precipitation event data, the user can view the plot of precipitation data by clicking “View Plot” button and “Clear Plot” to clear the plot from the screen. A view plot example is as shown below:

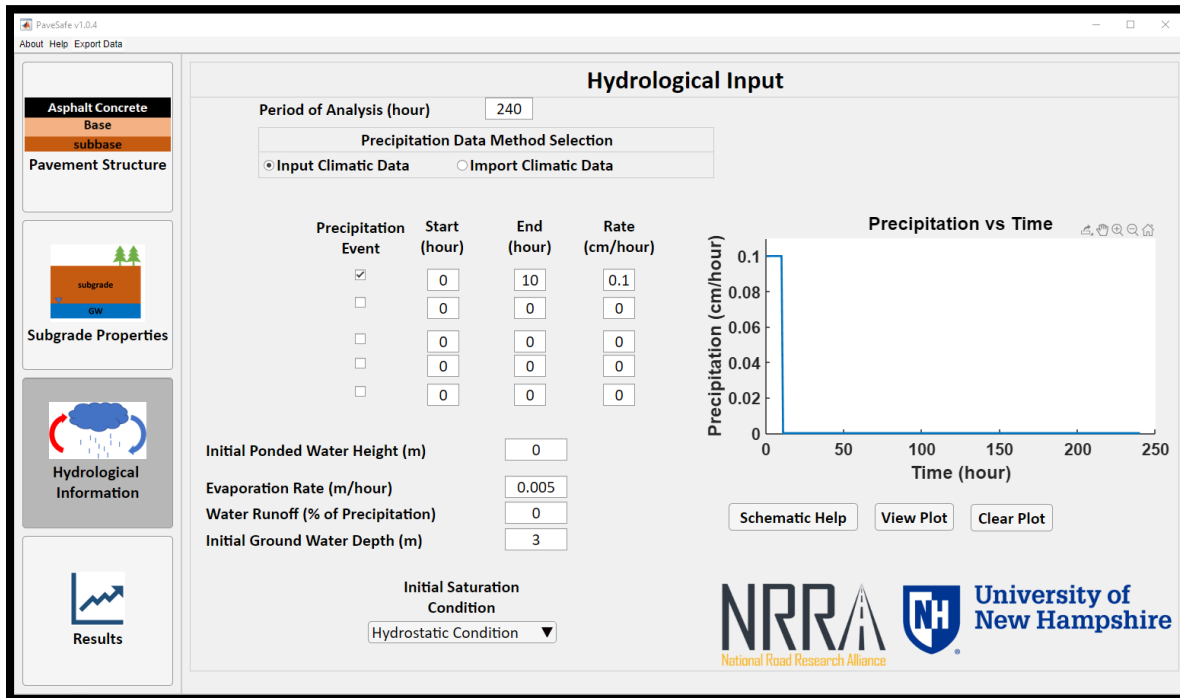


Figure 5-22. A screenshot of hydrological input panel with example precipitation time history.

The other option is “Import Climatic Data”. The default screen that appears when selecting this option is shown below:

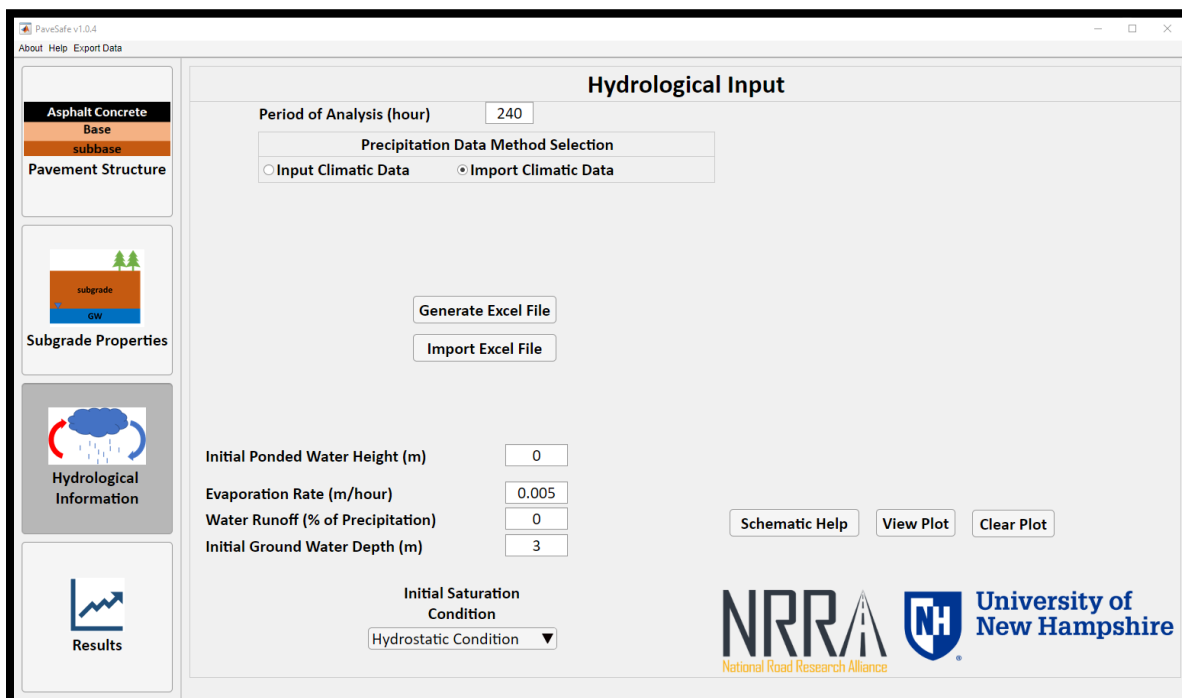






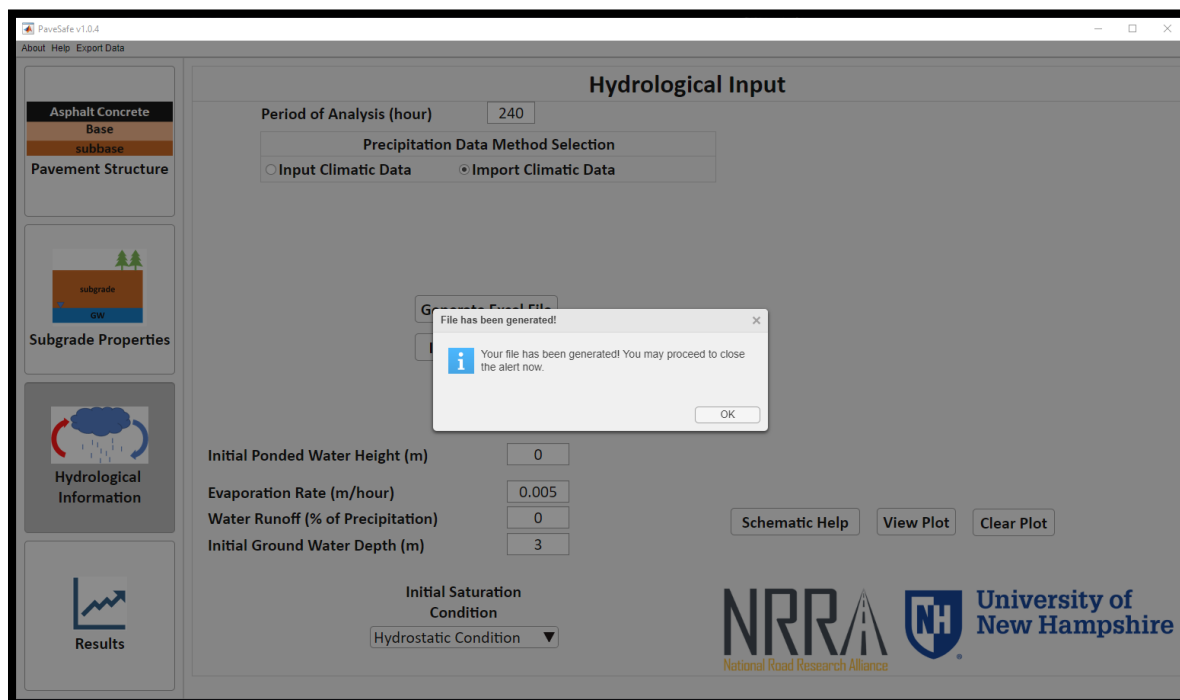
Figure 5-23. A screenshot of hydrological input panel with import climate data option.

When clicking on “Generate Excel File” a window named “Select Folder to Open” will pop up. Simply clicking on “Select Folder” without need to select any specific folder, an excel file named “Import\_Precipitation\_histories.xlsx” is going to be generated in the PaveSafe Application Folder as shown below:

	Import_Precipitation_histories.xlsx	5/21/2021 8:44 AM	Microsoft Excel W...	6 KB
	PaveSafe.exe	5/21/2021 8:14 AM	Application	3,035 KB
	readme.txt	5/21/2021 8:14 AM	Text Document	2 KB
	splash.png	5/21/2021 8:14 AM	PNG File	226 KB

**Figure 5-24. Generated climate data file name.**

When the Excel file is generated and ready to use the App will show the notification shown below:



**Figure 5-25. Message box for climate data generation.**

When opening the Excel file, its format is going to be as shown in the screenshot below:



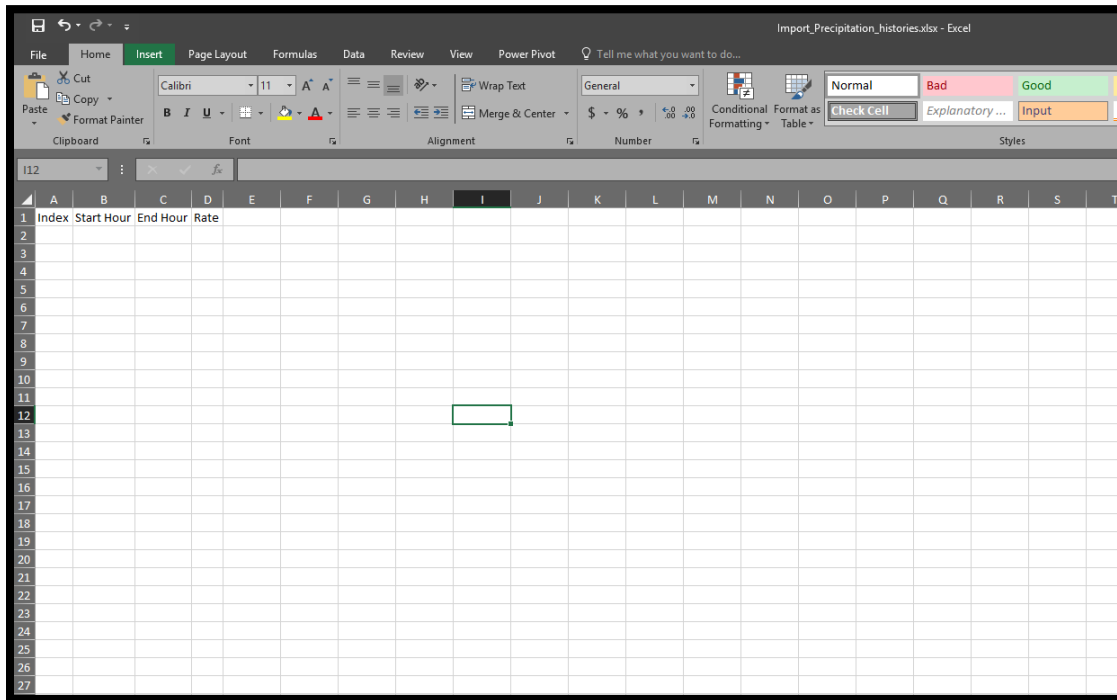


Figure 5-26. A screenshot of Excel file format.

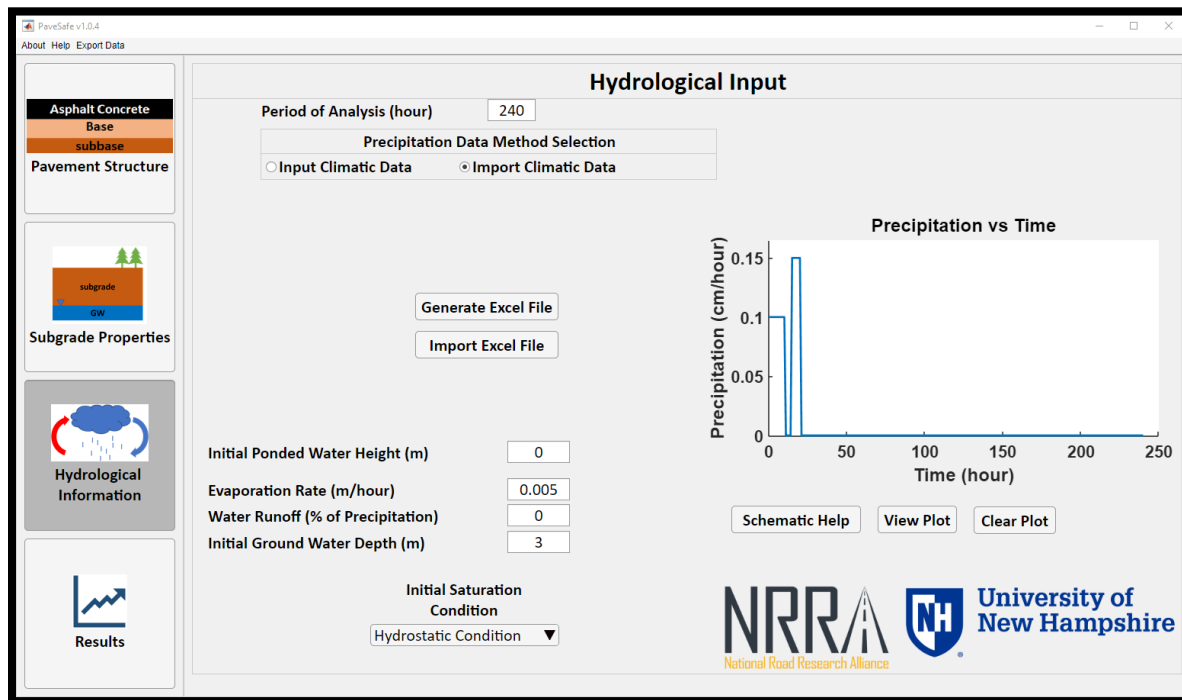
At this point the Start Hour, End Hour and Rate for the precipitation events can be inputted as shown below:

	A	B	C	D	E	F	G	H	I	J
1	Index	Start Hour	End Hour	Rate						
2		0	10	0.1						
3		15	20	0.15						
4										
5										
6										
7										
8										
9										
10										
11										
12										
13										
14										

Figure 5-27. A screenshot of Excel file basic inputs.

The user can also insert the ID or # of the precipitation event in the index column but it is not necessary for the input Excel file to work.

After saving the Excel file, the user can go back to the PaveSafe App and click on “Import Excel File” and select the Excel file from the PaveSafe Application folder. At this point, the user can click on “View Plot” to see a plot of the inputted precipitation events as shown below:



**Figure 5-28. A screenshot of hydrological input panel with example precipitation time history from input climate data file.**

Also, in PaveSafe v1.0.4, a “Schematic Help” button was introduced explaining the underlying model. The schematic help is mentioned below for reference.

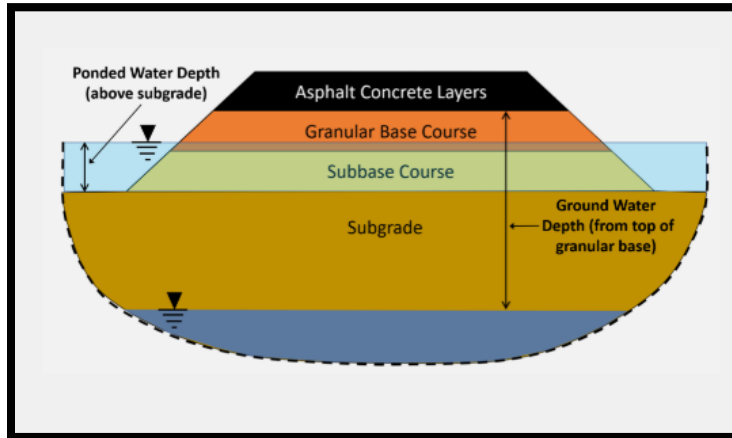


Figure 5-29. A schematic of pavement layer system with water table elevation.

### 5.2.9 Results Panel

By default, the results panel has the following appearance:

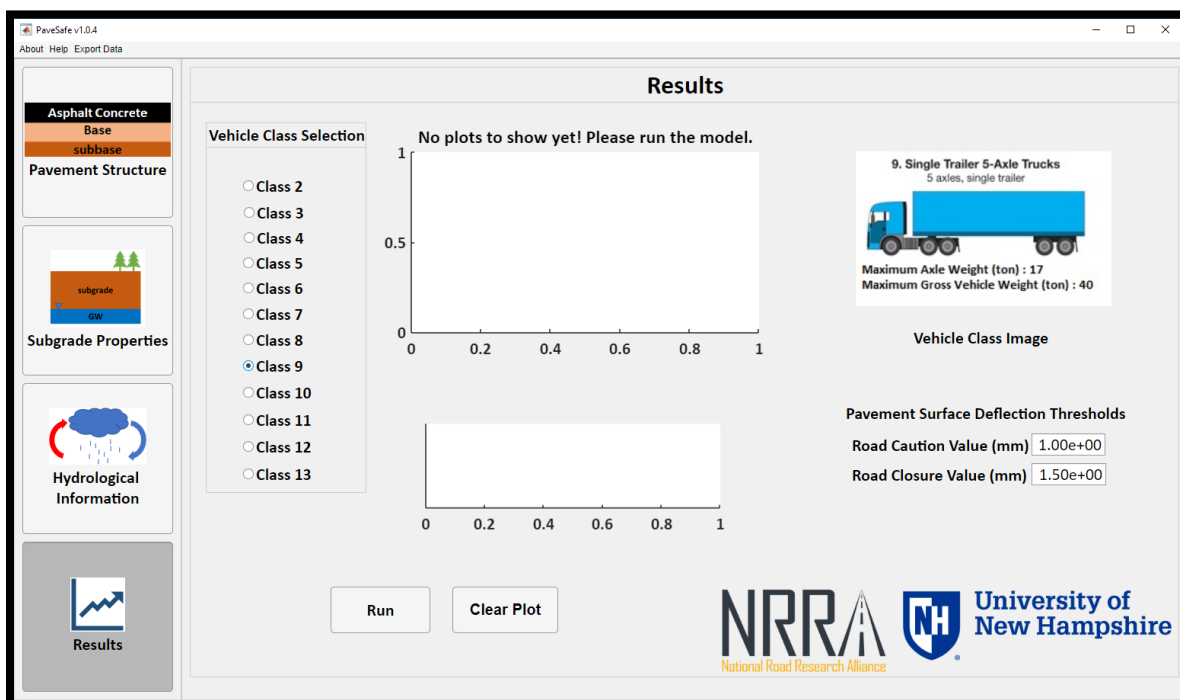


Figure 5-30. A screenshot of results panel.

The users can opt to select the desired vehicle class and a representative image of that vehicle class will appear on the screen.

As input to the application, users can set the Pavement Surface Deflection Threshold for Road Caution and Road Closure (in mm or inch). By default, these values are set to 1 mm (0.04 inch) and 1.5 mm (0.06 inch) for Road Caution and Road Closure, respectively.

After the inputs are provided or retained, the application is ready to run. To run the application please press the “Run” button appearing on the screen.

While the model is running the “Run” button turns **Yellow** in color and users must wait until the model has completed the run cycle. The running state appears as below:

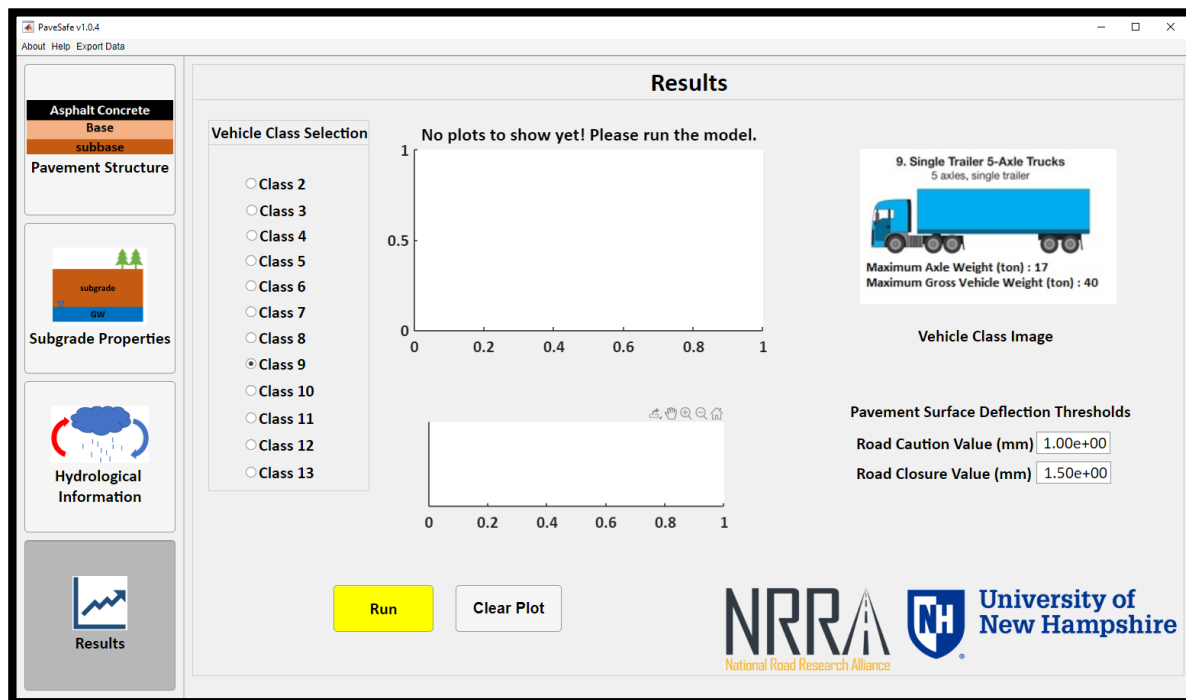


Figure 5-31. A screenshot of results panel while program is running.

Once the model has finished its run cycle, the “Run” button turns **Green** and the deflection results are displayed on the figure at the top as a graph. A bell sound alerts the user of completed run. Also, safe passage information is visible at the bottom of the graph giving information about the condition of the road with respect to the selected vehicle class. **Green** Passage means the vehicle is safe to pass, **Yellow** means it is a caution zone and **Red** means completely unsafe. After the run cycle the Results Panel appears as below:

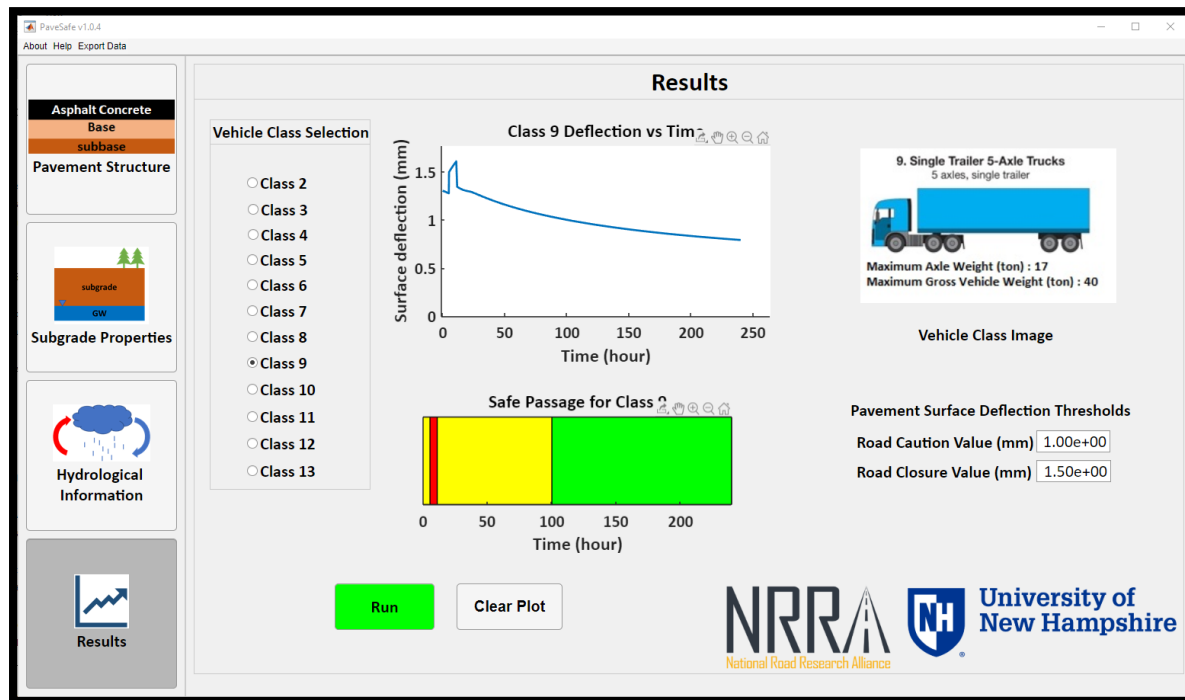


Figure 5-32. A screenshot of results panel when the analysis is completed.

The users are provided the freedom to change the Road Caution and Road Closure values to view the effect on safe passage with the new values. Users must keep in mind that it is required to change the vehicle class to reflect changes with new Road Caution and Road Closure values. Also, any change in the application inputs (excluding changes to Project Information Panel) turns the “Run” button to **Gray**, which means a new analysis and run are needed.

Note that, users are also provided with a feature to export the analysis data. This feature is available in the Menu Tab and will be explained in detail in the following section.

### 5.2.10 Menu Tab

---

The Menu Tab appears at the top of the application and contains the following options:

- About
- Help
- Export Data

The About menu brings up details about the application in the default browser. It is a pdf file and it has a possibility to be opened within the default pdf viewer on the system.

The Help menu brings up the User Manual for detailed information about the application.

The Export Data menu brings down “Export Excel File” dropdown. When this dropdown is clicked, it asks the users to provide the location where the generated file would be saved. Also, an alert box appears on the screen informing the user about the file generation process. Users may close this alert box, but they must wait until “File Generated” alert appears on the screen before they continue to interact with the application. The output file generated is a Microsoft Excel Worksheet with name “PaveSafe\_ExportData”.

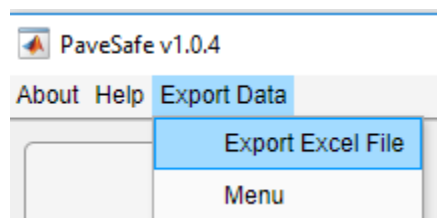


Figure 5-33. A screenshot of the menu tab to export the results excel file.

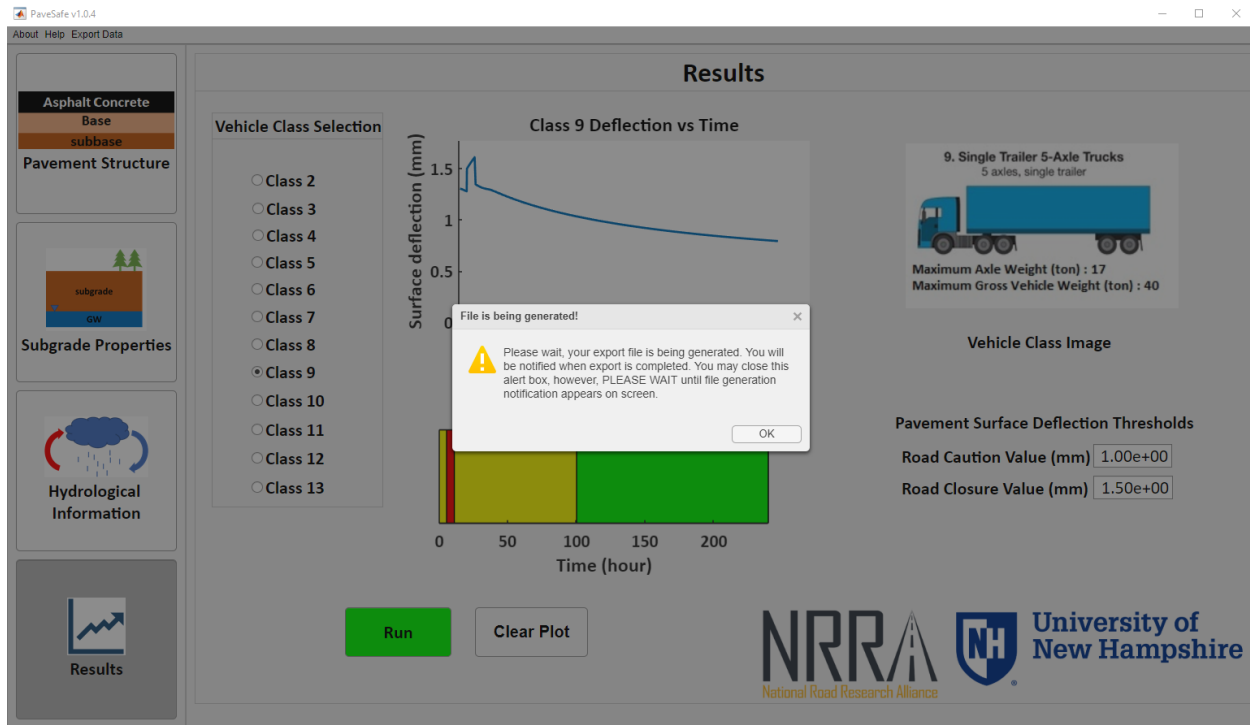


Figure 5-34. A screenshot of results panel when the results Excel file is successfully generated.



Figure 5-35. An example of generated results Excel file.

An example of the “PaveSafe\_ExportData.xlsx” Excel file is shown below:

	Class 2	Class 3	Class 4	Class 5	Class 6	Class 7	Class 8	Class 9	Class 10	Class 11	Class 12	Class 13
0	0.070199474	0.185714791	0.71726502	0.774632007	1.1508043	1.420161171	1.08132828	1.302403341	1.347541389	0.866366203	1.116096045	1.494420892
0.01	0.070178729	0.185708377	0.71723985	0.774604807	1.150770191	1.420119785	1.081296135	1.302361635	1.347507331	0.866335792	1.116062916	1.494777189
0.02	0.070176314	0.185701396	0.717214667	0.774577591	1.150738601	1.42007831	1.081263923	1.302319863	1.347473173	0.86630536	1.116029718	1.494733391
0.03	0.070173893	0.185695525	0.71718941	0.774550296	1.150701708	1.420036684	1.081231596	1.302277952	1.347438879	0.866274837	1.115996401	1.494689436
0.04	0.070171463	0.1856897	0.717164075	0.774522916	1.150667281	1.419995907	1.081199153	1.302235896	1.347404451	0.866244217	1.115962964	1.494645332
0.05	0.070169027	0.185682595	0.71713866	0.77449545	1.150632731	1.419952978	1.081165994	1.302193695	1.34736989	0.866213501	1.115929407	1.494601045
0.06	0.070166582	0.1856761	0.717113166	0.774467898	1.150598059	1.4199109	1.08113392	1.302151352	1.347335199	0.866182687	1.115895732	1.494556612
0.07	0.070164128	0.185669579	0.717087567	0.774440233	1.150563227	1.419868627	1.081101095	1.302108821	1.347300338	0.866151745	1.115861902	1.494511974
0.08	0.070161664	0.185663031	0.717061866	0.774412458	1.150528237	1.41982616	1.081068123	1.302066104	1.347265307	0.866120678	1.115827919	1.494467132
0.09	0.070159198	0.185656479	0.717036143	0.774384659	1.150493217	1.419783656	1.08103512	1.302023351	1.347230245	0.866089585	1.115793905	1.49442225
0.1	0.070156724	0.185649905	0.717010339	0.774356772	1.150458073	1.419741002	1.081002003	1.301980452	1.347195052	0.866058392	1.115759773	1.494377209
0.11	0.070154238	0.185643286	0.716984402	0.774328743	1.150422729	1.419698102	1.080968996	1.301937318	1.347159644	0.86602704	1.115725445	1.494333191
0.12	0.070151756	0.185636702	0.716958511	0.77430076	1.150387458	1.419655293	1.080935458	1.301894267	1.347124233	0.865995729	1.115691189	1.494288707
0.13	0.070149261	0.185630073	0.716932486	0.774272633	1.150351982	1.419612232	1.080902027	1.301850974	1.347088778	0.865964276	1.115656733	1.4942441237
0.14	0.070146759	0.185623425	0.716906388	0.774244428	1.1503164	1.419569043	1.080868497	1.301807557	1.347053125	0.865932725	1.115622173	1.494199533
0.15	0.070144251	0.18561676	0.716880222	0.77421615	1.150280713	1.419525725	1.080834868	1.301764016	1.347017358	0.86590109	1.115587515	1.494149993
0.16	0.070141741	0.18561009	0.716854039	0.774187853	1.15024501	1.419482388	1.080801223	1.301720452	1.346981582	0.865869436	1.115552839	1.494104123
0.17	0.070139215	0.185603377	0.716827685	0.774159371	1.150209039	1.419438722	1.080767326	1.301676575	1.346945511	0.865837572	1.115517902	1.494058025
0.18	0.070136693	0.185596675	0.716801373	0.774130935	1.150173144	1.419395152	1.080733501	1.301632784	1.346909534	0.86580576	1.115483041	1.494012019
0.19	0.070134158	0.18558994	0.716774929	0.774102356	1.150137044	1.419351329	1.080699462	1.301588753	1.346873332	0.865773787	1.115447979	1.493965746
0.2	0.070131618	0.18558319	0.716748429	0.774073716	1.150100961	1.419307406	1.080665387	1.301544623	1.346837046	0.865741744	1.115412838	1.493919568
0.21	0.070129072	0.185576424	0.716721865	0.774045007	1.150064584	1.419263368	1.080631202	1.301500382	1.34680066	0.865709625	1.115377605	1.493872668
0.22	0.070126519	0.185569641	0.716695236	0.774016228	1.150028213	1.419219215	1.080596928	1.301456028	1.346764176	0.865677427	1.11534228	1.493826246
0.23	0.07012396	0.185562842	0.71666854	0.773987377	1.149991738	1.419174935	1.080562557	1.301411553	1.346727582	0.865645146	1.115306855	1.493779492
0.24	0.070121396	0.185556028	0.716641787	0.773958463	1.149955181	1.419130554	1.080528108	1.301366978	1.346690902	0.865612796	1.11527135	1.493732631
0.25	0.070118826	0.185549197	0.716614966	0.773929477	1.14991852	1.419088048	1.080493562	1.301322282	1.346654112	0.865580363	1.115235744	1.493685637
0.26	0.07011625	0.185542353	0.716588094	0.77390034	1.149881766	1.41904452	1.080458947	1.301277698	1.346617247	0.865547868	1.115200060	1.493638549
0.27	0.070113668	0.185535492	0.716561157	0.773871322	1.149844954	1.418999677	1.08042424	1.301232599	1.346580278	0.865515293	1.115164296	1.493591335
0.28	0.070111081	0.185528616	0.71653416	0.773842144	1.149808032	1.418955911	1.080389448	1.301187593	1.346543214	0.865482645	1.115128437	1.493544004
0.29	0.070108488	0.185521726	0.716507107	0.773812907	1.14977103	1.418909687	1.08035458	1.301142491	1.346506065	0.86544993	1.1150925	1.49349657
0.3	0.07010589	0.185514822	0.716479996	0.773783607	1.14973394	1.418861956	1.08031963	1.301097285	1.346468825	0.86541743	1.115056477	1.493449023
0.31	0.070103286	0.185507902	0.716452825	0.773754242	1.149696759	1.418816815	1.080284595	1.301051972	1.346431488	0.865384283	1.115020367	1.49340136
0.32	0.070100677	0.185500989	0.716425603	0.773724821	1.149659504	1.418771583	1.080249489	1.301006571	1.346394075	0.865351361	1.114984185	1.49335336
0.33	0.070098062	0.185494021	0.716398318	0.773695333	1.149622155	1.418726236	1.080214295	1.300961058	1.346356596	0.865318363	1.114947911	1.493305719
0.34	0.070095442	0.18548706	0.716370965	0.773665792	1.149584735	1.418680802	1.080179034	1.300915461	1.346318973	0.865285306	1.114911560	1.493257748
0.35	0.070092817	0.185480084	0.716343596	0.77363619	1.14954723	1.418635266	1.080143694	1.300869764	1.346281296	0.865252179	1.114875144	1.493209667
0.36	0.070090187	0.185473095	0.71631615	0.773606528	1.149509642	1.41859826	1.080108274	1.300823968	1.346243531	0.865218985	1.114838637	1.493161479
0.37	0.070087563	0.185466093	0.716288743	0.773576915	1.149471961	1.418560789	1.080072787	1.300778085	1.34620566	0.865185729	1.114802063	1.493113282

Figure 5-36. A screenshot of final results Excel file.

The file is organized in 13 columns. The first column represents all the times at which the deflection on top of the pavement surface was calculated, and all of the other columns show deflection values for all the different vehicle classes (Class 2 to 13).

## 5.3 TOOLKIT SUMMARY

### 5.3.1 Summary

PaveSafe™ v1.0.4 is the latest official version of the toolkit. The toolkit is able to assess the pavement performance during and after high moisture events (such as storms or flooding) given the initial pavement structure, subgrade, and hydrological information. Future refinement, enhancement, and modifications are expected.

The toolkit app and corresponding information and details are available to public through the following website. This will facilitate the updates and new versions when become available.

<https://mypages.unh.edu/pavesafe>



## CHAPTER 6: CALIBRATION AND PRELIMINARY VALIDATION OF THE TOOLKIT

This chapter is organized in two sections. The first section describes the approach that was followed for the verification of the toolkit with comparison to a layered elastic analysis software (GAMES) and the results obtained for different scenarios and vehicle classes. The second section presents all the results for the verification portion, where post-flooding field FWD testing results are compared with the ones from simulations using GAMES software and PaveSafe app.

### 6.1 VERIFICATION PROCEDURE AND RESULTS

#### 6.1.1 Introduction

A pavement analysis software GAMES (developed by Maina and Matsui, 2004), which is based on layered elastic solution, was used for the verification of PaveSafe. The procedure that was followed and the assumptions that were made to build the pavement structure model in GAMES is presented herein. In addition, all the results obtained using GAMES software and PaveSafe for different scenarios and vehicle classes are presented and compared in this chapter.

#### 6.1.2 Adopted Procedure for the Verification of PaveSafe

##### Simulated Scenarios

Three scenarios were taken into consideration for the verification of PaveSafe including one scenario representing a regular condition with no flooding, and two fully saturated scenarios (flooded condition) with different ponded water heights. The scenario details in terms of hydrological information for the three scenarios are shown in Table 6-1: Hydrological information for the three scenarios taken into consideration..

**Table 6-1: Hydrological information for the three scenarios taken into consideration.**

Case scenario #	Condition	GWT depth (m) (from top of granular base)	Ponded water height (m) (above subgrade layer)	Fully Saturated Layers
1	Hydrostatic	3.8	0	Subgrade below GWT
2	Fully Saturated	3.8	0.05	Subgrade + 5 cm of Subbase
3	Fully Saturated	3.8	0.8	Subgrade + Subbase + Aggregate Base

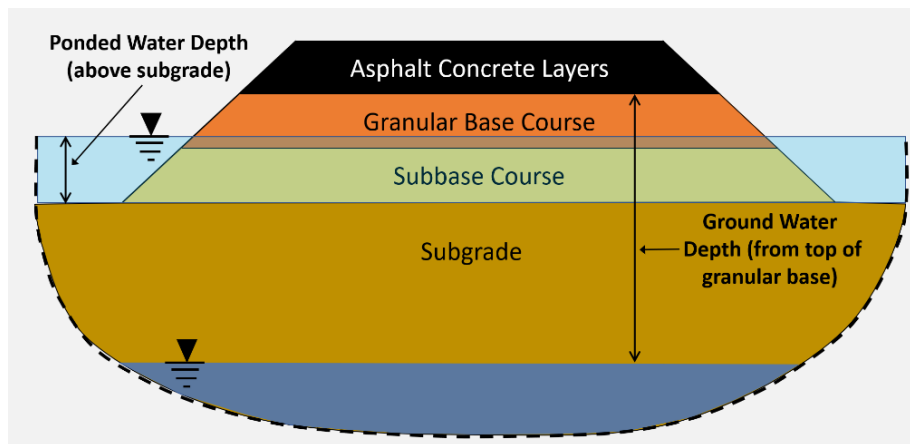
The reference pavement cross-section that was utilized is shown in Table 6-2. As can be seen from the table, all of the aforementioned scenarios were simulated considering both a fine sand subgrade

(AASHTO A-3) and a high-plasticity clay subgrade (AASHTO A-7-6). This was done in order to verify the models for pavement systems with both coarse and fine grained soil types.

**Table 6-2: Cross-section with either A-3 or A-7-6 subgrade type.**

Layer	Material type	Thickness [cm]	MR [MPa] (at OMC for subsurface layers)
HMA	Dense-graded	10	3000
BASE	AASHTO A-1-a	30	275.8
SUBBASE	AASHTO A-1-b	50	275.8
SUBGRADE	AASHTO A-3	Semi-infinite	65
	AASHTO A-7-6	Semi-infinite	37

The GWT depth is calculated from the top of granular base layer while the ponded water height was estimated above the top of subgrade layer as can be seen in Figure 6-1. As shown in Table 6-2, the combined thickness of aggregate base and subbase layers is 0.8 m. Therefore, Scenario 3 in Table 6-1, represents a condition where all the subsurface layers are fully saturated. Scenario 2 instead represents a fully saturated subgrade with 5 cm of fully saturated subbase layer while the rest of the 45 cm of subbase layer and the whole aggregate base layer are unsaturated.

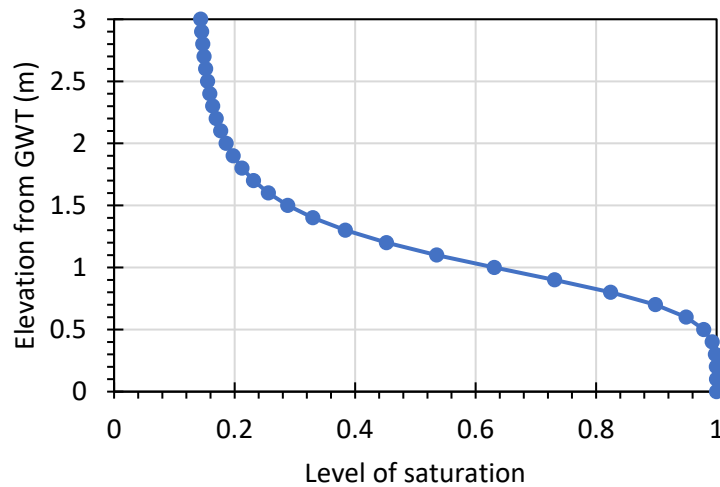


**Figure 6-1. Schematic of the pavement cross section.**

### 6.1.3 Saturation Profile and Resilient Modulus Calculation

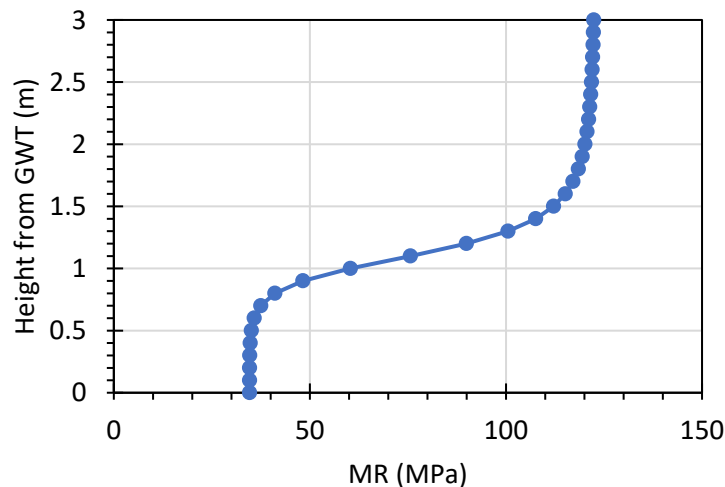
For Scenario 1, the initial moisture content of the subgrade was estimated based on the soil water retention curve (SWRC) data and initial groundwater level (GWL) (i.e., depth of groundwater to the subgrade natural surface). In this regard, van Genuchten's formula (van Genuchten 1980) (Equation 3-6) was utilized to correlate the height above the groundwater level and the moisture content. The saturation

profile was calculated based on the soil water retention curve (SWRC). In Figure 6-2, an example of saturation profile for the AASHTO A-3 subgrade type is shown.



**Figure 6-2. Saturation profile for the hydrostatic scenario with AASHTO A-3 soil type.**

The Resilient Modulus at different depth was estimated based on the foreshown degree of saturation profile. This was performed by using 3-14, which estimates unbound pavement layers' resilient modulus ( $M_R$ ) based on their resilient modulus at the optimum degree of saturation ( $M_{R-OPT}$ ) (Zapata et al. 2007) with fitting parameters as in Table 5-1. In Figure 6-3, an example of the Resilient Modulus at different elevations above the GWT is shown for the scenario with AASHTO A-3 subgrade type.



**Figure 6-3: Resilient Modulus profile for the hydrostatic scenario with AASHTO A-3 soil type.**

To model the Resilient Modulus variation with depth in GAMES, the subgrade was divided into sublayers of 0.5 m thickness. Each sublayer was assigned a constant Resilient Modulus calculated as the

average of the distribution in each selected gap. The bottom subgrade layer (below GWT), was considered fully saturated and modeled as semi-infinite layer.

For Scenarios 2 and 3, the subgrade was considered fully saturated (constant saturation level of 1), and consequently modeled as a single semi-infinite layer with constant Resilient Modulus value. The aggregate base and subbase layers' degree of saturation were calculated based on the weighted average of the inundated portion and the unsaturated portion of each layer. In Scenario 2, 0.05 m of the subbase layer was considered fully saturated while in scenario 3, both base and subbase layers were considered fully saturated (based on ponded water height). The variation of Resilient Modulus for aggregate base and subbase layers between the fully saturated and unsaturated condition was calculated accordingly.

### Vehicle Classes and Load Configurations

Two FHWA vehicle classes were selected for the verification of all the aforementioned scenarios. The two vehicle classes that were selected are the number 5 (Single Unit 2-Axle Trucks) and number 9 (Single Trailer 5-Axle Trucks). These two vehicle types were selected due to their most prevalent usage on highways as well as their ability to capture most significant range of commercial vehicles from perspective of highway loadings. In addition, for Scenario 1 with AASHTO A-3 subgrade type, all the FHWA vehicle classes were simulated. More information on the vehicle classes can be found in Figure 5-1.

The simulation of the vehicle load in GAMES was performed by modeling the actual tire configuration for the different vehicle classes. Nonetheless, PaveSafe is based on the assumption of equivalent tire footprint for the modeling of the vehicle load on the asphalt concrete (AC) surface. The difference between the two methods is shown in Figure 5-2 and was extensively discussed in Chapter 5. In the bottom left of the figure, the actual tire load configuration is shown, which indicates the approach that was utilized to model the load on the pavement surface in GAMES software. In the right bottom end, the equivalent tire footprint method is shown, which replicates the approach adopted within PaveSafe for modeling the load distribution on the pavement surface.

#### 6.1.4 Results for the Verification of PaveSafe

---

##### Verification of Different Case Scenarios

In this section, all the results obtained from GAMES software and PaveSafe are presented for three different case scenarios (flooded with high ponded water, hydrostatic condition and flooded with lower amount of ponded water), two different soil types (AASHTO A-3 and AASHTO A-7-6) and for two vehicle classes (5 and 9).

In Figure 6-4 and Figure 6-5, the results in terms of deflection on the AC surface from GAMES and PaveSafe are presented and compared.

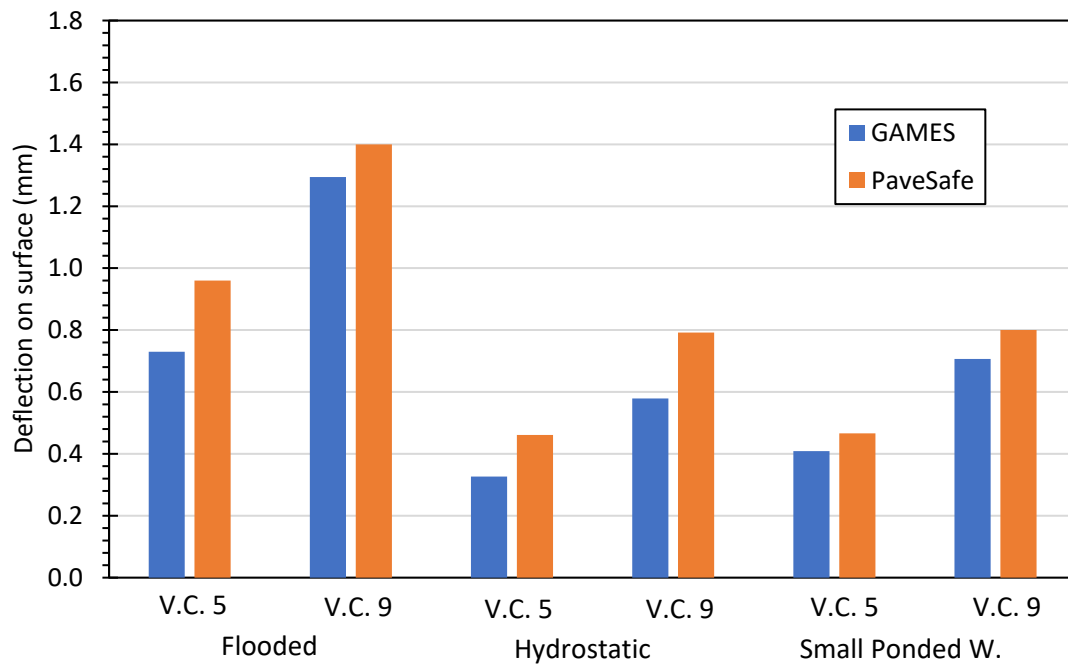


Figure 6-4. Comparison results from GAMES and PaveSafe for the three scenarios with A-3 subgrade type for vehicle class (V.C.) 5 and 9.

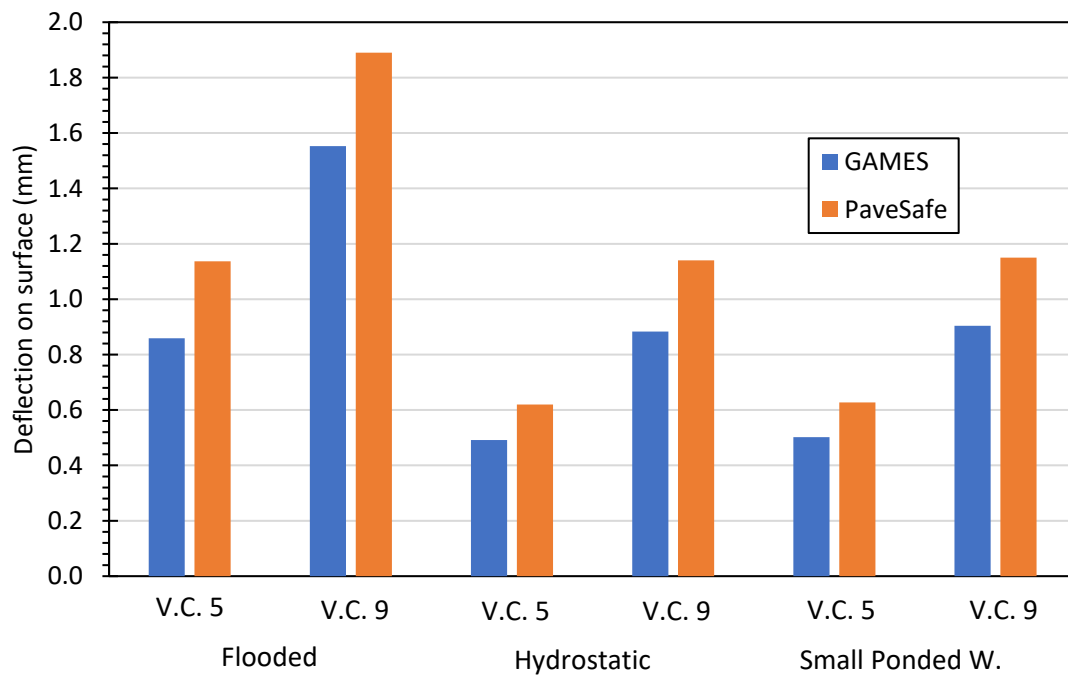
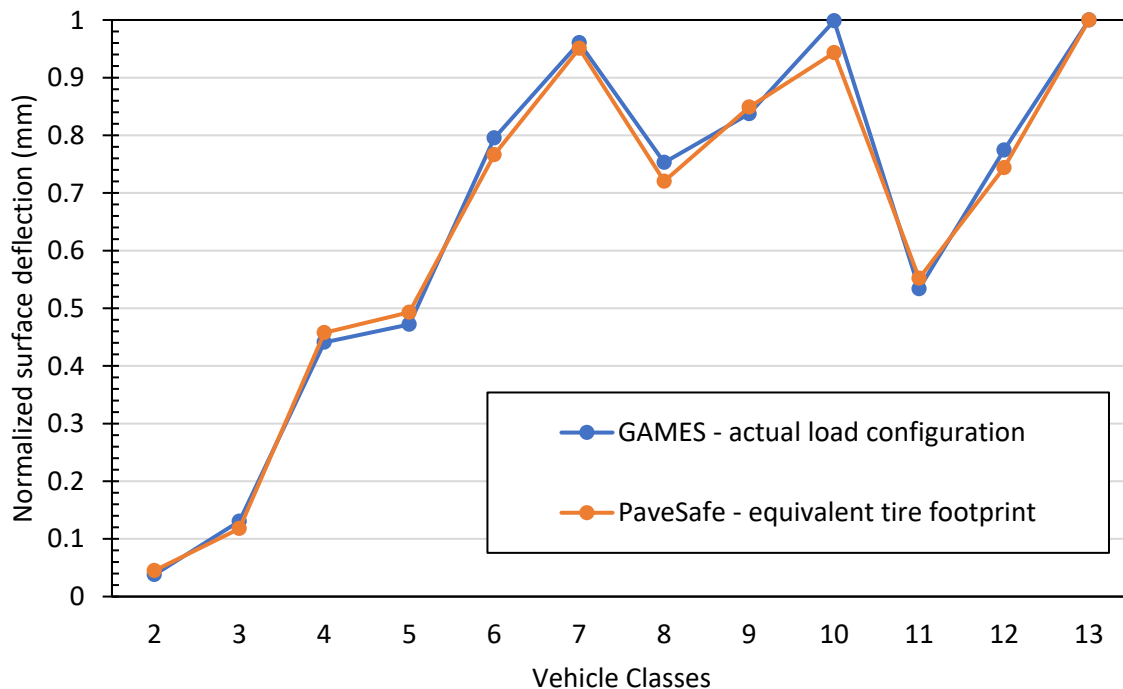


Figure 6-5. Comparison results from GAMES and PaveSafe for the three scenarios with A-7-6 subgrade type for vehicle class (V.C.) 5 and 9.

Results of analyses indicate that the equivalent footprint method implemented in PaveSafe leads to a conservative estimation of AC surface deflection. In general, the surface deflections estimated considering the equivalent footprint method were approximately 30% higher than the ones estimated considering the actual tire configuration. At present, the predictions are left as is (they can be easily calibrated since difference is constant), however research team believes that this approximately 30% increase in predicted deflection provides for a factor of safety in decision process and also serves to account for some in-situ variabilities (due to construction, natural soils variabilities etc.).

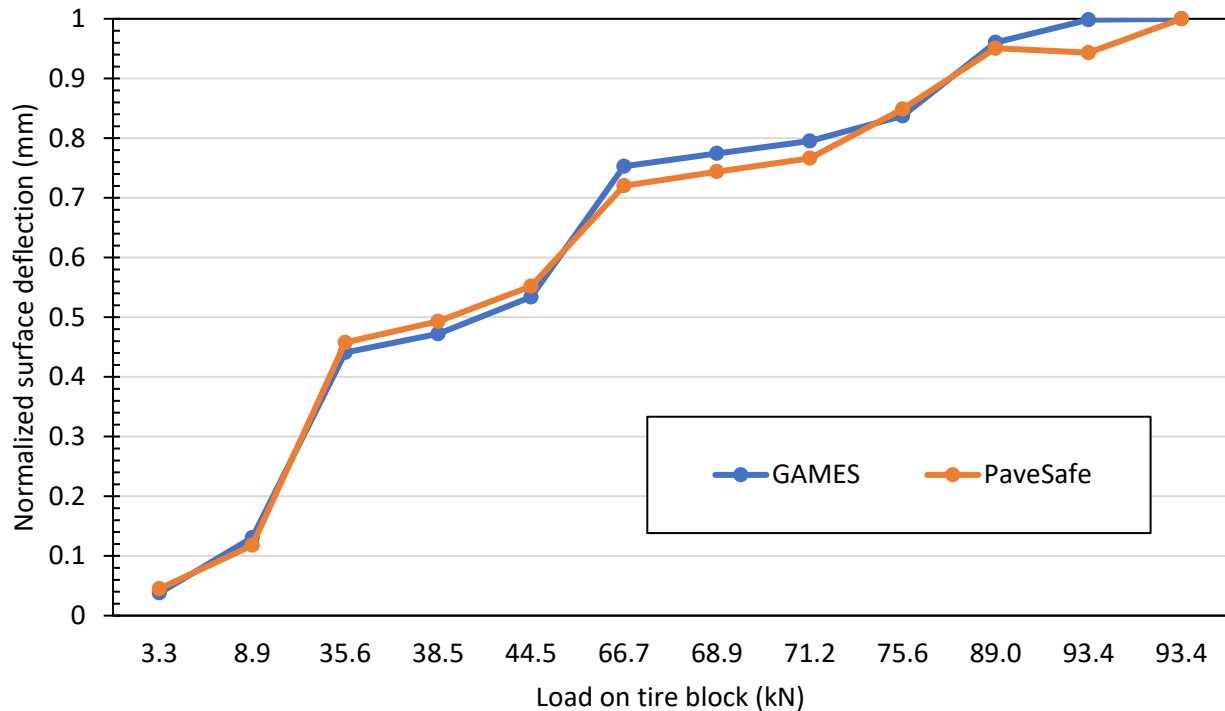
### Verification Using All Vehicle Classes

For the case scenario 1 (hydrostatic condition) with AASHTO A-3 subgrade type, all the vehicle classes were simulated in order to verify the consistency between the two software for all the possible loading scenarios. In Figure 6-6, the normalized surface deflection values for vehicle classes 2 to 13 are shown. The results were normalized for both the utilized methods by dividing all the surface deflections by the highest deflection calculated (in both cases the one from vehicle class 13) and this was done in order to verify the trend of correlation between the two simulation methods for all the FHWA vehicle classes implemented in PaveSafe.



**Figure 6-6. Normalized surface deflection for all vehicle classes in hydrostatic scenario with A-3 subgrade type from GAMES and PaveSafe.**

In Figure 6-7, the same results are shown but ordered using actual load on the tire block (i.e. tires composing of half of the heaviest axle for each vehicle were considered as actual tire configuration for GAMES and as equivalent tire footprint in PaveSafe) instead of vehicle classes.



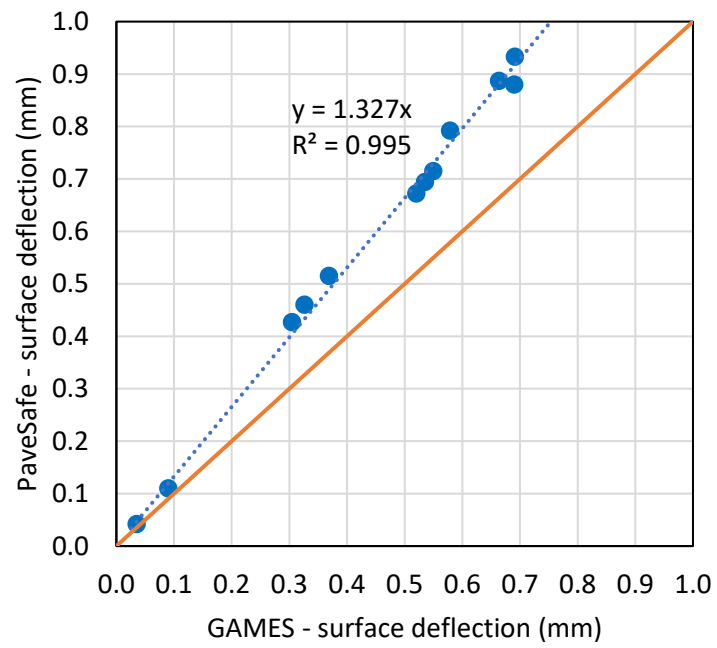
**Figure 6-7. Normalized surface deflection for all axle loads in hydrostatic scenario with A-3 subgrade type from GAMES and PaveSafe.**

It is clear how the two different methods utilized for the simulations are consistent for all the vehicle classes. These results confirm that the increased deflection in PaveSafe (shown in previous section) is tied both to the use of equivalent tire footprint method and to the different type of analysis performed in PaveSafe (i.e. Equivalent Thickness Method) with respect to actual tire configuration and layered elastic solution adopted in GAMES.

The only vehicle class that resulted in bigger discrepancy between GAMES and PaveSafe is vehicle class 10. Vehicle class 10 represents Single Trailer 6-Axle Trucks, which is the heaviest vehicle type in terms of maximum axle weight together with vehicle class 13. In addition, vehicle 10 is modeled in the software as three dual tires mounted on three parallel axles. The combination of very high load together with a higher discrepancy between the actual load configuration and equivalent tire footprint method, might be the factor causing the higher discrepancy between the two calculated surface deflections. However, it should be re-emphasized that PaveSafe yielded higher value than GAMES.

In Figure 6-8, a correlation between results obtained with PaveSafe and GAMES is shown. The values that were utilized to build the plot are the actual values of surface deflection calculated using the

two software. It is clear how the trend of correlation between the two simulations is very close to linear, proving again the consistency of the two different analysis methods.



**Figure 6-8. Correlation of results from GAMES and PavSafe simulations.**



## 6.2 FIELD-BASED VALIDATION PROCEDURE AND RESULTS

### 6.2.1 Introduction

The results obtained with FWD testing in Minnesota and North Dakota, respectively on MN 93 and ND 200, are compared with the simulations performed with GAMES software and PaveSafe. Multiple realistic scenarios were simulated, and all the results are presented using box plots (whiskers, quartiles and median values) in this chapter.

### 6.2.2 Field-Based Validation of PaveSafe

#### FWD Data Provided

Falling Weight Deflectometer (FWD) testing results were provided for two testing locations, one in Minnesota and the other one in North Dakota. These two tested sections were used for preliminary validation of PaveSafe application.

The FWD testing in Minnesota was carried out on MN 93 between Le Sueur and Henderson from RP 1.8 to RP 5.4 in Control Section 7212. This section of roadway often experiences spring flooding from the nearby Minnesota River and in the spring of 2011, water over the road closed it from March 21 until April 15. This roadway is classified as Rural Minor Arterial. Minnesota DOT Highway Pavement Management Application (HPMA) shows that it is an HMA road paved 24' wide with 4.3' wide gravel shoulders. The current roadway was initially constructed in 1946 and the last rehab was a thin overlay in 1998, a chip seal was placed in 2003. HPMA shows that this road has 2350 ADT with 8.9% trucks. Soil maps show that the soils in this area are predominately A-6 with some areas of A-4 in the vicinity of the Rush River crossing. The cross section for MN 93 is shown in Table 6-3.

**Table 6-3: Cross section for MN 93.**

Layer	Thickness (inches)	Thickness (cm)
HMA	5	12.7
Aggregate Base (CL 5)	6	15.24
Subbase (Granular material)	19	48.26
Subgrade (AASHTO A-4 and A-6)	Semi-infinite	Semi-infinite

The roadway section was first tested on 24<sup>th</sup> of April 2010 prior to flooding event. On March 21<sup>st</sup>, 2011 the section was closed since the water level reached 733.7 ft. and it crested at 737.66 ft. on March 27<sup>th</sup>. The roadway section was reopened on April 15<sup>th</sup>, 2011 and it was tested on April 18<sup>th</sup>, 2011 with a water level at 732.4 ft. It was subsequently tested again on April 25<sup>th</sup> of the same year with water level at 731.0 ft. and on May 9<sup>th</sup> with water level at 728.8 ft.

The FWD testing in North Dakota was carried out on ND 200 from RP 1 to RP 3.1 in 2019. The cross section for ND 200 is shown in Table 6-4.

Table 6-4: Cross section for ND 200.

Layer	Thickness (inches)	Thickness (cm)
HMA	8	20.32
Base (Granular material)	10	25.4
Subgrade	Semi-infinite	Semi-infinite

In this case, information on the subgrade type was not available but Resilient Modulus calculation for the subgrade (tested on April 3<sup>rd</sup>, 2019 in unflooded condition) was provided and it can be seen in Figure 6-9.

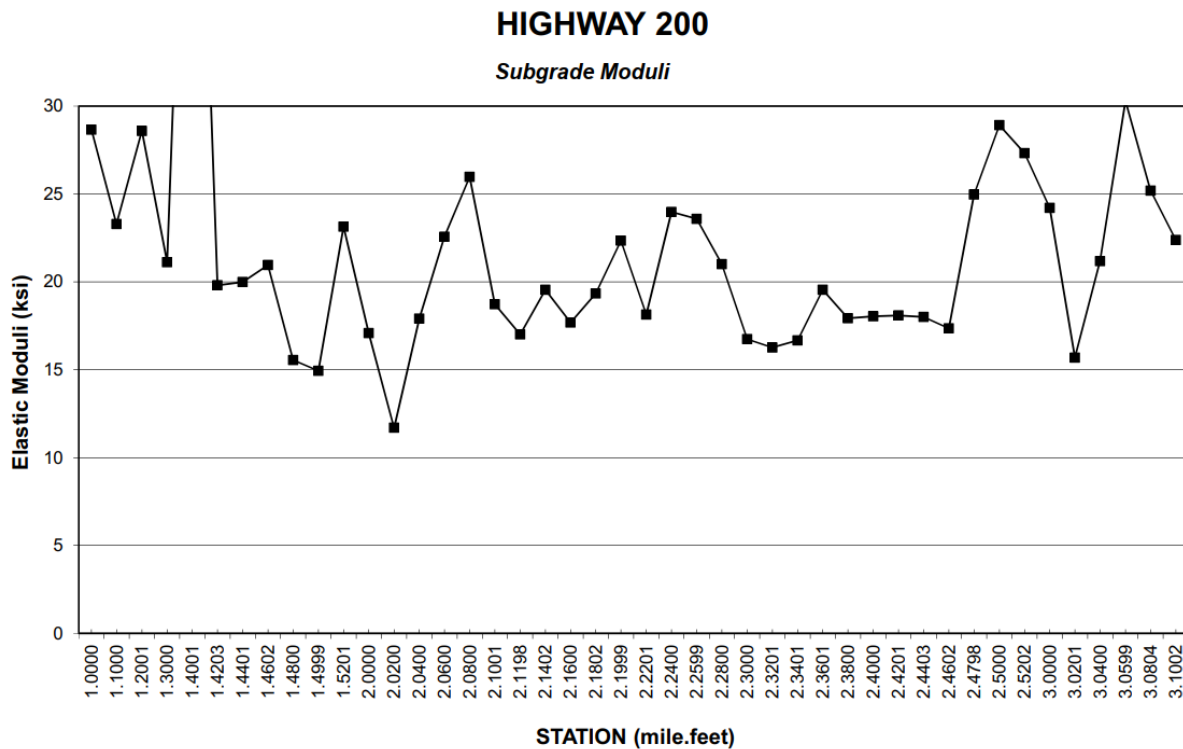


Figure 6-9. Resilient Modulus of subgrade on ND 200.

Data in terms of resilient modulus and pavement surface deflection determined using FWD testing results were provided for both unflooded and flooded conditions.

### Adopted Approach for Simulation

FWD testing on the aforementioned cross sections was simulated using GAMES software. GAMES software allows to model the exact shape of the FWD plate (300 mm diameter), assign the same force as recorded in the field and eventually calculate the deformation on the pavement surface.

The same procedure as mentioned in the previous Chapter was adopted to build the pavement structure model for the different locations and scenarios. Information were collected both on thicknesses of different layers in the pavement cross sections and materials used along with soil type. For each day of simulation, depending on the measured water level on site, the depth of the GWT was calculated. Based on that, the saturation profile in the pavement structure was determined and the Resilient Modulus accordingly calculated (Equation 3-6 and Equation 3-14). GAMES software allows to divide each layer in multiple sub-layers and assign different properties for the same material in different locations with depth. This feature allowed to accurately describe the variation of Resilient Modulus with depth in the pavement structure and within each pavement layer.

It could be argued that GAMES software does not allow to solve the water flow problem, but in this validation procedure, only a “single day” was simulated at a time while the water level was provided for that specific day. Therefore, including the water flow was not required. Nevertheless, the assumption to have the same saturation profile in the pavement structure during the testing hours was made, but this is a realistic assumption.

Based on the deformation obtained from GAMES, a surface deflection that would have been predicted by PaveSafe was estimated considering that PaveSafe (based on equivalent tire footprint method) was shown to provide more conservative results. Specifically, the earlier verification chapter showed an approximately 30% overestimation of surface deflection in PaveSafe. In addition, in order to have a direct surface deflection estimated from PaveSafe simulation, deflection caused by vehicle classes 3 and 4 were compared with the previously mentioned simulations. Vehicle classes 3 and 4 were selected since they are comparable in terms of applied pressure on the AC surface to FWD testing pressures.

For both MN 93 and ND 200, the GWT position for the unflooded scenario was considered at a depth of 1 m from the subgrade surface. For MN 93, since water level data were available for all the testing days, the level of saturation of subgrade and subsurface layers for the different models were calculated. For ND 200, the flooded scenario was simply modeled as a pavement structure with fully saturated subsurface layers.

#### 6.2.3 Results for the Field-Based Validation of PaveSafe

---

All of the results are presented for the different testing days and locations using box and whisker plots. These plots were used because the available FWD data were measured at multiple points/locations along the pavement sections. Therefore, this was considered the best approach to present and consider the data in order to keep the variability of the results at the site in perspective while making comparison with GAMES and PaveSafe results.

In these plots, FWD represents the data coming from field testing on the pavement sections, G represents results coming from GAMES software based on layered elastic solution, and PS represents results from PaveSafe calculated as 20-25% increment with respect to GAMES software on the basis of the 30% difference evaluated in the verification section. Lastly, PS – 3 & 4 represents the actual surface deflection results obtained using PaveSafe and specifically for vehicle classes 3 and 4. As mentioned earlier, vehicle classes 3 and 4 were selected since the applied pressure on the surface calculated based on the load on tire block and area of application are comparable with the pressure applied by FWD.

#### Results from MN 93 Roadway Section

The simulations in GAMES and PaveSafe were implemented with variability associated to the soil type present in the area (AASHTO A-3 and AASHTO A-6). A range for the Resilient Modulus between 39.5 and 62 MPa was utilized based on Ji et al. (2014). In addition, SWRC parameters for each soil type, such as  $n$  and  $\alpha$ , were varied between ranges identified based on literature studies: Ghanbarian-Alavijeh et al. (2010), Puckett et al. (1985), Huang et al. (2005), and Nemes et al. (2001).

Results associated with the FWD data for June 24<sup>th</sup>, 2010 are shown in Figure 6-10.

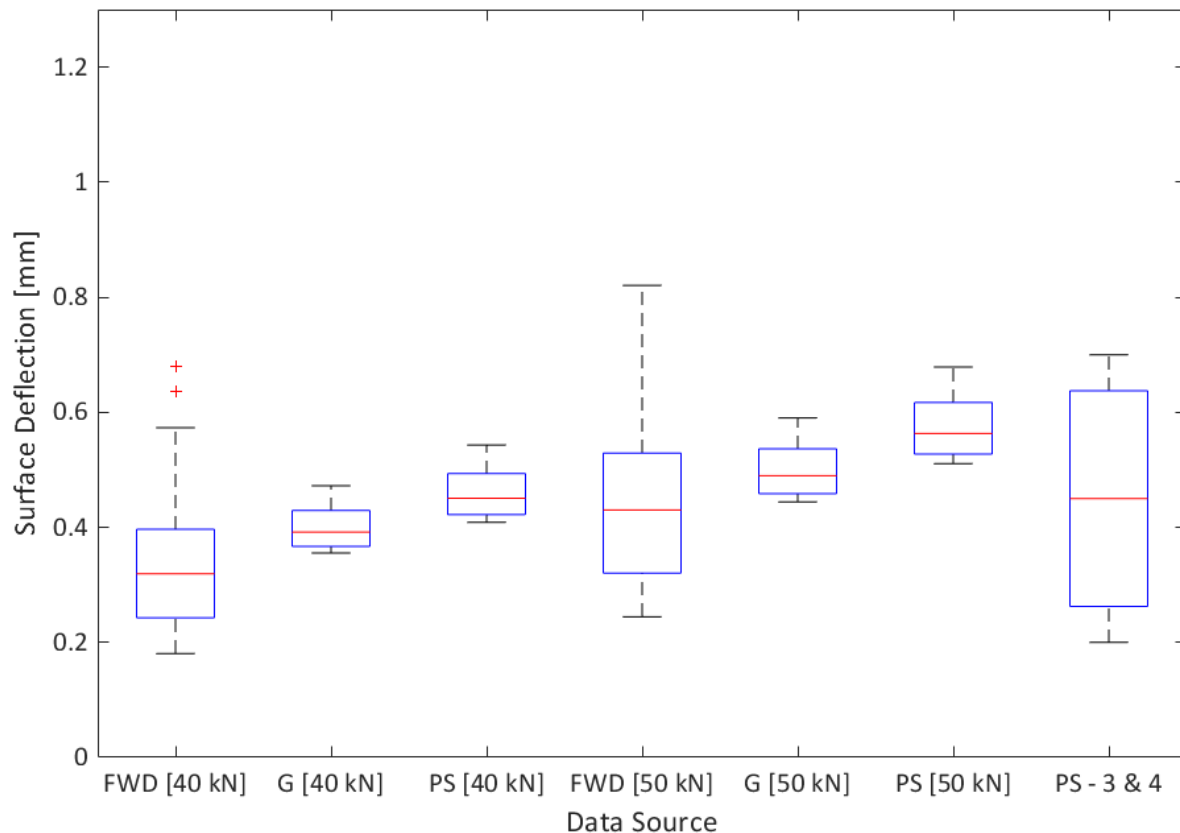
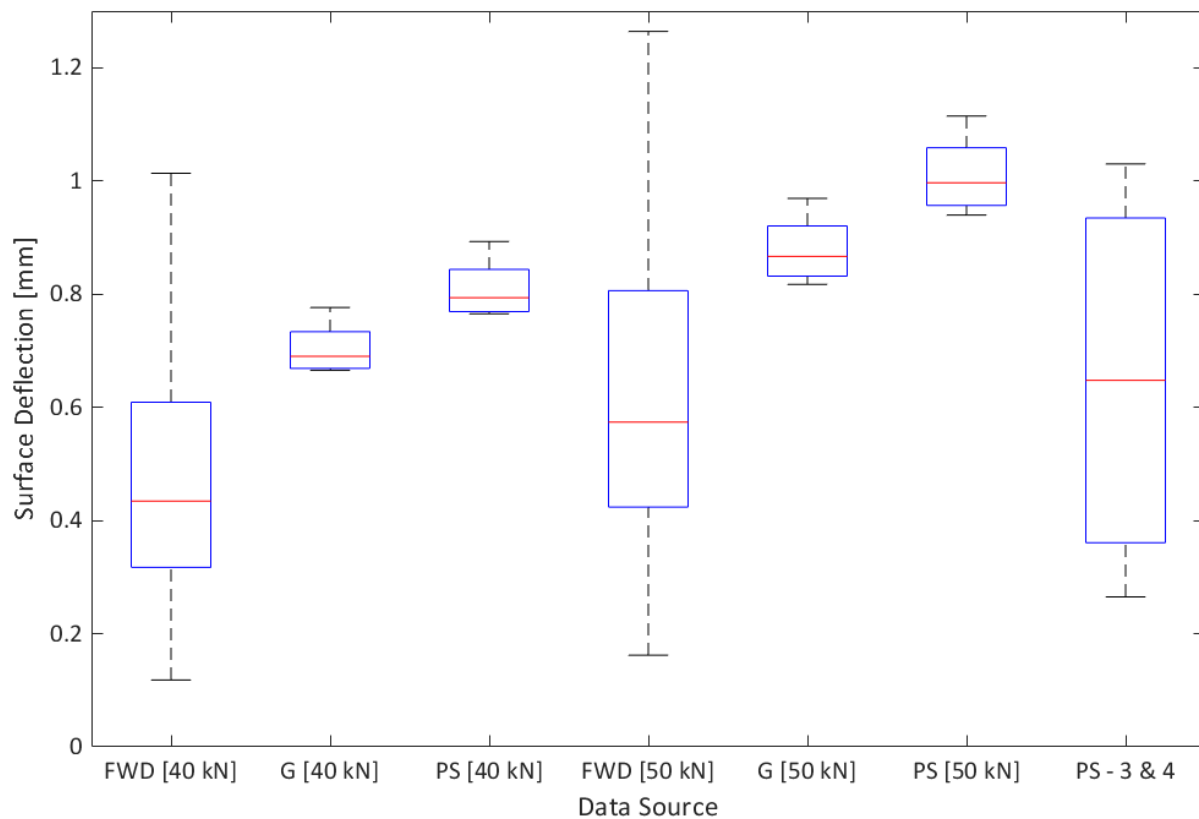


Figure 6-10. Results MN 93 (6/24/2010).

From Figure 6-10, it can be seen how results from both GAMES and PaveSafe under both loading conditions (40 and 50 kN) are inside the range of the results obtained from the field with FWD testing. The pressure applied on the surface by vehicle classes 3 and 4 is between the pressure generated with FWD performed at 40 kN and FWD performed at 50 kN, and this is reflected in the results obtained from direct PaveSafe simulation (PS – 3 & 4).

In addition, PaveSafe results are not only within FWD measurement range but also always within or slightly above the upper quantile. This result is preferable to be considered in order to ensure that instead of the average response, the actual weaker part of pavement section is taken into consideration, since that is what will control the ability to reopen the roadway section to traffic.

In Figure 6-11, the results obtained in April 18<sup>th</sup>, 2011 on MN 93 are shown. On this day, the water level was measured to be at 732.4 ft. or 223.3 m, which means approximately 1.5 m higher with respect to the hydrostatic condition scenario shown in Figure 6-10 for June 24<sup>th</sup>, 2010.

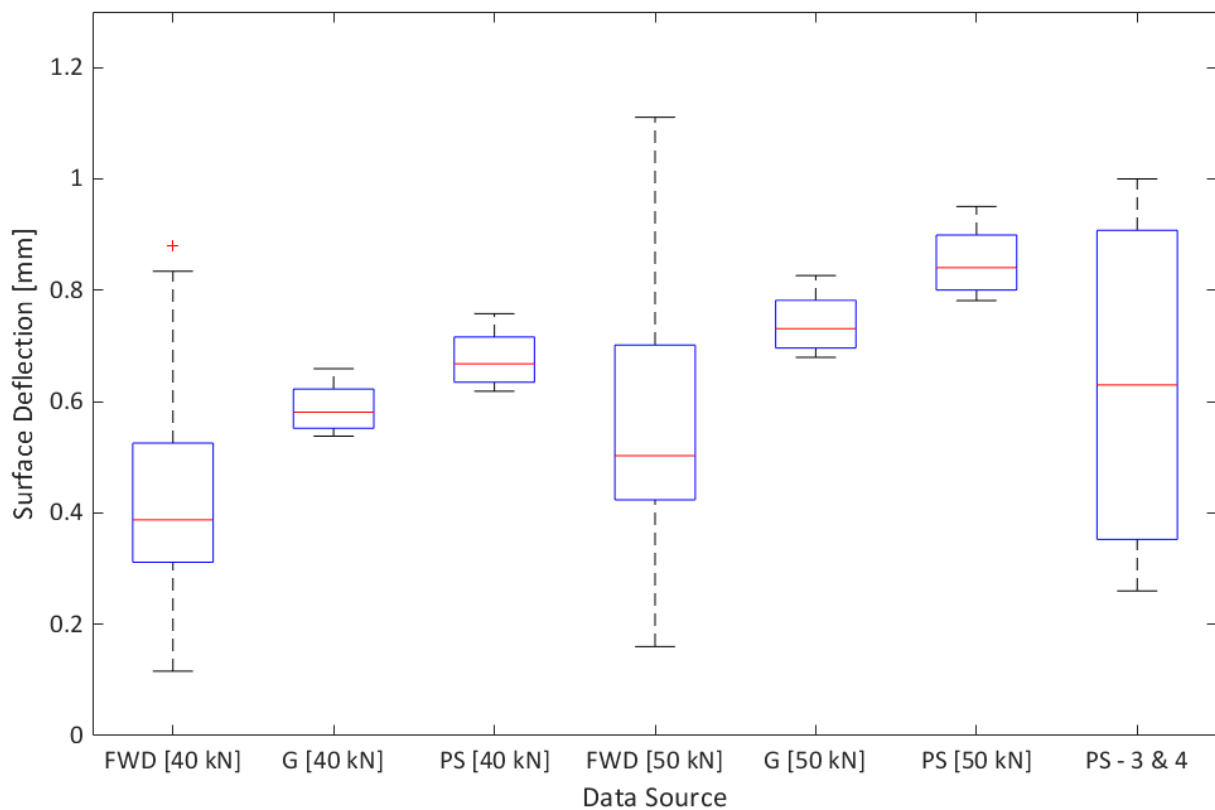


**Figure 6-11. Results MN 93 (4/18/2011).**

The first thing that can be noticed from Figure 6-11 is that the results in terms of surface deflection under the loading application are higher when compared with Figure 6-10. This is the effect of the level of saturation in different pavement layers, which in this case, based on the cross-section information and measured water level, they are fully saturated. Nonetheless, even in this case, GAMES and PaveSafe can

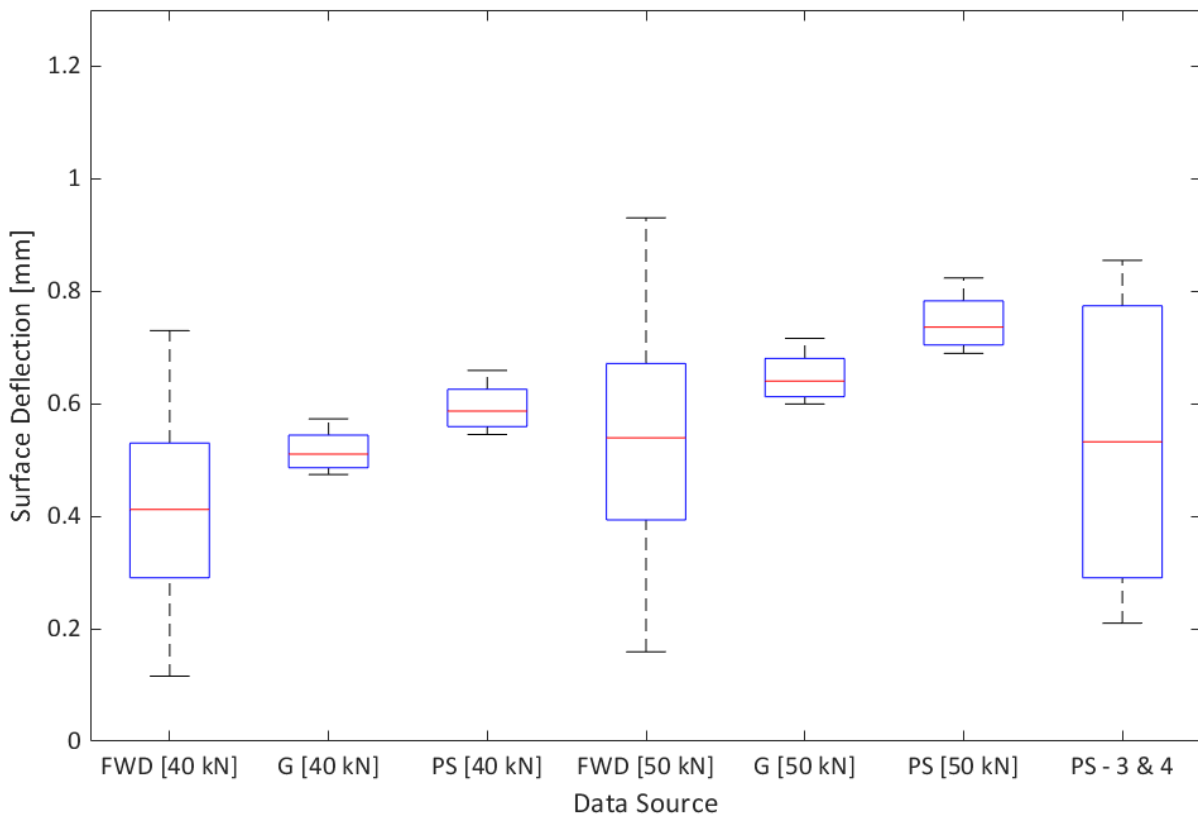
capture the increment in surface deflection caused by flooding and all the simulations results are inside the range of variability of FWD data at both load levels.

Also in this case, PaveSafe results are not only within FWD measurement range but also always within or slightly above the upper quantile. In Figure 6-12, Figure 6-13 and Figure 6-14, results from FWD testing at 40 and 50 kN and from simulations performed with GAMES and PaveSafe are shown.



**Figure 6-12. Results MN 93 (4/21/2011).**

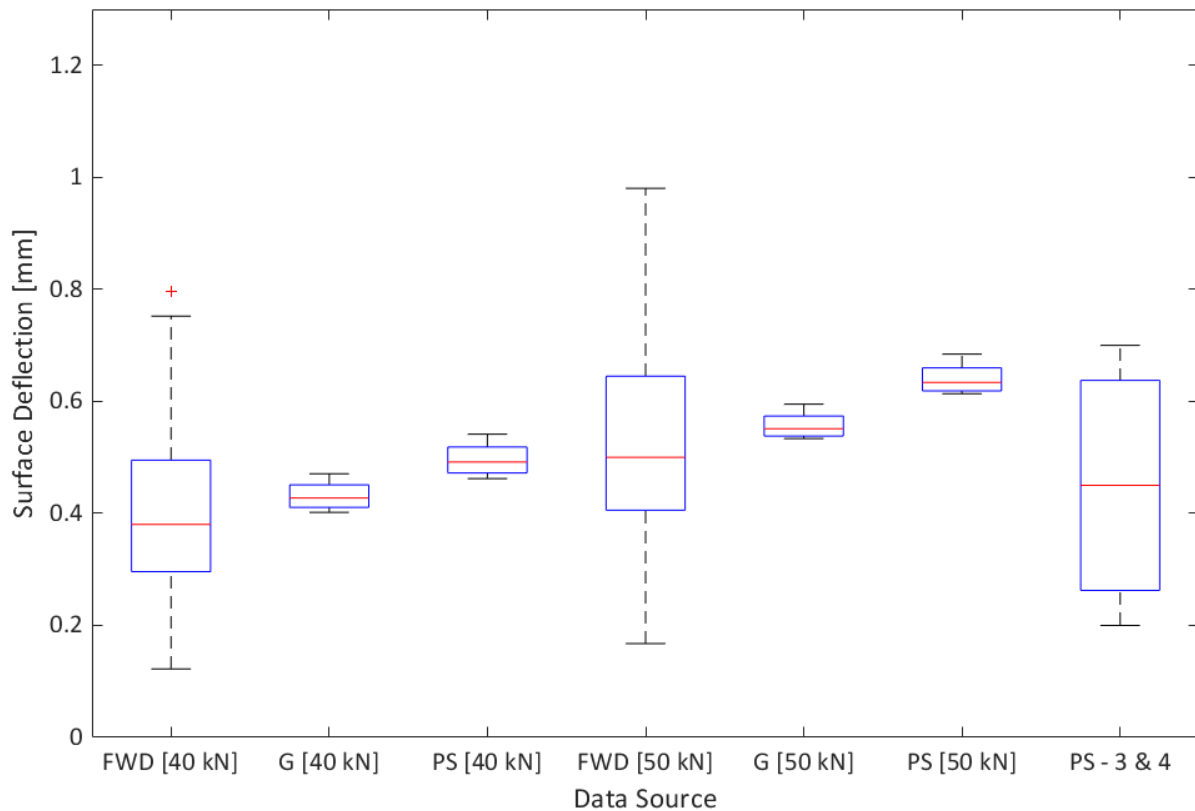
The FWD data shown in Figure 6-12 were collected on April 21<sup>st</sup>, 2011. In this case, the saturation profile was considered partially flooded. The water level measured in that day was of 731.7 ft. or 223 m, which, based on cross section information, means fully saturated subgrade and fully saturated subbase with a completely unsaturated aggregate base layer.



**Figure 6-13. Results MN 93 (4/25/2011).**

This case scenario can be also considered as partially flooded. The water level measured in April 25<sup>th</sup>, 2011 was of 731 ft. or 222.8 m, which, based on pavement cross section information, means fully saturated subgrade, partially saturated subbase and completely unsaturated aggregate base layer.

The results in Figure 6-13 reflect the lower level of saturation of the pavement layers with respect to Figure 6-12. In addition, the simulation results were consistent with the field data.



**Figure 6-14. Results MN 93 (5/9/2011).**

Data on May 9th, 2011 were collected in a scenario where the measured water level was of 728.8 m or 222.1 m. This means that aggregate base and subbase were completely unsaturated and subgrade was still in fully saturated condition. The results obtained in this day are comparable to the ones that were obtained on the previous testing day (shown in Figure 6-13). Once again, the results from simulation were inside the range of variability of FWD testing data for both loading conditions.

For all those last three scenarios, PaveSafe results are not only within FWD measurement range but also always within or slightly above the upper quantile. As mentioned earlier, this result is preferable to be considered in order to ensure that instead of the average response, the actual weaker part of pavement section is taken into consideration, which will control the ability to reopen the roadway section to traffic.

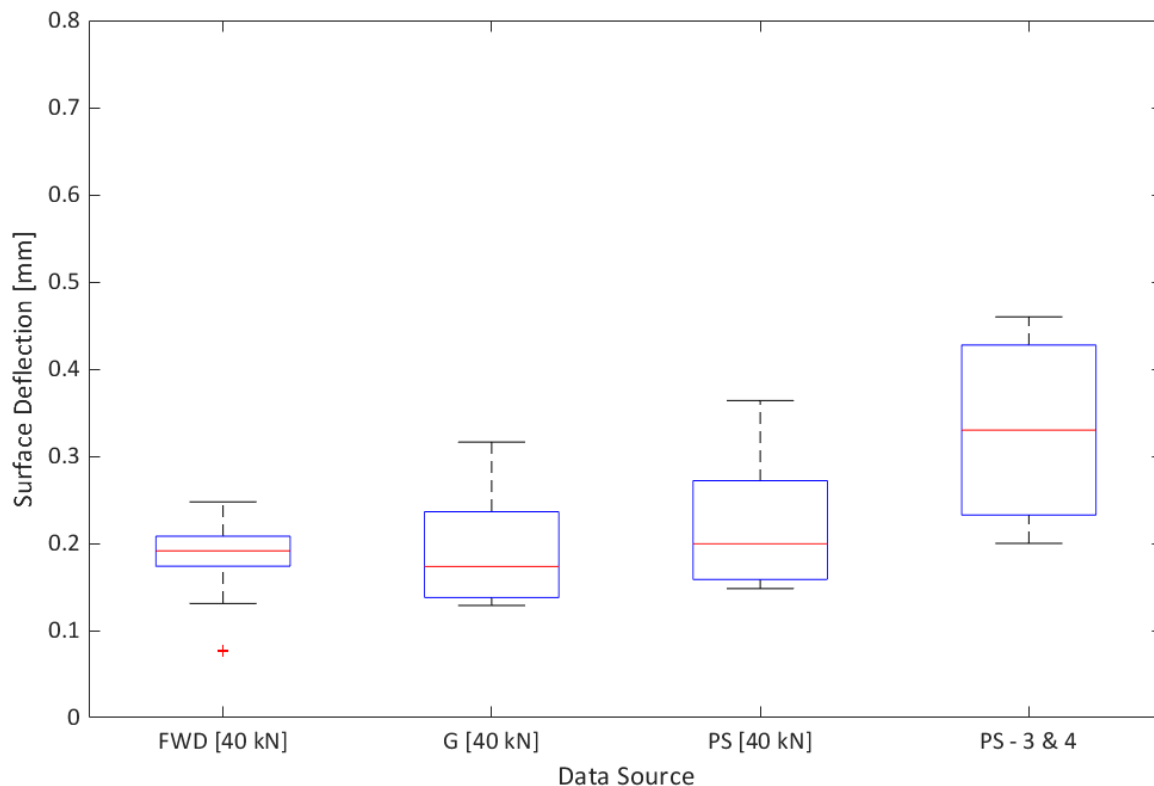


### Results from ND 200 Roadway Section

The same approach followed for MN 93 was adopted for ND 200. Variability of subgrade Resilient Modulus and SWRC parameters were implemented in the simulations based on literature information: Ji et al. (2014), Ghanbarian-Alavijeh et al. (2010), Puckett et al. (1985), Huang et al. (2005), and Nemes et al. (2001).

For ND 200, water level data were not available for the different testing days and consequently it would have been difficult to estimate the GWT position in the different case scenarios. For this reason, it was decided to simulated only two case scenarios: one in hydrostatic condition with GTW level at -2 m from subgrade surface (based on USGS data in Carrington, ND) and a fully saturated scenario with all the pavement layers in fully saturated condition.

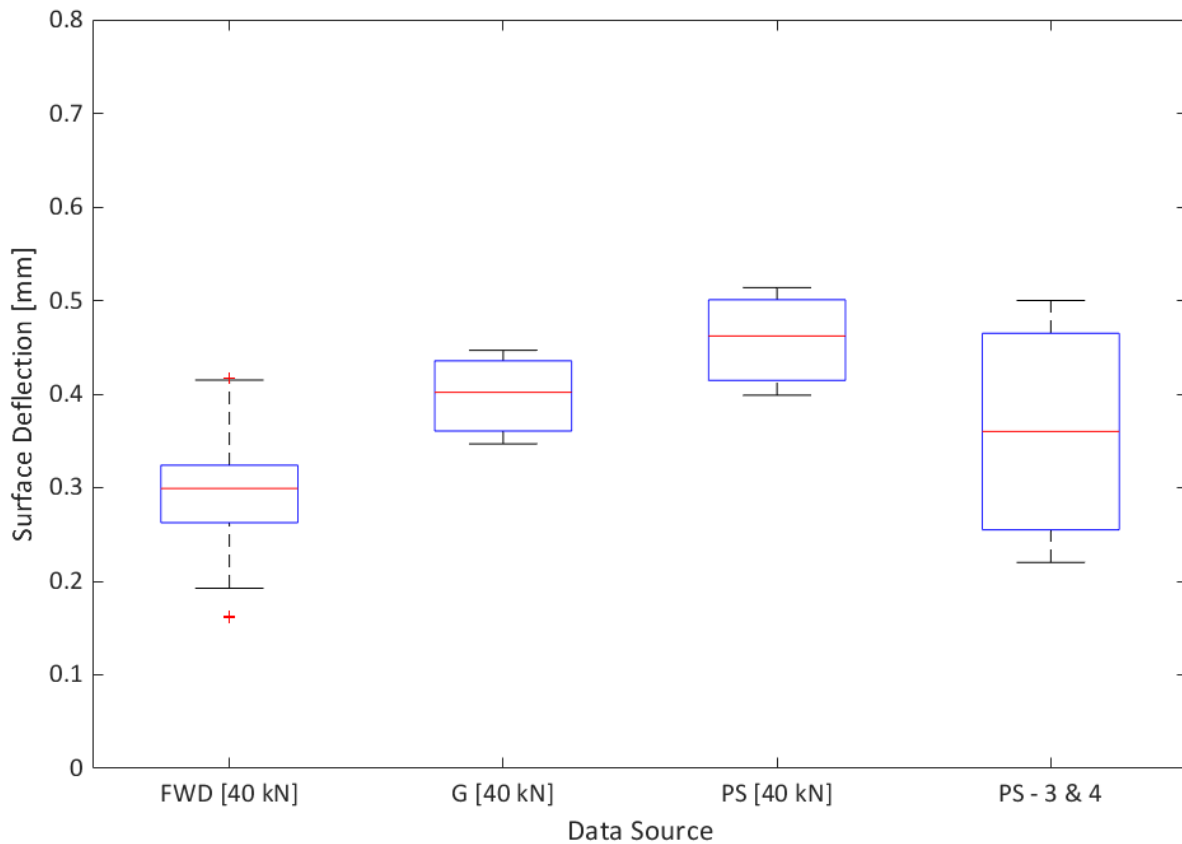
Figure 6-15 shows results for ND 200 in the hydrostatic condition.



**Figure 6-15. Results ND 200 before flood.**

In Figure 6-15, it can be noticed that only 40 kN was used as testing load for FWD in ND 200. For this reason, the higher values obtained from PaveSafe using vehicle classes 3 and 4 make sense since they are obtained with pressure values that, as mentioned earlier, are between the pressure applied using FWD at 40 and 50 kN.

In Figure 6-16, results for ND 200 in flooded condition are shown. Here, it can be noticed again that results were available just at 40 kN load application which justifies the higher surface deflection obtained with vehicle classes 3 and 4 using PaveSafe, since the pressure applied on the surface by those vehicles is higher than the pressure generated with FWD performed at 40 kN. In addition, it can be noticed that the surface deflection data recorded on this day reflect the higher level of saturation of the pavement layers with respect to Figure 6-15.



**Figure 6-16. Results ND 200 flooded.**

In this case scenario, the simulations were able to predict the increment of surface deflection with respect to the previous scenario. In addition, results obtained from both PaveSafe and GAMES, are very close to the field recorded ones for both scenarios.

## 6.3 CALIBRATION AND VALIDATION SUMMARY

### 6.3.1 Summary

---

The PaveSafe application was verified by comparing the results in terms of surface deflection with layered elastic analysis (LEA) using the commercial software for pavement evaluation GAMES. The correlation between the two methods was proven consistent even though PaveSafe (utilizing equivalent tire footprint) resulted in deflections that were conservative for every scenario and vehicle type (approximately 30% higher surface deflection than GAMES).

Subsequently, PaveSafe performance was validated by comparing the results with field data from FWD testing performed on roadway sections in Minnesota (MN 93) and North Dakota (ND 200). PaveSafe surface deflection was estimated by increasing the results from GAMES by 30%, since the ability of simulating FWD plate dimension and load magnitude has not been integrated in the toolkit yet. Nonetheless, results directly obtained from PaveSafe simulation for vehicle classes 3 and 4 were included in the comparison for all the scenarios since they apply a pressure on the pavement surface which is between the ones generated by FWD testing at 40 kN and 50 kN.

## CHAPTER 7: SUMMARY, CONCLUSIONS AND FUTURE WORK

### 7.1 SUMMARY

This project involved three core thrusts: (1) literature search; (2) system dynamics modelling and sensitivity analysis; and (3) development and evaluation of a load restriction toolkit. The literature search involved reviewing state-of-the-art and practice related to flooded pavement response. This included hydrological models, moisture-dependent soil properties, pavement performance models, and current load restriction protocols.

System dynamics modeling was leveraged to simulate the real-time behavior of pavement systems due to moisture variations using three main structures: hydrological, geotechnical, and pavement response structures. Components and variables required to model each structure and the interaction between them was provided in the context of a typical flexible pavement system. Capitalizing on the system dynamics platform, a set of univariate and multivariate sensitivity analysis was performed with respect to various climatic-, geotechnical-, and pavement-related system parameters. The pavement performance was interpreted in terms of four key performance measures: (1) peak surface deflection during moisture variation and under a certain traffic load, (2) the ratio of peak surface deflection and the surface deflection before precipitation event, (3) time to reach peak surface deflection, and (4) time required for recovery of pavement system.

Identifying key influencers from the sensitivity analysis, the PaveSafe App was developed and the latest version (PaveSafe™ v1.0.4) was described in detail. This report is accompanied by both technical guidance and a user manual to aid in implementation efforts. The PaveSafe application was verified by comparing the results in terms of surface deflection with layered elastic analysis (LEA) and with field data from FWD testing performed on two roadway sections in Minnesota and North Dakota.

### 7.2 CONCLUSIONS

Over the course of this research project, several pertinent conclusions with respect to pavement capacity assessment and forecasting with respect to excess subsurface moisture conditions were identified. A summary of key findings is provided below:

- The performance of flexible pavements during and after a moisture variation event and the significance of input parameters are highly dependent on the permeability of subgrade soil.
- Regardless of the type of subgrade soil, climate data including precipitation rate and duration play a significant role in estimation of pavement performance. Accurate estimation of these parameters is of critical importance for a reasonable prediction of pavement performance during flooding or pavement planning and management for forecasted events.
- Thickness and mechanical properties of an AC layer may significantly impact the peak surface deflection during excessive moisture conditions; however, they may have a minimal impact on the extent of the impact of moisture variation relative to the initial condition and the required time for recovery of the pavement.

- Thickness of compacted granular base and subbase layers with relatively high permeability can significantly impact the performance of pavement systems during and after excessive moisture variation. This impact is expected to be more substantial in pavements with subgrades with relatively lower permeability.
- For pavements with relatively permeable granular base and subbase layers, variation of the layers' hydraulic conductivity may not substantially impact the performance of pavement systems with fine-grained subgrade; however, it may substantially impact the performance of pavement systems with coarse-grained subgrade.
- Hydraulic properties of subgrade soil including hydraulic conductivity and water retainability can substantially impact its behavior during moisture variations. For soils with relatively high permeability (such as clean sand), a decrease in permeability can adversely impact pavement performance, while for subgrades with relatively very low permeability (i.e., clay), reduction in permeability may improve the pavement capacity during moisture variation.
- Groundwater level may have a complex impact on the performance of pavement systems during moisture variations. While an increase in the depth of groundwater may lower peak surface deflection experienced during moisture variation, it may increase the recovery time.
- System dynamics modeling can holistically incorporate pavement structure, climate forecast, traffic loads, and moisture movement processes within a pavement response and facilitate a system-based response assessment.
- The PaveSafe app is able to assess pavement performance during and after high-moisture events (such as storms or flooding) given the initial pavement structure, subgrade, and hydrological information. However, future refinement, enhancement, and modifications are expected.
- PaveSafe provided reasonable approximation of pavement response when compared with other linear elastic analysis software and limited field FWD data pre- and post-flooding.

### 7.3 FUTURE WORK

While the research study resulted in sound and implementable research products, there were areas of future work that were identified. These areas would help to improve the PaveSafe app in terms of user functionality and prediction reliability as well as aid in implementation efforts. Recommended future research directions are listed below:

- Additional sites and roadway sections can be tested in the future using FWD under different flooded or hydrostatic conditions and the toolkit can be furtherly validated.
- The toolkit could be implemented with the ability of using LEA for the simulations and the FWD plate and loading conditions can be added to the traffic spectrum portion to facilitate future verifications.
- The graphical interface can be enhanced.
- The toolkit's computational efficiency could be improved both with regard to input data, analysis efficiency, and output generation.

- Physical modeling of the saturation profiles and hydraulic conductivity can be performed using available commercial software to further verify the reliability of the hydrological structure of the toolkit.
- The toolkit could be implemented with the ability of running a probabilistic analysis and include the variability associated with SWRC parameters for the different subgrade materials. Once probabilistic distribution functions are implemented in the hydraulic and mechanical response portion, Monte Carlo simulation could be implemented in the toolkit to enhance reliability.

## REFERENCES

- AASHTO. (1993). *Guide for Design of Pavement Structures* (Vol. Part III). Washington DC: AASHTO.
- Ahlvin, R. E., & Ulery, H. H. (1962). Tabulated Values for Determining the Complete Pattern of Stresses, Strains, and Deflections Beneath a Uniform Circular Load on a Homogeneous Half Space (Highway Research Bulletin No. 342, Stress Distribution in Earth Masses).
- Amiri, H. (2004). Impact of Moisture Variation of Stiffness Response of Pavements through Small Scale Models (Master Thesis), University of Texas, El Paso, TX.
- Badiane, M., Yi, J, Dore., G, Bilodeau, J.-P., & Prophate, F. (2015). Monitoring of Flexible Pavement Structures during Freezing and Thawing. 16th International Conference on Cold Regions Engineering, American Society of Civil Engineers, Salt Lake City, Utah, July 19-22, 2015.
- Bilodeau, J.-P., Cloutier, J.-P., & Dore, G. (2017) Experimental Damage Assessment of Flexible Pavements during Freeze-Up. *Journal of Cold Regions Engineering*, 31(4), p16.
- Bilodeau, J.-P., & Dore, G. (2012). Water Sensitivity of Resilient Modulus of Compacted Unbound Granular Materials Used as Pavement Base. *International Journal of Pavement Engineering*, 13(5), 459-471.
- Bixler, T. S., Houle, J., Ballesterio, T., & Mo, W. (2019). A Dynamic Life Cycle Assessment of Green Infrastructures. *Science of The Total Environment*, 692, 1146-1154.
- Boussinesq, J. (1885). Application des Potentiels à L'étude de L'équilibre et du Mouvement des Solides élastiques: Principalement au Calcul des Déformations et des Pressions que Produisent, Dans ces Solides, des Efforts Quelconques Exercés Sur une Petite Partie de Leur Surface ou de Leur Intérieur: Mémoire Suivi de Notes étendues Sur Divers Points de Physique. *Mathematique et d'Analyse*, 4. P724.
- Brooks, R. H., & Corey, A. T., (1964). Hydraulic Properties of Porous Media (Hydrology Paper No. 3, March). Fort Collins, CO: Colorado State University.
- Burmister, D. M. (1943), The Theory of Stresses and Displacements in Layered Systems and Application to the Design of Airport Runways. *Proceedings, Highway Research Board*, 23, 126-148.
- Camacho-Garita, E., Aguiar-Moya, J. P., Avila-Esquivel, T., & Loria-Salazar, L. G. (2020). Effect of Moisture on Full-Scale Pavement Distress. *Journal of Testing and Evaluation*, 48(1), 235-246.
- Carmichael, R. F. III, & Stuart, E. (1985). Predicting Resilient Modulus: A Study to Determine the Mechanical Properties of Subgrade Soils. *Transportation Research Record*, 1043, 145-148.
- Cary, C. E., & Zapata, C. E. (2011). Resilient Modulus for Unsaturated Unbound Materials. *Road Materials and Pavement Design*, 12(3), 615-638.
- Cary, C. E., & C. E. Zapata. (2010) Enhanced Model for Resilient Response of Soils Resulting from Seasonal Changes as Implemented in Mechanistic–Empirical Pavement Design Guide. *Transportation Research Record*, 2170, 36–44.
- Ceratti, A., Gehling, W., & Nunez, W. P. (2004). Seasonal Variations of a Subgrade Soil Resilient Modulus in Southern Brazil. *Transportation Research Record*, 1874, 165–173.

- Chandra, D., Chua, K. M., & Lytton, R. L. (1989). Effects of Temperature and Moisture on the Load Response of Granular Base Material in Thin Pavements. *Transportation Research Record*, 1252, 33-41.
- Chapuis, R. P. (2004). Predicting the Saturated Hydraulic Conductivity of Sand and Gravel Using Effective Diameter and Void Ratio. *Canadian Geotechnical Journal*, 41(5), 787–795.
- Charlier, R., Horny, P., Srsen, M., Hermansson, A., Bjarnason, A., Erlingsson, S., & Pavisic, P. (2009) Water Influence on Bearing Capacity and Pavement Performance: Field Observations. In Dawson A. (ed.) *Water in Road Structures. Geotechnical, Geological and Earthquake Engineering* (vol 5). Dordrech, Springer.
- Chen, X., & Zhang, Z. (2014). Effects of Hurricanes Katrina and Rita Flooding on Louisiana Pavement Performance. *Pavement Materials, Structures, and Performance*, Ge-shanghai, 2014, 212-221.
- Chiglo, J. M. (2014). Technical Memorandum. St. Paul: MNDOT.
- Christopher, B. R., Schwartz, C. W., Boudreaux, R., & Berg, R. R. (2006). Geotechnical Aspects of Pavements (No. FHWA-NHI-05-037). Washington, DC: United States Federal Highway Administration.
- Currie, D. J., Smith, C., & Jagals, P. (2018). The Application of System Dynamics Modelling to Environmental Health Decision-Making and Policy-A Scoping Review. *BMC Public Health*, 18(1), 402.
- Daniel, J. S., Jacobs, J. M., Douglas, E., Mallick, R. B., & Hayhoe, K., (2014). Impact of Climate Change on Pavement Performance: Preliminary Lessons Learned Through the Infrastructure and Climate Network (ICNet). In *Climatic Effects on Pavement and Geotechnical Infrastructure*. Reston, VA: American Society of Civil Engineers.
- Drumm, E. C., Reeves, J. S., Madgett, M. R., & Trolinger, W. D. (1997). Subgrade Resilient Modulus Correction for Saturation Effects. *J. Geotech. Geoenviron. Eng.*, 123(7), 663–670.
- Edris, Earl V. Jr., & Lytton, R. L., (1976). Dynamic Properties of Subgrade Soils Including Environmental Effects (Report No. TTI-2-18-74-164-3). College Station, TX: Texas A&M University, Texas Transportation Institute.
- Elkins, G. E., Schmalzer, P., Thompson, T., & Simpson A. (2003). Introduction to the LTPP Information Management System (IMS) (Rep. No. FHWA-RD-03-088). Washington, DC: Federal Highway Administration, U.S. Department of Transportation.
- Elshaer, M., Ghayoomi, M., & Daniel, J. S. (2017). “Bearing Capacity Analysis of Pavement Structures for Short Term Flooding Events. *10th International Conference on the Bearing Capacity of Roads, Railways, and Airfields*, Athens, Greece, 2127-2133.
- Elshaer, M., Ghayoomi, M., & Daniel, J. S. (2018a). Methodology to evaluate performance of pavement structure using soil moisture profile. *Road Materials and Pavement Design*, 19(4), 952-971. DOI: 10.1080/14680629.2017.1283356
- Elshaer, M., Ghayoomi, M., & Daniel, J. S. (2018b). The Role of Predictive Models for Resilient Modulus of Unbound Materials in Pavement FWD-Deflection Assessment. *Road Materials and Pavement Design*, 19(4), 952-971. DOI: 10.1080/14680629.2017.1283356
- Elshaer, M., Ghayoomi, M., & Daniel, J. S. (2019). Impact of Subsurface Water on Structural Performance of Inundated Flexible Pavements. *International Journal of Pavement Engineering*, 20(8), 947-957.



- Elshaer, M. H. (2017-May). Assessing the Mechanical Response of Pavements During and After Flooding, (PhD Dissertation). University of New Hampshire, Durham, NH.
- EPA, (2017). Climate Impacts on Transportation. Environmental Protection Agency. Retrieved from <https://archive.epa.gov/epa/climate-impacts/climate-impacts-transportation.html>
- Espinoza, R. D., & Bourdeau, P. L. (1992). Numerical Modelling of Moisture Infiltration in Pavement Systems, *Canadian Geotechnical Conference*, Toronto, Canada.
- FHWA. (1995). Comprehensive Truck and Weight (Phase 1-Synthesis, Pavement and Truck Size Regulations). Retrieved from <https://www.fhwa.dot.gov/reports/tswstudy/TSWwp3.pdf>
- FHWA. (2002). User's Guide for Drainage Requirements in Pavements (DRIP 2.0 Microcomputer Program). Washington, DC: Federal Highway Administration.
- FHWA. (2014). Verification, Refinement, and Applicability of Long-Term Pavement Performance Vehicle Classification Rules (Report FHWA-HRT-13-091). Washington, DC: Federal Highway Administration.
- FHWA. (2019). Traffic Monitoring Guide. U.S. Department of Transportation/Federal Highway Administration. Retrieved from [https://www.fhwa.dot.gov/policyinformation/tmguidetmg\\_2013/traffic-data-pavement.cfm](https://www.fhwa.dot.gov/policyinformation/tmguidetmg_2013/traffic-data-pavement.cfm)
- Forrester, J. W. (1987). Lessons from System Dynamics Modeling. *System Dynamics Review*, 3(2), 136-149.
- Foster, C. R. & R. G. Ahlvin. (1954), Stresses and Deflections Induced by a Uniform Circular Load. *Proceedings, Highway Research Board*, 33, 467-470.
- Fredlund, D. G., & Morgenstern, N. R. (1977). Stress state variables for unsaturated soils. *Journal of Geotechnical and Geoenvironmental Engineering*, 103, ASCE 12919.
- Fredlund, D. G., & Xing, A., (1994). Equations for the Soil-Water Characteristic Curve. *Canadian Geotechnical Journal*, 31, 521-532.
- Fredlund, D. G., Xing, A., & Huang, S. (1994). Predicting the permeability function for unsaturated soil using the soil-water characteristic curve. *Canadian Geotechnical Journal*, 31, 533-546.
- Freeze, A. (1969). The Mechanism of Natural Ground-Water Recharge and Discharge: 1. One-Dimensional, Vertical, Unsteady, Unsaturated Flow above a Recharging or Discharging Ground-Water Flow System. *Water Resources Research*, 5(1), 153-171.
- Gardner, W. R. (1958). Some steady state solutions of the unsaturated moisture flow equation with application to evaporation from a water table. *Soil Science*, 85(4), 228-232.
- Gaspard, K., Martinez, M., Zhang, Z., & Wu, Z., (2007). Impact of Hurricane Katrina on roadways in the New Orleans Area (Technical Assistance Report No. 07-2TA). Baton Rouge, LA: LTRC Pavement Research Group, Louisiana Department of Transportation and Development.
- Ghanbarian-Alavijeh, B., Liaghat, A., Huang, G. H., & Van Genuchten, M. T. (2010). Estimation of the van Genuchten soil water retention properties from soil textural data. *Pedosphere*, 20(4), 456-465.
- Green, W. H., & Ampt, G. (1911). Studies of soil physics, part I – the flow of air and water through soils. *J. Ag. Sci*, 4, 1-24.

- Haider S. W., & Masud, M. M. (2018). Effect of Moisture Infiltration on Flexible Pavement using the AASHTOWare Pavement-ME. *Advances in Materials and Pavement Performance Prediction*, CRC Press, 1st Edition, 31-35.
- Han, Z., & Vanapalli, S. K. (2015). Model for Predicting Resilient Modulus of Unsaturated Subgrade Soil Using Soil-Water Characteristic Curve. *Canadian Geotechnical Journal*, 52(10), 1605-1619.
- Han, Z., & Vanapalli, S. K. (2016). State-of-the-Art: Prediction of Resilient Modulus of Unsaturated Subgrade Soils. *International Journal of Geomechanics*, 16(4), p15.  
[https://ascelibrary.org/doi/abs/10.1061/\(ASCE\)GM.1943-5622.0000631](https://ascelibrary.org/doi/abs/10.1061/(ASCE)GM.1943-5622.0000631)
- Hazen, A. (1911). Dams on Sand Formations: Discussion. *Trans ASCE*, 73, 199–203.
- Helali, K., Robson, M., Nicholson, R., & Bekheet, W. (2008) Importance of A Pavement Management System in Assessing Pavement Damage from Natural Disasters: A Case Study to Assess the Damage from Hurricanes Katrina and Rita in Jefferson Parish, Louisiana. Paper presented at the 7th International Conference on Managing Pavement Assets, Preserving What We Have, investing in the Future, and Finding the Balance, Transportation Research Board, Washington, DC.
- Heydinger, A. (2003). Monitoring Seasonal Instrumentation and Modeling Climatic Effects on Pavements at the Ohio/SHRP Test Road. FHWA/OH-2003/018,, Final Report , Washington, DC, TRB.
- Hicks, R. G., & Monismith, C. L. (1971) Factors Influencing the Resilient Response of Granular Materials. *Highway Research Record*, 345, 15-31.
- Holtz, R. D. (2011). An Introduction to Geotechnical Engineering: International Version. Upper Saddle River, NJ: Pearson Education.
- Huang, G., & Zhang, R. (2005). Evaluation of soil water retention curve with the pore–solid fractal model. *Geoderma*, 127(1-2), 52-61.
- Huang, Y. H. (2012). Pavement Analysis and Design. Upper Saddle River. NJ: Pearson Prentice Hall.
- Ji, R., Siddiki, N., Nantung, T., & Kim, D. (2014). Evaluation of Resilient Modulus of Subgrade and Base Materials in Indiana and its Implementation in MEPDG. *The Scientific World Journal*, 214, p14.
- Jones, A. (1962). Tables of Stresses in Three-Layer Elastic Systems. Highway Research Board Bulletin No. 342, Stress Distribution in Earth Masses, 176-214.
- Khan, M. U., Mesbah, M., Ferreira, L., & Williams, D. J. (2015). Development of A Post-Flood Road Maintenance Strategy: Case Study Queensland, Australia. *International Journal of Pavement Engineering*, 18(8), 702-713.
- Khan, S., Yufeng, L., & Ahmad, A. (2009). Analyzing complex behavior of hydrological systems through a system dynamics approach. *Environmental Modelling & Software*, 24(12), 1363-1372.
- Khosravifar, S., Afsharikia, Z., & Schwartz, C. W. (2015). Evaluation of Resilient Modulus Prediction Models for Cohesive and Non cohesive Soils. *Airfield and Highway Pavements*, ASCE, Miami, FL, 778-788.
- Khoury, C. K., & Khoury, N. K. (2009). The Effect of Moisture Hysteresis on Resilient Modulus of Subgrade Soils. Paper presented at the 8th Int. Conf. Bearing Capacity Roads, Railways, and Airfields, Univ. of Illinois–Urbana-Champaign, Champaign, IL.

- Khoury, C., Khoury, N., & Miller, G. (2010) Effect of Suction Hysteresis on Resilient Modulus of Fine-Grained Soil. Transportation Research Board 89th Annual Meeting Compendium Papers (CD-ROM), Transportation Research Board, Washington, DC.
- Khoury, N. N., & Zaman, M. (2004). Correlation Among Resilient Modulus, Moisture variation, and Soil Suction for Subgrade Soils. *Transportation Research Record*, 1874, 99–107.
- Kirkwood, C. W. (1998). System Dynamics Methods. Tempe, AZ: Arizona State University, College of Business.
- Knott, J. F. (2019). Climate Adaptation for Coastal Road Infrastructure in the Northeast (Doctorate Thesis), University of New Hampshire, Durham, NH.
- Laliberte, G. E., Corey, A. T., & Brooks, R. H. (1966). Properties of Unsaturated Porous Media (Hydrology Paper 17). Fort Collins, CO: Colorado State University.
- Lamborn, M. J. (1986). A Micromechanical Approach to Modeling Partly Saturated Soils (MSc Thesis). College Station, TX: Texas A&M University.
- Larson, G., & Dempsey, B. J. (1997). *Enhanced Integrated Climatic Model: Version 2.0* (Rep. No. Report number DTFA MN/DOT 72114). Minneapolis: Minnesota Road Research Project and Federal Highway Administration.
- Lary, J. A., & Mahoney, J. P. (1984). Seasonal Effects on the Strength of Pavement Structures. *Transportation Research Record*, 954, 88-94.
- Liang, R., Rabab'ab, S., & Khasawneh, M. (2008). Predicting Moisture Dependent Resilient Modulus of Cohesive Soils using Soil Suction Concept. *ASCE Journal of Transportation Engineering*, 134(1) 34–40.
- Long, X., Aubeny, C. P., Bulut, R., & Lytton, R. L. (2006). Two-Dimensional Moisture Flow-Soil Deformation Model for Application to Pavement Design. *Transportation Research Record*, 1967, 121-131.
- Lu, D., Tighe, S. L., Xie, W.-C. (2017). Pavement Fragility Modeling Framework and Build-in Resilience Strategies for Flood Hazard. Paper presented at the Transportation Research Board 96th Annual Meeting, Transportation Research Board, Washington, DC.
- Lu, N., & Likos, W. Unsaturated Soil Mechanics. Hoboken, NJ: J. Wiley.
- Maina, J. W., & Matsui, K. (2004). Developing Software for Elastic Analysis of Pavement Structure Responses to Vertical and Horizontal Surface Loadings. *Transportation Research Record*, 1896(1), 107–118.
- Mallick, R., & El-Korchi, T. (2013). Pavement Engineering Principals and Practice (Second Edition). Boca Raton, FL: CRC Press, Taylor and Francis Group.
- Mallick, R. B., Tao, M., Daniel, J. S., Jacobs, J., & Veeraragavan, A. (2015). Development of A Methodology and A Tool for The Assessment of Vulnerability of Roadways to Flood Induced Damage. *Journal of Flood Risk Management*, 10, 301-313.
- Mallick, R. B., Tao, M., Daniel, J. S., Jacobs, J. M., & Veeraragavan, A. (2017). Combined Model Framework for Asphalt Pavement Condition Determination After Flooding. *Transportation Research Record*, 2639, 64-72.

- Mbonimpa, M., Aubertin, M., Chapuis, R. P., & Bussière, B. (2002). Practical Pedotransfer Functions for Estimating the Saturated Hydraulic Conductivity. *Geotechnical and Geological Engineering*, 20(3), 235–259.
- Minnesota Department of Transportation. (2012). *MnPAVE User's Guide*. St. Paul, MN: MnDOT.
- Mitchell, P. W., & Avalle, D. L. (1984). A Technique to Predict Expansive Soil Movements. Paper presented at the 5th International Conference on Expansive Soils, Adelaide, South Australia.
- Mndawe, M. B., Ndambuki, J. M., Kupolati, W. K., & Badejo, A. A., (2015). Assessment of The Effects of Climate Change on the Performance of Pavement Subgrade. *African Journal of Science, Technology, Innovation and Development*, 7(2), 111-115.
- MnDoT. (2019). Minnesota Department of Transportation. Retrieved from <https://www.dot.state.mn.us/>
- Moossazadeh, J., & Witczak, M. W. (1981). Prediction of subgrade moduli for soil that exhibits nonlinear behavior. *Transportation Research Record*, 810, 9–17.
- Mualem, Y. (1976). A new model for predicting the hydraulic conductivity of unsaturated porous media. *Water Resources Research*, 12(3), 513–522.
- Natural Resources Conservation Service. (2019). NRCS. Retrieved from <https://www.nrcs.usda.gov/wps/portal/nrcs/site/national/home/>
- NDDOT. ND Load Restrictions. (2019). NDDOT. Retrieved from <https://www.dot.nd.gov/roadreport/loadlimit/loadlimitinfo.htm#restrictioninfo>
- Nemes, A. D., Schaap, M. G., Leij, F. J., & Wösten, J. H. M. (2001). Description of the unsaturated soil hydraulic database UNSODA version 2.0. *Journal of Hydrology*, 251(3-4), 151-162.
- Newmark, N. M. (1942), Influence Charts for Computation of Stresses in Elastic Foundations. *Univ. of Illinois Bulletin*, 40(12), p28.
- Ng, C. W. W., Zhou, C., Yuan, Q., & Xu, J. (2013). Resilient modulus of unsaturated subgrade soil: Experimental and theoretical investigations. *Can. Geotech. J.*, 50(2), 223–232.
- Noureldin, A. S. (1994) Influence of Stress Levels and Seasonal Variations on In Situ Pavement Layer Properties. *Transportation Research Record*, 1448, 16-24.
- Oh, J. H., Fernando, E. G., Holzschuher, C., & Horhota, D. (2012). Comparison of Resilient Modulus Values for Florida Flexible Mechanistic-Empirical Pavement Design. *Int. J. Pavement Eng.*, 13(5), 472–484.
- Ovik, J. M., Siekmeier, J. A., & Van Deusen, D. A., (2000). *Improved spring load restrictions guidelines using mechanistic analysis*. St. Paul, MN: Minnesota Department of Transportation.
- Pathak, S. P., & Singh, T. (2014). An Analysis on Groundwater Recharge by Mathematical Model in Inclined Porous Media. *International Scholarly Research Notices*, 2014, 1–4.  
<https://doi.org/10.1155/2014/189369>
- Pavement Interactive. (2019). Pavement Interactive. Retrieved from <https://www.pavementinteractive.org/>

- Pregolato, M., Ford, A., Wilkinson, S. M., & Dawson, R. J. (2017). The Impact of Flooding on Road Transport: A Depth-Disruption Function. *Transportation Research Part D: Transport and Environment*, 55, 67–81. <https://doi.org/10.1016/j.trd.2017.06.020>
- Puckett, W. E., Dane, J. H., & Hajek, B. F. (1985). Physical and mineralogical data to determine soil hydraulic properties. *Soil Science Society of America Journal*, 49(4), 831-836.
- Qiao, Y., Medina, R. A., McCarthy, L. M., Mallick, R. B., & Daniel, J. S. (2017). Decision Tree for Post flooding Roadway Operations. *Transportation Research Record*, 2604, 120-130
- Rada, G., & Witczak, M. W. (1981). Comprehensive Evaluation of Laboratory Resilient Moduli Results for Granular Material. *Transportation Research Record*, 810, 23-33.
- Rashedi, R., & Hegazy, T. (2016). Holistic Analysis of Infrastructure Deterioration and Rehabilitation using System Dynamics. *Journal of Infrastructure Systems*, 22(1), 04015016.
- Ravi, V., & Williams, J. R. (1998). Estimation of Infiltration Rate in the Vadose Zone: Compilation of Simple Mathematical Models (Volume I.). Ada, OK: U.S. Environmental Protection Agency, Subsurface Protection and Remediation Division, National Risk Management Research Laboratory.
- Richards, L. A. (1931). Capillary Conduction of Liquids through Porous Mediums. *Physics* 1(5), 318–333.
- Richter, C. A. (2006). *Seasonal Variations in the Moduli of Unbound Pavement Layers* (Rep. No. FHWA-HRT-04-079). Washington, DC: Federal Highway Administration, U.S. Department of Transportation
- Saevarsdottir, T., & Erlingsson, S. (2013). Effect of Moisture Content on Pavement Behavior in a Heavy Vehicle Simulator Test. *Road Materials and Pavement Design*, 14(S1), 274-286.
- Sahin, H., Gu, F., Tong, Y., & Lytton, R. L. (2013). Unsaturated soil mechanics in the design and performance of pavements. Keynote address at the 1st Pan-Am. Conf. on Unsaturated Soils, CRC Press/Balkema, Rotterdam, the Netherlands.
- Salour, F., Erlingsson, S., & Zapata, C. E. (2015). Model for Seasonal Variation of Resilient Modulus in Silty Sand Subgrade Soil Evaluation with Falling Weight Deflectometer. *Transportation Research Record*, 2510, 65–73.
- Saltelli, A., Ratto, M., Andres, T., Campolongo, F., Cariboni, J., Gatelli, D., Saisana, M., & Tarantola, S. (2008). Global Sensitivity Analysis: The Primer. John Wiley & Sons, p304.
- Santero, N., Masanet, E., & Horvath, A. (2011). Life-Cycle Assessment of Pavements. Part I: Critical Review. *Resources, Conservation and Recycling*, 55(9), 801–809.
- Sauer, E. K., & Monismith, C. L. (1968). Influence of Soil Suction on Behavior of a Glacial Till Subjected to Repeated Loading. *Highway Research Record*, 215, 8-23.
- Sawangsurriya, A., Edil, T. B., & Benson, C. H. (2009). Effect of Suction on Resilient Modulus of Compacted Fine-Grained Subgrade Soils. *Transportation Research Record*, 2101, 82-88.
- Seed, H. B., Mitry, F. G., Monismith, C. L., & Chan, C. K. (1967). Prediction of Pavement Deflection from Laboratory Repeated Load Tests. (NCHRP Rep. No. 35) Washington, DC: Transportation Research Board.

- SHRP. (1994). The SUPERPAVE Mix Design System Manual of Specifications, Test Methods, and Practices (SHRP-A-379). National Research Council, Washington, DC.
- Sias, J., Mallick, R., Ghayoomi, M., Jacobs, J., Medina, R., McCarthy, L., Tao, M., Maser, K., Qiao, Y., Elshaer, M., & Gallishaw, N. (2018). Flooded Pavement Assessment (FHWA Report, Contract No. DTFH61-13-C-00022). Washington, DC: FHWA
- Sivakumar, V., Kodikara, J., O'hagan, R., Hughes, D., Cairns, P., & McKinley, J. D. (2013). Effects of Confining Pressure and Water Content on Performance of Unsaturated Compacted Clay under Repeated Loading. *Géotechnique*, 63(8), 628-640.
- Sultana, M., Chai, G., Martin, T., & Chowdhury, S., (2016). Modeling the Post flood Short-Term Behavior of Flexible Pavements. *Journal of Transportation Engineering, American Society of Civil Engineers*, 142(10), 04016042.
- Tang, Y., Reed, P., Wagener, T., Van Werkhoven, K., & Wagener, T. (2007). Comparing Sensitivity Analysis Methods to Advance Lumped Watershed Model Identification and Evaluation. *European Geosciences Union, Hydrol. Earth Syst. Sci.*, 11, 793-817.
- Thom, N. H., & Brown, S. F. (1987). Effect of Moisture on the Structural Performance of a Crushed-Limestone Road Base. *Transportation Research Board, Washington, DC*. 50-56.
- Ueshita, K., & Meyerhof, G. G. (1967). Deflection of Multilayer Soil Systems. *Proc. ASCE*, 93(SM5), 257-282
- Ullidtz, P. (1987). *Pavement Analysis*. New York: Elsevier Science.
- VADOSE/W. (2014). Vadose Modeling with VADOSE/W: An Engineering Methodology. GEO-SLOPE International Ltd., Calgary, Alberta, Canada.
- van Genuchten, M. T. (1980). A Closed-form Equation for Predicting the Hydraulic Conductivity of Unsaturated Soils. *Soil Science Society of America Journal*, 44(5), 892–898.
- Vennapusa, P., White, D. J., & Miller, D.K., (2013). Western Iowa Missouri River Flooding - Geo-Infrastructure Damage Assessment, Repair and Mitigation Strategies (Iowa DOT Project TR-638, Federal Highway Administration). Washington, DC: FHWA.
- Vennapusa, P. K. R., & White, D. J. (2015). Performance Assessment of Secondary-Roadway Infrastructure in Iowa after 2011 Missouri River Flooding. *Journal of Infrastructure Systems*, 21(4), p11.
- Wang, J., & Yuan, H. (2017). System Dynamics Approach for Investigating the risk Effects on Schedule Delay in Infrastructure Projects. *Journal of Management in Engineering*, 33(1), 04016029.
- Wei, T. (2013). A review of Sensitivity Analysis Methods in Building Energy Analysis. *Renewable and Sustainable Energy Reviews*. 20, 411-419.
- WisDOT. (2019). Highway Maintenance Manual. Bureau of Highway Maintenance, Madison, WI.
- WisDOT. (2019). Wisconsin Department of Transportation. Retrieved from <https://wisconsin.dot.gov/Pages/home.aspx>
- Witczak M. W., Houston, W. N., Zapata, C. E., Richter, C., Larson, G., & Walsh, K. (2000). Improvement of the Integrated Climatic Model for Moisture Content Predictions. Development of the 2002 Guide for the

Development of New and Rehabilitated Pavement Structures (NCHRP 1-37 A, Inter Team Technical Report, Seasonal 4). Washington, DC.

Yang, D., Zhang, T., Zhang, K., Greenwood, D. J., Hammond, J. P., & White, P. J. (2009). An Easily Implemented Agro-hydrological Procedure with Dynamic Root Simulation for Water Transfer in the Crop–Soil system: Validation and Application. *Journal of Hydrology*, 370(1-4), 177-190.

Yang, R. R., Huang, W. H., & Tai, Y. T. (2005). Variation of Resilient Modulus with Soil Suction for Compacted Subgrade Soils. *Transportation Research Record*, 1913, 99–106.

Zapata, C. E., Andrei, D., Witczak, M. W., & Houston, W. N. (2007). Incorporation of Environmental Effects in Pavement Design. *RoadMater. Pavement Des.*, 8(4), 667–693.

Zapata, C. E., Witczak, M. W., Houston, W. N., & Andrei, D. (2007). Incorporation of Environmental Effects in Pavement Design. *Road Materials and Pavement Design*, 8(4), 667–693.

Zhang, Z., Wu, Z., Martinez, M., & Gaspard, K., (2008). Pavement Structures Damage Caused by Hurricane Katrina Flooding. *Journal of Geotechnical and Geoenvironmental Engineering*, 134(5), pp. 633-643.

## **APPENDIX A. SUMMARY OF RESILIENT MODULUS EQUATIONS**



**Table A-1: Resilient Modulus Equations (1).**

TYPES OF SOIL USED = PM= Pulverized mudstone; DT= Decomposed Tuff; SCL= Silty Clay Loam			Group (Type of Equation)	Recommended Soil Type	Where Implemented	When it was used	Supported by Others / Notes	Soil Suction Range (kPa)
MEPDG	Used to calibrate the optimum resilient modulus values; also developed with degree of saturation where SWCC describes the relationship	Eq. (3) is used in MEPDG to calibrate the $M_{RSAT}$ values considering the influence of seasonal moisture content fluctuations $\log \left( \frac{M_R}{M_{RSAT}} \right) = a + \frac{b-a}{1 + \exp \left[ \ln \left( \frac{b}{a} \right) + k_w(S - S_{OFT}) \right]}$ (3)	(A) Empirical	-	-	2004	One of the main equations used with a variety of soil types and scenarios; R <sup>2</sup> = 0.88 when compared	-
Swangsuriya et al.	Four fine-grained soils (2 A-4 and 2 A-7-6)	$M_R/M_{RSAT} = -5.61 + 4.54 \log(\psi)$	(A) Empirical	Fine-Grained	Minnesota	2009	R <sup>2</sup> = 0.68 tends to under predict most data; sensitive to saturated resilient modulus; small differences contribute to significant variations in predicted resilient modulus	0-10,000
Yang et al.	Two fine-grained subgrade soils (A-7-5 and A-7-6)	$M_R = k_1(\sigma_d + \chi\psi)^{k_2}$	(B) Constitutive Models	R <sup>2</sup> >0.9; predicts different non-linear Mr- $\omega$ at various levels of shearing stress for PM and SCL; Extend the independent stress state variable approach and reasonably takes into account of soil suction	Taiwan, China	2005	R <sup>2</sup> =0.56; reasonably captures increase in Mr with $\omega$ ; most suitable to predict Mr- $\omega$ correlations for subgrade soils that exhibit hardening behavior (with respect to applied shearing stresses)	0-10,000
Liang et al.	Two fine-grained subgrades (A-4 and A-6); also validated using 8 sets of experimental data on fine-grained soils from lit.	$M_R = k_1 p_a \left( \frac{\theta_b + \chi\psi}{p_a} \right)^{k_2} \left( 1 + \frac{\tau_{oct}}{p_a} \right)^{k_3}$	(B) Constitutive Models	Fine-Grained	-	2008	R <sup>2</sup> =0.95; predicted behavior of Mr with respect to $\sigma_d$ for PM and SCL are not consistent	150-380
Khoury et al.	Several subgrade soils (range from A-4 to A-7)	$M_R = k_1 p_a \left( \frac{\theta_b}{p_a} \right)^{k_2} \left( k_4 + \frac{\tau_{oct}}{p_a} \right)^{k_3} + \alpha_1 \psi^{\beta_1} = M_{RSAT} + \alpha_1 \psi^{\beta_1}$	(C) Consecutive models extending the independent stress state variable approach	Subgrade Soils (Range from A-4 to A-7)	Oklahoma	2009	R <sup>2</sup> >0.9; predicts variation of Mr regardless of influence of applied shearing stress; does not consider influence of applied stress on the Mr- $\omega$ relationships	0-6,000
Ng et al.	Subgrade soil	$M_R = M_0 \left( \frac{p}{p_r} \right)^{k_1} \left( 1 + \frac{q_{cyc}}{p_r} \right)^{k_2} \left( 1 + \frac{\psi}{p} \right)^{k_3}$	(C) Consecutive models extending the independent stress state variable approach	Subgrade Soils	Hong Kong, China	2013	R <sup>2</sup> >0.9; predicts different non-linear Mr- $\omega$ at various levels of shearing stress for PM and SCL; Extend the independent stress state variable approach and reasonably takes into account of soil suction and provide reliable predictions within boundary effect and transition zones	0-250
Johnson et al.	-	$M_R = 1.35 \times 10^6 \times (101.36 - \psi)^{2.36} (J_1)^{3.25} (\gamma_d)^{3.06}$	(A) Empirical	Sandy Soils	-	1986	-	-
Parreira and Gonçalves	A-7-6 Soils	$M_R = 14.10 \sigma_d^{0.782} \psi^{0.076}$	(A) Empirical	Lateritic Soil	Brazil	2000	-	0-87,500 kPa
Ceratti et al.	A-7-6 Soils	$M_R = 142 + 16.9 \psi$	(A) Empirical	Lateritic Soil	Brazil	2004	-	0-14 kPa

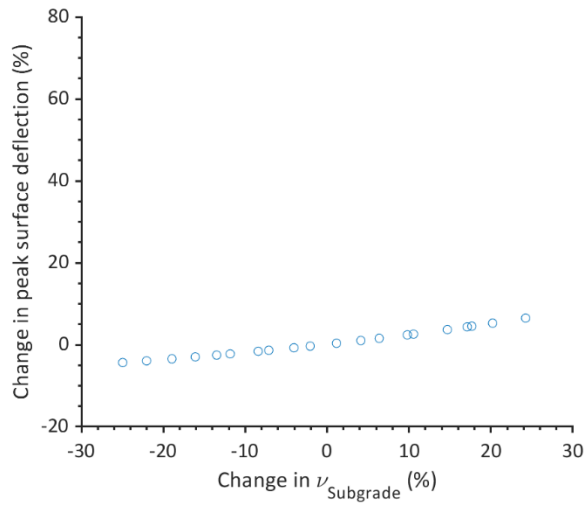
**Table A-2: Resilient Modulus Equations (2).**

Doucet and Dore	Also developed for several "partially crushed materials"	$M_R = 1060\theta_b - 8700\psi + 57000$	(A) Empirical	Crushed Granular Materials	Quebec, Canada	2004	-	
Swangsuriya et al.	Four fine-grained soils (2 A-4 and 2 A-7-6)	$M_R/M_{ROPT} = -0.24 + 0.25 \log(\psi)$	(A) Empirical	Fine-Grained	Minnesota	2009	-	0-10,000 kPa
Ba et al.	Derived for four unbound granular base materials	$M_R/M_{ROPT} = 0.385 + 0.267 \log(\psi)$	(A) Empirical	Granular	Senegal	2013	-	0-100 kPa
Moossazadeh and Witczak	Relates applied stress using model parameters	$M_R = k_1 \left( \frac{\sigma_d}{p_a} \right)^{k_2}$	(B) Constitutive Models	-	-	1981	Most commonly used constitutive models	-
Uzan	Relates applied stress using model parameters	$M_R = k_1 p_a \left( \frac{\theta_b}{p_a} \right)^{k_2} \left( \frac{\tau_{oct}}{p_a} \right)^{k_3}$	(B) Constitutive Models	-	-	1985	Most commonly used constitutive models	-
Loach	-	$M_R = \frac{\sigma_d}{k_1} \left[ \frac{c\sigma_c + \psi}{\sigma_d} \right]^{k_2}$	(B) Constitutive Models	Fine Grained Soils	United Kingdom	1987	-	0-100 kPa
Jin et al.	granular base materials	$\Delta M_R = K_1 K_2 \theta_b^{K_2-1} (\Delta\theta_{bT} + \Delta\theta_{b\psi})$	(B) Constitutive Models	Granular	Rhode Island	1994	-	-
Lytton	granular base materials	$\Delta M_R = K_1 K_2 \theta_b^{K_2-1} (\Delta\theta_{bT} + \Delta\theta_{b\psi})$	(B) Constitutive Models	Granular	-	1995	-	-
Gu et al.	Verification of eq. 14	$M_R = k_1 p_a \left( \frac{\theta_b - 3f\theta\psi}{p_a} \right)^{k_2} \left( \frac{\tau_{oct}}{p_a} \right)^{k_3}$	(B) Constitutive Models	Granular	Texas	2014	Derived off of nine granular base materials from Texas	-
Heath et al. 2004	Based off of a typical base material located in California	$M_R = k_1 p_a \left[ \frac{(\theta_b/3) - u_a + \chi\psi}{p_a} \right]^{k_2} \left( \frac{\sigma_d}{p_a} \right)^{k_3}$	(B) Constitutive Models	Most likely granular "base material"	California	2004	-	-
Oh et al.	derived for both base and subgrade materials	$M_R = k_1 p_a \left( \frac{\theta_b + 3k_4\psi\theta}{p_a} \right)^{k_2} \left( \frac{\tau_{oct}}{p_a} + 1 \right)^{k_3}$	(B) Constitutive Models	Granular	Florida	2012	-	-
Sahin et al.	Base materials	$M_R = k_1 p_a \left[ \frac{\theta_b - 3f\theta(\psi_0 + \beta \frac{\theta_b}{3} + \alpha\tau_{oct})}{p_a} \right]^{k_2} \left( \frac{\tau_{oct}}{p_a} + 1 \right)^{k_3}$	(B) Constitutive Models	Granular	-	2013	-	-

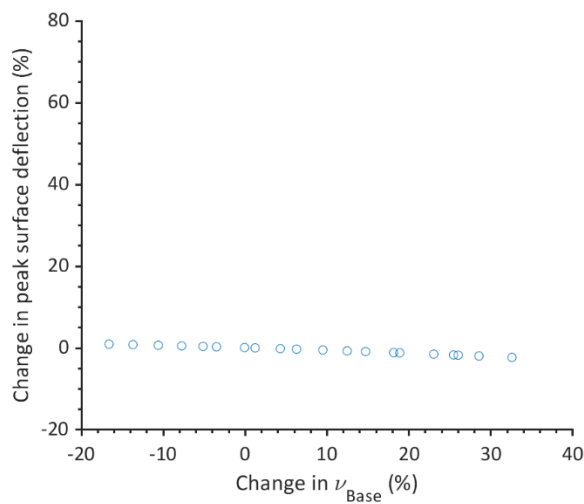
**Table A-3: Resilient Modulus Equations (3).**

Fredlund et al.	-	$\log M_R = c_{ld} - m_{ld}(\sigma_d)$	( C ) Consecutive models extending the independent stress state variable approach	Glacial Till	Saskatchewan, Canada	1977	-	0-1000 kPa
Oloo and Fredlund 1998	Coarse-grained soils (eq.22); Fine-grained soils (eq.23 & 24)	$M_R = k \theta_b^{m_b} + k_s \psi$ $M_R = k_2 - k_3(k_1 - \theta_b) + k_s \psi$ when $k_1 > \theta_b$ $M_R = k_2 + k_4(\theta_b - k_1) + k_s \psi$ when $k_1 < \theta_b$	( C ) Consecutive models extending the independent stress state variable approach	Coarse-Grained and Fine-grained	-	1998	-	-
Gupta et al. 2007	Two a-4 soils and two A-7-6 soils	$M_R = k_1 p_a \left( \frac{\theta_b - 3k_4}{p_a} \right)^{k_2} \left( k_5 + \frac{\tau_{oct}}{p_a} \right)^{k_3} + \alpha_1 \psi^{\beta_1}$ $M_R = k_1 p_a \left( \frac{\theta_b}{p_a} \right)^{k_2} \left( 1 + \frac{\tau_{oct}}{p_a} \right)^{k_3} + k_{as} p_a \Theta^e \psi$	( C ) Consecutive models extending the independent stress state variable approach	Fine-Grained	Minnesota	2007	-	10-10000 kPa
Caicedo et al.	derived from three nonstandard base materials	$M_R = k_1 p_a \left( 1 + k_2 \frac{\sigma_d}{p_a} \right) \left( \frac{\psi}{p_a} \right)^{k_3} \frac{f(e)}{f(0.33)}$	( C ) Consecutive models extending the independent stress state variable approach	Granular	Andes Cordillera, Colombia	2009	-	0-200 kPa
Khoury et al.	Derived from manufactured soil	$M_R = \left[ k_1 p_a \left( \frac{\theta_b}{p_a} \right)^{k_2} \left( 1 + \frac{\tau_{oct}}{p_a} \right)^{k_3} + (\psi - \psi_0) \times \left( \frac{\theta_d}{\theta_v} \right)^{\left( \frac{k_1}{\theta_v} \right)} \right] \times \left( \frac{\theta_d}{\theta_w} \right)$	( C ) Consecutive models extending the independent stress state variable approach	Silty Soil	-	2011	Hysteresis behavior in Mr	0-100 kPa
Cary and Zapata	Further verified by Salour et al. 2014 in Sweden; Two sandy subgrade soils (A-4 and A-2-4 with soil suction range 0-450kPa)	$M_R = k_1 p_a \left( \frac{\theta_{net} - 3\Delta u_{w-sat}}{p_a} \right)^{k_2} \left( \frac{\tau_{oct}}{p_a} + 1 \right)^{k_3} \left( \frac{\psi_0 - \Delta \psi}{p_a} + 1 \right)^{k_4}$	( C ) Consecutive models extending the independent stress state variable approach	Granular Soil and Clayey Soil (further research needed for fine cohesive soils)	Arizona	2011	Considers dynamic loading and resulting change in pore water pressure; model proposed is modification of the MEPDG that accommodates changes in matrix suction and effects of drainage conditions; triaxial testing	0-250 kPa
Azam et al.	derived from recycled unbound materials	$M_R = k \left( \frac{\sigma_m}{p_a} \right)^{k_1} \left( \frac{\tau_{oct}}{\tau_{ref}} \right)^{k_2} \left( \frac{\psi}{p_a} \right)^{k_3} \left[ \frac{DDR(1 - k_4 RCM/100)}{100} \right]^{k_5}$	( C ) Consecutive models extending the independent stress state variable approach	Granular	Australia	2013	-	0-10 kPa
Han and Vanapalli	Derived from experiments from 11 compacted fine-grained subgrade soils	$M_R = k \left( \frac{\sigma_m}{p_a} \right)^{k_1} \left( \frac{\tau_{oct}}{\tau_{ref}} \right)^{k_2} \left( \frac{\psi}{p_a} \right)^{k_3} \left[ \frac{DDR(1 - k_4 RCM/100)}{100} \right]^{k_5}$ $\frac{M_R - M_{RSAT}}{M_{ROPT} - M_{RSAT}} = \frac{\psi}{\psi_{OPT}} \left( \frac{S}{S_{OPT}} \right)^\epsilon$	( C ) Consecutive models extending the independent stress state variable approach	Fine-Grained	-	2015	Has large list of protocols followed during testing (listed in paper)	-

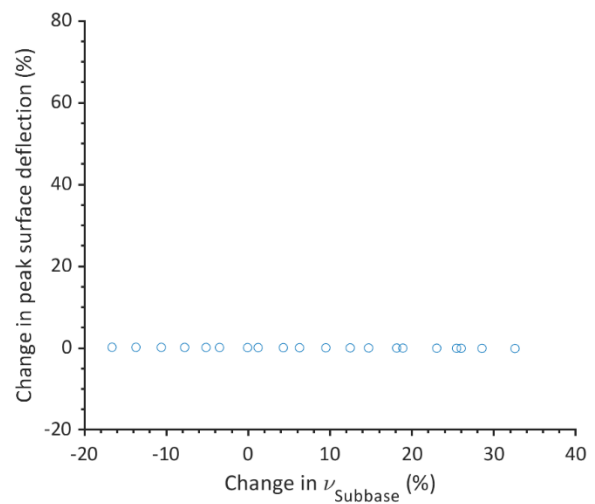
## **APPENDIX B. SENSISTIVITY ANALYSIS RESULTS**



**Figure B-1. Sensitivity of peak surface deflection to the variations of subgrade Poisson's ratio for coarse-grained subgrade model.**

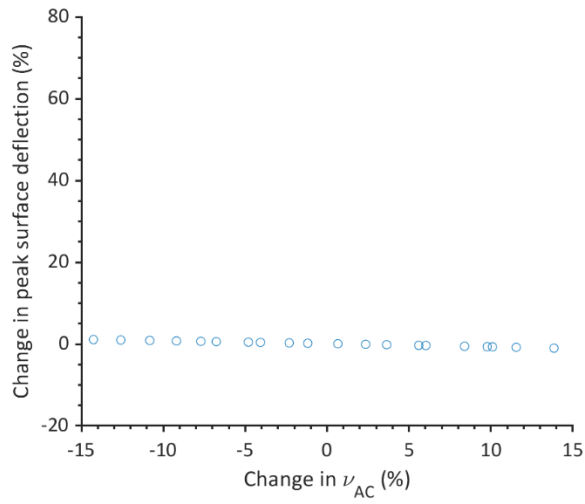


(a)

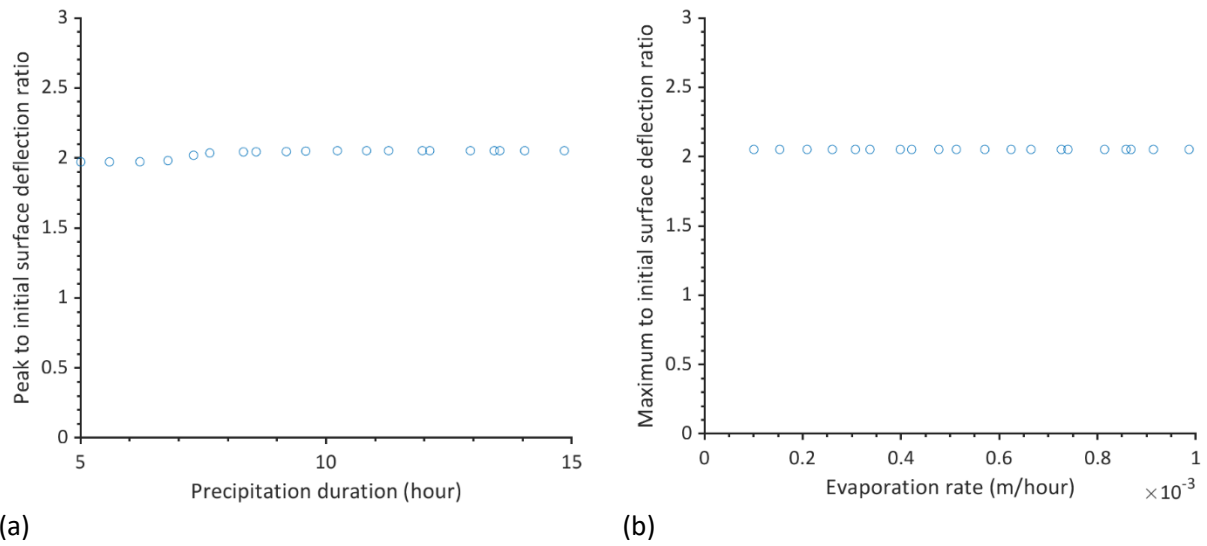


(b)

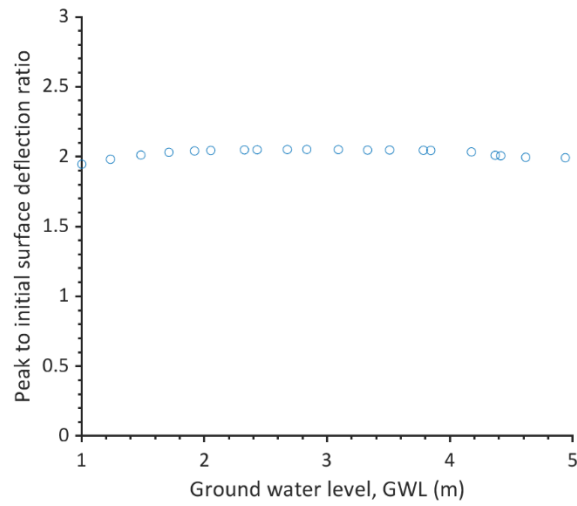
**Figure B-2. Sensitivity of peak surface deflection to the variations of (a) aggregate base and (b) subbase Poisson's ratio for coarse-grained subgrade model.**



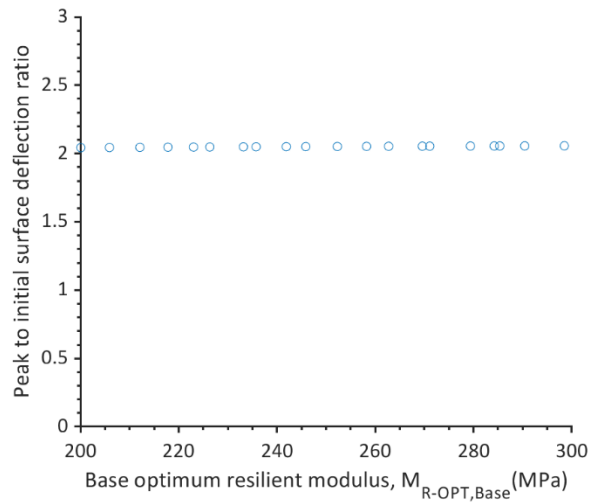
**Figure B-3. Sensitivity of peak surface deflection to the variations of AC Poisson's ratio for coarse-grained subgrade model.**



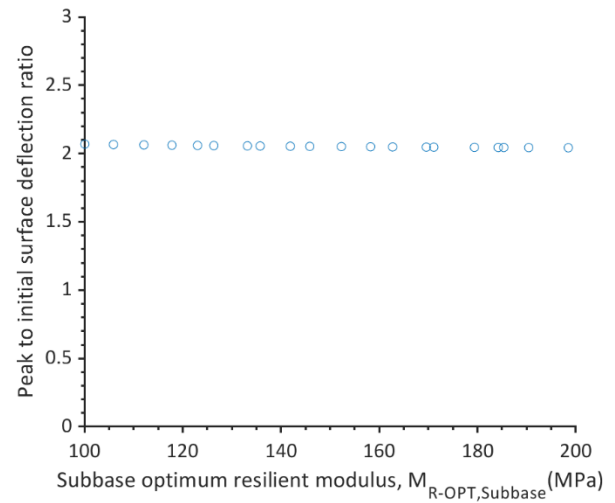
**Figure B-4. Sensitivity of  $\delta_p/\delta_0$  to variations in (a) precipitation duration and (b) evaporation rate for coarse-grained subgrade model.**



**Figure B-5. Sensitivity of  $\delta_p/\delta_0$  to variations in initial GWL for coarse-grained subgrade model.**

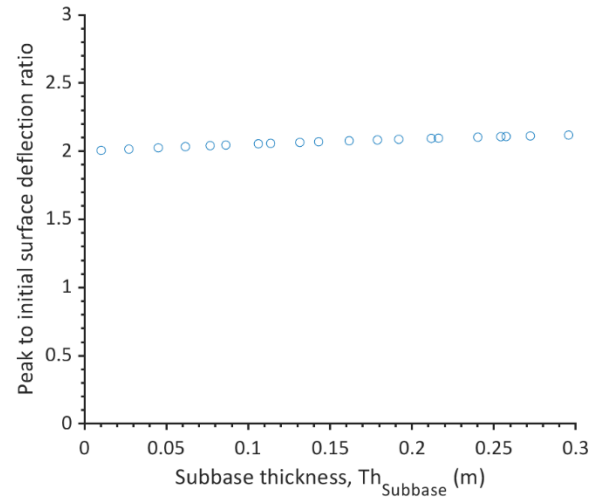
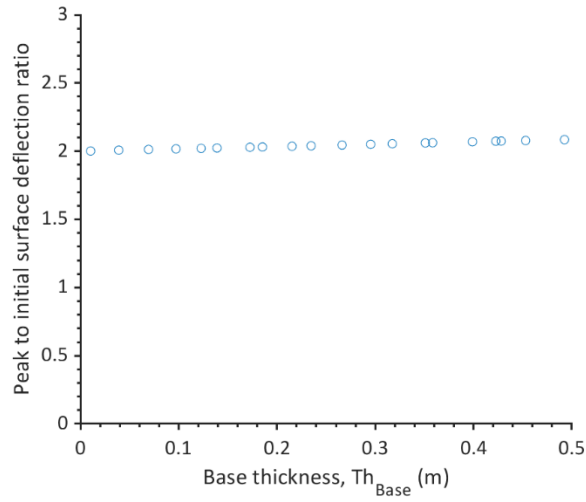


(a)



(b)

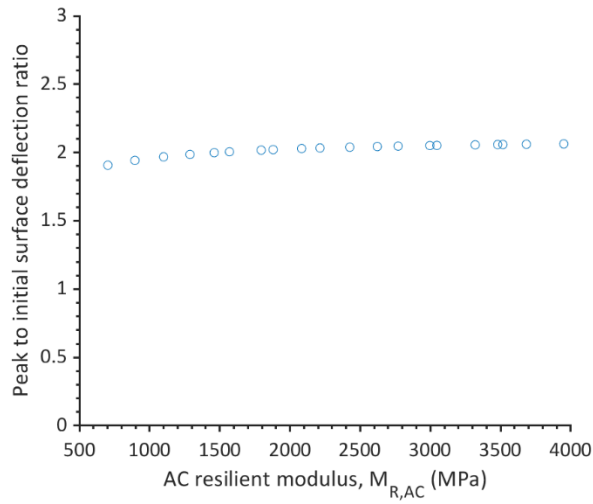
**Figure B-6. Sensitivity of  $\delta_p/\delta_0$  to variations in (a) aggregate base and (b) subbase optimum resilient moduli for coarse-grained subgrade model.**



(a)

(b)

**Figure B-7. Sensitivity of  $\delta_p/\delta_0$  to variations in (a) aggregate base and (b) subbase thicknesses for coarse-grained subgrade model.**



**Figure B-8. Sensitivity of  $\delta_p/\delta_0$  to variations in AC resilient modulus for coarse-grained subgrade model.**



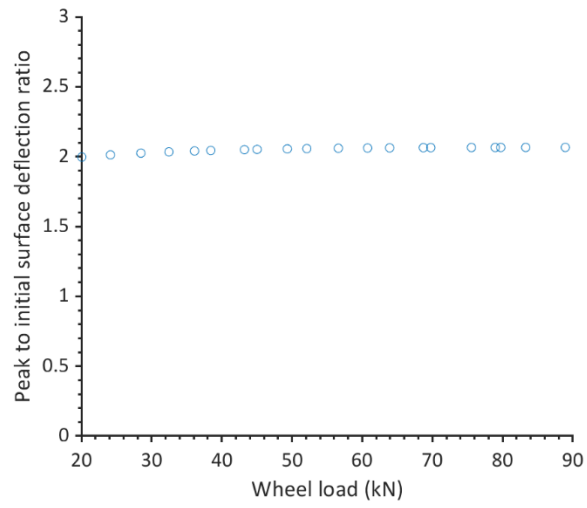


Figure B-9. Sensitivity of  $\delta_p/\delta_0$  to variations in wheel load for coarse-grained subgrade model.

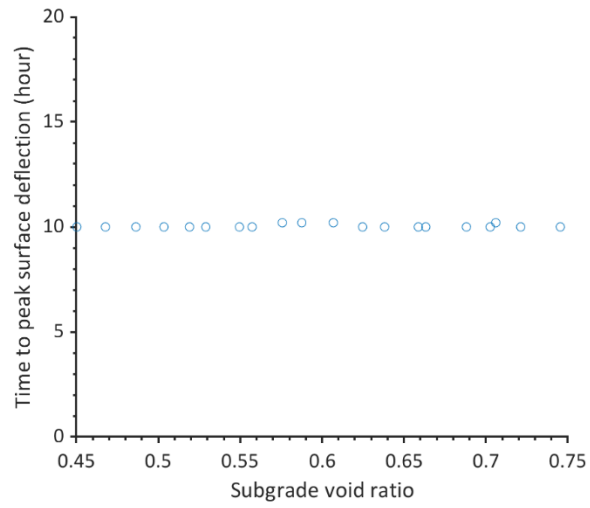
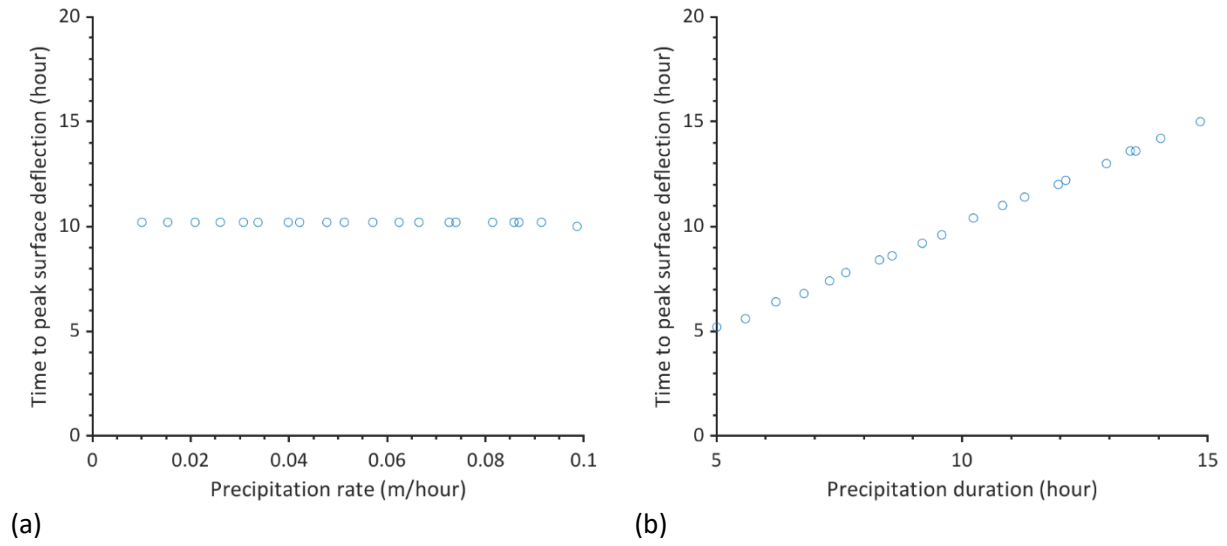
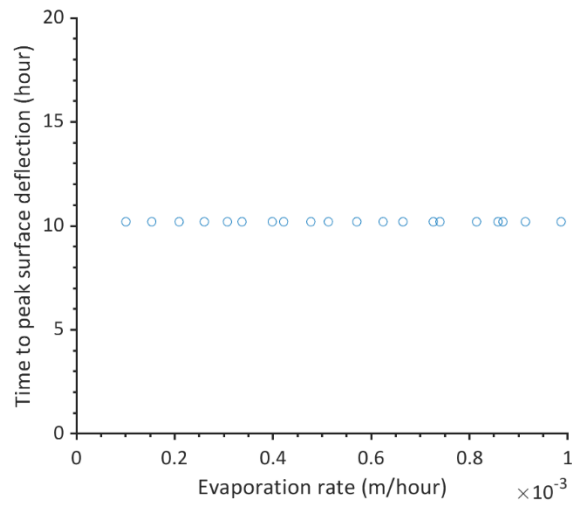


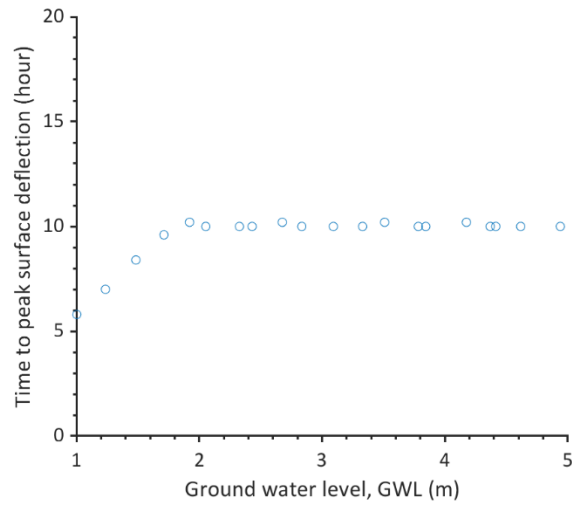
Figure B-10. Sensitivity of  $t_p$  to variations in subgrade void ratio for coarse-grained subgrade model.



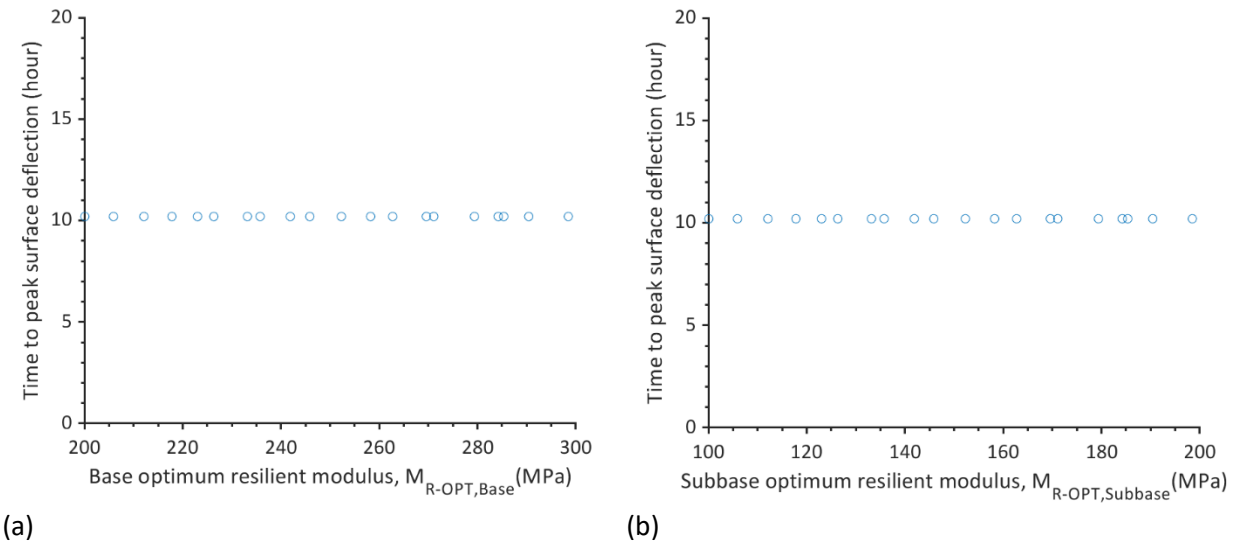
**Figure B-11. Sensitivity of  $t_p$  to variations in precipitation (a) rate and (b) duration for coarse-grained subgrade model.**



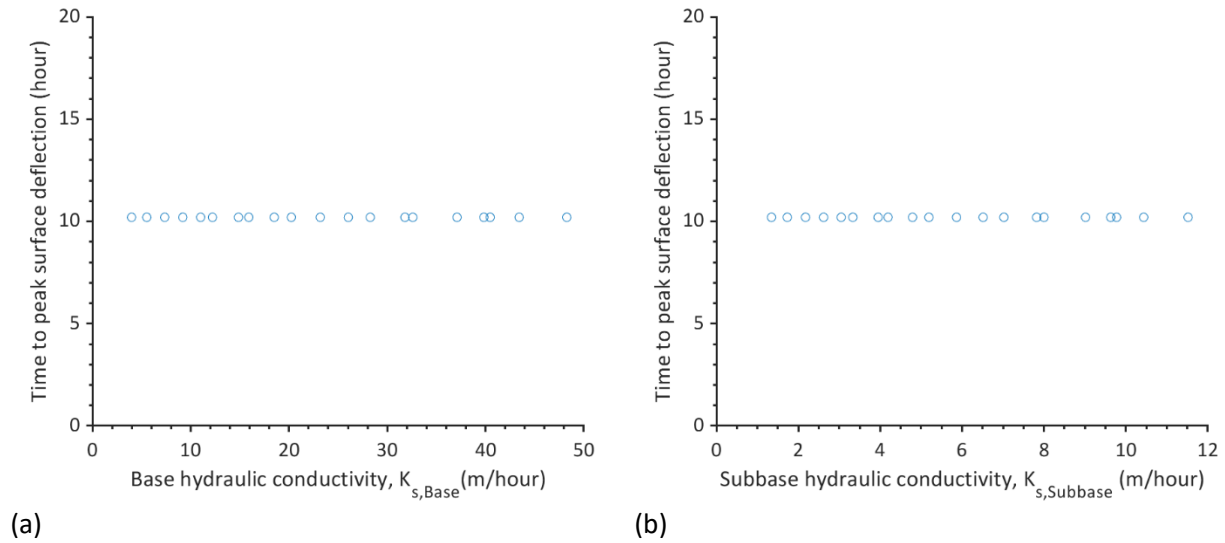
**Figure B-12. Sensitivity of  $t_p$  to variations in evaporation rate for coarse-grained subgrade model.**



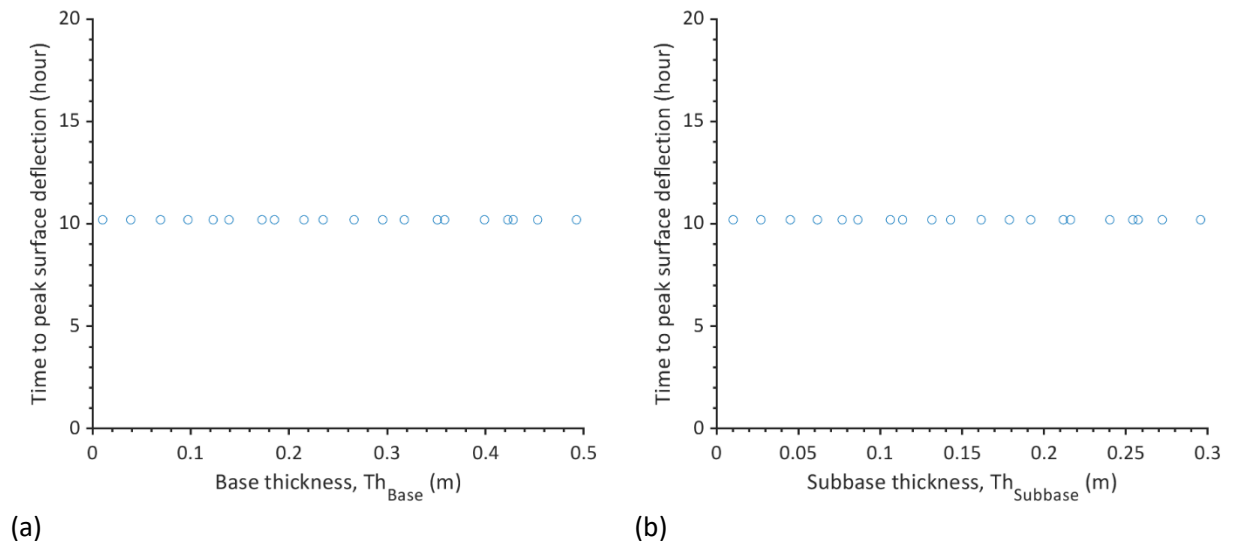
**Figure B-13. Sensitivity of  $t_p$  to variations in initial GWL for coarse-grained subgrade model.**



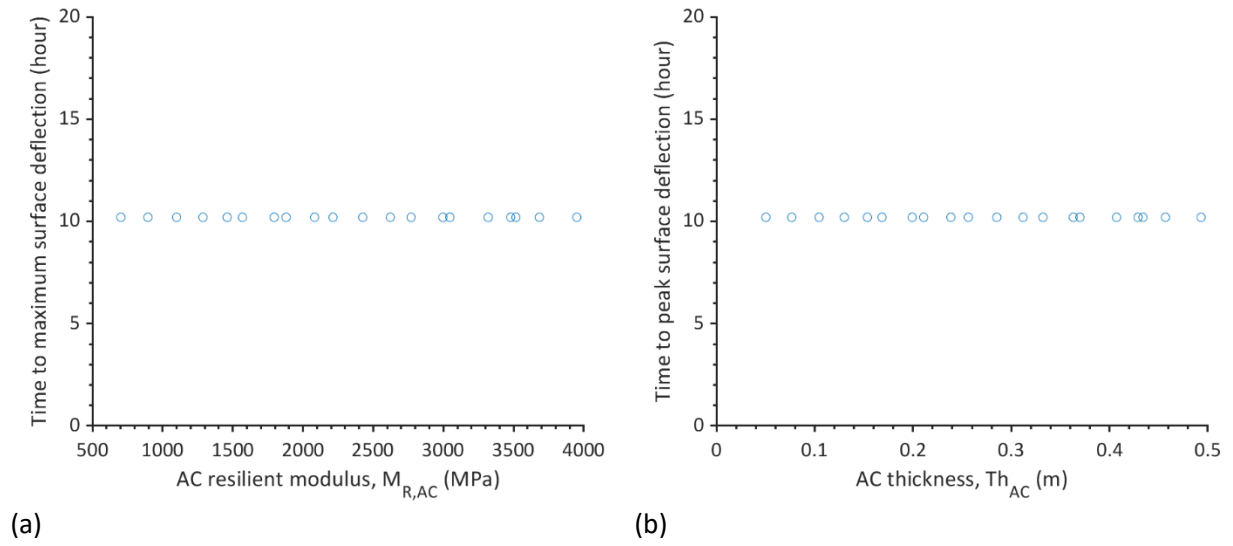
**Figure B-14. Sensitivity of  $t_p$  to variations in (a) aggregate base and (b) subbase optimum resilient moduli for coarse-grained subgrade model.**



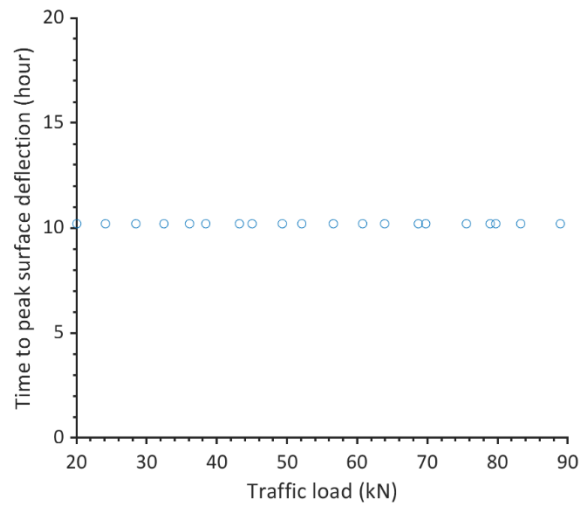
**Figure B-15. Sensitivity of  $t_p$  to the variations of (a) aggregate base and (b) subbase hydraulic conductivities for coarse-grained subgrade model.**



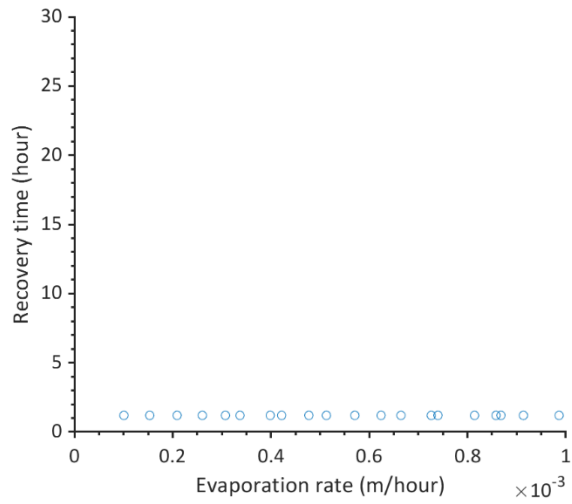
**Figure B-16. Sensitivity of  $t_p$  to variations in (a) aggregate base and (b) subbase thicknesses for coarse-grained subgrade model.**



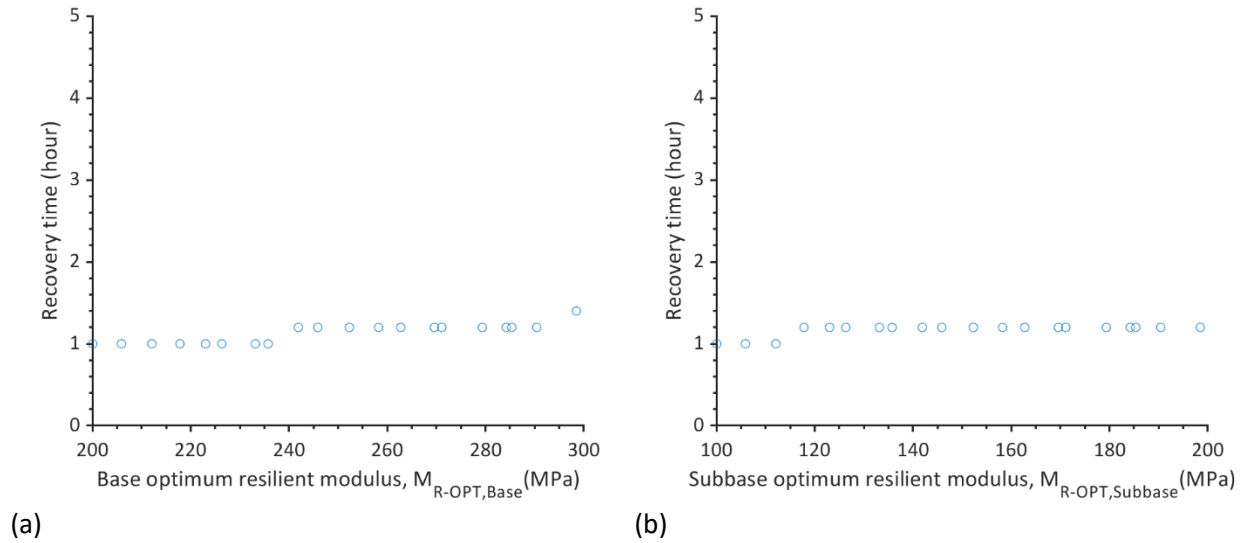
**Figure B-17. Sensitivity of  $t_p$  to variations in AC (a) resilient modulus and (b) thickness for coarse-grained subgrade model.**



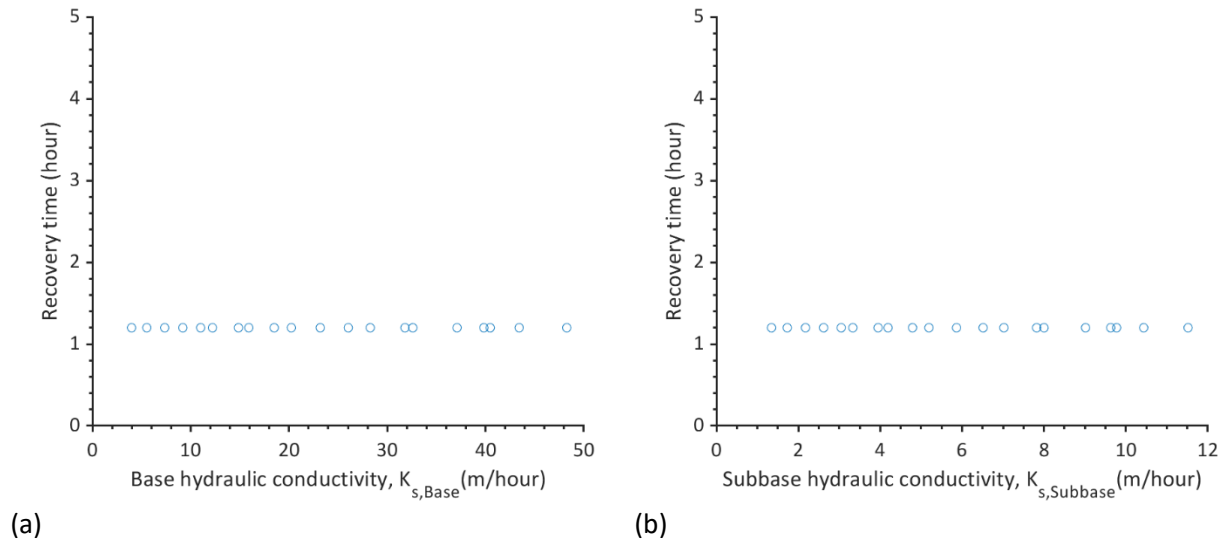
**Figure B-18. Sensitivity of  $t_p$  to variations in wheel load for coarse-grained subgrade model for coarse-grained subgrade model.**



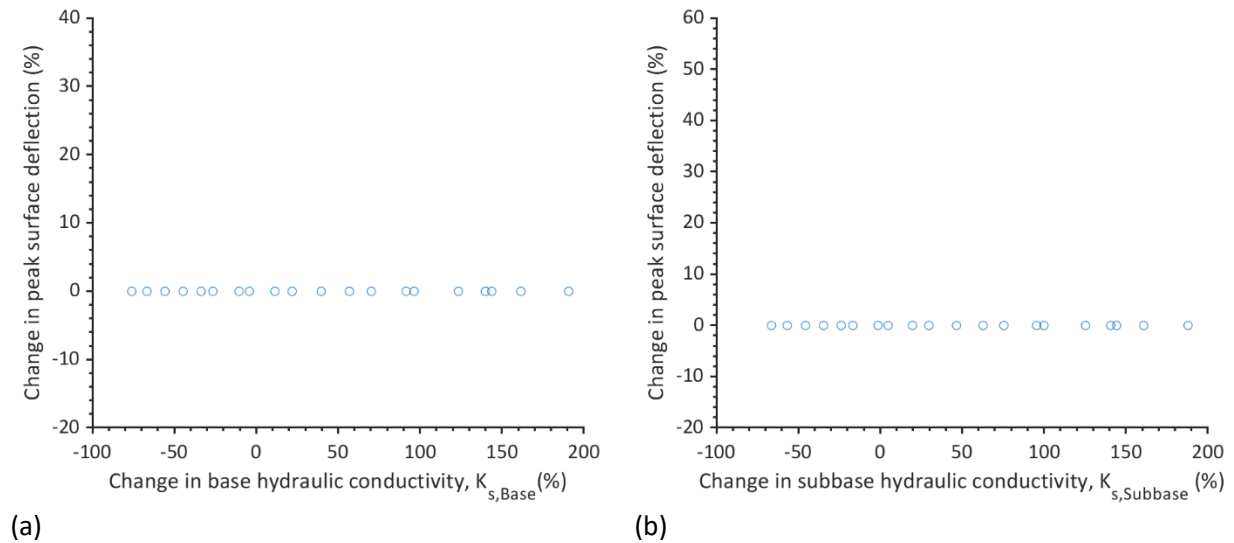
**Figure B-19. Sensitivity of  $t_R$  to variations in evaporation rate for coarse-grained subgrade model.**



**Figure B-20. Sensitivity of  $t_R$  to variations in (a) aggregate base and (b) subbase optimum resilient moduli for coarse-grained subgrade model.**



**Figure B-21. Sensitivity of  $t_R$  to the variations of (a) aggregate base and (b) subbase hydraulic conductivities for coarse-grained subgrade model.**



**Figure B-22. Sensitivity of peak surface deflection to the variations of (a) aggregate base and (b) subbase hydraulic conductivities for fine-grained subgrade model.**

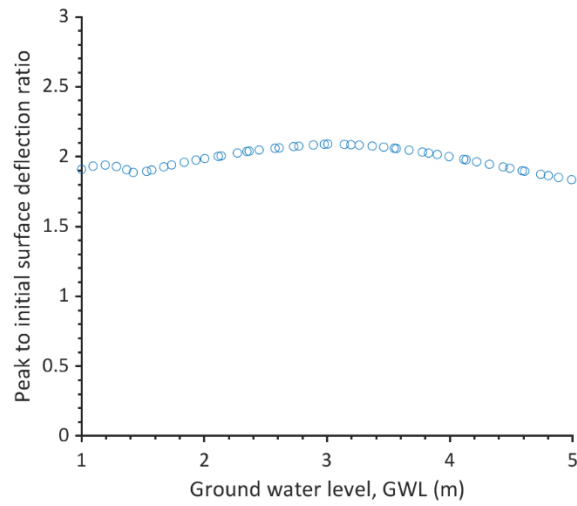


Figure B-23. Sensitivity of  $\delta_p/\delta_0$  to variation in initial GWL for fine-grained subgrade model.

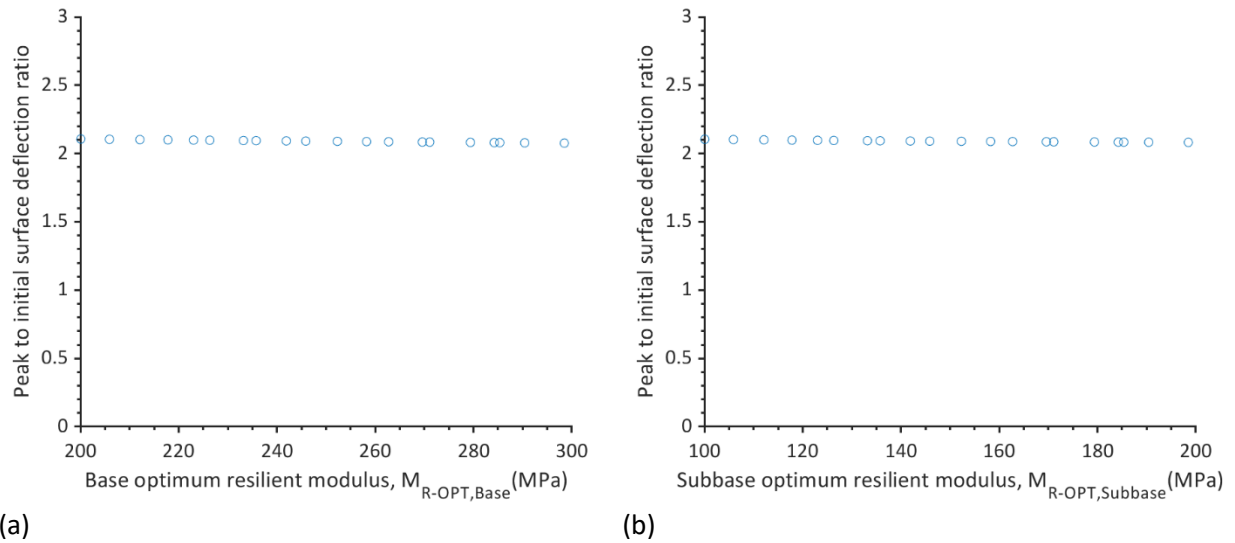
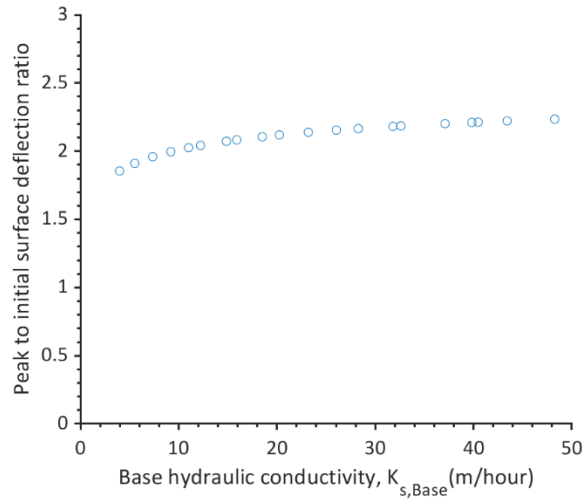
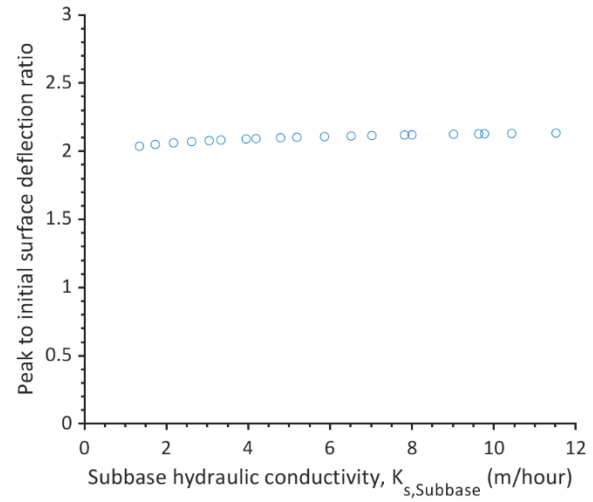


Figure B-24. Sensitivity of  $\delta_p/\delta_0$  to variations in (a) aggregate base and (b) subbase optimum resilient moduli for fine-grained subgrade model.



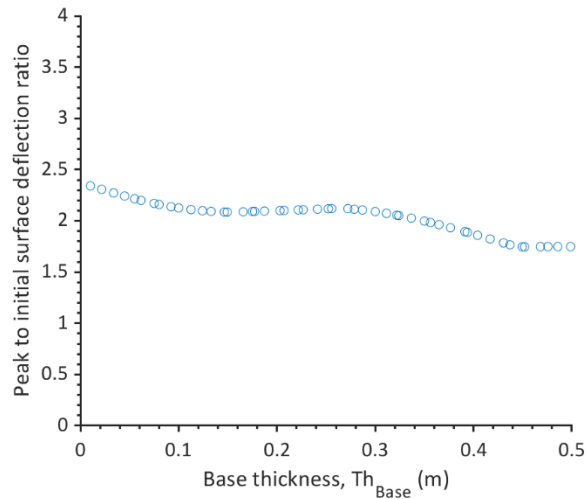


(a)

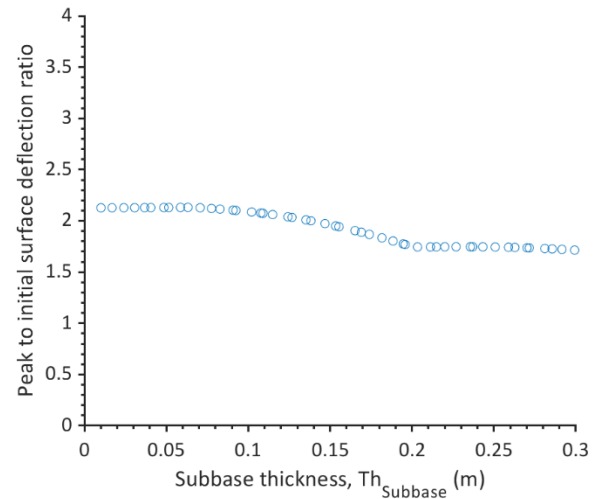


(b)

**Figure B-25. Sensitivity of  $\delta_p/\delta_0$  to the variations of (a) aggregate base and (b) subbase hydraulic conductivities for fine-grained subgrade model.**



(a)



(b)

**Figure B-26. Sensitivity of  $\delta_p/\delta_0$  to variations in (a) aggregate base and (b) subbase thicknesses for fine-grained subgrade model.**

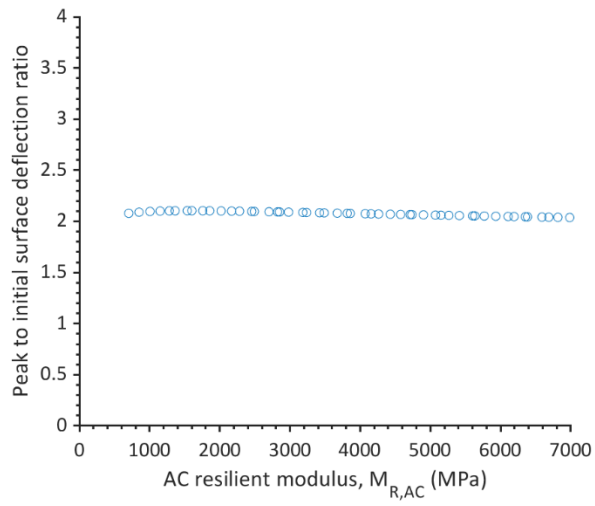


Figure B-27. Sensitivity of  $\delta_p/\delta_0$  to variations in AC resilient modulus for fine-grained subgrade model.

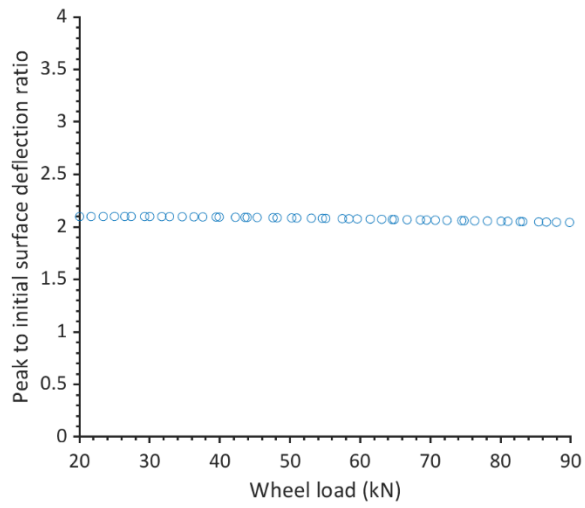
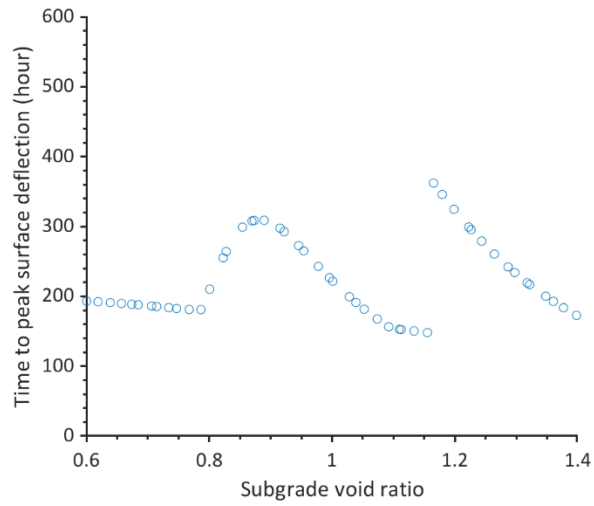
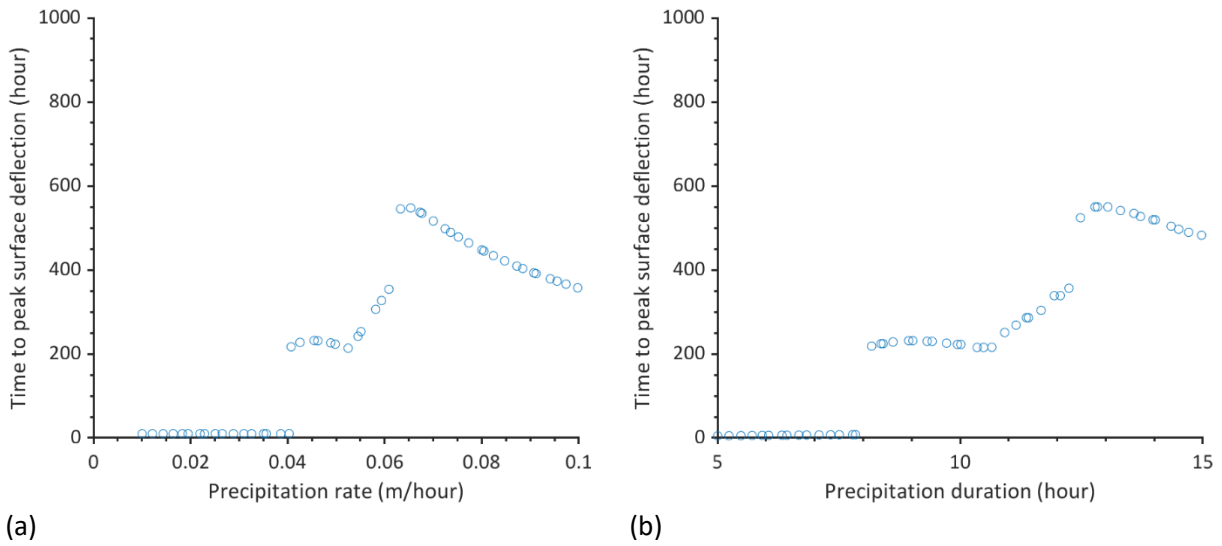


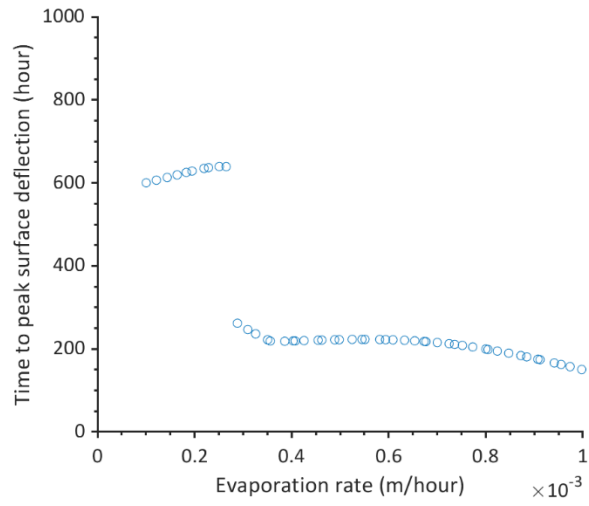
Figure B-28. Sensitivity of  $\delta_p/\delta_0$  to variations in wheel load for fine-grained subgrade model.



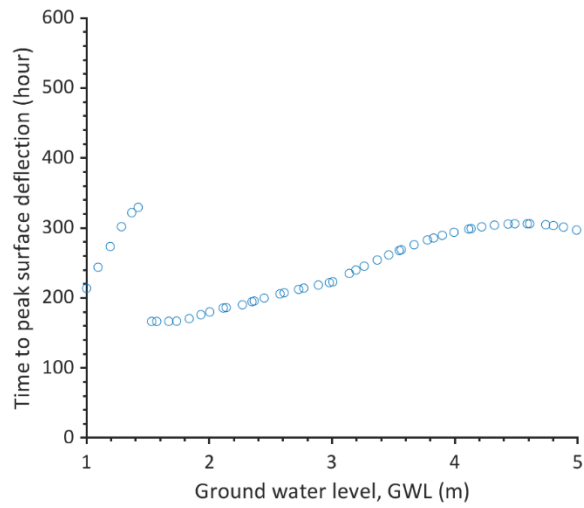
**Figure B-29. Sensitivity of  $t_p$  to variations in subgrade void ratio for fine-grained subgrade model.**



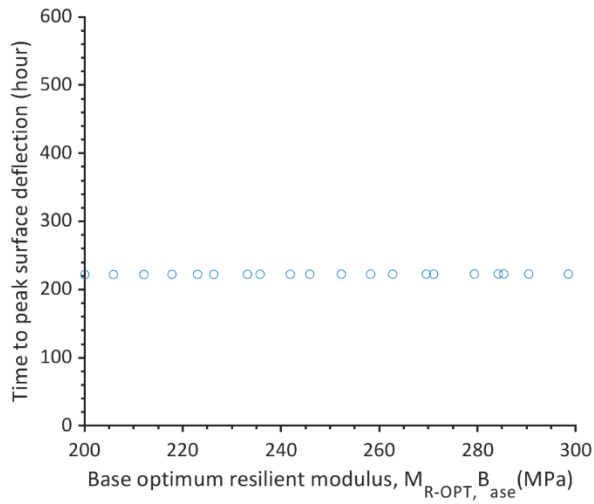
**Figure B-30. Sensitivity of  $t_p$  to variations in precipitation (a) rate and (b) duration for fine-grained subgrade model.**



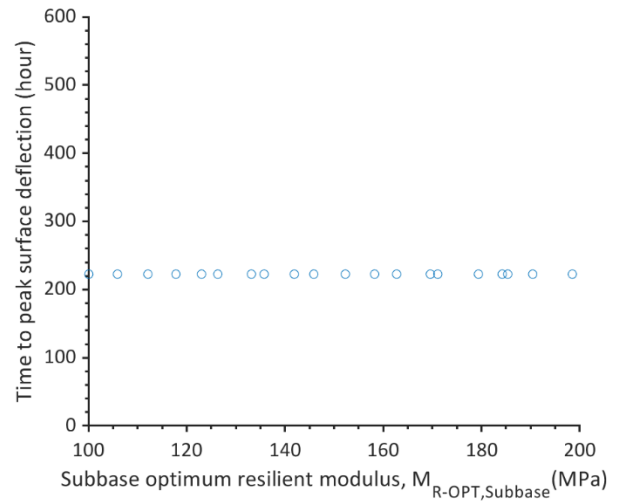
**Figure B-31. Sensitivity of  $t_p$  to variations in evaporation rate for fine-grained subgrade model.**



**Figure B-32. Sensitivity of  $t_p$  to variations in initial GWL for fine-grained subgrade model.**

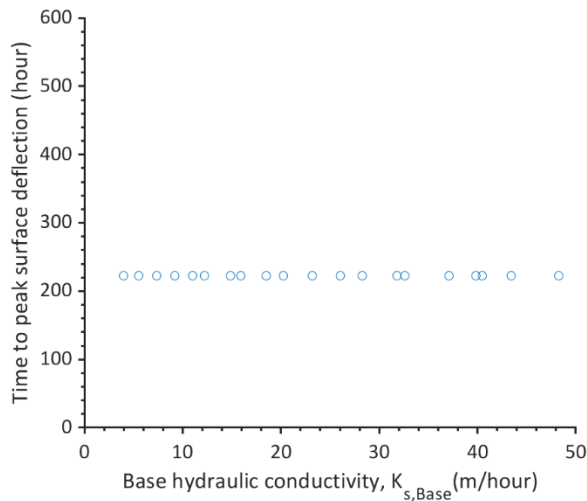


(a)

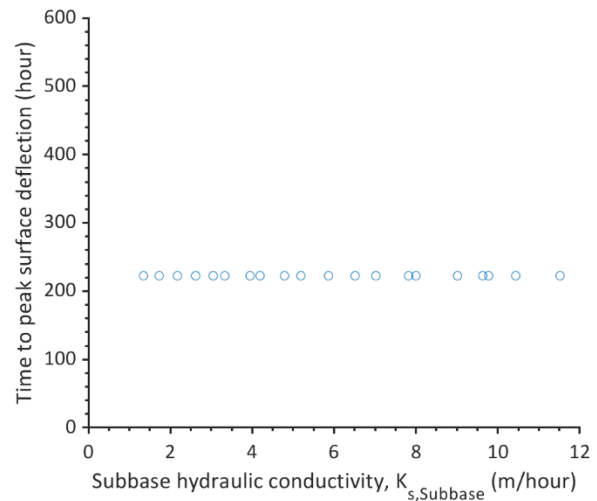


(b)

**Figure B-33. Sensitivity of  $t_p$  to variations in (a) aggregate base and (b) subbase optimum resilient moduli for fine-grained subgrade model.**

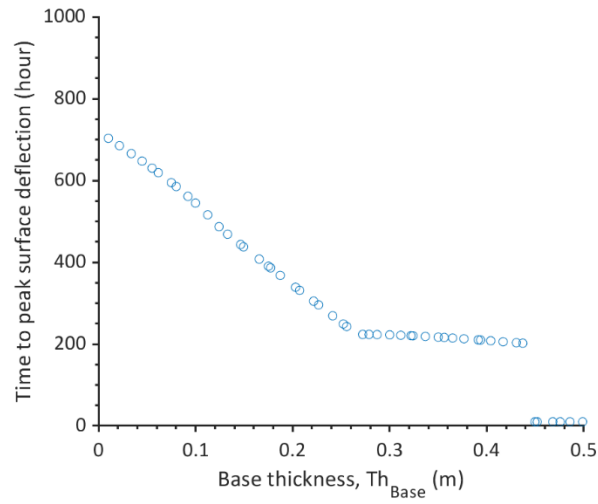


(a)

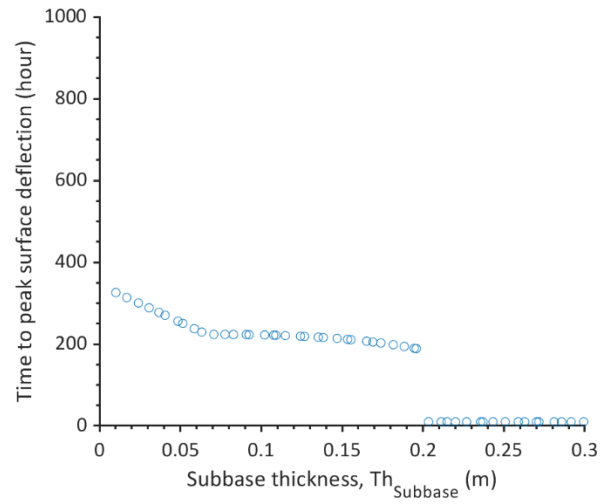


(b)

**Figure B-34. Sensitivity of  $t_p$  to the variations of (a) aggregate base and (b) subbase hydraulic conductivities for fine-grained subgrade model.**

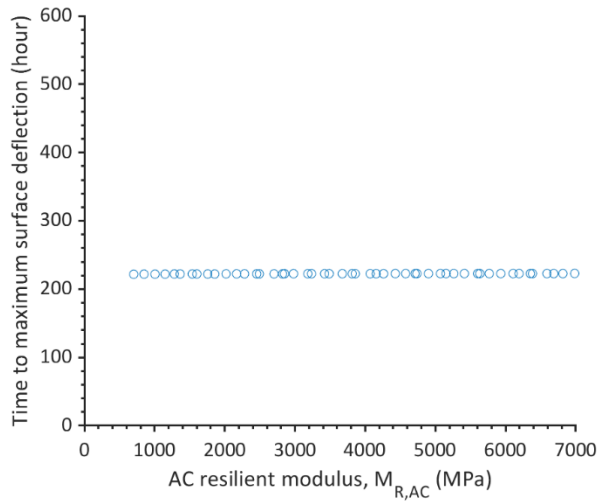


(a)

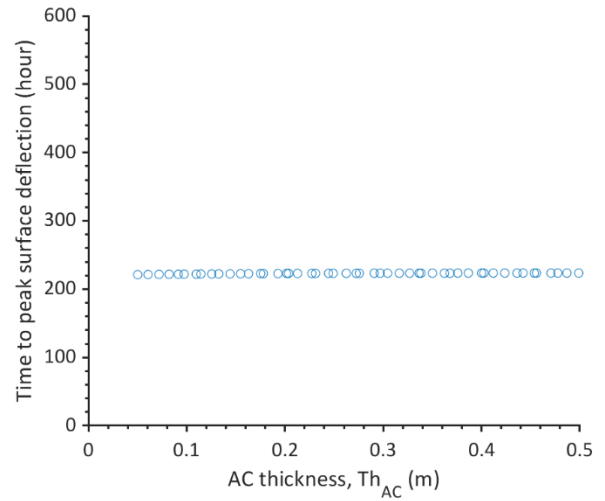


(b)

**Figure B-35. Sensitivity of  $t_p$  to variations in (a) aggregate base and (b) subbase thicknesses for fine-grained subgrade model.**

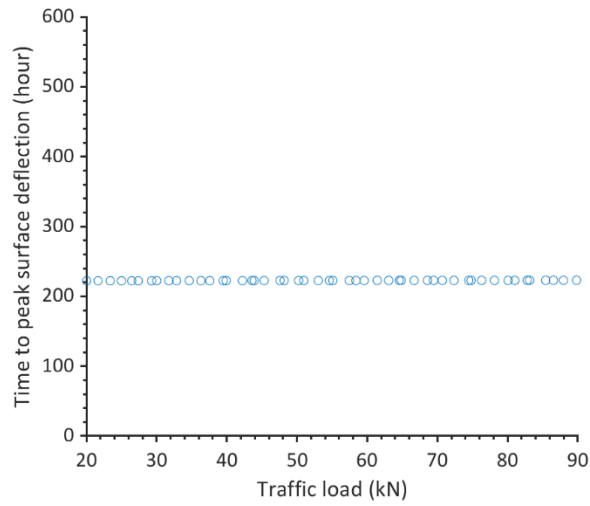


(a)

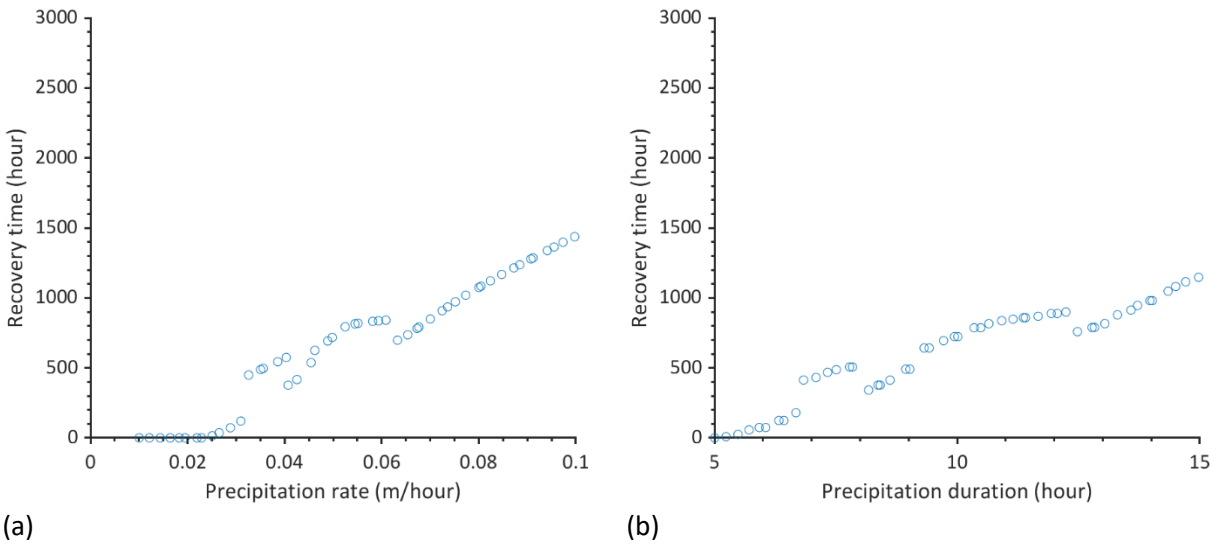


(b)

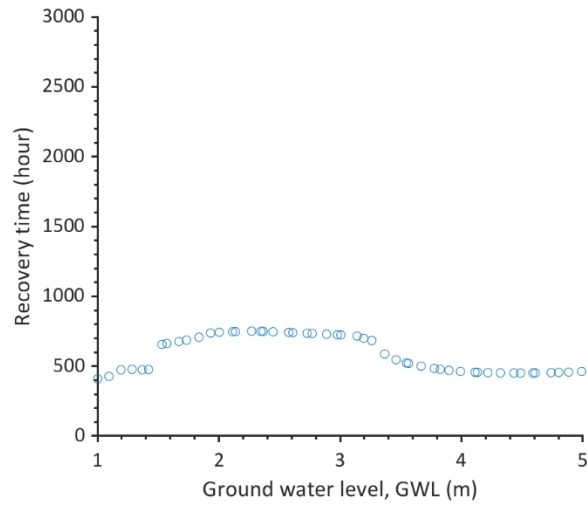
**Figure B-36. Sensitivity of  $t_p$  to variations in AC (a) resilient modulus and (b) thickness for fine-grained subgrade model.**



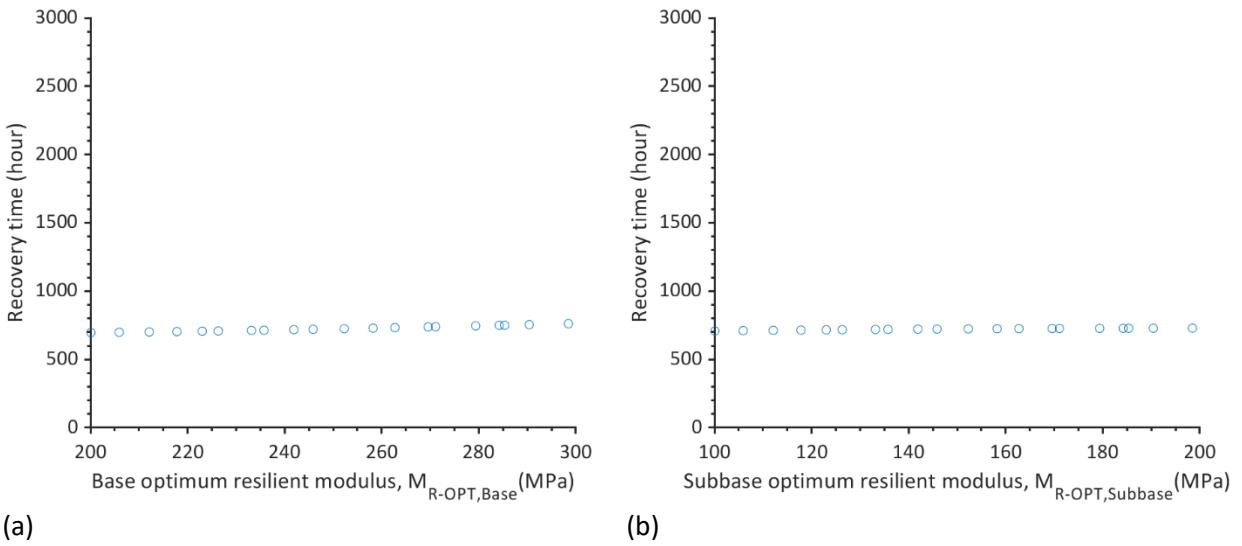
**Figure B-37. Sensitivity of  $t_p$  to variations in wheel load for coarse-grained subgrade model for fine-grained subgrade model.**



**Figure B-38. Sensitivity of  $t_R$  to variations in precipitation (a) rate and (b) duration for fine-grained subgrade model.**

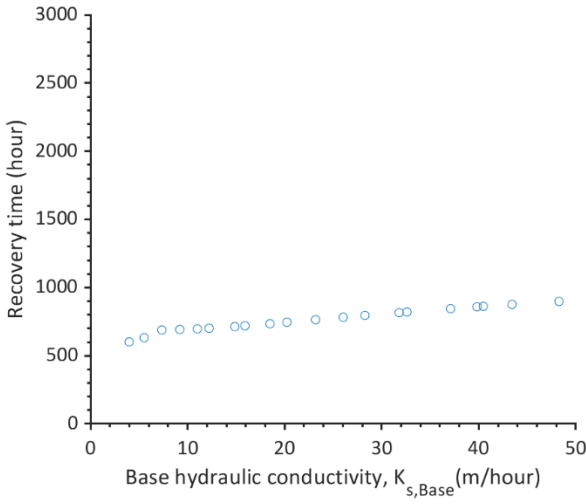


**Figure B-39. Sensitivity of  $t_R$  to variations in initial GWL for fine-grained subgrade model.**

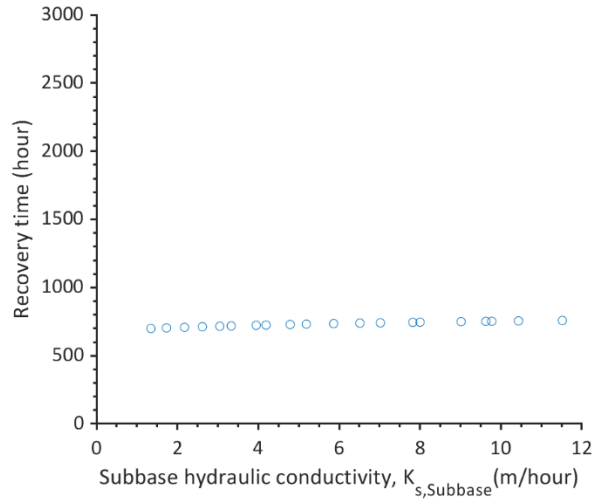


**Figure B-40. Sensitivity of  $t_R$  to variations in (a) aggregate base and (b) subbase optimum resilient moduli for fine-grained subgrade model.**



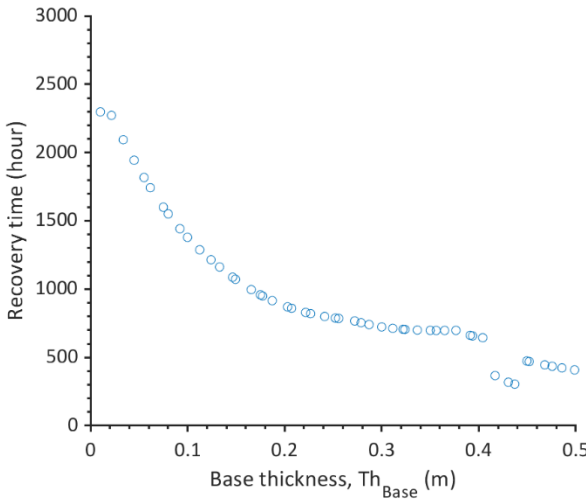


(a)

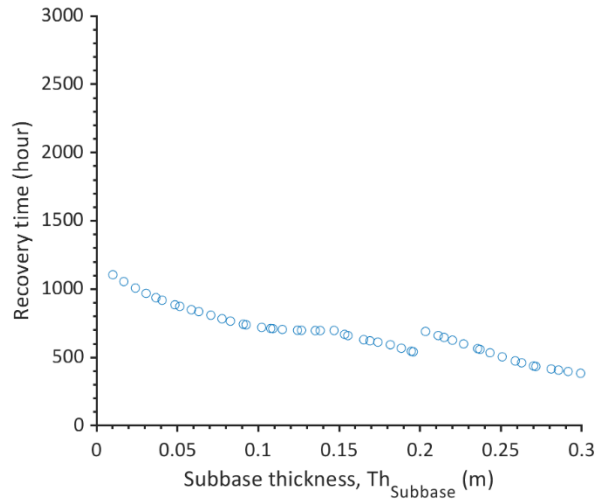


(b)

**Figure B-41. Sensitivity of  $t_R$  to the variations of (a) base and (b) subbase hydraulic conductivities for fine-grained subgrade model.**

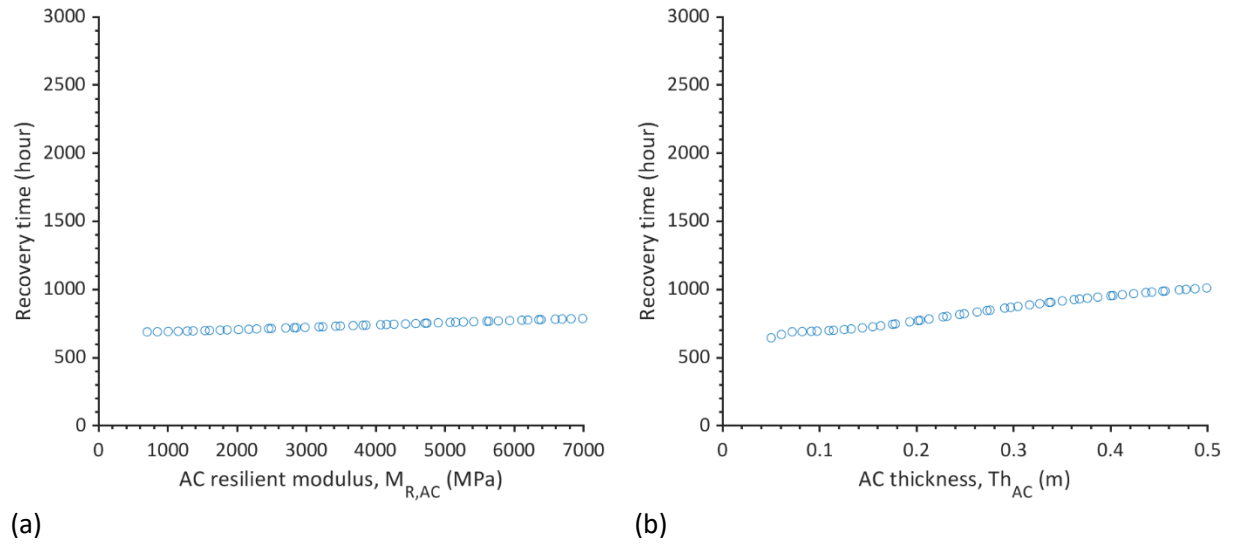


(a)

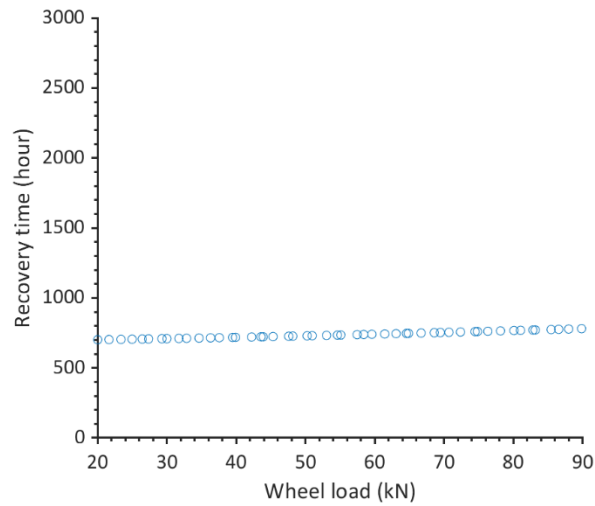


(b)

**Figure B-42. Sensitivity of  $t_R$  to variations in (a) base and (b) subbase thicknesses for fine-grained subgrade model.**



**Figure B-43. Sensitivity of  $t_R$  to variations in AC (a) resilient modulus and (b) thickness for fine-grained subgrade model.**



**Figure B-44. Sensitivity of  $t_R$  to variations in wheel load for coarse-grained subgrade model for fine-grained subgrade model.**